MARCH 1990
ENVIRONMENTAL SCIENCE & TECHNOLOGY

ES&T

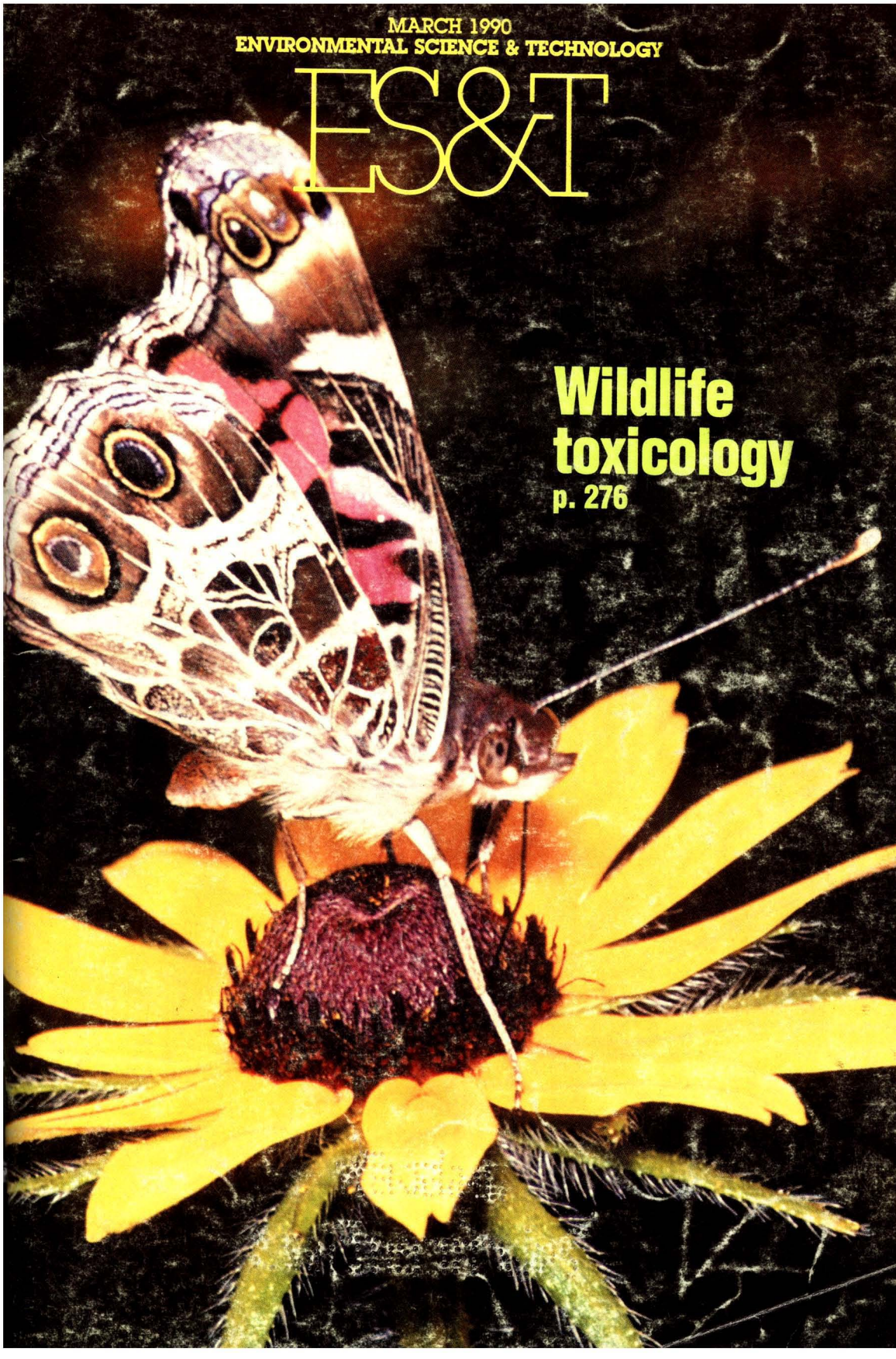

Wildlife toxicology

p. 276

CETAC U-5000 ULTRASONIC NEBULIZER

For Superior Limits of Detection

Several years ago, CETAC TECHNOLOGIES began research on an ultrasonic nebulizer that would provide today's chemist with a faster, more sensitive, stable, and reliable method of obtaining vastly improved detection limits. They succeeded.

SUPERIOR ANALYTICAL PERFORMANCE When used in conjunction with an ICP, the CETAC ULTRASONIC NEBULIZER will allow the analyst to achieve significant improvement in detection limits.

HOW THE U-5000 WORKS A peristaltic pump delivers the sample to the transducer face which is vibrating at 1.40 MHz. Instantly, the sample is nebulized into an extremely fine aerosol mist and swept away by the argon carrier gas. The dense aerosol mist then enters a "U" shaped tube which is heated to a temperature determined to best aid the desolvation process. The water component is then "stripped" away through condensation, thus resulting in a dry aerosol dense in analyte being introduced into the plasma.

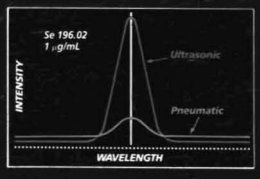

STABLE, RELIABLE PERFORMANCE Superior reliability and precision resulting from an air-cooled transducer and thermostatically controlled desolvation.

SAMPLE HANDLING FLEXIBILITY Whether your analysis needs call for the analysis of selenium in dolphin livers or arsenic in water, the U-5000 can do the job.

IMPORTANT FACTS ON THE MOST IMPORTANT INSTRUMENT IN YOUR LAB

- Installation can be performed in as little as fifteen minutes.
- Perfect for food, environmental, clinical, pharmaceutical analyses.
- Extremely cost effective.
- Total size of just 11¼" high X 17" wide X 13" deep.
- Total weight of just 35 pounds.

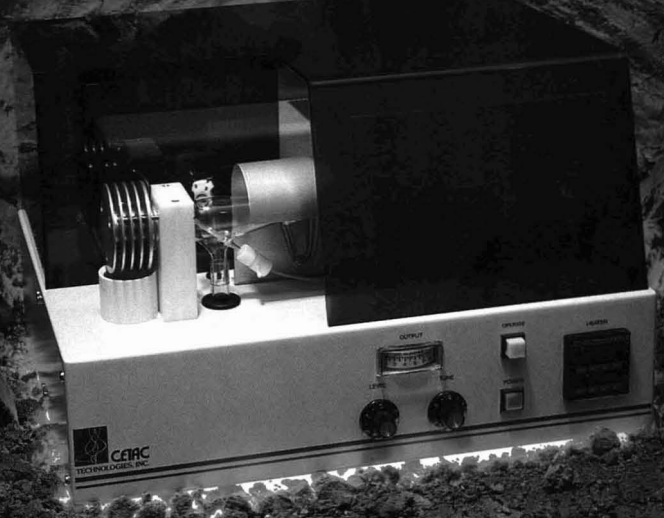

CETAC
TECHNOLOGIES, INC.
Expanding The Scope Of Measurement.

P.O. Box 31118
302 South 36th Street
Omaha, NE USA 68131
(402) 346-4345
FAX: (402) 346-9256

CIRCLE 2 ON READER SERVICE CARD

Environmental Science & Technology

Please send *research* manuscripts to Manuscript Reviewing, *feature* manuscripts to Managing Editor. For editorial policy, author's guide, and peer review policy, see the January 1990 issue, page 41, or write Yvonne D. Curry, Manuscript Reviewing Office, *ES&T.* A sample copyright transfer form, which may be copied, appears on the inside back cover of the January 1990 issue.

Environmental Science & Technology, ES&T (ISSN 0013-936X), is published monthly by the American Chemical Society at 1155 16th Street, N.W., Washington, D.C. 20036. Second-class postage paid at Washington, D.C., and at additional mailing offices. POSTMASTER: Send address changes to *Environmental Science & Technology,* Membership & Subscription Services, P.O. Box 3337, Columbus, Ohio 43210.

SUBSCRIPTION PRICES 1990: Members, $36 per year; nonmembers (for personal use), $67 per year; institutions, $276 per year. Foreign postage, $14 additional for Canada and Mexico, $29 additional for Europe including air service, and $36 additional for all other countries including air service. Single issues, $23 for current year; $24 for prior years. Back volumes, $282 each. For foreign rates add $3 for single issues and $14 for back volumes. Rates above do not apply to nonmember subscribers in Japan, who must enter subscription orders with Maruzen Company Ltd., 3-10 Nihon bashi 2 chome, Chuo-ku, Tokyo 103, Japan. Tel: (03) 272-7211.

SUBSCRIPTION SERVICE: Orders for new subscriptions, single issues, back volumes, and microform editions should be sent with payment to Office of the Treasurer, Financial Operations, ACS, 1155 16th St., N.W., Washington, D.C. 20036. Phone orders may be placed, using VISA, MasterCard, or American Express, by calling the ACS Sales Office at (614) 447-3776 or toll free (800) 333-9511 from anywhere in the continental U.S. (In the Washington, D.C., area call 872-4600.) Changes of address, subscription renewals, claims for missing issues, and inquiries concerning records and accounts should be directed to Manager, Membership and Subscription Services, ACS, P.O. Box 3337, Columbus, Ohio 43210. Changes of address should allow six weeks and be accompanied by old and new addresses and a recent mailing label. Claims for missing issues will not be allowed if loss was due to insufficient notice of change of address, if claim is dated more than 90 days after the issue date for North American subscribers or more than one year for foreign subscribers, or if the reason given is "missing from files."

ES&T

CONTENTS

Volume 24, Number 3, March 1990

FEATURES

CRITICAL REVIEW

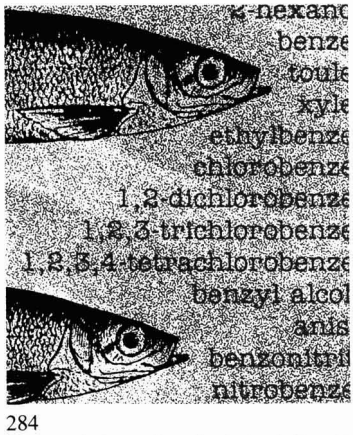

REGULATORY FOCUS

DEPARTMENTS

UPCOMING

20th anniversary Earth Day issue of *ES&T;* 14 essays by leading experts in their respective fields will address current environmental issues and problems

RESEARCH

ESTHAG 24(3)269–390 (1990)
ISSN 0013 936X

Cover: U.S. Fish & Wildlife Service: Jon R. Nickles

Credits: p. 275, Kyocera

CORRESPONDENCE

*To whom correspondence should be addressed

This issue contains no papers for which there is supplementary material in microform.

ES&T
EDITORIAL

Confirmation of structure

Research articles in this journal often involve the study of new or rare organic compounds the identity of which is central to the purpose of the paper. For example, the compounds may be by-products of a chemical or biological process or may be identified in a particular environmental setting. Although most authors are aware of the necessity for detailed proof of structure and submit such proof as a routine practice, this is not always the case. Worse still, some reviewers fail to notice the lack of such proof. In the future we will ask reviewers to be more careful on this point and to require appropriate data to indicate proof of structure for all compounds that are used or identified in an investigation.

We are also concerned that authors who propose mechanistic chemical pathways should provide evidence that such pathways are actually followed. In these cases, not only should the structure of each compound be thoroughly proven, but authors should also provide data (e.g., time-sequenced data) that show how the proposed path from one compound to another has been determined. Lacking such data, authors should refrain from proposing complex chemical schemes.

Confirmation of structure is often made more difficult by the fact that in many environmental studies we are compelled to deal with analyte concentrations that are extremely low. Here isolation of compounds and proof of structure are very demanding, even for the expert. Seldom are we able to isolate an amount of analyte sufficient to obtain elemental composition, boiling or melting point, and so forth, as in classical studies. Isolating enough for NMR studies is often out of the question. There are still a substantial number of investigators who propose identification based on a chromatographic retention time. In such cases, reviewers should be extremely careful to satisfy themselves that the evidence is conclusive. For example, confirmatory columns or Standard Methods should be used and the samples should not be excessively complex. For more confident proof of structure, spectroscopic data are required, and in the environmental field this has usually meant mass spectral data.

However, as spectroscopic methods become increasingly sophisticated we are seeing other methods become more and more credible for determining proof of structure. FTIR methods are becoming more routine, and we expect these methods to become even more popular as special libraries increase and instrument costs come down. Full spectrum UV/VIS or fluorescence spectra, especially of HPLC fractions, are also becoming powerful confirmatory methods for some classes of analytes, especially when combined with class separation procedures. Even in the field of environmental mass spectrometry, the monopoly of GC/MS is giving way to new methods such as HPLC/MS, dynamic FAB/MS, and others.

The editors recognize that each investigation has unique characteristics and that it would be inappropriate for this or any other journal to specify what methods must be used for proof of structure. What is more important is that authors should be required to establish by an appropriate number of confirmatory methods that the correct structure is proposed. The principles of environmental analytical chemistry are now well enough elucidated that, with the help of reviewers and authors, we should be able to maintain the standards of the journal with respect to confirmation of chemical structure.

0013-936X/90/0924-0271$02.50/0

ES&T
LETTERS

The Environmental Index

Dear Sir: The Environmental Index in the November 1989 issue of *ES&T* (p. 1337) contains some significant errors which lead to gross overstatement of conclusions. I am referring specifically to the data in the section comparing ethanol and gasoline fuels quoted from the *Ethanol Report* of the Renewable Fuels Association.

Simple stoichiometric calculations, outlined in the worksheet below, show that the number of pounds of carbon dioxide emitted per gallon of ethanol is 12.6, not 5.26, and per million Btu of combustion energy is 145, not 69.4. These errors lead to further errors in the last two lines of this section, which purport to give percentage comparisons.

Furthermore, the value of 186.6 pounds of carbon dioxide per million Btu given in the Index is correct for pure benzene, which has the highest C:H ratio of any gasoline component; but it is not true for the mixture commonly sold as gasoline. For paraffins, which make up a considerable portion of gasolines, the value is much lower. (See calculation for 2,2,4-trimethyl pentane, called "iso-octane" in the petroleum industry, for instance.) For substituted aromatics, such as toluene, which is also present in gasoline, the value is also lower than 186.6.

In conclusion, the data you quote from the *Ethanol Report* are incorrect and misleading. You have a well-established policy of careful review of feature and research articles. You need the same policy for the Environmental Index.

David Kauffman
Associate Dean and Associate Professor
Chemical and Nuclear Engineering
The University of New Mexico
Albuquerque, NM 87131

The carcinogenicity of radon

Dear Sir: The recent *ES&T* View on radon by Rhonda S. Berger (January 1990, p. 30) illustrates the difficulty of assessing and communicating the risks associated with human exposure to radon. Radon is a difficult problem, largely because risk levels associated with exposure to radon are exceptionally high. The risk levels (number of excess cancer deaths) reported by the author were taken from EPA's 1986 publication, *A Citizen's Guide to Radon,* and are consistent with EPA's current position on the risks associated with human exposure to radon.

Risk levels for radon are extrapolated in part from epidemiological data describing lung cancer rates in underground miners exposed to radon-contaminated dust particles. Although some have criticized these risk levels as having a tenuous correlation to the clinical data, the approach used by EPA to extrapolate risks to nonoccupationally exposed individuals is consistent with current risk assessment methodologies. Due to uncertainties associated with these estimates, however, projected risk levels should not be viewed as definitive numbers. More precise risk estimates cannot be made until the studies of miners are extended to cover the entire lifetime of exposed individuals and additional studies are initiated to evaluate the relationship between lung cancer and indoor radon levels.

Several points related to indoor radon levels, risks, and public perception should be emphasized. First, EPA recommends implementation of remedial action in homes where radon levels exceed 4 pCi/L. The risk associated with this exposure level is one to five in 100 (10^{-2}). Thus, the maximum tolerable risk level for radon is about three orders of magnitude higher than the threshold level generally adopted for exposure to chemical carcinogens (10^{-5}).

Second, there is a correlation between lung cancer, radon, and smoking. Only 5–10% of the expected lung cancer cases per year will occur in nonsmokers. The risk of developing lung cancer is about 10 times higher for a smoker relative to a nonsmoker and about 20 times higher for heavy smokers. Because data on the combined effect of radon exposure and smoking are scarce, definitive conclusions about the effect of smoking on radon dosimetry cannot be drawn.

Third, there is currently no federal regulation governing radon levels in homes. The Indoor Radon Abatement Act of 1988 authorizes (among other things) the *measurement* of radon levels in schools and federal buildings but not private residences. Should the results of this testing program (which are due later in 1990) show that radon levels are consistently elevated in these buildings, regulation of these structures is a strong possibility. Given the difficulty of enforcing regulation aimed at private residences, it is doubtful EPA will promulgate radon regulation for homes.

Given the lack of data on the association between radon exposure and lung cancer, continued discussion of the accuracy of published risk levels seems pointless. A more beneficial strategy would be to focus our resources on conducting epidemiological studies in areas with high background radon levels and on basic research to better understand the biology of radon-induced lung cancer.

Curtis C. Travis
Holly A. Hattemer-Frey
Office of Risk Analysis
Oak Ridge National Laboratory
Oak Ridge, TN 37831-6109

	sp gr (liq.)	ΔH_c (gross value) Btu/lb
Ethanol	0.789	13161
Benzene	0.879	18172
2,2,4-trimethyl-pentane	0.692	19197

Source: *Perry's Chemical Engineers' Handbook.*

Combustion chemistry

Ethanol $C_2H_5OH + 3O_2 \rightarrow 2CO_2 + 3H_2O$
Benzene $C_6H_6 + 7.5O_2 \rightarrow 6CO_2 + 3H_2O$
2,2,4-tmp $C_8H_{18} + 12.5O_2 \rightarrow 8CO_2 + 9H_2O$

	Ethanol	Benzene	2,2,4-tmp
Mol wt	46	78	114
Moles CO_2/mol fuel	2	6	8
Lbs CO_2/lb fuel	1.913	3.385	2.316
Lbs fuel/gal	6.58	7.33	5.77
Lbs fuel/million Btu	75.98	55.03	52.091
Lbs CO_2/gal	12.6	24.8	13.4
Lbs CO_2/million Btu	145	186	121
CO_2 yield (by volume)	ethanol: benzene = 0.51		49% less
	ethanol: 2,2,4-tmp = 0.94		6% less
CO_2 yield (by energy)	ethanol: benzene = 0.78		22% less
	ethanol: 2,2,4-tmp = 1.20		20% more

0013-936X/90/0924-0272$02.50/0

INTERNATIONAL

The state of the environment in the changing countries of central and eastern Europe generally is not a happy one. In Poland, for instance, it is estimated that only 1% of that country's surface water can be used for drinking water. Czechoslovakian interim President Vaclav Havel told his people Jan. 1, "We have the worst environment in the whole of Europe today." He may have been referring to acute air pollution and forest decline problems that originate from local industries and from industries in neighboring East Germany. Like Poland, Romania suffers from severe water pollution; the country's interim Prime Minister, Petre Roman, a hydrogeologist by training, says that one of his country's priorities will be to try to redress environmental wrongs.

The international drug trade is taking its environmental toll, according to part of a report released Jan. 10 by the U.N. International Narcotics Control Board (Vienna). Drug producers are destroying tropical forests and soils by slash-and-burn methods. In addition, they are contaminating rivers and streams with chemicals they use to process cocaine and heroin, according to the report.

EPA administrator William Reilly and his counterpart from the U.S.S.R., Nikolai Vorontsov, with members of their staffs, met to plan cooperative work between the two countries for 1990 and future years. This work will include studies of the climate; the prevention of air, water, and agricultural pollution; the biological and genetic effects of pollution; and arctic and subarctic ecosystems. One proposal calls for the establishment of an international park and wildlife refuge on both sides of the Bering Strait. This cooperative effort originally was called for in the Reagan–Gorbachev Washington summit of December 1987.

FEDERAL

President Bush has signed a bill that forbids U.S. support for international lending projects unless their environmental impact is assessed. That provision had been added by Sen. Frank Lautenberg (D-NJ) to the National Environmental Policy on International Financing Act of 1989. Its purpose is to put pressure on lending agencies such as the World Bank and the Inter-American Development Bank to take into account potential environmental consequences of development projects in less developed countries.

In EPA administrator William Reilly's opinion, a $10 remedy can reduce some automobile pollution. His proposal calls for an increase in the size of activated carbon canisters that trap gasoline fumes during hot weather and reroute them to the engine to burn. EPA officials estimate that the use of these larger canisters could reduce hydrocarbon emissions in summer by 5%. Moreover, because the recycled gasoline vapor can fuel the engine, fuel savings could offset the cost of the canisters. By contrast, proposals before Congress to trap gasoline fumes emitted during refueling or to cut tailpipe emissions might reduce summer hydrocarbon emissions by about 2% and 1%, respectively.

EPA supports a plan to forestall global warming that allows nations to buy and sell emissions rights for CO_2 and fossil fuels so long as reduction goals are achieved, agency spokesman Dave Cohen said Jan. 10. The plan would work similarly to U.S. plans for air pollution control that allow industrial firms in a given area to trade emission rights so long as overall air pollution standards are met in that area. The plan was proposed by Assistant Attorney General Richard Stewart, an environmental lawyer. Two questions arise, however: Given differing political situations and interpretations of national sovereignty, how well will the trade-off concept be accepted worldwide? Also, how can exchange rates for different types of emissions be specified accurately?

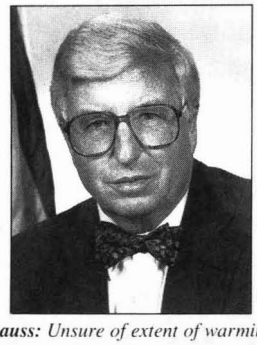

Knauss: Unsure of extent of warming

John Knauss, administrator of the National Oceanic and Atmospheric Administration (NOAA), agrees that there is a threat of significant global warming. He notes, however, that there is much uncertainty over its magnitude. Knauss says that NOAA scientists are carefully analyzing climate and sea-level data to detect the first signal that the Earth is, in fact, warming because of greenhouse gases. NOAA's current budget is $1.2 billion, and it has a staff of 2200 scientists, a uniformed corps of 400 sailors and pilots, 23 ships, 6 satellites in orbit, and several aircraft. Before coming to NOAA, Knauss was a professor at the Graduate School of Oceanography at the University of Rhode Island.

The National Institute of Standards and Technology is developing standard reference materials (SRMs) for vehicle emissions. Among the SRMs will be nitric oxide in nitrogen and methane in air. The SRMs will serve as national standards for calibrating instruments and methods to measure automotive emissions. In partnership with the Motor Vehicle Manufacturers Association, NIST is developing seven such SRMs. They will be offered in the

0013-936X/90/0924-0273$02.50/0

form of bottled gas mixtures and are expected to become available during the fall of 1990.

STATES

The New York Department of Environmental Conservation has announced a $280-million plan to remove sediments contaminated with polychlorinated biphenyls (PCBs) from the Hudson River. This plan replaces a $40-million plan that DEC Commissioner Thomas Jorling had rejected as inadequate. Financing would come from Superfund. The plan calls for removing 250,000 lb of PCBs from a stretch of the Hudson between Fort Edward and Troy. The old plan had called for removing 24,000 lb as a demonstration project. EPA could stymie the plan with a no-action recommendation, approve the plan with modifications, or, as New York officials hope, approve the entire plan for extended PCB removal.

The Illinois Environmental Protection Agency has developed a proposed list of 108 airborne toxic chemicals. Chemicals are added to this list on the basis of emissions data, the toxic properties of the chemicals, and their potential threat to human health. The list includes air contaminants that are deemed to be able to cause or contribute to an increase in mortality or in serious irreversible illness. For more information, contact the Illinois Environmental Protection Agency, P.O. Box 19276, Springfield, IL 62794-9276.

The City of New York is developing a 20-year, comprehensive solid-waste management plan. It must provide for programs to reduce, recycle, compost, incinerate, and landfill about 30,000 tons per day of solid and medical waste, sewage sludge, harbor drift, and construction and demolition debris. Roy F. Weston, Inc. (West Chester, PA), has received a $3 million, one-year contract to assist the city in preparing the plan.

In most states, proposals for new hazardous-waste treatment facilities eventually are approved despite public opposition and the complex and time-consuming siting process. A National Governors Association (NGA) work group found that of the applications filed between 1980 and 1986, 71% acted upon during that time were approved. Group members also observed that it is easier to locate a waste management facility on-site (at the waste generator's) than off-site; that it is easier to locate facilities on already industrialized land parcels; and that it is easier to find sites for storage, transfer, and mobile treatment facilities than for other kinds of facilities. The NGA report, "Siting New Treatment and Disposal Facilities," is available for $15 from NGA Publications, 444 N. Capitol St., Suite 250, Washington, DC 20001-1572.

The world's largest steel can recycling facility will be built in St. Paul, MN. When completed later this year, the plant will process 40,000 tons per yr of steel food, beverage, and aerosol cans. Surrounding counties in Minnesota and Wisconsin are expected to send in this type of waste. Currently, they spend a total of about $18,000 a week ($936,000 a year) to bury the steel in a landfill. Robert Chevalier, director of steel can recycling for AMG Resources (Pittsburgh, PA), which will build and operate the plant, estimates that the counties will save more than $1 million a year. That amount includes what AMG will pay for the steel.

AWARDS

A new Air & Waste Management Association award recognizes excellence in the waste management field. Its criteria will be outstanding technical achievement in the science and art of waste management; outstanding achievement in management, prevention, and regulation that minimizes adverse effects; and distinguished achievement as an educator in the field. Nominations should be sent to Joe Padgett, 4509 Bartlette Drive, Raleigh, NC 27609.

SCIENCE

The damage that lead inflicts on children continues to affect them when they reach adulthood, says Herbert Needleman of the University of Pittsburgh School of Medicine. Lead harms the central nervous system. A study by Boston and Pittsburgh researchers examined 132 of 270 young adults who were exposed to lead as children and initially studied during the 1970s. At that time, they performed poorly on behavioral and intelligence tests. In later life, many of the study subjects did not graduate from high school and showed reading disabilities, poor hand–eye coordination, and several other problems. The follow-up study is described in the January 1990 issue of the *New England Journal of Medicine.*

The new International Society of Exposure Analysis (Princeton, NJ) held its first technical meeting in Las Vegas, NV, in late November; 300 people attended. Myron Mehlman is its executive director. The organization aims to identify and assess the cumulative inputs and effects of contaminants of air, drinking water, and food, as well as those of contaminants in the workplace. Some of its members suggest the use of total exposure assessment methodology, a means of monitoring health effects of known doses of pollutants on humans.

A new tool for studying air pollution may be found in tree rings. Pollutants could be deposited in the rings, says James Bockheim of the University of Wisconsin–Madison. He notes that researchers in some states have observed that trees are growing more slowly and that the wood in their newest growth rings—just below the bark—contains more aluminum, lead, and sulfur than do older growth rings. The researchers believe that their findings are related to higher levels of air pollution and soil acidification observed during the last 40 years. Increased acidification of soil solubilizes pollutants such as aluminum, lead, and sulfur, thereby making them more available to the trees. Bockheim now is developing a method known as stem analysis, by which samples will be taken at regular sites along a tree to help determine the type and distribution of pollutants the tree may have taken up.

Very low levels of nicotine are found in the air of smokers' offices, report C. J. Proctor and his colleagues of BAT(UK&E) Research and Development Centre (Southampton, England) (*Environmental Technology Letters* 1989, *10,* 1003–18). They also report that smoking has "very little influence" on levels of volatile organic compounds in office air. The net result, the researchers say, is that a nonsmoking male, for instance, would have to work in a smoker's office for an average of 11 weeks to be exposed to the nicotine equivalent of one cigarette and for 15 weeks to be exposed to the particulate equivalent of one cigarette. For females, these numbers are 20 and 25 weeks, respectively. The British

researchers say that their data indicate that levels of components such as nicotine and particulates of environmental tobacco smoke in offices in the "relatively well ventilated" building they studied "are extremely small."

The 1980s were indeed the hottest years in more than a century, according to the Meteorological Office (MO) of the United Kingdom. James Hansen of NASA says, "It's not conclusive, but it's one more strong piece of evidence" that the greenhouse effect is happening. MO's David Parker remarks that it will be "some time before we. . . know what the cause is. . . but it looks more likely all the time that there has been a definite warming of the globe." Earlier in the decade, it was estimated that average temperatures would increase 4–9 °F by 2050. These forecasts recently have been revised downward slightly.

TECHNOLOGY

A sensor for detecting liquid organic contaminants in soil has been developed at Battelle (Richland, WA). Its developer, John Cary, explains that the sensor consists of an optical switch containing an infrared light-emitting device that is attached to a porous disk made of ceramic material, Teflon, or other polymer. The amount of organic liquid or water detected in the soil is proportional to the light transmitted. Cary explains that currently available detectors, such as gypsum blocks, do not measure organic liquids and that most other sensors that are used to detect organic liquids actually detect vapors.

A hybrid diesel–electric car has successfully completed tests, according to spokespersons for Volkswagen (Wolfsburg, West Germany) and the Swiss Technical College. Over the next two years, 40–50 Volkswagen Golfs will be converted to hybrid drive. In the city, they can be run on a sodium-sulfur battery with low-noise and exhaust-free performance. On open roads and at high speeds, when increased power loads are necessary, the drive would switch automatically to diesel. One advantage is that exhaust emissions may be shifted away from urban areas. Two problems still need to be overcome, however. One is the need to improve the efficiency of the output of braking energy. A second is that although the electric drive itself weighs about 35 kg, the battery weighs at least 90 kg (198 lb).

The world's first all-solar-powered tract home is being shown in Lake Placid, FL, by The Charles Wayne Group, a firm of developers. Its photovoltaic modules have been supplied by Kyocera America (San Diego, CA). The solar system on the roof supplies 100% of the electricity needed to power the 2480-ft^2, three-bedroom home, even after seven days of continuous cloudy weather.

All-solar-powered home

There are 108 photovoltaic modules, each 59 watts, installed on the roof with a single-axis sun-tracking system. Gel-cell batteries on the garage wall store the energy. An inverter converts the batteries' DC current to AC. The system can run all of the home's appliances, including the water and space heaters, air conditioning, lights, refrigerator, microwave oven, and freezer, according to a spokesperson for Kyocera.

BUSINESS

The Edison Electric Institute (EEI, Washington, DC) warned that if the Department of Energy does not accept spent nuclear fuel for storage beginning January 31, 1998, a funding mechanism will have to be set up to pay additional costs of storage at reactors. That is the date DOE is supposed to accept the waste for monitored retrievable storage (MRS). EEI spokespersons called on DOE to proceed expeditiously with studies at a proposed repository at Yucca Mountain, NV, to determine its suitability as a storage site and what, if any, disqualifying conditions may exist there. The repository was supposed to start operations in 2003, but DOE announced not only a delay until 2010, but also plans to detach MRS from the repository program. DOE plans to sue Nevada to obtain needed environmental permits. Opposition to the repository currently is running strong in Nevada.

Jeffrey Zelms, chairman of the Lead Industries Association (LIA, New York City), says that lead shielding beneath the foundation of a home could protect it from naturally occurring radon gas. He says that the National Association of Home Builders, funded by LIA, is conducting tests to determine whether sheet lead would be a cost-effective means to block the infiltration of radon into a home's air, where it becomes a cancer threat. One test involved the installation of a lead membrane under a slab-built home in Gainesville, FL. A second is taking place in Port Charlotte, FL. The lead sheeting used generally is 0.04 in. thick. The Florida sites were chosen because they are underlain by phosphate ore that contains uranium and emits radon.

Amoco (Chicago, IL) will begin marketing compressed natural gas (CNG) as an alternative motor fuel for fleet vehicles this year at four service stations in and near Denver, CO. The pilot test is being conducted in cooperation with Public Service Company of Colorado. Public Service will transport the CNG through its pipelines to the designated Amoco stations. The CNG will be available to any customer with a vehicle equipped to use the fuel. About 20,000 vehicles in the United States can run on CNG. Amoco's marketing vice president, Robert Rauscher, sees CNG as "a promising motor fuel, especially for fleet use. It's clean-burning and can play a significant role in reducing carbon monoxide and ozone levels."

ES&T SERIES

Wildlife toxicology

Third part of a four-part series

David J. Hoffman
Barnett A. Rattner
Russell J. Hall
U.S. Fish and Wildlife Service
Patuxent Wildlife Research Center
Laurel, MD 20708

Ecotoxicology series

Ecotoxicology is the study of the fate and effect of toxic agents in ecosystems. In the second part of this series John Cairns and Donald Mount addressed aquatic toxicology from several perspectives. They noted that more standard toxicity tests were needed along with multiassay test batteries. They called for predictive models that address ecosystem functioning and resilience and for methods to assess ecological changes at hazardous-waste sites. (See the February 1990 issue, p. 154.)

In the first part of this series John Bascietto, Dexter Hinkley, and colleagues provided an overview of applications of ecotoxicology through the various regulatory acts and programs of EPA. They reported that new directions within EPA reflect an increased emphasis on the role of sediments, biomarkers, and ecosystem assessments in regulating environmental pollutants. (See the January 1990 issue, p. 10.)

The fourth and last part of this series will appear in the May issue. Hallet Harris, Paul Sager, and colleagues will discuss ecotoxicology from an ecosystem integrity standpoint and use the Great Lakes as the example.

Scientists who have investigated the effects of pollutants on wildlife and habitats for many years are not comfortable with the appellation "wildlife toxicology." To some, it still brings forth im-

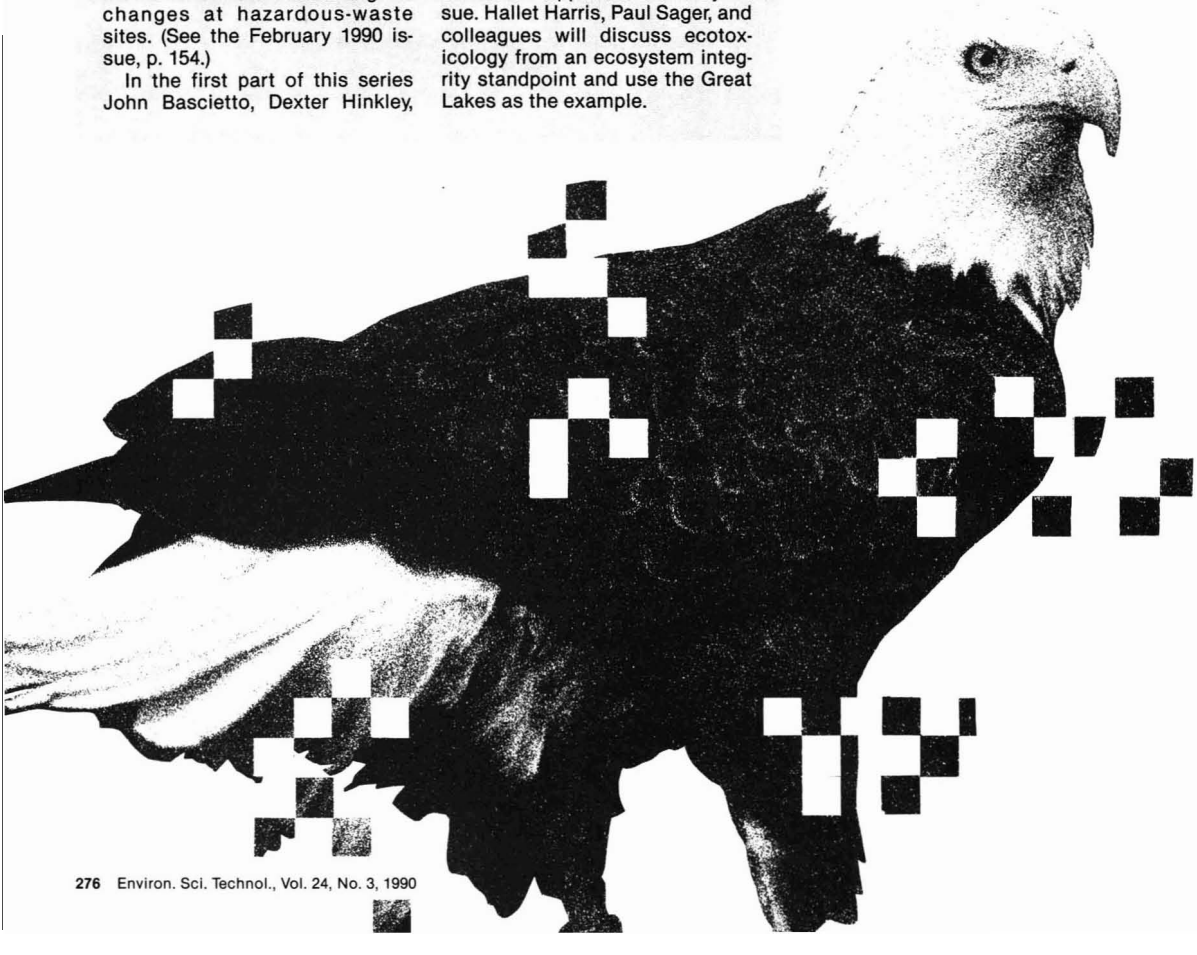

TABLE 1
Integrated strategies for wildlife toxicology

Test systems	Volume of data produced per unit cost	Repeatability and precision of data	Control of variables	Sensitivity	Confidence in applicability to field	Special capabilities
Chemical screening	High	High	High	High within confidence of test system	Moderate	Test many chemicals singly and in combination. Utilize many end points (e.g., lethality, reproduction, teratogenicity, growth, behavior, physiology)
Field ecology	Moderate	Low	None	High for total impact, low for individual variables	High	Evaluate total impact of complex interactions of xenobiotics and other environmental stressors. Determine effects on population distribution and abundance.
Controlled field and mesocosm studies	Moderate	Moderate	Moderate	High	Moderately High	Examine interaction of xenobiotics and other stressors under moderately controlled conditions. Evaluate individual variables. Utilize different end points.

ages of white-coated technicians extracting venom from rattlesnakes. To many, it suggests intellectual restrictions in a truly multidisciplinary field that relies on the knowledge and skills of ecologists, chemists, physiologists, toxicologists and, increasingly, biometricians and systems ecologists. Environmental contamination problems are complex, and useful knowledge often results from research begun from several vantage points.

Three principal strategies for understanding xenobiotic effects on wildlife are chemical screening, field ecology, and controlled field studies. In chemical screening, a variety of toxicological tests are performed with what are thought to be representative species. The purpose of screening is to predict likely effects in natural populations by identifying those chemicals toxic to wildlife. Endpoints of these tests may include lethality, reproductive impairment, behavioral aberrations, alterations in growth and development, or changes in physiological indicators (or "markers") that may foreshadow effects crucial to reproduction and survival.

A strategy at the other end of the spectrum is field ecology. Wildlife populations in environments believed to be polluted are studied to estimate distribution, absolute and relative abundance, mortality and recruitment, and interactions with other components of the ecosystem. Indications of population effects may be related to contaminant body burdens as detected by analytical chemistry.

The third strategy seeks to optimize both control of variables and resemblance of test systems to natural environments. It is known as a controlled field or mesocosm study. Each of these three strategies has strengths and weaknesses (see Table 1). In practice, integrated investigations that involve more than one research strategy are necessary to study and correct environmental problems. Contributions of the various approaches and disciplines will become evident as we discuss past and present endeavors in wildlife toxicology.

Brief history

Even in ancient times an awareness of the condition of wild birds existed—hence the Greek maxim "a bad crow lays a bad egg." Reports of anthropogenic environmental contaminants affecting wildlife began to accumulate during the industrial revolution of the 1850s. One account described the death of fallow deer (*Dama dama*) caused by arsenic emissions from a silver foundry in Germany *(1)*. Another report identified hydrogen sulfide fumes near a Texas oil field as the cause of death of many wild birds and mammals *(1)*. The hazard of spent lead shot was recognized as early as 1874, when lead-poisoned water fowl and pheasants were observed in Texas and North Carolina *(2)*.

Prior to the Second World War, most agricultural pesticides were derived from naturally occurring minerals and plant products, and were neither very toxic nor environmentally persistent. Thereafter, the variety and total worldwide production of synthetic organic insecticides rose dramatically. It soon became apparent that modern insecticides had immense biological potency, not merely to poison but often to persist in the environment in nontarget organisms, including fish and wildlife.

Studies of the effects of modern pesticides on wildlife began soon after the introduction of DDT in 1943. Several of these early studies conducted by Stickel *(3)* and others at the Patuxent Wildlife Research Center cautioned users of the potential hazards of DDT to wildlife *(4)*. Despite this concern, use of DDT continued. Decline in the population of American robins (*Turdus migratorius*) was linked to DDT spraying for Dutch elm disease by the early 1950s. Soon it became evident that the bald eagle (*Haliaeetus leucocephalus*), osprey (*Pandion haliaetus*), and certain fish-eating mammals were at risk *(5)*.

Further research revealed that dietary exposure to DDT and other organochlorine (OC) insecticides (e.g., DDD, endrin, aldrin, and dieldrin) impaired reproductive success of pheasants and quail even when direct adverse effects on adults were not evident *(6)*. Eggshell thinning related to DDT, and specifically its metabolite DDE, caused reproductive failure in European *(7)* and North American raptors and fish-eating birds *(8–10)*. Other modern insecticides causing more recent wildlife losses include organophosphorus (OP) and carbamate (CB) compounds that act principally by inhibiting the enzyme acetylcholinesterase *(11, 12)*.

Agricultural tillage practices and irrigation may also affect wildlife. Recent focus on subsurface drainage has demonstrated that irrigation water contain-

ing seleniferous compounds is highly toxic to water bird embryos *(13, 14)*.

Toxicological testing

With the advent of modern insecticides and consequent wildlife losses, screening of pesticides for adverse effects became important *(15–17)*. Standardized avian testing protocols were developed by the U. S. Fish and Wildlife Service, and several of these (acute oral and subacute dietary tests; [*15*]) are currently required for regulatory purposes by EPA under the Federal Insecticide, Fungicide, and Rodenticide Act (FIFRA) and the Toxic Substances Control Act (TSCA).

These basic protocols have lethality as the principal end point and are used as a first-line toxicity screen (Figure 1). Single oral dose LD_{50} data have been published for 75 species of birds and over 1000 chemicals *(16)*. Pesticide registration in the U.S. requires acute oral toxicity tests on two species of birds, the mallard (*Anas platyrhynchos*) and northern bobwhite (*Colinus virginianus*), as well as product analysis and generation of dose–response curves. Acute oral toxicity testing has utilized bobwhite and passerines to compare toxicities and potential hazards of technical grade and granular formulations *(18, 19)*. The subacute test allows evaluation of both feeding behavior and other responses, thus serving as a composite indicator of species' vulnerability to contaminated diets.

More than 300 standardized pesticide trials have been conducted with young northern bobwhite, Japanese quail (*Coturnix japonica*), ring-necked pheasants (*Phasianus colchicus*) and mallards *(20, 21)*. Routine embryo tests treat eggs by immersion, topical application, or injection, depending on likely route of contaminant exposure. Results of over 70 mallard embryo tests for lethality and teratogenicity have been conducted with pesticides, petroleum pollutants, aromatic hydrocarbons, heavy metals, and industrial effluents *(22, 23)*. Investigations of lethal toxicity usually include doses that bracket concentrations encountered in the field, thereby providing indices of absolute toxicity and potential hazard.

Two protocols have been used for examining contaminant effects on avian reproduction. One is used for persistent environmental chemicals, with test concentrations based on observed contaminant residues and effect levels. The other protocol is for less persistent chemicals (e.g., OP and CB pesticides), using 3-week observation phases for pretreatment, treatment, and posttreatment effects *(15)*. In practice, these large and costly investigations also generate sublethal-effects data useful for integrated risk assessments.

FIGURE 1
Protocols used in avian toxicity testing

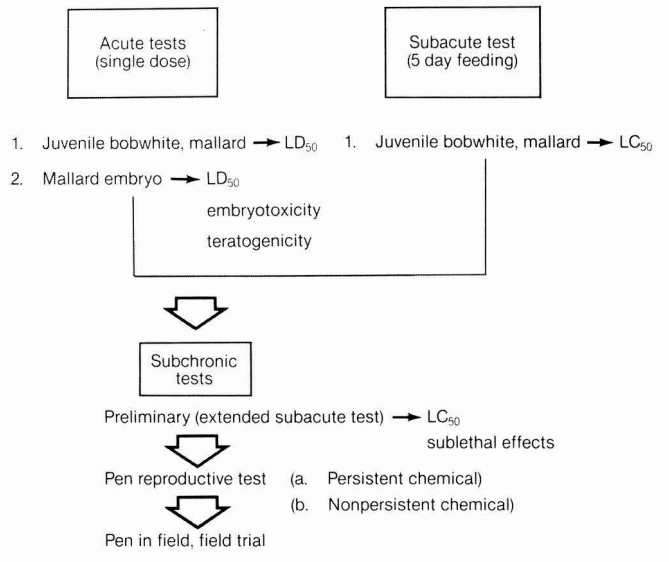

For example, effects of cadmium on reproduction revealed that concentrations in mallard eggs were poor indicators of exposure and reproductive hazard *(24)*. A new subchronic dietary toxicity test emphasizes sublethal indicators of toxicity to ascertain the necessity for full-scale reproductive tests and to provide a better hazard index using the ratio of sublethal and lethal toxicity values. Other less commonly conducted subchronic tests include pen-in-field and full-scale field trials *(25)*.

Specific protocols and species for mammalian wildlife toxicity testing have not been established. Potential methods include both 5- and 10-day acute LD_{50} and 10-day subacute LC_{50} tests *(26, 27)*. In the past, data from human health effects research based on studies with common laboratory mammals have been used in an attempt to assess risk to mammalian wildlife. However, no representative species have yet been designated under FIFRA or TSCA. Ringer *(28)* recommended tests with a wild herbivore species (vole, *Microtus pennsylvanicus*), an omnivore (deer mouse, *Peromyscus maniculatus*), and a carnivore. Schafer and Bowles *(17)* have presented acute oral toxicity data for 933 chemicals in deer mice and house mice. When oral LD_{50} and 30-day dietary LC_{50} tests from four microtine species were compared with published values for laboratory rats and mice, Cholakis and coworkers *(26)* concluded that laboratory rodents were generally more sensitive.

However, oral LD_{50} and 5-day sublethal responses simultaneously conducted with laboratory mice (*Mus musculus*), meadow voles, and white-footed mice (*Peromyscus leucopus*) revealed equal sensitivity to the OP insecticide acephate *(29)*. The semi-domesticated mink (*Mustela vison*) may be an ideal carnivore because mink are indigenous to North America, can be propagated in the laboratory, and have a large biological data base *(28, 30)*.

Contaminant interactions

Evaluation of interactive effects of simultaneously applied pesticides and other pollutants occurring in an ecosystem is warranted. Limited testing suggests the occurrence of additivity and occasional synergism and antagonism. Of 13 pairs of chemicals fed to pheasants and quail, two showed moderate synergism, whereas additive effects were noted for others *(31)*. Methylmercury and parathion were synergistic, and DDE pretreatment enhanced parathion toxicity *(32)*. Toxicity of a mixture of aromatic hydrocarbons to mallard embryos was greater than the sum of individual components, indicating moderate synergism *(22)*. Because different agrichemicals may be applied from the same tank mix, there is potential for interactions to occur in the field. The toxic trace elements selenium and arsenic in agricultural drainwater in the western United States affect duckling development and growth, but combina-

tions of the two act antagonistically *(33)*.

Knowledge of specific pesticide formulations and vehicles is important in evaluating toxicity and hazard of agricultural chemicals. For example, granular formulations are often equally or less toxic than active ingredients alone *(18, 19)*. However, the field hazard of granular pesticides is more dependent on the size and feeding behavior of species inhabiting a treated area than on the application rate. Many liquid formulations are more toxic to quail than the active components alone *(34)*.

Embryolethality, teratogenesis, and brain acetylcholinesterase inhibition by OP insecticides applied to mallard eggs was greater with an oil vehicle than with aqueous emulsifiable concentrate *(35)*. This is presumably caused by increased pesticide transfer through the shell and its membranes. Thus, OP insecticides in oil vehicles may pose greater potential field hazard to avian embryos than aqueous emulsifiable concentrates.

Other factors influencing toxicity of xenobiotics to wildlife include naturally occurring stressors (i.e., temperature extremes, nutritional deficits, and disease). A twofold enhancement of parathion toxicity was observed when quail were chronically exposed to heat or cold *(36, 37)*. Similarly, methyl parathion caused 60% mortality in American kestrels (*Falco sparverius*) at −5 °C, but at 22 °C comparable doses caused only sublethal effects *(38)*.

Cold was identified as contributing to the death of about 1500 geese (*Anser anser* and *A. brachyrhynchus*) that fed on carbophenthion-treated winter wheat in the United Kingdom *(39)*, and elevated temperature has been suggested to exacerbate dimethoate toxicity to sage grouse (*Centrocerus urophasianus*) in Idaho *(40)*.

Cold winter weather is thought to increase lead toxicity. There were increased mortality and higher blood and liver lead concentrations in ringed turtle-doves (*Streptopelia risoria*) exposed to 6 °C, compared with birds maintained at 21 °C *(41)*. High temperature can also increase lead toxicity in mammals but appears to have less impact on birds *(42)*. Nutritional deficit enhances lead and selenium toxicity in mallards and black ducks (*Anas rubripes*) *(33, 43, 44)*. Several environmental contaminants including petroleum, lead, selenium, and plant growth regulators can cause immunosuppression in birds and mammals, possibly rendering them more susceptible to disease *(45–46)*.

Bioaccumulation and toxicokinetics

Bioaccumulation of contaminants in food chains with resulting biomagnification in wildlife first became evident when mortality of American robins was linked to DDT in earthworms *(5)*. Experiments on kinetics of pesticide residues indicated that DDT and other persistent organochlorines in the brain could be diagnostically related to lethality *(47, 48)*. Although average concentrations of persistent organochlorine pesticides and PCBs in wildlife have decreased over the past decade, historical and current contamination remain sufficiently high to reduce recruitment and survival in certain wildlife populations *(49)*.

More recent sources of contamination have included heptachlor seed treatment, use of endrin to control cutworms and rodents, DDT contamination from illegal use, and burdens acquired by birds wintering outside of the United States. Several species, particularly predatory birds *(50)* and insectivorous bats *(51)*, continue to be at risk. However, persistent OCs do not universally increase along food chains *(52)*, and the ultimate effect depends on both the species and the chemical.

Bioaccumulation of contaminants in food chains with resulting biomagnification in wildlife first became evident when mortality of American robins was linked to DDT in earthworms.

Similarly, caution must be exercised in interpreting the accumulation of metals; metal contaminants that are biomagnified at low concentrations in ecosystems do not necessarily behave similarly at high concentrations *(53)*. Metabolism, hepatic mixed-function-oxygenase (MFO) inducibility, lipid content, and species growth rate are all important determinants in rate of bioaccumulation.

There are, in general, marked differences in the rate of xenobiotic metabolism by vertebrates: small vertebrates > large vertebrates; omnivores and herbivores > predators; and mammals > birds > fish *(54)*. Bioaccumulation tends to be inversely related to rate of xenobiotic metabolism.

Biomagnification of selenium in aquatic ecosystems has received much attention recently. Selenium is made available for biological uptake through oxidation and methylation. Aquatic plants can bioconcentrate selenium at least 500 times, with additional biomagnification of 2 to 6 times by invertebrates and forage fish. Total bioaccumulation of 30,000 times has been reported in fish chronically exposed to selenium *(55)*.

Accumulation of selenium in water birds seems dependent on its form; selenomethionine readily accumulates in liver, muscle, and eggs, whereas selenite and selenocystine do not *(56)*. In some instances, relatively high body burdens of selenium appear to protect animals from toxic effects of metals (e.g., mercury and cadmium). Additional field and interpretive studies are needed to elucidate protective metal interactions.

Field and ecosystem investigations

Avian die-offs due to OP and CB insecticide exposure vary from small-scale poisonings in barnyards to massive die-offs of colonial breeding birds *(57)*. There are over 100 confirmed reports of wildlife die-offs following pesticide use involving at least 30 different families of birds and a smaller number of mammals *(11, 58)*. Secondary poisoning of predators that consumed prey tainted with OP insecticides also contributes to wildlife mortality *(59)*. These observations no doubt reflect highly visible situations, and there may be a multitude of undetected incidents for every one observed. Although large losses occur, the impact on populations remains uncertain.

Current studies by the U.S. Fish and Wildlife Service and EPA are focusing on sage grouse die-offs associated with increased agricultural applications of OP insecticides. Radiotelemetric monitoring of sage grouse in Idaho revealed that nearly 20% of the monitored birds were seriously affected by OP insecticides *(60)*. Because of their limited migratory range and the ease of tracking, this species may aid in further elucidation of pesticide impacts on population dynamics.

The prairie potholes region of the northern plains provides breeding habitat for at least 50% of North American water fowl. Intensive drainage of prairie wetlands for agriculture has left only 35% of the original area. The potential for agrichemicals to enter the remaining wetlands and affect wildlife is great (Figure 2). The most widely used OP and CB insecticides in the region are highly toxic to aquatic invertebrates and birds. Both bird mortality and loss of invertebrate prey base were greater than expected when ethyl or methyl parathion was aerially applied according to product recommendations *(61, 62)*.

Of the 16 insecticides most widely used in North Dakota in 1984, nine

FIGURE 2
Potential effects of environmental contaminants on survival and reproduction of wild birds[a]

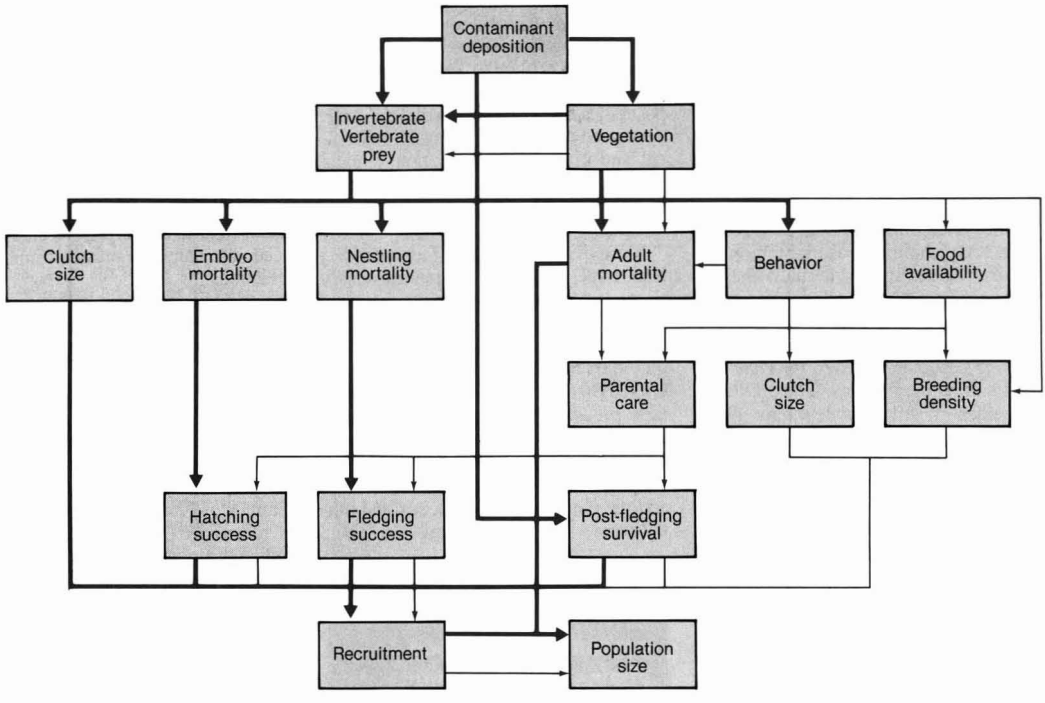

[a]Bold lines indicate direct toxic effects; narrow lines indicate indirect effects. Adapted from Reference 61.

have been implicated elsewhere in wildlife mortality. Thirteen of 16 insecticides most frequently used were highly toxic to aquatic invertebrates and birds *(61, 62)*. Reduced availability of aquatic invertebrate food resources to ducklings and egg-laying hens appeared to decrease water fowl productivity. The spraying of tank mixture combinations of pesticides could further intensify these effects.

Estuaries, including Chesapeake Bay and San Francisco Bay, are complex ecosystems affected by a multitude of pollutants *(63)*. Direct exposure to contaminants and altered habitat may both contribute to wildlife losses. For example, changes in winter abundance and distribution of canvasbacks (*Aythya valisineria*) in Chesapeake Bay have been attributed to loss of submerged aquatic vegetation, formerly a major food resource *(64)*. As a consequence, canvasbacks and other water fowl now feed primarily on invertebrates rather than vegetation. This may result in a combination of nutritional deficits and exposure to greater quantities of contaminants.

Potentially harmful levels of trace elements and organics are found in invertebrates in San Francisco Bay. Reproductive problems including congenital malformations, reduced hatching success, and decreased survival of hatchlings have been observed in colonial water birds nesting there *(65, 66)*.

The Great Lakes Basin of North America comprises a complicated ecosystem that contains 20% of the world's freshwater resources *(67)*. Persistent toxic substances seriously threaten wildlife residing around the Great Lakes *(68)*. Concentrations of certain restricted or banned toxicants (e.g., DDT, dieldrin, heptachlor, and PCBs) in water have declined considerably over the past decade, but biomagnification in fish feeding near sediments containing PCBs, dioxins, and other OCs poses a continuing hazard to wildlife.

Populations of bald eagles, Forster's terns (*Sterna forsteri*), and Caspian terns (*Sterna caspia*) are experiencing reproductive failure; congenital malformations have been reported in terns, gulls, and double-crested cormorants (*Phalacrocorax auritus*) *(69)*. Tissue samples from these birds have among the highest OC burdens in the world *(70–72)*. Correlations between OC concentrations in fish and fish-eating wild mammals are apparent, and PCB concentrations in wild mink around Lake Ontario are similar to those reported to affect reproduction in controlled studies *(29, 73)*.

Tissues of aquatic birds and their eggs collected from irrigation drainage ponds on the Kesterson National Wildlife Refuge in California contained up to 130 ppm (dry wt.) selenium. Embryonic mortality and congenital deformities were associated with selenium concentrations in eggs *(13, 14)*. Of nearly 350 nests examined, 41% had at least one dead embryo and 20% had one or more deformed embryos or chicks. Multiple gross malformations of the eyes, brain, and feet were often present. Concurrent examination of a control population and published records indicated that the incidence of embryonic mortality and deformities was nine to 30 times greater than expected. Some adult birds in the area were emaciated or exhibited hepatic and biochemical lesions *(74)*. Boron concentrations were also high at Kesterson, but not considered the primary

cause of reproductive problems *(75)*. Aquatic bird eggs in other western U.S. sites, including the Tulare Lake Basin in California, exhibit deformities apparently linked to agricultural drainwater.

Biomarkers in risk assessment

Use of biomarkers for documenting injury or damage caused by contaminant exposure has recently gained considerable attention. In addition to mortality and impaired reproduction, several other indicators of xenobiotic-mediated toxicity in wildlife have been identified. Congenital malformations in wild birds have been described in at least three pollution assessments in the Great Lakes, Long Island Sound, and in central California *(13–15)*. Defects including deformed bills, eye malformations, reduced mandibles, and foot deformities have been attributed to halogenated aromatic hydrocarbons, mercury, and selenium.

Eggshell thinning by DDE and other contaminants has been recognized as a biomarker associated with impaired hatching success of wild birds. Thinning is detected by measuring shell thickness directly or by weight per unit of shell area (Ratcliffe index). More recently, measurement of eggshell breaking strength has emerged as a sensitive index of shell fragility *(76, 77)*.

Alterations in biochemical processes can be used to demonstrate exposure and injury from hazardous substances. Measurement of acetylcholinesterase activity, for example, can indicate exposure to OP and CB pesticides. Laboratory and field studies of wild birds and mammals have linked brain acetylcholinesterase inhibition to deleterious effects on reproduction, stress tolerance, and survival *(11, 57)*. Delta-amino levulinic acid dehydratase (ALAD), an enzyme in the biosynthetic pathway of heme, is inhibited by lead. ALAD activity and lead concentration in water fowl blood are inversely related, and studies with raptors have reported reduced hematocrit and hemoglobin concentration accompanying ALAD inhibition *(78, 79)*. ALAD activity has been utilized as a sensitive indicator of lead exposure in free-ranging birds and mammals *(80)*. A quantitative index of lead exposure at concentrations causing nearly complete inhibition of ALAD activity is afforded by measurement of free erythrocyte protoporphyrin *(81, 82)*. Mixed-function oxygenases in avian embryos and hatchlings seem particularly promising as a bioeffect monitor for documenting contaminant exposure *(83)*. Porphyria, the concentration of highly carboxylated porphyrins, has been reported in the livers of adult herring gulls (*Larus argentatus*) in the Great Lakes and may reflect disturbed heme biosynthesis due to polyhalogenated aromatic hydrocarbon exposure *(84)*.

Malformed mallard (Anas platyrhnchos) *duck embryo near hatching from parents that received 10 ppm Se as selenomethionine in the diet. Note hydrocephaly of the brain, micropthalmia of the eyes, reduced mandible, and ectrodactyly.*

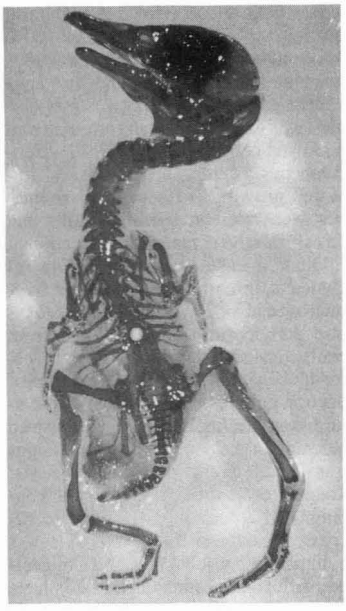

Alizarin-stained skeleton of gadwall (Anas strepera) *duck embryo near hatching from Kesterson Reservoir. Note reduced mandible and ectrodactyly. Malformations were associated with agricultural drainwater containing high selenium concentrations.*

Contaminant-induced behavioral aberrations in wildlife may occur well below lethal exposure levels and provide a sensitive indicator of toxic response. In the laboratory, subtle alterations in behavior have been associated with exposure to hazardous substances *(85)*. Peakall reviewed behavioral responses of birds to pesticides and other contaminants and concluded that certain operant tests are promising due to simplicity and reproducibility, but that more complex tests, such as breeding behavior and prey capture, should also be considered as relevant indices of survival in the wild *(86)*.

Confounding interactive factors, such as weather, should not preclude attempts to evaluate wildlife behavior in the field. Studies have been conducted on behavioral aberrations in wild birds exposed to acetylcholinesterase-inhibiting insecticides *(87)* and OCs *(88)* where decreased nest attentiveness depressed reproduction.

Integrated approaches

Field, laboratory, and mesocosm approaches have been successfully utilized to address wildlife risk assessments such as acid precipitation, persistent OCs in the Great Lakes, and irrigation drainwater in the western United States.

Acid precipitation in eastern North America has altered freshwater ecosystems essential for breeding water fowl. Survival, growth, and physiological condition were monitored in black duck ducklings in mesocosms where fish-free emergent wetlands were experimentally acidified to pH 5.0 *(89, 90)*. Acidification markedly reduced phytoplankton and algal growth and invertebrate biomass. Survival and growth of broods of ducklings maintained on the acidified ponds were reduced and alterations in metabolism and development were apparent. Broods on acidified wetlands exhibited increased distress behavior and spent more time seeking food, possibly rendering them at greater risk to predation in nature.

Reproductive failure and anomalies in fish-eating colonial birds on the Great Lakes have caused concern, owing to the presence of persistent OCs. Field observations have attributed low reproductive success to direct toxicity of contaminants present in eggs and indirectly to aberrant parental behavior caused by contaminants, resulting in poor incubation and care of nestlings. To determine the extent of direct chemical toxicity, studies were conducted in which eggs from "clean" and contaminated colonies were artificially incubated.

Hatching success for Lake Ontario herring gulls in the 1970s was 60% lower than controls *(91)*. In the 1980s hatching success for Forster's tern eggs collected from Green Bay, Lake Michigan, was 48% lower than for eggs from an inland control colony *(69, 92)*. Subcutaneous edema, hepatomegaly, impaired growth, and congenital anomalies were seen in hatchling gulls and terns from the contaminated locations.

Other manifestations of toxicity included a three-fold elevation of liver microsomal aryl hydrocarbon hydroxylase activity in tern hatchlings from contaminated colonies. Abnormal parental behavior also depressed reproduction in gulls and terns; this observation was confirmed by the improved hatching success of contaminated eggs transferred to "clean" colony nests. Transfer of control colony eggs to contaminated colony nests resulted in decreased hatching success *(69, 93)*.

Impaired reproduction and congenital malformations in aquatic birds have been associated with trace elements in agricultural drainwater. Studies with mallards were conducted to predict potential hazard for other sites based on concentrations of selenium, boron, and arsenic in food items and bird eggs. Selenium was the primary causative agent and selenomethionine was particularly teratogenic, presumably because of its enhanced accumulation in eggs *(56, 94)*. Using logistic regression, the statistical relationship between hatching success and selenium concentrations in sample eggs from wild aquatic birds yielded a threshold similar to that observed in controlled studies *(95)*.

Future directions

Public resistance to large-scale animal testing may preclude generation of data bases on lethal toxicity as large as previous ones. This challenges toxicologists and statisticians to develop effective methods of predicting hazards to wildlife using minimum numbers of animal subjects. Similarly, it is necessary to determine the degree to which extensive data bases developed on a few species serve to assess hazard to the broad array of taxa at risk. Amphibians and reptiles, for example, are extremely diverse groups about which little is known; whether they are adequately protected by regulations based on avian and mammalian species remains to be determined.

Increased use of innovative techniques to better control and monitor field experimentation and to determine limitations of extrapolation of laboratory and pen studies to nature is needed. Every local wildlife population at risk is unique with respect to blend of contaminants, likely duration of exposure, and other interactive factors such as seasonal food availability and predator–prey relationships.

Construction of mesocosms, such as experimental wetlands, to simulate brood habitat for ducks can be used for risk assessments. Food abundance can be manipulated in wetland mesocosms by maintaining them fish-free, in order to maximize invertebrate availability as occurs in seasonal wetlands that are highly attractive to water fowl. The impact of pesticide application can be more precisely assessed in carefully controlled spray operations with respect to application rate and time and frequency of spraying. Radiotelemetry of exposed individuals can yield better information on individual movements and survival, leading to better inferences on population effects.

Hall *(4)* concluded that further studies are needed to address interactive factors. Although most combinations of xenobiotics may be additive, one synergistic combination could have far-reaching effects on wildlife populations. For example, spraying OP insecticide and fungicide combinations in orchards was reported to be highly toxic to dove eggs *(96)*. Whether this phenomenon can be attributed to synergistic effects of two pesticides or is caused in part by species sensitivity is uncertain. Further studies are needed to test possible interactions of chemicals and effects of natural stressors.

Analytical chemistry has traditionally been employed to detect contaminants in the environment and in wildlife tissues. However, increasing costs have made certain applications nearly prohibitive. One suggested strategy for detecting biologically active chemicals in environmental samples involves screening samples with a bioassay system before the commitment is made for costly analytical chemistry. Bioassay systems utilizing microorganisms, plants, or vertebrate embryos have been tested or are under development. These may be particularly helpful in the analysis of hazardous-waste sites, where complex mixtures of harmful chemicals may be separated by solvent extraction and fractions may be used in bioassays.

Use of more sensitive and expedient biomarkers is crucial to effective monitoring when contaminants and other ecological factors come into play. Better understanding of the relationship between biomarkers and impending biological damage is needed. Immunological quantification of cytochrome P450 isozymes, utilized in mammalian and aquatic toxicological studies, is being adapted to avian species. Increased automation of micromethods will permit rapid and precise evaluations of microsomal MFO activities in embryonic and other tissues of limited quantity.

Oxyradical-mediated responses for biomonitoring have been useful in aquatic toxicology because there are probably more xenobiotics occurring in contaminant mixtures that are "redox-active" than in mixtures that are "MFO-inducers" *(97)*. Preliminary studies on wildlife have afforded a similar conclusion. Other promising biomarkers for wildlife risk assessments include measurements of immunotoxicity and genotoxicity.

Ultimately, better predictability at the population level is needed. Models that combine multiple impact assessment on wildlife populations for contaminant effects, hunting and predation, and habitat disturbance may help to address this issue.

Acknowledgment

We thank Dr. Ronald Eisler, Dr. Gary Heinz, and Ms. Paula Henry for reviewing this manuscript.

References

(1) Newman, J. R. *Biological Conservation* **1979,** *15,* 181–90.
(2) Forbes, R. M.; Sanderson, G. C. In *The Biogeochemistry of Lead in the Environment,* Part B; Nriagu, J. O., Ed.; Elsevier North-Holland Biomedical Press: Amsterdam, 1978, pp. 238–60.
(3) Stickel, L. F. *J. Wildl. Manage.* **1946,** *10,* 216–18.
(4) Hall, R. J. In *Silent Spring Revisited;* Marcu, G. J.; Hollingworth, R. M.; Durham, W., Eds.; American Chemical Society: Washington, DC, 1987, pp. 85–111.
(5) Carson, R. *Silent Spring;* Houghton Mifflin: Boston, 1962; pp. 103–127.
(6) De Witt, J. B. *Agric. Food Chem.* **1955,** *3,* 672–76.
(7) Ratcliffe, D. A. *Nature* **1967,** *215,* 208–10.
(8) Hickey, J. J.; Anderson, D. W. *Science* **1968,** *162,* 271–73.
(9) Wiemeyer, S. N.; Porter, R. D. *Nature* **1970,** *227,* 737–38.
(10) Blus, L. J.; Belisle, A. A.; Prouty, R. M. *Pestic. Monit. J.* **1974,** *7,* 181–94.
(11) Grue, C. E. et al. *Trans. North Am. Wildl. Nat. Resour. Conf.* **1983,** *48,* 200–220.
(12) Hardy, A. R.; Stanley, P. I. In *Agriculture and the Environment;* Jenkins, D., Ed.; Institute of Territorial Ecology: Cambridge, 1984, pp. 72–80.
(13) Ohlendorf, H. M. et al. *Sci. Total Environ.* **1986,** *52,* 49–63.
(14) Hoffman, D. J.; Ohlendorf, H. M.; Aldrich, T. W. *Arch. Environ. Contam. Toxicol.* **1988,** *17,* 519–25.
(15) Hill, E. F.; Hoffman, D. J. *J. Am. Coll. Toxicol.* **1984,** *3,* 357–76.
(16) Hudson, R. H.; Tucker, R. K.; Haegele, M. A. U.S. Fish and Wildlife Service Resour. Publ. 153. U.S. Department of the Interior: Washington, DC, 1984.
(17) Schafer, E. W.; Bowles, W. A., Jr. *Arch. Environ. Contam. Toxicol.* **1985,** *14,* 111–29.
(18) Balcomb, R. *J. Wildl. Manage.* **1984,** *48,* 1353–59.
(19) Hill, E. F.; Camardese, M. B. *Ecotoxicol. Environ. Saf.* **1984,** *8,* 551–63.
(20) Hill, E. F. et al. U.S. Fish and Wildlife Service Special Scientific Report: Wildlife No. 191; U.S. Government Printing Office: Washington, DC, 1975.
(21) Hill, E. F.; Camardese, M. B. U.S. Fish

and Wildlife Service: Fish and Wildlife Service Technical Report 2; U.S. Government Printing Office: Washington, DC, 1986.
(22) Hoffman, D. J.; Albers, P. H. *Arch. Environ. Contam. Toxicol.* **1984,** *13,* 15-27.
(23) Hoffman, D. J. *Rev. Environ. Contam. Toxicol.* (in press).
(24) White, D. H.; Finley, M. T. *Environ. Res.* **1978,** *17,* 53-59.
(25) Tucker, R. K.; Leitzke, J. S. *Pharmacol. Ther.* **1979,** *6,* 167-220.
(26) Cholakis, J. M. et al. In *Avian and Mammalian Wildlife Toxicology: Second Conference;* STP 757; Lamb, D.W.; Kenaga, E.E., Eds.; American Society for Testing Materials: Philadelphia, PA, pp. 143-54.
(27) Linder, G. *Abstracts of Papers,* Ninth Annual Meeting of the Society of Environmental Toxicology and Chemistry, Arlington, VA; Society of Environmental Toxicology and Chemistry: Washington, DC, 1988; p. 44.
(28) Ringer, R. K. *Environ. Toxicol. Chem.* **1988,** *7,* 339-42.
(29) Rattner, B. A.; Hoffman, D. J. *Arch. Environ. Contam. Toxicol.* **1984,** *13,* 483-91.
(30) Aulerich. R. J.; Ringer, R. K. *Arch. Environ. Contam. Toxicol.* **1977,** *6,* 279-92.
(31) Kreitzer, J. F.; Spann, J. W. *Bull. Environ. Contam. Toxicol.* **1973,** *9,* 250-56.
(32) Ludke, J. L. *Bull. Environ. Contam. Toxicol.* **1976,** *16,* 253-60.
(33) Hoffman, D. J. *Abstracts of Papers,* Tenth Annual Meeting of the Society of Toxicology and Chemistry, Toronto, Ontario, Canada; Society of Environmental Toxicology and Chemistry: Washington, DC, 1988, p. 79.
(34) Hill, E. F. U.S. Fish and Wildlife Service Research Information Bulletin No. 686; U.S. Fish and Wildlife Service: Washington, DC, 1986.
(35) Hoffman, D. J.; Eastin, W. C., Jr. *Environ. Res.* **1981,** *26,* 472-85.
(36) Rattner, B. A.; Sileo, L.; Scanes, C. G. *Pestic. Biochem. Physiol.* **1982,** *18,* 132-38.
(37) Rattner, B. A.; Becker, J. M.; Nakatsugawa, T. *Pestic. Biochem. Physiol.* **1987,** *27,* 330-39.
(38) Rattner, B. A.; Franson, J. C. *Can. J. Physiol. Pharmacol.* **1984,** *62,* 787-92.
(39) Stanley, P. I.; Bunyan, P. J. *Proc. R. Soc. London, B* **1979,** *205,* 31-45.
(40) Blus, L. J. et al. *J. Wildl. Manage.* **1989,** *53,* 1139-46.
(41) Kendall, R. J.; Scanlon, P. F. *J. Environ. Pathol. Toxicol. Oncol.* **1984,** 183-92.
(42) Srebocan, E.; Rattner, B. A. *Bull. Environ. Contam. Toxicol.* **1988,** *40,* 165-69.
(43) Finley, M. T.; Dieter, M. P. *J. Wildl. Manage.* **1978,** *42,* 32-39.
(44) Pain, D. J.; Rattner, B. A. *Bull. Environ. Contam. Toxicol.* **1988,** *40,* 159-64.
(45) Franson, J. C. In *Lead Poisoning in Wild Waterfowl—A Workshop;* Feierabend, J. S.; Russell, A. B., Eds.; National Wildlife Federation: Washington, DC, 1986, pp. 106-9.
(46) Fairbrother, A.; Yuill, T. M.; Olson, L. J. *Arch. Environ. Contam. Toxicol.* **1986,** *15,* 265-75.
(47) Bernard, R. F. *Publ. Mus. Mich. State Univ., Biol. Ser.* **1963,** *2,* 155- 92.
(48) Stickel, L. F. In *Environmental Pollution in Pesticides;* Edwards, C. A. Ed.; Plenum Press: London, 1973, pp. 254-312.
(49) Fleming, W. J.; Clark, D. R.,Jr.; Henny, C. J. *Trans. North Am. Wildl. Nat. Resour. Conf.* **1983,** *48,* 186-99.
(50) Henny, C. J.; Blus, L. J.; Stafford, C. J. *J. Wildl. Manage.* **1983,** *47,* 1080-87.
(51) Clark, D. R., Jr.; LaVal, R. K.; Krynitsky, A. J. *Pestic. Monit. J.* **1980,** *13,* 137-40.
(52) Moriarty, F.; Walker, C. H. *Ecotoxicol. Environ. Safety* **1987,** *13,* 208-15.
(53) Beyer, W. N. *Environ. Toxicol. Chem.* **1986,** *5,* 863-64.
(54) Walker, C. H. *Prog. Drug Metab.* **1980,** *5,* 113-65.
(55) Lemly, A. D.; Smith, G. J. U.S. Fish and Wildlife Leaflet 12; National Technical Information Service: Springfield, VA, 1987.
(56) Heinz, G. H. et al. *Environ. Toxicol. Chem.* **1987,** *6,* 423-33.
(57) Hill, E. F.; Fleming, W. J. *Environ. Toxicol. Chem.* **1982,** *1,* 27-38.
(58) Stone, W. B. *N.Y. Fish Game J.* **1979,** *26,* 37-47.
(59) Henny, C. J. et al. *J. Wildl. Manage.* **1985,** *49,* 648-58.
(60) Blus, L. J. et al. *J. Wildl. Manage.* **1989,** *53,* in press.
(61) Grue, C. E. et al. *Trans. North Am. Wildl. Nat. Resour. Conf.* **1986,** *51,* 357-83.
(62) Grue, C. E. et al. U.S. Fish and Wildlife Service Biological Report 88 (16); U.S. Government Printing Office: Washington, DC, 1988.
(63) Ohlendorf H. M.; Fleming, W. J. *Mar. Pollut. Bull.* **1988,** *19,* 487-95.
(64) Perry, M. C.; Uhler, F. M. *Estuaries* **1988,** *11,* 57-67.
(65) Hoffman, D. J. et al. *J. Toxicol. Environ. Health* **1986,** *19,* 383-91.
(66) Ohlendorf, H. M. et al. *Colonial Waterbirds* **1988,** *11,* 85-94.
(67) Fox, G. A.; Weseloh, D. V. In *The Value of Birds;* ICBP Technical Publication No. 6; Diamond, A.W.; Fillion, F., Eds; Page Brothers: Norfolk, England, 1987; pp. 209-16.
(68) Gilbertson, M. In *Toxic Contaminants and Ecosystem Health: A Great Lakes Focus;* Evans, M. S., Ed.; Wiley: New York, 1988; pp. 133-52.
(69) Kubiak, T. J. et al. *Arch. Environ. Contam. Toxicol.* **1989,** *18,* 706-27.
(70) Haseltine, S. D. et al. *Pestic. Monit. J.* **1981,** *15,* 90-97.
(71) Heinz, G. H. et al. *Environ. Monit. Assess.* **1985,** *5,* 223-36.
(72) Mineau, P. et al. In *Toxic Contaminants in the Great Lakes, Advances in Environmental Sciences and Technology;* Nriagu, J.O.; Simmons, M. S., Eds.; Wiley: New York, 1984; pp. 425-52.
(73) Foley, R. E. et al. *Environ. Toxicol. Chem.* **1988,** *7,* 363-74.
(74) Ohlendorf, H. M. et al. *J. Toxicol. Environ. Health* **1988,** *24,* 67-92.
(75) Smith, C. J.; Anders, V. P. *Environ. Toxicol. Chem.* **1989,** *8,* 943-50.
(76) Carlisle, J. C.; Lamb, D. W.; Toll, P. A. *Environ. Toxicol. Chem.* **1986,** *5,* 887-89.
(77) Bennett, J. K. et al. *Environ. Toxicol. Chem.* **1988,** *7,* 351-57.
(78) Dieter, M. P.; Finely, M. T. *Environ. Res.* **1979,** *19,* 127-35.
(79) Hoffman, D. J. et al. *Comp. Biochem. Physiol.* **1985,** *80C,* 431-39.
(80) Beyer, W. N. et al. *Environ. Poll. Ser. A.* **1985,** *38,* 63-86.
(81) Roscoe, D. E. et al. *J. Wildl. Dis.* **1979,** *15,* 127-36.
(82) Scheuhammer, A. M. *Environ. Poll.* **1987,** *46,* 263-95.
(83) Rattner, B. A.; Hoffman, D. J.; Marn, C. M. *Environ. Toxicol. Chem.* **1989,** *8,* 1093-1102.
(84) Fox, G. A. et al. *Environ. Toxicol. Chem.* **1988,** *7,* 831-39.
(85) Heinz, G. H. *J. Wildl. Manage.* **1979,** *43,* 394-401.
(86) Peakall, D. B. *Residue Rev.* **1985,** *96,* 45-47.
(87) White, D. H.; Mitchell, C. A.; Hill, E. F. *Bull. Environ. Contam. Toxicol.* **1983,** *31,* 93-97.
(88) Fox, G. A. et al. *J. Wildl. Manage.* **1978,** *42,* 477-83.
(89) Haramis, G. M.; Chu, D. S. In *The Value of Birds;* ICBP Technical Publication No. 6. Diamond, A. W.; Fillion, F., Eds.; Page Brothers Ltd.: Norfolk, England, 1987; pp. 173-81.
(90) Rattner, B. A. et al. *Can. J. Zool.* **1987,** *65,* 2953-958.
(91) Gilbertson, M.; Fox, G. A. *Environ. Pollut.* **1977,** *12,* 211-16.
(92) Hoffman, D. J. et al. *Environ. Res.* **1987,** *42,* 176-84.
(93) Peakall, D. B. et al. *Environ. Sci. Res. Ser.* **1978,** *16,* 337-44.
(94) Hoffman, D. J.; Heinz, G. H. *J. Toxicol. Environ. Health* **1988,** *24,* 477-90.
(95) Ohlendorf, H. M. et al. *Trans. N. Am. Wildl. Nat. Resour. Conf.* **1986,** *51,* 330-42.
(96) Putera, J. A.; Woolf, A.; Klimstra, W. D. *Wildl. Soc. Bull.* **1985,** *13,* 496-501.
(97) DiGiulio, R. T. et al. *Environ. Toxicol. Chem.* **1989,** *8,* 1103-23.

David J. Hoffman *is a research physiologist in the Environmental Contaminants Research Branch of the Patuxent Wildlife Research Center. He has a Ph.D. in developmental zoology from the University of Maryland and received post-doctoral training in molecular biology as an NIH post-doctoral fellow at Oak Ridge National Laboratory. For the past 10 years, his research has focused on developmental toxicology, including morphological and biochemical effects of environmental contaminants on wildlife.*

Barnett A. Rattner *(l) is deputy chief of the Environmental Contaminants Research Branch of the Patuxent Wildlife Research Center. He has a Ph.D. in zoology from the University of Maryland and received post-doctoral training at the Naval Medical Research Institute and the National Institutes of Health. For the past 10 years his research has focused on comparative toxicology and the biochemical and physiological effects of pollutants on wildlife.*

Russell J. Hall *(r) recently became staff biologist in the Washington office of the U.S. Fish and Wildlife Service after having served in various research and management positions for over 10 years at the Patuxent Wildlife Research Center. He has a Ph.D. in zoology from the University of Kansas. His research in wildlife and conservation has included studies of the effects of environmental contaminants on amphibians, reptiles, and other vertebrates.*

ES&T
CRITICAL REVIEW

Determining chemical toxicity to aquatic species

The use of QSARs and surrogate organisms

Diane J. W. Blum
Bala Cynwyd, PA 19004

R. E. Speece
Vanderbilt University
Nashville, TN 37235

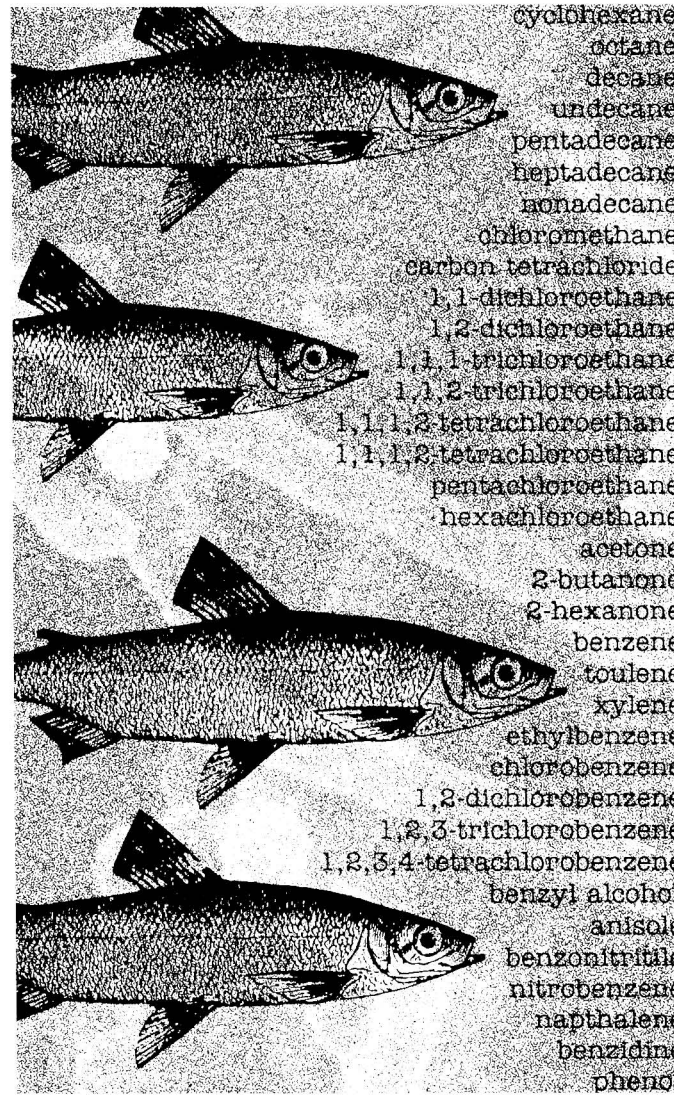

In the past, the major concern in municipal and industrial wastewater treatment was reducing oxygen-consuming pollutants. Currently, health concerns, particularly toxicity, are being superimposed on the objectives of wastewater treatment. The quantity of toxicants finding their way into the aquatic environment is alarming.

The wastewater treatment systems we have spent billions of dollars to construct are being called upon to handle many of these toxicants. Yet often we do not even know the effects of the toxicants. Will they be removed in the treatment system? Will they cause the biological treatment processes to fail? What effect will they have on bacteria and other aquatic species when they are discharged into the environment? Basic information needed to understand the toxic nature of chemicals and effectively regulate their use is sparse.

To handle and treat wastes effectively, we must know the degree of toxicity of the chemicals they contain. Worldwatch Institute estimates that there are 70,000 synthetic chemicals in everyday use, with between 500 and 1000 new ones added to the list each year. But for approximately 79% of the chemicals in commerce, no information on their toxic effects is available, reports Worldwatch *(1)*.

Clearly, we have huge gaps to fill in our data base, and this means large expenditures of money and time to test the toxicity of chemicals to species of concern.

Because there are a multitude of toxic compounds that can be present in

0013-936X/90/0924-0284$02.50/0

wastewater and a multitude of living organisms that can be affected by the treated wastewater discharge, tools for the efficient development of toxicity data must be found. Two such techniques are Quantitative Structure–Activity Relationships (QSARs) and the use of surrogate testing organisms. This article describes these two techniques and their potential for helping to find data on the toxicity of chemicals to species in the aquatic environment. QSARs correlate and predict the toxic properties of chemicals from physical and chemical descriptors. Surrogate testing organisms are used to estimate the response of an organism or an ecosystem to toxicants. We focus on four bacteria and a fish species, comparing and correlating their response to toxicants, in order to estimate their potential to act as surrogates for one another.

Our research

We tested or collected data for the toxicity of a broad range of chemicals including substituted benzenes, substituted phenols, chlorinated aliphatic hydrocarbons, and alcohols. Each of the chemicals was tested individually. Although most toxic wastes include a combination of toxicants, evaluating individual constituents is a first step in assessing the toxicity of a mixture.

We collected laboratory data for three groups of bacteria of central interest in the natural environment and in wastewater treatment systems: aerobic heterotrophs, *Nitrosomonas*, and methanogens. Aerobic heterotrophs predominate in activated sludge systems and natural aerobic environments, converting organic material to carbon dioxide and water. *Nitrosomonas* convert ammonia nitrogen to nitrite as the first and more sensitive step in the biological oxidation of inorganic nitrogen. Methanogens are a key organism in the conversion of organic matter to carbon dioxide and methane in anaerobic environments. Data were also collected from the literature for the fathead minnow and the Microtox test. We collected toxicity data for 50–130 chemicals per species to compare the toxicity of the same chemicals to five organisms. We then used the data to develop QSARs and interspecies correlations for nonreactive toxicants. (See Table 1 for a list of chemicals considered.)

We found highly successful QSARs covering a broad range of chemical toxicants for all species tested. Our work identifies the advantages and disadvantages of three QSAR methods: octanol–water partitioning (log P), linear solvation energy relationships (LSERs), and molecular connectivity. LSER QSARs were most accurate and covered the greatest range of chemicals. Parameters are more readily available for log P and molecular connectivity QSARs. Molecular connectivity indices can be computed with no knowledge of chemical properties, simply from structural formulas. It is therefore easy to see how changes in structure affect predicted toxicity. However, log P and LSER QSARs afford a more intuitive understanding of the properties affecting toxicity.

Our QSARs are valuable to practicing engineers for predicting the toxicity of untested chemicals to the species considered, provided the chemicals are related to our test chemicals. The QSAR equations can be interpreted to find clues about the relationship between toxicity and chemical structure.

We also found many successful correlations between the toxicity to different species that illustrate the potential savings gained by using surrogate organisms in this manner. Microtox results can be obtained in as little as five minutes, once the chemical dilutions and other solutions are made. In addition, because the test is easily reproducible, the results available in the literature can be drawn upon with fair confidence. Obviously, where Microtox testing can substitute for or even provide a first estimate of toxicity to other species, a huge savings in time and money can be realized. Our research found that toxicity to other environmental bacteria can be correlated with each other and with fish. Methods for testing environmental bacteria, typically based on measures of activity such as respiration, take several hours to a few days to yield results and require little expenditure for materials.

This paper will discuss the role of QSARs and interspecies correlations in extracting the greatest quantity of information possible from toxicity tests. We draw illustrations from our research as well as that of others. (Details of our research are found in Reference 2; findings from the research are used here.) The methods we used are not unique. However, the use of three common QSAR methods for one extensive data set allows a good overview of the pros and cons of the methods.

QSARs and surrogate testing organisms are methods first developed in the area of pharmacology. They have more recently been applied to aquatic toxicology. Our work takes the methods a step further, applying the ideas to bacteria of environmental interest. The equations developed can be used by practicing engineers for estimating the toxicity of a chemical to key environmental bacteria based on its structure or toxicity to a surrogate testing organism.

Structure–activity relationships

A QSAR is a mathematical relationship between a property (activity) of a chemical, in this case toxicity, and a number of descriptors of the chemical. The descriptors are chemical or physical characteristics obtained experimentally or from the structure of the chemical. First, a training set of toxicity data is used to statistically establish the mathematical relationship between chemical toxicity and the descriptors. The QSAR can then be used to predict the toxicity of untested chemicals for which the descriptors are known. In this way, the easily calculated or measured descriptors of a chemical can be used with a QSAR equation to estimate its toxicity.

Quantitative Structure–Activity Relationships (QSARs) can predict what change in toxicity would be accompanied by a given change in structure.

One criticism often lodged against correlations such as QSARs is that they are not based on a fundamental understanding of the mechanisms of toxicity. They provide quick answers but not basic understanding. It is the greater understanding of toxicity mechanisms that can ultimately answer many of our toxicity questions. However, in the short run, we still need some guidance. And in fact QSARs used in conjunction with more fundamental research may serve both needs.

A high-quality QSAR, although it cannot prove any causal relationships between chemical structure and toxicity, can indicate useful areas of research into such relationships. Clues can be discovered in the types of parameters found to be significant in correlations with toxicity. QSARs can predict what change in toxicity would be accompanied by a given change in structure. Chemicals found to be outliers from a QSAR may have a different toxicity mechanism than the other compounds that is worth investigating. In these ways, if QSARs are used in conjunction with more fundamental toxicity research, both the need for more toxicity data and the long-term search for a fundamental understanding of toxicity can be served.

Many people are skeptical of statisti-

cal correlations because of the sometimes specious use of statistics. Some skepticism is warranted. It is important to critically evaluate the methods used in deriving a statistical relationship. For instance, for multiple linear regressions often used in QSARs, one must be sure that the observation-to-parameter ratio is not too low. Studies should be done to validate the relationship either statistically or with additional independent data. A clear and compelling rationale must be given to justify the omission of any outlying data points. Finally, remember that statistical correlations are not models and do not prove a causal relationship.

History of QSARs

Although recognition of the relationship between chemical structure and activity began long ago, the use of formal structure–activity relationships started with the pioneering work of Hammett in the 1930s, Taft in the 1950s, and Hansch in the 1960s. QSAR methodology was developed and has been used most extensively in the areas of drug and pesticide research. In the 1970s, spurred by the burgeoning number of chemicals being released to the environment, QSAR methodology began to be applied to environmental toxicology.

The primary focus in the area of environmental toxicology has been bioconcentration and toxic effects on fish and other aquatic life. Some work has been done in relating chemical structure characteristics to toxicity in bacteria of environmental interest without deriving mathematical relationships *(3)*. However, few studies have applied QSAR methodology to mathematically model these relationships in environmental microbiology. Our work takes the methods a step further, applying them to bacteria of environmental interest.

Nonreactive toxicity

When considering toxicity QSARs, it is vital to differentiate the types of toxicity. QSARs developed to describe one mode of toxicity cannot be expected to predict the toxicity of a chemical acting by a different mechanism. As pointed out by Veith et al. *(4)* and Lipnick *(5)*, predicting the mode of action of a chemical can be difficult, and this uncertainty increases the potential for the erroneous use of QSAR equations.

The most fundamental differentiation is between reactive and nonreactive toxicity. (Reactive toxicity is also called specific toxicity. Nonreactive toxicity is also called nonspecific toxicity or narcosis.) Reactive toxicity is that which is associated with a specific reactive mechanism such as a chemical reaction with an enzyme or inhibition of a meta-

TABLE 1
Chemicals considered in Blum and Speece research

	Chemical class	Toxicant	Priority pollutants
Aliphatics	Alkanes	cyclohexane	
		octane	
		decane	
		undecane	
		dodecane	
		pentadecane	
		heptadecane	
		nonadecane	
	Chlorinated alkanes	chloromethane	X
		methylene chloride	X
		chloroform	X
		carbon tetrachloride	X
		1,1-dichloroethane	X
		1,2-dichloroethane	X
		1,1,1-trichloroethane	X
		1,1,2-trichloroethane	X
		1,1,1,2-tetrachloroethane	X
		1,1,2,2-tetrachloroethane	X
		pentachloroethane	X
		hexachloroethane	X
		1-chloropropane	
		2-chloropropane	
		1,2-dichloropropane	X
		1,3-dichloropropane	X
		1,2,3-trichloropropane	
		1-chlorobutane	
		1,2-dichlorobutane	
		1,2,3,4-tetrachlorobutane	
		1-chloropentane	
		1,5-dichloropentane	
		1-chlorohexane	
		1-chlorooctane	
		1-chlorodecane	
		1,2-dichloro-2-methylpropane	
		1-chloro-2,2-dimethylpropane	
		bromomethane	X
		bromodichloromethane	X
		1,1,2-trichlorotrifluoroethane	
	Chlorinated alkenes and alkynes	1,1-dichloroethylene	
		1,2-dichloroethylene	X
		cis-1,2-dichloroethylene	X
		trans-1,2-dichloroethylene	X
		trichloroethylene	X
		tetrachloroethylene	X
		1-chloro-2-methylpropene	
		1,3-dichloropropene	X
		3-chloropropyne	
		5-chloro-1-pentyne	
	Alcohols	methanol	
		ethanol	
		1-propanol	
		1-butanol	
		1-pentanol	
		1-hexanol	
		1-octanol	
		1-decanol	
		1-dodecanol	
	Chlorinated alcohols	2,2-dichloroethanol	
		2,2,2-trichloroethanol	
		3-chloro-1,2-propanediol	
	Ethers	ethylether	
		isopropylether	
	Ketones	acetone	
		2-butanone	
		2-hexanone	
		4-methyl-2-pentanone	
		1,4-benzoquinone	
	Carboxylic acid esters	ethyl trichloroacetate	
	Acrylates	ethyl acrylate	
		butyl acrylate	
		octyl acrylate	
	Carbonic acids	2-chloropropionic acid	
		trichloroacetic acid	
	Amines	diethanolamine	
		1-methylpyrrolidine	
	Nitriles	acetonitrile	
		2-methylpropionitrile	
		acrylonitrile	X

	Chemical class	Toxicant	Priority pollutants
	Amides	*N,N'*-dimethyl acetamide	
	Sulfides and sulfoxides	carbon disulfide dimethyl sulfoxide	
Aromatics	Benzene and alkyl benzenes	benzene	X
		toluene	X
		xylene	
		ethylbenzene	X
	Chlorinated benzenes	chlorobenzene	X
		1,2-dichlorobenzene	X
		1,3-dichlorobenzene	X
		1,4-dichlorobenzene	X
		1,2,3-trichlorobenzene	X
		1,2,4-trichlorobenzene	X
		1,3,5-trichlorobenzene	X
		1,2,3,4-tetrachlorobenzene	X
		1,2,3,5-tetrachlorobenzene	X
		1,2,4,5-tetrachlorobenzene	X
		hexachlorobenzene	X
		2-chlorotoluene	X
		2-chloro-*p*-xylene	X
	Alcohols	benzyl alcohol	
	Methoxy benzenes	anisole 4-chloroanisole	
	Aldehydes	2-furaldehyde	
	Nitriles	benzonitrile *m*-tolunitrile	
	Nitros	nitrobenzene	X
		2,6-dinitrotoluene	X
		pentachloronitrobenzene	
		4-nitroaniline	
		1-nitronapthalene	
	Other cyclics	naphthalene	X
		phenanthrene	X
		benzidine	
	Hetero atom cyclics	pyridine quinoline	
	Phenol and misc. substituted phenols	phenol	X
		m-cresol	
		p-cresol	
		2,4-dimethylphenol	X
		3-ethylphenol	
		4-ethylphenol	
		catechol	
		resorcinol	
		hydroquinone	
		2-aminophenol	
		4-aminophenol	
		2-nitrophenol	X
		3-nitrophenol	X
		4-nitrophenol	X
		2,4-dinitrophenol	X
	Halogenated phenols	2-chlorophenol	X
		3-chlorophenol	X
		4-chlorophenol	X
		2,3-dichlorophenol	X
		2,4-dichlorophenol	X
		2,5-dichlorophenol	X
		2,6-dichlorophenol	X
		3,4-dichlorophenol	X
		3,5-dichlorophenol	X
		2,3,4-trichlorophenol	X
		2,3,5-trichlorophenol	X
		2,3,6-trichlorophenol	X
		2,4,5-trichlorophenol	X
		2,4,6-trichlorophenol	X
		2,3,5,6-tetrachlorophenol	X
		pentachlorophenol	X
		2-bromophenol	
		3-bromophenol	
		4-bromophenol	
		2,6-dibromophenol	
		2,4,6-tribromophenol	
		pentabromophenol	

bolic pathway. Nonreactive toxicity, in contrast, is not associated with a specific mechanism but rather is related directly to the quantity of toxicant acting upon the cell.

Hence, the toxic mechanisms of reactive toxicants are extremely dependent on their specific structures, whereas a large array of differing chemicals can act as nonreactive toxicants. This latter group includes chlorinated hydrocarbons, alcohols, ethers, ketones, weak acids, weak bases, and aliphatic nitro-compounds *(6)*. Nonreactive toxicity can be considered to be a baseline toxicity; a chemical can have greater but not lesser toxicity than that attributable to nonreactive toxicity *(5)*.

A theoretical explanation for nonreactive toxicity was first developed by E. Overton and H. Meyer in the late 19th century. Their theory relates the toxicity of a nonreactive chemical to its solubility in lipids. Depressant effects increase with rising partition coefficient between a lipid and water.

Ferguson extended this theory in the 1940s and 1950s by applying the concept of thermodynamic activity. In an aqueous environment in which there is an equilibrium between the water and the biophase, the physiologic effect of a chemical can be related to its activity in the aqueous phase. This activity can be estimated as the ratio of toxicant concentration to its saturation concentration. Thus, as aqueous solubility increases, the concentration of toxicant required to produce a given biological effect increases.

This relationship is not absolute. Within a congeneric series of chemicals, as solubility decreases, one reaches a limit (sometimes called the Ferguson cut-off) such that a very insoluble chemical is not toxic even at saturation. For instance, Veith et al. found that the relationship between toxicity to fish and saturation concentration was linear for alkyl alcohols up to decanol but became nonlinear above decanol *(4)*. Tridecanol produced no mortality even at its solubility limit. Abernathy et al. developed QSARs based on aqueous solubility but found it necessary to introduce a correction into the model in the form of a term expressing the reduction in organic solubility experienced by molecules of larger molar volume *(7)*. Lipnick argued that more research is needed in investigating the upper boundaries of linearity for very hydrophobic compounds *(5)*. The decrease in chemical activity of very insoluble chemicals could be related to a lack of equilibrium between the water and the lipid phases or to a decrease in the chemical activity of chemicals occupying larger molecular volumes *(4)*. Nonetheless, the toxi-

cant concentration measured relative to its saturation concentration varies much less than the absolute toxicant concentration producing a given effect.

Albert describes nonreactive toxicants as acting simply like foreign bodies *(6)*. They accumulate in some part of the cell and disorganize a chain of metabolic processes. His explanation for the phenomenon is that "accumulation of depressants in the lipoprotein membranes of simple cells must cause swelling. This could bring about the mechanical separation of enzymes responsible for an orderly sequence of reactions. The swelling could also alter the pores which exist for the ingress of sodium cations." Similar explanations are offered by numerous authors, although there does not seem to be definitive proof of any theory. Donald Mackay has found that the LC_{50} of a chemical corresponds to a chemical concentration in the fatty tissues of 0.6% *(8)*.

The focus of this article is QSARs involving nonreactive toxicity . . . toxicants acting simply like foreign bodies.

It should be noted that the original theories and observations regarding nonreactive toxicity were based on work relating to anesthetic drugs. However, the same ideas have been successful in explaining similar observations in the area of aquatic toxicology.

Although nonreactive toxicity is not related to specific chemical reactions and thus involves a wide variety of structurally diverse chemicals, it is still appropriate for study by structure–activity relationships. The elements of structure most closely related to nonreactive toxicity are those that describe the partitioning of the toxicant into the organism and thus involve solubility.

The focus of this article is QSARs involving nonreactive toxicity. QSARs for reactive toxicity are much less common in the environmental toxicology literature. They follow more closely the methods and parameters that are used in pharmacologic QSARs. A discussion of some of these methods applied to toxicity is found in Weinstein et al. *(9)*.

We consider three types of parameters that have been found to be successful in QSAR studies of nonreactive toxicity in environmental toxicology: octanol–water partition coefficient (log P); the solvatochromic parameters used in LSERs; and molecular connectivity. The log P and LSER methods are based on Hansch-type analyses using descriptors of physical and chemical properties. Molecular connectivity is based on molecular topology rather than on physical and chemical properties.

Requirements of QSARs

In order for a QSAR to be useful, three requirements must be met. First, the relationship must be accurate enough to be useful for the particular application. For instance, for engineering purposes, a reasonable goal for the accuracy of a QSAR in predicting toxicity to bacteria may be about one order of magnitude (standard error of one-half order of magnitude). This judgment is based in part on the variability inherent in toxicity tests as well as additional variability in applying the test condition data to any real situation such as a wastewater treatment application.

Second, a QSAR is only valid for the types of compounds used in its derivation, that is, the types of compounds found in the training set. Some QSAR methods are oriented to distinguishing differences among similar, often congeneric sets of data. Others are oriented toward distinguishing among broad ranges of toxicants. The latter type has greatest utility for engineers or applied scientists who need an estimate of the toxicity of a pollutant. This is true for three reasons. First, engineers and scientists may not have sufficient chemical intuition to select the best QSAR equation among a range of narrowly defined equations and be sure of its applicability. Second, because of the limitations in accuracy with which QSARs and even toxicity testing can be applied to field conditions, the knowledge of where, on a broad spectrum of toxicity, a type of chemical falls may have more utility than distinguishing among the toxicity of closely related toxicants. Third, when an equation is derived for a relatively small group of chemicals, the toxicity data itself may have just as much utility as the equation. For instance, there are 13 chlorobenzenes. To develop a QSAR equation, it would be necessary to test at least half of them. The test results alone would probably define their range of toxicity with sufficient accuracy for many applications. The greatest utility of a QSAR for a congeneric series of chemicals would be in understanding the small structural differences that give rise to variations in toxicity. This type of QSAR would be useful to someone looking for fundamental mechanisms of toxicity.

The third requirement for a useful QSAR is that the descriptors used should be relatively easy to obtain either through experiment or from existing data bases. For example, QSARs using aqueous solubility are limited by the fact that determining solubility experimentally is often difficult and the results reported in the literature are erratic.

QSAR methods

The three QSAR methods mentioned previously—octanol–water partitioning, LSERs, and molecular connectivity—were used in our research of toxicity of chemicals to environmental bacteria. Each method is described with examples from our research and others' to indicate its strengths and weaknesses.

The octanol–water partition coefficient used as log P is the most common parameter used in toxicity QSARs. It models the relative partitioning between the aqueous phase and the more nonpolar lipid-like biophase. As log P increases, toxicity increases. At high values of log P, the low aqueous solubility will begin to decrease the toxicity of a compound. For this reason, a second-order P term or a bilinear term is often introduced.

Log P values can be determined experimentally fairly easily and accurately for most compounds. They can also be calculated empirically by adding fragment constants for substructures of the compound and applying correction factors for various types of chemical structures, as shown by Lyman et al. *(10)*. They can be estimated by a computer-based expert system (CLOGP3) developed by Hansch and Leo at Pomona College. The availability of accurate methods for computation of log P make this parameter easy to use.

We found log P to be quite successful at correlating toxicity. For instance, for a training set of 53 chemicals tested for aerobic heterotrophs, we found an adjusted r^2 of 0.82 and a root mean square error of 0.39 (see Figure 1). Log P was sometimes more successful in correlations for chemicals separated by chemical class. For instance, for Microtox bacteria, a QSAR covering a wide range of chemical classes had an adjusted r^2 of 0.68 and a root mean square error of 0.80. However, a QSAR covering just substituted benzenes achieved an adjusted r^2 of 0.77 and a root mean square error of 0.29.

Many previous studies have found very successful QSARs using log P in the field of aquatic toxicology. Konemann related the toxicity to guppies of industrial pollutants to log P in a linear relationship ($n = 50$, $s = 0.237$, $r^2 = 0.976$) *(11)*. Veith et al. used a two-

FIGURE 1
Aerobic heterotroph log P QSAR

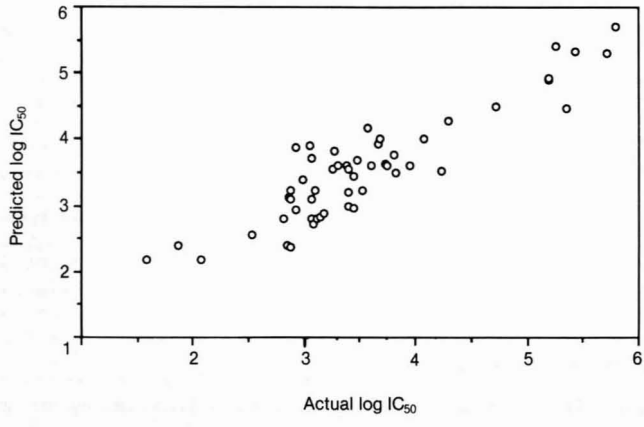

Log IC_{50} = 5.12 – 0.76 log P ; n = 53, s = 0.39, adj. r^2 = 0.82.

FIGURE 2
Aerobic heterotroph LSER QSAR

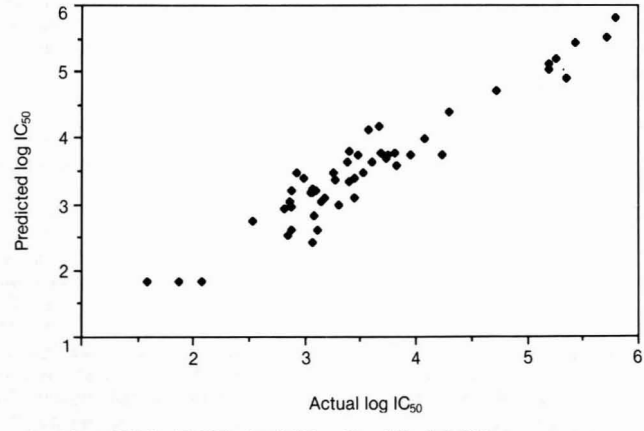

Log IC_{50} = 5.24 – 4.15 VI/100 + 3.71 BETA – 0.41 ALPHA; n = 52, s = 0.27, adj. r^2 = 0.92.

term log P relationship to describe the toxicity of a variety of industrial chemicals to the fathead minnow *(4)*. Even more common than log P QSARs for diverse chemical sets is the application of this method to smaller congeneric series of chemicals.

LSERs developed by Kamlet and coworkers have successfully correlated many diverse chemical properties, including toxicity, that depend on solute–solvent interactions. They are based on four molecular characteristics called solvatochromic parameters: V_i, the intrinsic molecular volume; π^*, a measure of polarity or polarizability; and α_m and β_m, measures of the ability to participate in hydrogen bonding as a hydrogen donor or acceptor, respectively. A particularly good overview of the LSER method is found in Kamlet et al. *(12)*.

A limitation of the LSER method is that the parameters are only available for a finite number of chemicals. V_i can be computed using a number of molecular modeling systems based on structural fragments and standard bond lengths and angles such as those described in Leahy et al. *(13)*. In addition, V_i can be estimated with sufficient accuracy by the McGowan method *(14)*. Values for the remaining solvatochromic parameters were originally determined from solvent effects on ultraviolet and visible spectra. There are now a number of high-quality correlations, particularly with chromatographic data, that can be used to find additional parameters. The parameters also have clear chemical interpretations. Therefore it is possible to estimate parameters from closely related chemicals. A number of rules are available to help make these estimates. In spite of these options, obtaining parameters for the LSER method is more difficult than for other methods (notably for phenols).

Of the three methods we considered, LSER produced the most accurate QSARs covering the widest range of chemical classes. For example, a QSAR for aerobic heterotrophs that included 52 compounds in the training set achieved an adjusted r^2 of 0.92 and a root mean square error of 0.27 (see Figure 2).

Other successful toxicity QSARs for nonreactive toxicity have been established for a number of organisms including Microtox bacteria *(15)*, Golden Orfe fish *(16)*, and *Daphnia pulex (17)*. Chemicals acting by a reactive toxicity mechanism are outliers from these relationships. Identification of outliers can provide information and impetus for identifying reactive toxicity mechanisms.

For instance, the differences between the observed and predicted toxicities of the carboxylic acid esters for the Golden Orfe fish *(16)* were compared to the rate constants for hydrolysis of these compounds and found to correlate with an r^2 of 0.950. Thus, esters that hydrolyze rapidly showed enhanced toxicity and those that hydrolyze slowly showed lesser toxicity and, in the extreme, followed a nonreactive toxicity mechanism.

The toxicity QSARs using LSER are all similar in form and relate to the physical meaning of the parameters. As the intrinsic molar volume or the hydrogen bond donor acidity increases, aqueous solubility decreases and toxicity increases. As the hydrogen bond donor accepter basicity increases, aqueous solubility increases and toxicity decreases. The only term that runs counter to the trend expected on the basis of solubility is polarity–polarizability. As polarity increases, aqueous solubility increases and so does toxicity. Kamlet et al. hypothesized that this effect may relate to the mechanism of nonreactive toxicity *(16)*.

Molecular connectivity is a method of describing molecular structure based solely on bonding and branching patterns rather than physical or chemical characteristics. Based on earlier work by Randic, Kier and Hall have developed connectivity indices and demonstrated their utility *(18)*. They have found high-quality correlations of diverse physicochemical properties and

FIGURE 3
Aerobic heterotroph molecular connectivity QSAR

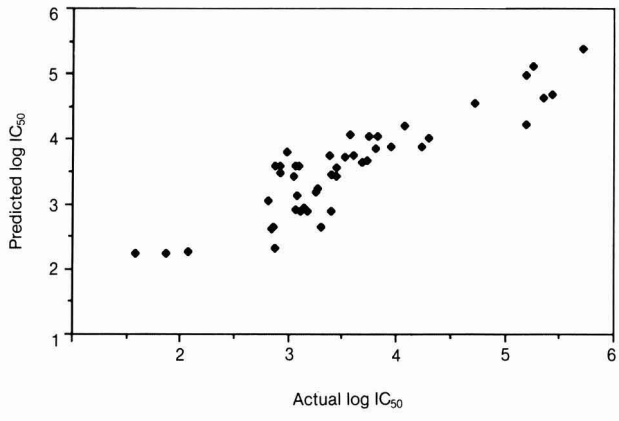

Log $IC_{50} = 6.09 - 0.59\ {}^0X + 2.29\ ({}^1X - {}^1X^v) + 0.37\ {}^3X^c$; n = 46, s = 0.43, adj. $r^2 = 0.78$

biological activity, particularly in medicinal chemistry.

Using a simple algorithm, a series of indices called zero-order (^0X), first-order (^1X), and so forth, describing increasingly larger molecular fragments are computed for chemicals. These computations are based solely on the chemicals' structural formula. "Valence indices" (denoted with a V superscript) include information on atom type, whereas "nonvalence" indices do not. One description of the method of calculating molecular connectivity indices is found in Hall and Kier *(19)*. Because the indices are based entirely on structural formula, the effect a change in structure would have on predicted toxicity can be easily determined.

We found very accurate QSARs using molecular connectivity. For example, for aerobic heterotroph data including 46 compounds, a correlation using two indices yielded an adjusted r^2 of 0.78 and a root mean square error of 0.43 (see Figure 3). Although we found molecular connectivity QSARs covering many classes of compounds, the accuracy was sometimes improved by separating compounds by class.

A common criticism of the molecular connectivity method is that the indices do not refer to any specific known physical qualities. Kier and Hall have interpreted the information contained in some indices. For instance, the simple first-order index ranks molecules according to their size and branching and is closely related to many of their physical properties *(18)*.

The valence index, $^1X^v$, carries information relating to both volume and electronic character. Higher order indices, based on larger substructures, encode more complex aspects of structure and often appear in multivariate regression analyses of molecules for physical and biological properties *(20)*. Additional information is contained in terms derived from the addition of valence and nonvalence indices and subtraction of valence and nonvalence indices for a given order *(21)*. Other researchers have tried to relate indices to known physical qualities with limited success *(22, 23)*. Therefore, although some molecular connectivity indices have been correlated with—or hypothesized to describe—specific characteristics, they are not defined well enough to be selected a priori for use in correlations. They are selected to optimize the correlation statistically.

In our work, the indices most often selected for inclusion in toxicity QSARs were a zero-order or first-order index. The second index selected was often a "difference index," derived from the subtraction of a valence from a nonvalence index. The similarities found between the indices used in our different toxicity QSARs support the presumption that these indices are describing fundamental aspects of toxicity.

Other researchers have used molecular connectivity in environmental toxicology. Murray et al. used molecular connectivity to correlate biological activity that had previously been described in QSARs using log P *(24)*. Hall and Kier derived equations describing the antimicrobial action of halogenated phenols in an inverse relationship to ^1X and a hyperbolic relationship with ^1X *(19)*. Schultz et al. developed a structure–activity relationship for the toxicity of nitrogenous heterocyclic compounds to the freshwater ciliate *Tetrahymena pyriformis (25)*. This correlation showed an improvement in r^2 over a previous correlation of the data using log P.

Koch used first- and second-order valence connectivity indices to correlate toxicological data *(26)*. He found that the accuracy of the linear relationships depended on the test organism and the similarity of the structure of chemical compounds. Better correlations were found for homologous series of chemicals rather than for more diverse sets. Koch developed QSARs for bioconcentration, sorption, and toxicity to guppies of a wide variety of environmental pollutants. All QSARs showed a linear dependence on $^1X^v$ *(27)*.

Sabljic and Protic showed the bioconcentration of a variety of halogenated environmental contaminants to be well correlated by a parabolic relationship with $^2X^v$ *(28)*. Sabljic demonstrated a correlation of toxicity to sheepshead minnows of chlorinated compounds with ^0X *(29)*.

Boyd et al. looked at a congeneric series of antimicrobial chemicals that had been previously correlated with log P *(30)*. They found that higher order (third-, fourth-, and fifth-order) connectivity indices provided improved correlations over log P.

Molecular connectivity relationships are often used to make structural interpretations of toxicity *(19, 20, 25)*. For instance, Hall and Kier developed a QSAR for toxicity of substituted phenols to fathead minnows *(20)*. They were able to show that an increase in molecular size (and hence ^1X) results in increased toxicity. The inclusion of $^3X_p^v$ in the equations showed that valence definition of the indices is influential in describing toxicity. Hall and Kier pointed out that similar structural interpretations of toxicity are not possible in correlations based on physicochemical properties such as log P *(19)*.

Surrogate testing organisms

Whenever toxicity standards are addressed, the immediate question that follows is, "Toxicity to what?" Because finances limit the number of bioassays that can be run, effective surrogate testing organisms must be found whose response can be related to target organisms or ecosystems, either natural or man-made (e.g., biological treatment systems).

The word *surrogate* is often associated in aquatic toxicology with using an organism to estimate in-stream toxicity. As ecosystem toxicity testing is not a reasonable option, surrogate organisms are required in this instance. However, surrogates can also be used in the more limited sense of one organism—the sur-

rogate—substituting for another specific organism. This can be accomplished by comparisons and correlations between the sensitivities of the two species. This more limited role of surrogates is the focus of this paper. It is a first step toward consideration of surrogates for more complex systems; the relationships between sensitivities of different organisms in an ecosystem will help define the requirements for an ecosystem surrogate. The use of surrogates to estimate toxicity to specific organisms is also particularly valuable when data for the target organism are difficult or costly to obtain.

Characteristics of surrogates. The ideal surrogate organism used to assay for toxicity should have the following characteristics:

- a response predictive of organisms in the natural or man-made system to be protected,
- a clear endpoint for the assay,
- ease of cultivation and assay of the organism, and
- a satisfactory response to all relevant toxicants.

This is a difficult set of criteria to meet. If one considers an entire ecosystem, the most sensitive organism must be protected, and there is usually a wide range of susceptibility to a given toxicant by the organisms in any ecosystem.

The endpoint of the toxicity assay may be a respiration rate that is 50% of a control. In the case of bioluminescent bacteria, it is 50% of the light emission rate. Thus, the range of toxicity assayed must include responses above and below the IC_{50} to allow interpolation of the IC_{50}. Endpoints such as motion of the assay organism are much more difficult to define.

The test organism must be relatively easy to cultivate. Ease, speed, and simplicity are desirable attributes of a toxicity assay; in some operations speed is essential to allow control measures to be taken to avert disaster.

The surrogate must have a satisfactory response to all relevant toxicants. Some test organisms, such as bacteria, respond to dissolved toxicants; others, such as protozoa, *daphnia,* or fish, respond to toxicants associated with the particulate phase as well as the dissolved phase. For instance, a toxicant with a high octanol–water coefficient may be very insoluble and partition strongly to organic particulates in the water. Thus, bacteria or the Microtox assay may not be adversely affected, whereas *daphnia* or fish may be strongly affected.

History of surrogates. Surrogate organisms have been used extensively in drug testing and some areas of aquatic toxicology. But their use can be expanded further in environmental engineering. Research into the human health effects of toxicants uses surrogate organisms and relationships between dose and response to estimate human response. Many aquatic toxicology studies have compared sensitivities of different organisms, looking for the more sensitive organisms to use as test organisms. The utility of comparisons is limited in that the results do not give specific estimates of toxicity. However, as we found in our work, it is also possible to use correlations of toxicity between organisms much the same way one can use QSAR correlations to estimate toxicity.

Requirements of interspecies correlations. Two major requirements must be met for the effective use of surrogate organisms in toxicity correlations. First, a good correlation must be developed between the toxicity to the two organisms. An accurate correlation can be more important than finding similarities in sensitivities of the two organisms. For instance, we found that the sensitivities of fathead minnows and Microtox bacteria are much closer than the sensitivities of fathead minnows and aerobic heterotrophs. But a more precise estimate of fathead minnow toxicity could be found from a correlation with aerobic heterotrophs ($n = 24$, adj. $r^2 = 0.90$, $s = 0.38$).

Sometimes a comparison of sensitivities can be useful, such as when two organisms are likely to be found in the same environment. For instance, we found that aerobic heterotrophs are an order of magnitude less sensitive than *Nitrosomonas* for the chemicals tested. This is useful information for designing and operating biological treatment systems that rely on both bacteria. Protecting *Nitrosomonas* from toxic effects will ensure that the aerobic heterotrophs are protected.

A second requirement for the use of interspecies correlations is that the domain over which the correlation holds must be well defined. One cannot define a relationship between organisms based on data for one chemical class and assume that it will hold for another untested class. We found excellent correlations between the toxicity to aerobic heterotrophs and methanogenic bacteria, with the important exception of chlorinated alkyl compounds. These compounds showed enhanced toxicity to the methanogens.

Correlations with Microtox. The Microtox test was developed by Beckman Instruments, Inc., as a quick screening test for toxicity. The test uses the bioluminescence of the marine bacterium *Photobacterium phosphoreum* as a measure of its activity. The degree of toxicity is measured by the decrease in light output in the presence of a toxicant. It is a quick, simple, and very reproducible test, albeit unrepresentative of freshwater ecosystems. One study found a coefficient of variation of 18% between tests with different operators, instruments, and production lots of reagent *(31).*

We found useful correlations between the Microtox test and the other bacteria tested (aerobic heterotrophs, *Nitrosomonas,* and methanogens) with r^2 values between 0.69 and 0.82 and root mean square error between 0.48 and 0.54. When we correlated Microtox test results with fathead minnow data, the equation had an r^2 value of 0.85 and a root mean square error of 0.46 (see Figure 4).

Many other researchers have looked

FIGURE 4
Correlation between toxicity to fathead minnows and Microtox bacteria

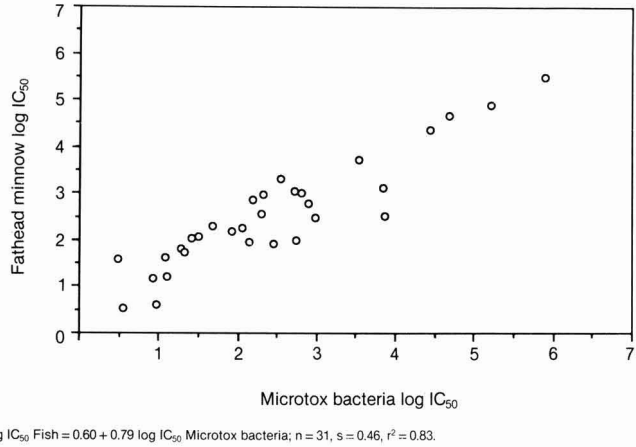

Log IC_{50} Fish = 0.60 + 0.79 log IC_{50} Microtox bacteria; $n = 31$, $s = 0.46$, $r^2 = 0.83$.

at the relationship between the toxicity in the Microtox test and toxicity to species of environmental concern, fish, and other bacteria. Many such studies have been reviewed by Bulich *(31)*. Correlations between Microtox bacteria and fish or *daphnia* involving organic chemicals and wastes showed r^2 values between 0.64 and 0.94. However, many studies reviewed found no successful correlations.

gate organisms include a comparison by Yoshioka et al. of the sensitivity of the 3-h activated sludge respiration inhibition test with toxicity tests conducted with aquatic invertebrates, fish, and algae *(33)*. They found that the microorganisms were not generally as sensitive as the other organisms, but a correlation was not developed. Vaishnav correlated the microbial respirometric IC_{50} and the fathead min-

FIGURE 5
Correlation between toxicity to aerobic heterotrophs and methanogens

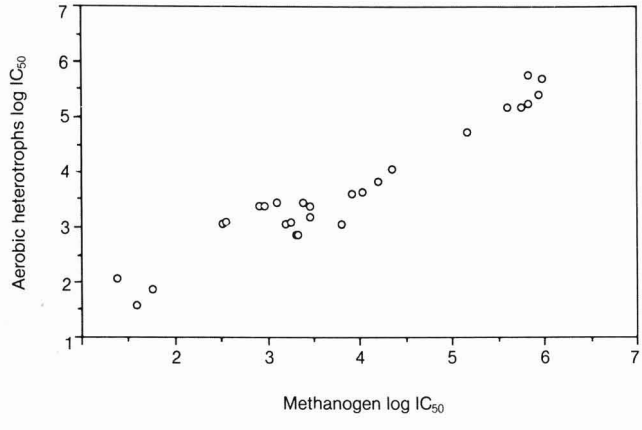

Log IC_{50} aerobic heterotrophs = 0.62 + 0.81 log IC_{50} methanogens; n = 27, s = 0.30, r^2 = 0.93.

Atkinson and Switzenbaum compared the toxicities of a wide variety of chemicals to Microtox bacteria and anaerobic bacteria *(32)*. They used both literature data and their own laboratory data. They found little correlation between the toxicities to the two species and concluded that Microtox would not be a good surrogate for anaerobic bacteria in toxicity tests. Our findings conflict with theirs probably because we restricted our correlation to nonreactive toxicants.

Correlations with environmental bacteria. Bacterial data can be used in interspecies correlations with each other and with fish. We found many useful relationships between aerobic heterotrophs, *Nitrosomonas,* Microtox bacteria, and fathead minnows. Some of the most accurate involved the aerobic heterotrophic bacteria. Correlations between aerobic heterotrophic bacteria and fathead minnows had an r^2 value of 0.90 and a root mean square error of 0.38. A correlation between aerobic heterotrophic bacteria and methanogens with the exclusion of chlorinated alkyl compounds had an r^2 of 0.93 and a root mean square error of 0.30 (see Figure 5).

Previous studies of bacteria as surro-

now acute toxicity (96-h LC_{50}) for seven primary alcohols and obtained a correlation coefficient of 0.992 *(34)*. The resulting equation was then used to predict the LC_{50} values of an additional 12 narcotic chemicals, mostly alcohols and ketones.

Areas for future research

Reactive toxicity. Our correlations, both interspecies and QSARs, were developed for nonreactive toxicants. Generally, QSARs have been most successful for chemicals acting by a nonreactive toxicity mechanism. Reactive toxicants should show enhanced toxicity above that predicted by a nonreactive chemical QSAR. In fact, the identification of outliers from a correlation involving nonreactive toxicants can indicate the possibility of a reactive toxic mechanism. In our studies, aldehydes, acryl functional groups, and compounds with low pKa values, were confirmed as reactive toxicants by showing enhanced toxicity above that predicted by the QSAR.

However, reactive toxicants pose two problems for QSARs and interspecies correlations. First, how does one know that a chemical is a reactive toxicant and cannot be accurately predicted by the QSAR? If a reactive toxicity mechanism for the chemical has not been previously identified, one can only rely on the fact that the chemical is similar to others in the training set to assume that it can be adequately predicted. For higher organisms such as fish, specific physiologic responses to a toxicant can be observed. For instance, when respiration is uncoupled from ATP formation by a reactive toxicant, the respiration rate of the fish increases. However, for microorganisms for which gross measures of vitality such as respiration rate are used to measure toxicity, specific responses are not observed. Future research should focus on defining and testing chemicals that act by reactive mechanisms.

Second, can interspecies correlations be used for predicting the toxicity of reactive toxicants? Our research indicates that this may be possible when the mode of action is not peculiar to a particular bacteria. We observed good correspondence between the toxicity of reactive toxicants to different bacteria groups we tested (aerobic heterotrophs, *Nitrosomonas,* and methanogens) for chemicals including acrylates, acrylonitrile, and compounds with low pKa values.

However, we found that compounds with nitro and amino groups have differing effects on aerobic and anaerobic cultures—perhaps due to the difference in oxidation–reduction potentials in the two cultures. We also found that Microtox bacteria correlated poorly for reactive toxicants with the other environmental bacteria groups. Firm conclusions cannot be drawn yet on the potential for correlating reactive toxicants between species. More work is needed to define areas in which these correlations are successful.

Combined toxicants. Our research considered the toxicity of individual chemicals. Rarely are chemicals found individually in a waste or in the environment. Information on the toxicity of individual toxicants in a mixture is a necessary starting point. However, the information would have much greater utility if we had a better understanding of the effects of combining toxicants. Is the toxicity simply additive? Are there synergistic or antagonistic effects? Is there some method we could use to express the toxicity so that it would be additive? Guidelines in this area would greatly enhance the value of toxicity estimates obtained from QSARs or interspecies correlations.

QSAR method development. The QSAR methods we examined—octanol–water partitioning, LSER, and molecular connectivity—were all successful in correlating toxicity. Further development of these methods to over-

come some of their limitations would be beneficial. The data base of LSER parameters must be enlarged, and clear methods made available to obtain parameters. These needs could be met by an expert system for calculating parameters and by an established experimental protocol for obtaining parameters from existing correlations. The molecular connectivity method should be improved by continued development of the understanding of what the different indices signify.

Toxicity testing protocols. If toxicity data are obtained by standard methods, QSARs and interspecies correlations can draw on this data to develop equations with wide applicability. For instance, the fact that Microtox is a well-standardized test makes it easy to use in correlations. Data were taken from a compendium of Microtox results *(35)* and used to validate our QSARs. More than 100 data points could be accurately predicted by our correlations (within the 95% confidence intervals). The reasons for almost all outliers were evident; either they were reactive toxicants or they were found to be experimentally inaccurate when compared to other data sources. In the area of bacteria toxicity testing, work is being done to standardize testing methods such as the OECD method. This standardization should allow us to draw on different data sources to continually update and expand QSAR and interspecies correlations.

Summing up

QSARs and surrogate organisms used in interspecies correlations have great potential as methods for helping to fill the great need for toxicity data. Depending on the accuracy required, predictions from these correlations can serve as estimates of toxicity, first guesses of toxicity to help guide further testing, or checks on existing data to help identify experimental errors.

We developed successful QSARs and interspecies correlations for a wide variety of chemical pollutants that act by nonreactive toxicity mechanisms for aerobic heterotroph bacteria, *Nitrosomonas*, methanogens, fathead minnows, and the Microtox test. The QSAR methods used log P, LSER, and molecular connectivity and were all successful in correlating toxicity.

Each method has advantages and disadvantages. LSER QSARs are most accurate and cover the greatest range of chemicals. Parameters are more readily available to apply log P and molecular connectivity QSARs. Molecular connectivity indices can be computed simply from structural formulas with no knowledge of chemical properties. It is therefore easy to see how changes in structure would affect predicted toxicity. However, log P and LSER QSARs afford a more intuitive understanding of the properties affecting toxicity.

We have also shown how the toxicity of chemicals to some bacteria can be used to estimate the toxicity to other bacteria and to fish using interspecies correlations and comparisons. The correlations between bacteria and fish are valuable, as are the correlations involving Microtox, due to the relative simplicity of obtaining bacteria (particularly Microtox) data.

Further research in several areas will enhance the development of high-quality correlations. Reactive toxicants must be identified and studied to better define the range of applicability for nonreactive toxicity correlations and to assess the potential for inclusion of reactive toxicants in interspecies correlations. The effects of combining toxicants need to be researched. Continued development of standard toxicity testing methods will provide data for future enlarged QSARs and interspecies correlations. Finally, development of the very promising QSAR techniques, particularly LSER and molecular connectivity, will aid use of these methods in toxicity work.

Acknowledgments

This research was funded by NSF Grant Number ECE-86-17101 to Drexel and Vanderbilt universities, Dr. Edward Bryan, Program Director.

References

(1) Postel, S. In *State of the World 1987;* Brown, et al., Eds.; W. W. Norton: New York, 1987; pp. 169–73.
(2) Blum, D.J.W. Ph.D. Dissertation, Drexel University, 1989.
(3) Chou, W. L. et al. Report no. NSF/GI/434; National Science Foundation: Washington, DC, 1977.
(4) Veith, G. D.; Call, D. J.; Brooke, L. T. *Can. J. Fish. Aquat. Sci.* **1983,** *40,* 743–48.
(5) Lipnick, R. L. *Environ. Toxicol. Chem.* **1985,** *4,* 255–57.
(6) Albert, A. *Selective Toxicity and Related Topics;* Butler and Tanner: London, 1968; pp.436–51.
(7) Abernathy, S. et al. *Aquat. Toxicol.* **1986,** *8,* 163–74.
(8) MacKay, D. *Environ. Toxicol. Chem.* **1988,** *7,* 469–81.
(9) Weinstein, H. et al. *Environ. Health Perspect.* **1985,** *61,* 147–62.
(10) Lyman, W. J.; Reehl, W. F.; Rosenblatt, D. H. *Handbook of Chemical Property Estimation Methods;* McGraw-Hill: New York, 1982; pp. 1.1–1.54.
(11) Konemann, H. *Toxicol.* **1981,** *19,* 209–21.
(12) Kamlet, M. J. et al. *Chemtech* **1986,** *9,* 566.
(13) Leahy, D. E. et al. *Chromtographia* **1986,** *21,* 473–78.
(14) Kamlet, M. J. et al. *J. Phys. Chem.* **1987,** *91*(7), 1996–2004.
(15) Kamlet, M. J. et al. *Environ. Sci. Technol.* **1986,** *20*(7), 690–95.
(16) Kamlet, M. J. et al. *Environ. Sci. Technol.* **1987,** *21*(2), 149–55.
(17) Passino, D.R.M.; Hickey, J. P.; Frank, A. M. Presented at 3rd International Workshop on Quantitative Structure–Activity Relationships in Environmental Toxicology; Knoxville, TN, May 1988.
(18) Kier, L. B.; Hall, L. H. *Molecular Connectivity in Chemistry and Drug Research;* Academic Press: New York, 1976.
(19) Hall, L. H.; Kier, L. B. *Eur. J. Med. Chem. Chim. Ther.* **1978,** *13*(1), 89–92.
(20) Hall, L. H.; Kier, L. B. *Bull. Environ. Cont. Toxicol.* **1984,** *32,* 354–62.
(21) Kier, L. B.; Hall, L. H. *J. Pharm. Sci.* **1981,** *70,* 583–89.
(22) Murray, W. J. *J. Pharm. Sci.* **1977,** *66,* 1352–54.
(23) Dearden, J. C. Presented at QSAR 88: 3rd International Workshop on Quantitative Structure–Activity Relationships in Environmental Toxicology; Knoxville, TN, May 1988.
(24) Murray, W. J.; Hall, L. H.; Kier, L. B. *J. Pharm. Sci.* **1975,** *64,* 1978–81.
(25) Schultz, T. W.; Kier, L. B.; Hall, L. H. *Bull. Environ. Contam. Toxicol.* **1982,** *28,* 373–78.
(26) Koch, R. *Chemosphere* **1982,** *11,* 925–31.
(27) Koch, R. *Toxicol. Environ. Chem.* **1983,** *6,* 87–96.
(28) Sabljic, A.; Protic, M. *Chem. Biol. Interactions* **1982,** *42,* 301–10.
(29) Sabljic, A. *Bull. Environ. Contam. Toxicol.* **1983,** *30,* 80–83.
(30) Boyd, J. C.; Millership, J. S.; Woolfson, A. D. *J. Pharm. Pharmacol.* **1982,** *34,* 158–61.
(31) Bulich, A. A., In *Toxicity Testing Using Microorganisms, Vol. 1;* Bitton, G.; Dutka, B. J., Eds.; CRC Press: Boca Raton, FL, 1986; pp. 57–74.
(32) Atkinson, D. S.; Switzenbaum, M. S. Presented at the International Conference on Biological Treatment of Toxic Wastewaters, Arlington, VA, June 26, 1986.
(33) Walker, J. D. *J. Water Pollut. Contr. Fed.* **1988,** *60,* 1106–20.
(34) Vaishnav, D. D. *Toxicity Assessment* **1986,** *1,* 227–40.
(35) Kaiser, K.L.E.; Ribo, J. M. *Toxicity Assessment* **1987,** *2*(4), 1987.

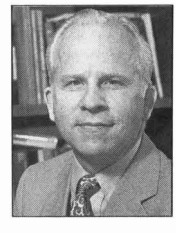

Diane J. W. Blum *(l), Ph.D., P.E., is a graduate of Stanford University and Drexel University in environmental engineering. Her professional employment has included EPA Region III and BCM Engineers. Presently, she is doing private consulting in research and engineering.*

Richard E. Speece *(r) is Centennial Professor of civil and environmental engineering at Vanderbilt University. The study described in this paper was funded by NSF while he was Betz Chair Professor of Environmental Engineering at Drexel University. His research interests are in toxic response of anaerobic treatment processes, the effect of chemical molecular structure on environmental response, and supplemental oxygenation for water quality management.*

The Department of the Environment

Alvin L. Alm

President George Bush has wisely endorsed upgrading EPA to cabinet status. This move, advocated by environmental groups and members of Congress, reflects the importance of EPA as a part of the government and environmental protection as a national priority. Although this gesture has real value, merely upgrading EPA to cabinet status would miss an unprecedented opportunity to strengthen the agency substantively.

The benefits of creating a Department of the Environment are either symbolic or are related to EPA's past lack of presidential support. The primary symbolic value would be to raise environmental quality to a higher national priority. Creation of a cabinet-level agency also creates a durable commitment. No cabinet-level agency has ever been abolished. In some cases, the name and structure are changed (e.g., the Department of Defense) or the department has fissioned into two entities (as the Department of Health, Education, and Welfare did), but no profound changes in status have occurred. EPA could be tucked into another agency under a reorganization plan, but as a cabinet agency, its status could be changed only by affirmative legislation.

Also, the EPA administrator lacks clout unless he or she has strong support from the president. Often the administrator must cajole other agencies to spend money on environmental protection or force them to abandon or change projects that adversely affect the environment. Yet the EPA administrator is outranked by the very officials he must convince to do unpleasant things.

Cabinet status would create a perception of greater stature. Cabinet status is perceived as a route of access to the president, which, in Washington, is often as valuable as reality.

Other reasons have been advanced for conferring cabinet status on EPA. Some argue, for example, that most of the Western nations have conferred ministerial rank on their environmental agencies, placing the administrator of EPA at a disadvantage in international environmental fora. (I personally question this argument, considering past and current U.S. leadership in world environmental efforts.)

Upgrading EPA to cabinet status provides minimal *immediate* benefits considering William Reilly's current relationship to the president. Greater benefits presumably would occur in the future should the environmental chief face a less supportive president.

More tangible benefits from reorganization would arise if EPA's upgrading were accompanied by a strengthening of its capabilities. Many government programs overlap EPA's authorities or could substantially increase EPA's scientific base. For example, the best environmental health research is conducted at the Department of Health and Human Services. The National Oceanic and Atmospheric Administration (NOAA) and the National Air and Space Administration (NASA) have substantial capabilities in predicting atmospheric transport and fate of pollutants. Department of Agriculture programs greatly affect soil erosion and pesticide accumulation. Occupational Safety and Health Administration and EPA authorities duplicate each other in certain areas.

Credible arguments can be made to transfer a list of programs to EPA. But most of these transfers would exact a high political cost that would doom the prospects for creating an environmental department. Moreover, many of these shifts would not be critical to the ultimate success of the new department. There does appear to be one exception, however. Transferring substantial parts of NOAA to the new department would make the new department a substantially stronger institution.

NOAA's capabilities in the atmospheric sciences would strengthen the environmental department's capability to understand many of the forces that drive global warming, atmospheric chemical reactions, and transport and fate of air pollutants. NOAA's marine laboratories would support the environmental department's regulatory and other responsibilities to deal with estuarine, coastal, and ocean pollution. Transfer of the Coastal Zone Management Act authorities would give EPA a useful tool to deal with the serious environmental problems facing coastal areas around the country. One result of this transfer would be a size reduction in the Department of Commerce, but this shift does not adversely affect its mission. Such a transfer would, on the other hand, substantially improve the environmental department's capability to discharge its missions.

The current congressional bills call for a commission to determine what additional authority should be vested in the new department. Similar commissions in the past have not been successful. Although there would be a political price to be paid if parts of NOAA were transferred to the new department now, the substantial benefits would be worth it. Because interest in upgrading EPA is now high, it seems an opportune time to give EPA some of the muscle it needs to carry out its mandates.

Alvin L. Alm is a director and senior vice-president for energy and the environment for Science Applications International Corp., a supplier of high-technology products and services related to the environment, energy, health, and national security.

0013-936X/90/0924-0294$02.50/0

ES&T PRODUCTS

AIR POLLUTION

Particulate filters. The 510 Series particulate filters are available in 14 models with capacities up to 15,000 standard ft^3/min at 100 psig. Pressure drops are low. Deltech Engineering **104**

Activated carbon adsorbers. Activated carbon adsorbers are designed to purify low flow-rate air (up to 1000 scfm) with no need for dedicated personnel or complicated process equipment. They also can purify water streams up to 50 gal/min. Hoyt **105**

Filter fibers. Fibers such as Nomex, Tefaire, and Teflon are available for high-temperature air filtration. A brochure assists users in selecting optimum fiber. Du Pont **106**

CFC substitutes. Company is offering HFC-134a and HCFC-123 as substitutes for chlorofluorocarbons for use in air conditioning, solvent, and other applications. Halocarbon Products **107**

Adsorbers. NIXTOX adsorber systems are designed to remove pollutants from air and treat process gases. Capacities up to 8000 ft^3/min are available. Company also has water treatment adsorber systems available. Tigg **108**

NO_x removal. Proprietary U-50 reagent uses buffering chemistry to convert NO_x to nitrogen gas. It can work in nitric acid baths or gas scrubbers. Environmental Technology **109**

HAZARDOUS MATERIALS

PCB spill cleanup. Envirosolv II solvent is designed to reduce contamination by polychlorinated biphenyls on concrete floors by up to 99%. Company spokespersons say effective removal has been proven through tests. Environmental Group **110**

Packaging tests. Company is carrying out tests of packaging for hazardous materials for U.S. Air Force. Certification tests are conducted. Wyle Laboratories **111**

Bioremediation of soils. Company uses consortia of microbes to carry out bioremediation of petroleum-contaminated soils. A technical paper is available to explain how. Solmar **113**

INSTRUMENTATION

Bioremediation testing. Respirometer package is designed to provide data on the biodegradability or treatability of a particular material and the rate at which organisms will decompose the material. Tech-Line Instruments **114**

Tank inspection. Tank Scope allows a viewer to look directly into a tank to check for cracks, perforations, water entry, corrosion, pump and valve integrity, and water entry. It fits through a 4-in. fitting or pipe. EnviroDynamics **115**

Sulfur detector. Model 350B sulfur chemiluminescence detector is used with gas chromatographs equipped with flame ionization detectors. Background noise is reduced. Sievers Research **116**

Testing for aromatics. Field test kit is designed to test water and soils for aromatics from 10 ppb to 1000 ppm. It contains enough material to conduct 30 analyses. Hanby Analytical Laboratories **117**

Ammonia analyzer. Continuous ammonia analyzer is designed to measure ammonia and NO in a flue-gas environment. It can be operated as an in situ or extractive instrument. ADA Technologies **118**

Sample preparer. Model SFE/50 supercritical fluid extraction instrument is designed to reduce the extraction time necessary to prepare for gas chromatography many types of environmental samples suspected of containing organic contaminants. Suprex **119**

TOC determination. Carlo Erba's NA1500 and EA 1108 can be used for the selective determination of organic carbon in sediments, soils, and composts, and to differentiate organic from inorganic carbon. Fisons Instruments **121**

H_2S measurement. Model 722R/102 analyzer measures hydrogen sulfide in fuel gases, in conformity with 1978 EPA regulations that allow measurement of H_2S in certain cases rather than measurement of SO_2 after combustion. Tracor Atlas **122**

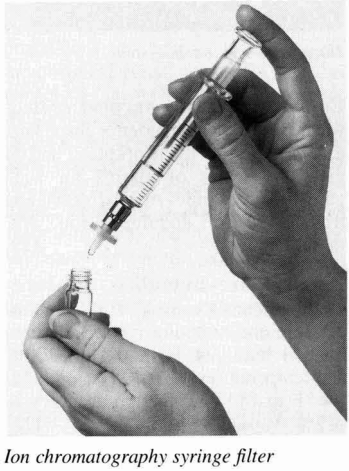

Ion chromatography syringe filter

Filter for IC. Acrodisc 13 syringe filter for ion chromatography is designed to eliminate the need for preflushing and to meet cleanliness criteria required for IC. Gelman Sciences **125**

Flow-through sampler. Model 3760 Stinger refrigerated flow-through sampler is designed to draw samples through a self-cleaning stainless-steel or Teflon "stinger" probe set directly in the flow stream. ISCO Environmental Division **123**

CO_2 monitor. Gas analyzer is designed to monitor carbon dioxide in ranges of 0–3000 ppm, 0–1%, 0–5%, and 0–10%. There is an alarm and a subsystem to start up an automatic vent to the atmosphere if an employee hazard is signaled. Automated Custom Systems **124**

Need more information about any items? If so, just circle the appropriate numbers on one of the reader service cards bound into this issue and mail in the card. No stamp is necessary.

Companies interested in a listing in this department should send their release directly to Environmental Science and Technology, *Attn: Products, 1155 16th St., N.W., Washington, DC 20036.*

0013-936X/90/0924-0295$02.50/0

Emission spectrometer. Plasma 40 inductively coupled plasma emission spectrometer is designed for high resolution and has new software that allows sample labeling and weight/volume correction and provides wavelength tables with 50,000 lines. Perkin-Elmer **126**

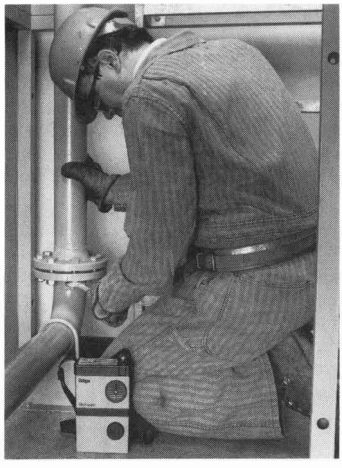

Hazardous-gas alarm system

Employee hazard warning. Multiwarn is designed to monitor three hazardous gases in the workplace and to give two levels of alarms for such gases. Daily profiles may be stored and transferred for documentation. National Dräger **127**

Temperature–humidity measurement. Battery-powered HM 34 temperature and humidity meter measures relative humidity from 0% to 100% and temperatures of −20 °C to 60 °C (-4 °F to 140 °F). Design accuracy is ±2%. Vaisala **128**

Groundwater monitoring. Products for groundwater monitoring are made of Teflon and other materials that are inert to components in a groundwater sample. Jensen Inert **129**

Water-level logger. Type A/F logger is designed for water-level recording in remote locations. It is battery-powered and stores data on a module slightly larger than a credit card. Leupold & Stevens **130**

Heavy metal detection. SEFA-P portable X-ray fluorescence analyzer is designed to detect heavy metal contaminants in soils and other materials at hazardous-waste sites. Data can be analyzed with a personal computer. HNU Systems **131**

Bacteria detector. Bacteria and fungus detector uses respirometry to detect contaminating microorganisms. It has 20 channels. The design sensitivity is 0.2 μL O_2/h. One application is aflatoxin detection in grains. Columbus Instruments International **132**

PUBLICATIONS

Environmental rules. Videotapes covering environmental laws and regulations, pollution prevention, hazardous waste, toxicology, and related topics are available. Government Institutes **133**

Groundwater references. Many books, brochures, publications, and other information sources on groundwater are available. Midwest Agricultural Chemicals Association **134**

Water products and services. The 1990 Products & Services Catalog lists publications, manuals of practice, educational materials, videos, and specialty items. Water Pollution Control Federation **135**

Wastewater Treatment (*ES&T* article series) reports on the processes for the treatment of wastewater, including removing particles and dissolved organic and inorganic contaminants, as well as aerobic treatment. ACS **136**

Computer Usage in Engineering (*ES&T* article series) discusses trends and applications of computers, including artificial intelligence and the impact of computer use in environmental engineering. The report tells how personal computers will change the practice of environmental engineering in the future. ACS **137**

Cancer Risk Assessment (*ES&T* article series) explores scientific topics of public concern regarding regulation of chemicals in the environment. Series reports on managing risk and communicating the results of risk assessment; also covered are exposure assessment and being realistic about chemical carcinogenesis. ACS **138**

SERVICES

Laboratory services. Company offers a full array of environmental laboratory capabilities that are listed in *Laboratory Services Reference Guide.* Scott Environmental Technology **139**

SOFTWARE

Mapping. QUIKMap Version 2 allows computer mapping for environmental, forestry, real estate, wildlife habitat, and numerous other applications. Environmental Sciences Limited **140**

Compliance. Audit Master Version 2.0 updates and expands environmental compliance auditing capabilities and presents improved warnings of potential compliance problems. Many parameters are user-defined. Utilicom **141**

Laboratory management. EasyLIMS software is written for the laboratory information management system. It features Microsoft Windows for use on IBM and compatible personal computers. Beckman Instruments **142**

STANDARDS

H_2S in air. Hydrogen sulfide in air standard has a guaranteed one-year stability. It is used to calibrate portable and fixed-point safety monitors at industrial facilities. Scott Specialty Gases **143**

Incinerator ash. Incinerator ash standard is reported to be the first commercially available reference for Toxicity Characteristic Leaching Procedure that mimics leaching of toxic materials at landfills by rain action. Fisher Scientific **144**

Performance evaluation. P.E.T. Organics provides performance evaluation for gas chromatography and GC/MS 600 series methods. Standard sets are available on a monthly basis for volatiles, acids, base/neutrals, and pesticides. Analytical Products Group **145**

Ozone generator. Ozone generator can be used for field-calibrating ozone monitoring instruments, as well as for laboratory studies. It produces a known concentration of 0.05–3 ppm. ENMET **146**

WATER TREATMENT

Solids removal. LME inclined-plate separators are designed to settle solids out of process water, potable water, and wastewater. Space requirements are markedly reduced. Zimpro/Passavant **147**

Potable water treatment. Microprocessor-controlled system uses ultraviolet and advanced software to optimize UV lamp intensity and flow capacity for UV disinfection of water. Aquionics **148**

Portable filtration system. Self-contained system for filtering water is designed to remove particles as small as 1 μm, as well as many microbial and chemical contaminants. It can be carried in a briefcase or handbag. Aqua City **149**

Water purifier. Aquafier water purifier uses a combination of distillation and both carbon and sediment filtration to transform even highly contaminated water to water company spokespersons say is 99.9% pure. Conklin **150**

ES&T BOOKS

Global Climate Change: Human and Natural Influences. S. Fred Singer, Ed. Paragon House, 90 Fifth Ave., New York, NY 10011. 1989. vii + 424 pages. $34.95, cloth.

The papers in *Global Climate Change* examine three categories of problems. The first involves inadvertent byproducts of human activities. The second category is undesirable long-range effects of intentional modification of the environment by humans. The third consists of consequences of changes humans did not cause and cannot control, such as volcanic eruptions, earthquakes, and other natural disasters; some of these changes are cataclysmic, but others can be as slow and as subtle as man-made effects. Among topics discussed are possible effects of acid rain, "nuclear winter," stratospheric ozone, and atmospheric CO_2 loadings.

Control of Radon in Houses, NCRP Report No. 103. National Council on Radiation Protection and Measurements. NCRP Publications, 7910 Woodmont Ave., Suite 800, Bethesda, MD 20814. 1989. vi + 90 pages. $15, paper.

This book starts by describing the sources of radon, especially ^{222}Rn. It continues with general approaches for control, source-dependent control techniques, source-independent control techniques, and recommendations. Among the recommendations is that the homeowner's best approaches to radon control are increased ventilation with outside air, enhanced convection or air circulation, and a combination of enhanced convection and unipolar space charging.

An Investigation of the Biodegradation Potential of Groundwater Contaminants. John T. Novak et al. Virginia Water Resources Research Center, 617 N. Main St., Blacksburg, VA 24060-3397. 1989. ix + 72 pages. $8 (single copies free for Virginia residents and organizations), paper.

This book examines biodegradation potential generally and does not confine itself to groundwater problems in Virginia. Topics include a literature review, the relationship between subsurface degradation rates and microbial density, and effects of site variations on degradation potential.

Combustion Processes and the Quality of the Indoor Environment. Air & Waste Management Association. Air & Waste Management Association, P.O. Box 2861, Pittsburgh, PA 15230. 1989. 392 pages. $75 ($50 for AWMA members), paper.

This work contains peer-reviewed papers on fuel use and tobacco smoke as they pertain to indoor combustion. It considers source characterization, exposure assessment, health effects, and policy. Specific topics include characterizing and controlling emissions from unvented and vented appliances, assessing indoor exposure to combustion byproducts, health effects, and tobacco smoke and other indoor air policy issues.

Chemicals, the Press and the Public. Environmental Health Center, National Safety Council, 1050 17th St., N.W., Suite 770, Washington, DC 20036. 1989. 124 pages. $9.95.

Chemicals, the Press and the Public aims at helping journalists communicate to the general public potential chemical risks in their communities. Specifically, this book offers reporters guidance in interpreting chemical information made available under the Superfund Community Right-To-Know provisions and reporting on it in an understandable manner.

Real Estate Transactions and Environmental Risks: A Practical Guide. Donald Nanney. Executive Enterprises Publications Co., Inc., 22 W. 21st St., New York, NY 10010-6904. 1989. 451 pages. $79.95.

These days, businesses and even individual homeowners may encounter difficulties selling their properties because of the possible presence of hazardous wastes. Moreover, they could risk civil and criminal penalties even though they did not themselves dispose of the wastes. The author explains how to assess environmental risks; avoid, minimize, or allocate environmental liability; negotiate protections; minimize personal liability under Superfund; and determine the right insurance to cover environmental risk.

Standard Methods for the Examination of Water and Wastewater, 17th Edition. Lenore S. Clesceri, Arnold E. Greenberg, R. Rhodes Trussell, Eds. American Public Health Association, 1015 15th St., N.W., Washington, DC 20005. 1989. $120 (20% discount for APHA, AWWA, and WPCF members).

Standard Methods sets forth more than 300 methods, each with step-by-step procedures for the precise analysis of the chemical constituents of water and wastewater, as well as of sanitary quality and physical and biological characteristics. More than 60 methods have been updated and 30 new ones have been added. New material includes statistics; detection limits; dissolved gas supersaturation; and new methods for aluminum, selenium, and arsenic.

Indoor Air Pollution Control. Thad Godish. Lewis Publishers, Inc., P.O. Drawer 519, Chelsea, MI 48118. 1989. $59.95. 401 pages, cloth.

Indoor Air Pollution Control defines the indoor air pollution problem and discusses source control measures for pollutants such as asbestos, combustion gases, radon, formaldehyde, volatile organics, pesticides, and biogenic particles. The book also reviews public policy and regulatory issues and suggests mitigation practices on a case-history basis.

ENVIRONMENTAL INDEX SOURCE BOX

(1) Ditz, D. W. *International Environmental Affairs* 1989, *1*(3), 175. ***(2)*** Op. cit., p. 177. ***(3, 4)*** Op. cit., p. 180. ***(5, 6)*** Osherenko, G. *International Environmental Affairs* 1989, *1*(3), 204. ***(7, 8)*** New York State Department of Environmental Conservation; January 12, 1990; press release 90-11.

0013-936X/90/0924-0297$02.50/0

Organic Substances and Sediments in Water—Pedagogical symposium planned for the ACS meeting in Boston.

Chemical sciences are often an integral aspect of scientific and engineering processes perceived as nonchemical in nature. To improve knowledge of such situations and to facilitate communication among interdisciplinary contributors, the American Chemical Society, through its Committee on Science, has established a Pedagogical Symposium program. These tutorial symposia typically offer overview and research presentations for ACS members by experts in related fields.

The Environmental Chemistry Division of the ACS will conduct a major interdisciplinary research symposium, "Organic Substances and Sediments in Water," at the national meeting in Boston, MA, April 23–27, 1990. Additionally there will be a pedagogical symposium of the same title on Tuesday, April 24, 1990. Leading engineers and scientists engaged in water treatment, biodegradation, ecotoxicology, and marine–estuarine processes will be speaking. Their presentations are expected to be of broad interest to all chemists regardless of divisional affiliation.

The Environmental Chemistry Division of ACS welcomes all participants in the ACS national meeting, regardless of divisional affiliation, to attend the pedagogical symposium.

April 24 Boston, MA
Organic Substances and Sediments in Water
Organizer, Presiding, R. A. Baker, U.S. Geological Survey

8:30—Introductory remarks
8:45—The Formation and Control of Organic Contaminants in Drinking Water, *James A. Symons*, University of Houston
9:30—Biologically Mediated Transformations of Organic Contaminants, *Edward J. Bouwer*, Johns Hopkins University
10:15—Intermission
10:30—Environmental Response to Hazardous Chemicals, *Richard E. Speece*, Vanderbilt University
11:15—Modeling the Fate of Organic Chemicals in the Water Column and Sediment: Difficulties and Challenges, *Dominic M. DiToro*, Manhattan College
1:30—Coastal and Estuarine Toxic Chemical Pollution: What Do We Know? What Should We Know? *John W. Farrington*, Gordon Wallace, Anne McElroy, University of Massachusetts–Boston
2:15—Making the Transition of Toxicology to Ecotoxicology, *James R. Pratt*, Pennsylvania State University
3:00—Intermission
3:15—Application of Biotechnology to Water Quality Monitoring, Rita R. Colwell and *Ivor T. Knight*, University of Maryland
4:00—Panel discussion and audience participation
(A week-long research symposium of the same title contains 95 papers and five poster presentations to complement the tutorial program of seven lectures.)

March 27–28, 1990 Shreveport, LA
New Developments: Ozone in Water and Wastewater Treatment
International Ozone Association

Papers will deal with ozone generator feed gas systems, generator selection, laboratory and pilot research and testing programs, water and wastewater treatment plant operating experience, and full-scale system modification. Equipment purchase also will be discussed. Registration $170 for IOA members; $210 for nonmembers.

IOA–Pan American Committee, 83 Oakwood Ave., Norwalk, CT 06850; (203) 847-8169; Fax: (203) 847-2683.

April 8–12 Las Vegas, NV
International High Level Radioactive Waste Management Conference & Expo
American Society of Civil Engineers and others

This conference will cover subjects such as geochemistry of the waste environment, tectonics, transport processes, hydrology, health effects assessment, vitrified waste, storage, and public involvement.

IHLRWM Conference & Exhibit, American Society of Civil Engineers, 345 E. 47th St., New York, NY 10017.

May 1–2 Amherst, MA
Drinking Water and Public Health
University of Massachusetts

This conference will offer sessions on federal regulations and control strategies and their probable impact on the control of lead, radon, microbes, and hazardous-waste contamination of groundwater.

Charles E. Gilbert, School of Public Health, University of Massachusetts, Amherst, MA 01003-0081; (413) 545-3164; Fax: (413) 545-4692.

May 15–17 Philadelphia, PA
Second Forum on Innovative Waste Treatment Technologies: Domestic and International
EPA

This conference will introduce and highlight innovative treatment technologies that show actual performance results. It will emphasize selected international technologies and technologies developed through the Superfund Innovative Technology Evaluation (SITE) program.

JACA Corp., 550 Pinetown Road, Fort Washington, PA 19034; (215) 643-5466.

May 21–23 Bethesda, MD
New Directions in Cancer Risk Assessment
Society for Risk Analysis

This course presents an overview of methodologies, assumptions, and new research concerning risk assessments. Special emphasis will be given to new developments in pharmacokinetics; biomonitoring; and reproductive, immunological, and neurological risks. Registration $525; $425 for government employees.

Mary Oran, Office of Risk Analysis, Oak Ridge National Laboratory, P.O. Box 2008, Oak Ridge, TN 37831; (615) 574-8438; FTS: (615) 624-8438.

0013-936X/90/0924-0298$02.50/0

May 22–23 Santa Monica, CA
Profiting from Water
Water Research Associates, L.P.

The theme of the conference is business and investment opportunities in drinking water. Topics include ultraviolet disinfection, ozonation, reverse osmosis, ultrafiltration, and ultrapure water.

Lou Olmos, Water Research Associates, L.P., 12233 W. Olympic Blvd., Suite 152, Los Angeles, CA 90064; (213) 207-8277; Fax: (213) 207-1280.

June 4–15 Baltimore, MD
The Third Summer Institute in Environmental Health Studies
The Johns Hopkins University

This graduate-level and continuing-education course is aimed at professionals with responsibility for health, safety, and environmental matters in the public and private sectors. Subjects include toxicology, industrial hygiene, radiation, risk assessment and management, and risk communication.

Dr. Jacqueline Corn, School of Hygiene and Public Health, The Johns Hopkins University, 615 N. Wolfe St., Room 1003, Baltimore, MD 21205; (301) 955-2609.

June 10–13 Washington, DC
International Conference on Pollution Prevention: Clean Technologies and Clean Products
UNIDO

This conference will focus on pollution prevention and technologies developed for that purpose. There will be analytical presentations of their current status and expected future directions.

United Nations Industrial Development Organization, P.O. Box 300, A-1400 Vienna, Austria.

June 18–22 New Hampton, NH
A Gordon Research Conference on Environmental Sciences: Water
Gordon Research Conferences

The theme is transport and transformations of pollutants. Principal topics will encompass chemical processes in soil and fresh water, transport processes in surface and groundwater, atmospheric processes, biological degradation and accumulation processes, and surfactants. There will be poster sessions.

Ronald A. Hites, Department of Chemistry, Indiana University, Bloomington, IN 47405; (812) 855-0193; Fax: (812) 855-7802.

June 24–29 Pittsburgh, PA
83rd Annual Meeting & Exhibition of the Air & Waste Management Association
Air & Waste Management Association

There will be more than 100 sessions on issues such as management, incineration, indoor air quality, tropospheric ozone, acid precipitation, global climate change, and toxic chemicals.

Jon Fedorka, Air & Waste Management Association, P.O. Box 2861, Pittsburgh, PA 15230; (412) 232-3444.

July 9–12 Cincinnati, OH
24th Annual Conference on Trace Substances in Environmental Health
University of Missouri

Sessions will deal with low-level lead exposures, biological modeling of trace substances, risk assessment of radionuclides, and alternative disinfection technologies for treatment of drinking water and the risks involved.

Dr. D. D. Hemphill, Environmental Trace Substances Research Center, University of Missouri, 5450 S. Sinclair Rd., Columbia, MO 65203; (314) 882-2151; Fax: (314) 445-5848.

July 16–20 Washington, DC
Sixth Annual Waste Testing and Quality Assurance Symposium
EPA and American Chemical Society

Major topics include analytical test methods, mobility assessment methods, sampling, quality assurance, monitoring, and enforcement.

American Chemical Society, 1155 16th St., N.W., Room 205, Washington, DC 20036.

Aug. 27–30 Saskatoon, SK, Canada
Conference on Aquatic Systems in Semi-Arid Regions: Implications for Resource Management
National Hydrology Research Institute and Rawson Academy of Aquatic Science

Discussions center on topics such as saline lakes, inorganically turbid reservoirs, oligotrophic to hypereutrophic freshwater lakes, and fish and wildlife protection.

Scientific Information Division, National Hydrology Research Institute, 11 Innovation Blvd., Saskatoon, SK S7N 3H5, Canada; (306) 975-4022; Fax: (306) 975-5143.

Aug. 28–30 Baltimore, MD
Measuring Waterborne Trace Substances
Electric Power Research Institute

Papers will cover new and existing methods of sampling and analysis, including successful methods and those that fail by current standards.

Maureen Barbeau, Electric Power Research Institute, P.O. Box 10412, Palo Alto, CA 94303; (415) 855-2127; Fax: (415) 855-2954.

Sept. 11–13 Montreal, Canada
ENVIROSOFT 90
Computational Mechanics Institute

This conference emphasizes software for environmental engineering; surface and groundwater hydrology; pollution; mathematical modeling; and environmental chemistry, physics, and biology. Software for personal computers and new computer languages also will be discussed.

The Conference Secretariat, Computational Mechanics Institute, Ashurst Lodge, Ashurst, Southampton SO4 2AA, England, U.K.; (0) 42129 3223; Telex: 47388 Attn COMPMECH; Fax: (0) 42129 2853.

Oct. 23–25 Vienna, Austria
ENVIROTECH VIENNA 1990
International Society for Environmental Protection

The theme is current problems in hazardous-waste management and contaminated sites. Topics include thermal-waste processing; transport of hazardous waste, especially with respect to the Convention of Basel; risk assessment; and improved technologies for site cleanup. There will be a colloquy on international legal and technical strategies of avoidance and risk management of major accidents.

Dr. Bernhard Zimburg, Austrian Embassy, 2343 Massachusetts Ave., N.W., Washington, DC 20008; (202) 667-8158; Fax: (202) 483-2743; or ISEP-Secretariat, A - Vienna, Spittelauer Lände 3; (43) 222-344511 510; Fax: (43) 222 344511 299.

July 23–26, 1991 Beijing, China
International Symposium on Advances in Chemistry and Molecular Biology of Cancer Research
Beijing Polytechnic University

Sessions will cover topics such as the molecular mechanism of carcinogenesis, structure-carcinogenic activity relationships, chemical factors in the etiology of cancer, and the fate and control of chemical carcinogens. Conference organizers need to be informed by April 20, *1990*, who will present papers or posters and who will attend.

Prof. Zheng Qingying, CMBC Secretary-General, Center for Chemistry and Bioengineering of Cancer, Beijing Polytechnic University, Beijing 100022, China.

ES&T

ENVIRONMENTAL INDEX

Number of tons of chlorinated organic chemical wastes from Western Europe that were burned aboard incineration ships in the North Sea in the past 20 years: > 1 million

Year that incineration of chemical wastes aboard ships in the North Sea is scheduled to end: 1994

Cost for incineration of chlorinated chemical wastes aboard ships: about $100 per ton

Cost for incinceration at a conventional land-based facility: $200–$450 per ton

---

Number of international agreements on environment and conservation that the Soviet Union is a party to: 36

Number of above agreements that are multilateral: 24

Percentage of solid waste recycled in New York state: 10

Expected statewide recycling rate by 1997: 40%

Sources are listed on p. 297.

0013-936X/90/0924-0300$02.50/0

CIRCLE NUMBERS FOR FREE INQUIRY SERVICE

ES&T **MARCH, 1990** VALID THROUGH SEPT. 1990

Please circle appropriate numbers to receive additional information

READER SERVICE

1	2	3	4	5	6	7	8	9	10	11	12	13	14	15
16	17	18	19	20	21	22	23	24	25	26	27	28	29	30
31	32	33	34	35	36	37	38	39	40	41	42	43	44	45
46	47	48	49	50	51	52	53	54	55	56	57	58	59	60
61	62	63	64	65	66	67	68	69	70	71	72	73	74	75
76	77	78	79	80	81	82	83	84	85	86	87	88	89	90
91	92	93	94	95	96	97	98	99	100	101	102	103	104	105
106	107	108	109	110	111	112	113	114	115	116	117	118	119	120
121	122	123	124	125	126	127	128	129	130	131	132	133	134	135
136	137	138	139	140	141	142	143	144	145	146	147	148	149	150

Principal product to which my work relates:

- ☐ A. Oil/Gas/Petroleum
- ☐ B. Plastics/Resins
- ☐ C. Rubber
- ☐ D. Drugs/Cosmetics
- ☐ E. Food/Beverages
- ☐ F. Textile/Fiber
- ☐ G. Pulp/Paper/Wood
- ☐ H. Soaps/Cleaners
- ☐ I. Paint/Coating/Ink
- ☐ J. Agrichemicals
- ☐ K. Stone/Glass/Cement
- ☐ L. Metals/Mining
- ☐ M. Machinery
- ☐ N. Auto/Aircraft
- ☐ O. Instrument/Controls
- ☐ P. Inorganic Chemicals
- ☐ Q. Organic Chemicals
- ☐ R. Other Manufacturing
- ☐ S. Design/Construction
- ☐ T. Utilities
- ☐ U. Consulting Services
- ☐ V. Federal Government
- ☐ W. State Government
- ☐ X. Municipal Government
- ☐ Y. Education

NAME: _____

POSITION: _____

ORGANIZATION: _____

STREET: _____

CITY: _____

STATE: _____ ZIP: _____

TELEPHONE: (___ ___ ___) - ___ ___ ___ - ___ ___ ___ ___

NO POSTAGE
NECESSARY
IF MAILED
IN THE
UNITED STATES

BUSINESS REPLY MAIL

FIRST CLASS PERMIT NO. 209 WESTPORT, CT

POSTAGE WILL BE PAID BY ADDRESSEE

Environmental
Science & Technology

CENTCOM, LTD.
P.O. BOX 231
WESTPORT, CT 06881-9919

ES&T

Reader Service Reply Card

It's computer processed for fast response to your inquiries AND, IT'S FREE

CLASSIFIED SECTION

CLASSIFIED ADVERTISING RATES

Rate based on number of insertions used within 12 months from date of first insertion and not on the number of inches used. Space in classified advertising cannot be combined for frequency with ROP advertising. Classified advertising accepted in inch multiples only.

Unit	1-T	3-T	6-T	12-T	24-T
1 inch	$105	$100	$95	$90	$85

(Check Classified Advertising Department for rates if advertisement is larger than 10″.)
SHIPPING INSTRUCTIONS:
Send all material to

Environmental Science & Technology
Classified Advertising Department
500 Post Road East
P.O. Box 231
Westport, CT 06881
(203) 226-7131
FAX: (203) 454-9939

PENNSTATE
Harrisburg The Capital College

FACULTY POSITION

Penn State-Harrisburg — Tenure track position starting August 1990. Individual will be teaching in programs leading to a B.S. in Environmental Engineering Technology, a Master of Engineering, and a Master of Environmental Pollution Control. A strong background in chemistry and engineering, and being able to teach environmental chemistry and microbiology is expected. Applicants should also desire involvement in research, service activities, and supervising master papers.

Qualifications: Ph.D. preferred and relevant experience in environmental engineering and/or sciences. Penn State-Harrisburg is a senior level college and graduate center located 8 miles southeast of the state capital at Harrisburg.

Apply to Dr. William A. Welsh, Jr., Division Head, Science, Engineering & Technology, c/o Mrs. Sandra Jackson, Box EST, Penn State-Harrisburg, The Capital College, Middletown, PA 17057. Position is open until filled.

An Affirmative Action/Equal Opportunity Employer
Women and Minorities Encouraged to Apply.

Join A Talented Team

EMCON ASSOCIATES

EMCON Associates, a leading environmental engineering and consulting firm, has an immediate opportunity in our San Jose corporate headquarters.

Senior Risk Assessment Specialist/Manager

Responsible for:

- Leading a team of professionals in quantitative risk assessment activities
- Agency & client liaison
- Report preparation
- Project management & business development

Minimum requirements are MS or Ph.D. in Toxicology, Environmental Health Science or related field and a minimum of 3 years related experience. Requires a strong knowledge of state and federal risk assessment procedures and excellent oral and written communication skills.

EMCON offers an excellent compensation and benefits package, including Employee Stock Purchase and 401(k) Plans. Please send your resume to: **EMCON Associates, 1921 Ringwood Avenue, Dept. C-005A, San Jose, CA 95131.** An Equal Opportunity Employer.

***Regional Offices* — California:** San Jose, Sacramento, Fresno, Burbank, Orange County & Ventura areas; **Washington:** Bothell, Kelso; **Oregon:** Portland; **Arizona:** Phoenix.

INDOOR AIR QUALITY

SENIOR SCIENTIST / PROGRAM MANAGER

GEOMET's Indoor Environment Division conducts research related to a variety of environmental stressors such as microbial aerosols, chemical pollutants, extremely low frequency electromagnetic fields and ionizing radiation.

We are seeking an individual with an advanced degree in analytical/environmental chemistry and experience in field monitoring and instrumentation. Demonstrated background in measurement of air quality and building ventilation parameters is essential. Good managerial and publication track records highly desirable.

GEOMET offers competitive salary, comprehensive benefits package, and outstanding opportunities for career advancement.

Please send resume and salary history to:

Personnel Manager
GEOMET Technologies, Inc.
20251 Century Blvd.
Germantown, MD 20874

EOE

Recruitment Notice

HEALTH EFFECTS SCIENTIST

The Chicago Office of the United States Environmental Protection Agency has an opening for a Health Effects Scientist to evaluate human health and toxicological matters relative to toxic environmental pollutants. Ability to assess, quantify, and communicate human health risk from the exposure to toxic chemicals, such as those at hazardous waste sites, and knowledge of computer modeling techniques is essential.

Salary range is $35,852 to $55,381 depending on your experience. All applications must be received or postmarked by March 30, 1990.

For application forms please contact:

U.S. Environmental Protection Agency
Attn: Personnel Branch, 16th Floor
(Recruitment Notice, RN-10)
230 South Dearborn Street
Chicago, Illinois 60604
(312) 353-2026

U.S. citizenship is required.

Applications will be considered without regard to race, religion, color, sex, national origin, or any other non-merit factors.

Carnegie Mellon University

Graduate Study in Engineering and Public Policy (EPP): The EPP Graduate Program leads to a research-based Ph.D. specializing in policy issues in areas including: mathematical modeling of energy and environmental systems; technical and economic issues of peace and international security; and risk analysis. We are particularly interested in a doctoral student in environmental science with Russian language skills to work on Soviet environmental problems. Applicants must hold a Bachelor's Degree in engineering, physical sciences, or mathematics. Education or experience beyond the Bachelor's Degree is very desirable. Contact **Dr. Indira Nair, Engineering and Public Policy (04), Carnegie Mellon University, Pittsburgh, PA 15213.**

ENDOWED PROFESSORSHIP in CHEMICAL & ENVIRONMENTAL ENGINEERING

The University of Alabama is pleased to announce the establishment of an Endowed Professorship in Chemical & Environmental Engineering in the Chemical Engineering Department. Nominations and applications are invited for this key leadership position in the University's environmental research program. Qualified applicants will have a proven track record in environmental research, possess good administrative skills, and hold an earned doctorate in engineering or science. The successful candidate will be expected to develop a funded multi-disciplinary research program, teach graduate courses, and foster relationships with personnel from industry, government agencies, and other academic institutions.

Applicants should send a resume which includes three references to:

Dr. Verle N. Schrodt, Assistant Dean
College of Engineering
The University of Alabama
P.O. Box 870200, Tuscaloosa, AL 35487-0200

The University of Alabama is an EO/AA employer.

ENVIRONMENTAL ENGINEER

Environmental Engineer to provide process/project engineering input to a wide variety of projects involving municipal water and wastewater treatment, industrial water and wastewater, solid waste, and hazardous waste projects. Perform computations, draft documents or portions thereof, produce designs/plans, participate in studies and pilot plant operations, organize and perform analysis on data.

Requirements: Doctor of Philosophy in Environmental Engineering. A minimum of one year working experience in environmental engineering. Educational emphasis and research in areas of water treatment and/or hazardous wastes with through background in laboratory analysis and procedures.

Position and job site interviewing will be conducted, for a full-time position with a consulting firm, in Santa Ana, California.

Salary: $42,000 per year plus benefits.

Send this ad and your resume, no later than March 28, 1990, to: **Job #BLW11788, P.O. Box 9560, Sacramento, CA 95823-0560.**

ENVIRONMENTAL RESEARCH SCIENTIST

The Research & Test Department of the Association of American Railroads has an immediate opening for a scientist interested in research on environmental issues facing the railroad industry. Skills in experimental design, statistical inference, research planning, and written and oral communication are essential. Training in any of the following areas would also be useful: chemistry, environmental engineering, EPA regulations, environmental fate of pollutants, pollution mitigation technology. Responsibilities will include development and oversight of research projects on industry related environmental issues, evaluation of proposed regulation and legislation, and interaction with railroad officers. MS or PhD in chemistry, environmental science, environmental engineering, or other appropriate discipline required. Approximate starting salary range $40K and excellent benefits. Applicants should send a letter of interest, resume, names of three references, and copies of recent publications or reports, to: **Christopher Barkan, Environmental & Hazardous Materials Research Division, EST, Research & Test Department, Association of American Railroads, 50 F St., N.W., Washington, DC 20001.** Application materials should be received as soon as possible. The AAR is an Equal Opportunity Employer, M/F/H/V.

CLASSIFIED ADVERTISING RATES

Rate based on number of insertions used within 12 months from date of first insertion and not on the number of inches used. Space in classified advertising cannot be combined for frequency with ROP advertising. Classified advertising accepted in inch multiples only.

Unit	1-T	3-T	6-T	12-T	24-T
1 inch	$105	$100	$95	$90	$85

(Check Classified Advertising Department for rates if advertisement is larger than 10″.)

SHIPPING INSTRUCTIONS:

Send all material to

Environmental Science & Technology
Classified Advertising Department
500 Post Road East
P.O. Box 231
Westport, CT 06881
(203) 226-7131

professional consulting services directory

INDEX TO THE ADVERTISERS IN THIS ISSUE

Advertising Management for the American Chemical Society Publications

CENTCOM, LTD.

President
James A. Byrne

Executive Vice President
Benjamin W. Jones

Clay S. Holden, *Vice President*
Robert L. Voepel, *Vice President*
Joseph P. Stenza, *Production Director*

500 Post Road East
P.O. Box 231
Westport, Connecticut 06880
(Area Code 203) 226-7131
Telex No. 643310
Fax No. (203) 454-9939

ADVERTISING SALES MANAGER
Bruce Poorman

ADVERTISING PRODUCTION MANAGER
Jane F. Gatenby

SALES REPRESENTATIVES

Philadelphia, Pa. . . . CENTCOM, LTD., GSB Building, Suite 405, 1 Belmont Ave., Bala Cynwyd, Pa. 19004 (Area Code 215) 667-9666, FAX: (215) 667-9353

New York, N.Y. . . . John F. Raftery, CENTCOM, LTD., 60 E. 42nd Street, New York 10165 (Area Code 212) 972-9660

Westport, Ct. . . . Edward M. Black, CENTCOM, LTD., 500 Post Road East, P.O. Box 231, Westport, Ct 06880 (Area Code 203) 226-7131, FAX: (203) 454-9939.

Cleveland, OH. . . . Bruce Poorman, John Guyot, CENTCOM, LTD., 325 Front St., Berea, OH 44017 (Area Code 216) 234-1333, FAX: (216) 234-3425

Chicago, Ill. . . . Michael J. Pak, CENTCOM, LTD., 540 Frontage Rd., Northfield, Ill 60093 (Area Code 708) 441-6383, FAX: (708) 441-6382

Houston, Tx. . . . Michael J. Pak, CENTCOM, LTD., (Area Code 708) 441-6383

San Francisco, Ca. . . . Paul M. Butts, CENTCOM, LTD., Suite 1070, 2672 Bayshore Frontage Road, Mountainview, CA 94043 (Area Code 415) 969-4604

Los Angeles, Ca. . . . Clay S. Holden, CENTCOM, LTD., 3142 Pacific Coast Highway, Suite 200, Torrance, CA 90505 (Area Code 213) 325-1903

Boston, Ma. . . . Edward M. Black, CENTCOM, LTD., (Area Code 203) 226-7131

Atlanta, Ga. . . . John F. Guyot, CENTCOM, LTD., (Area Code 212) 972-9660

Denver, Co. . . . Paul M. Butts, CENTCOM, LTD., (Area Code 415) 969-4604

RESEARCH

A Compact Coiled Denuder for Atmospheric Sampling†

David Y. H. Pui,*,‡ Charles W. Lewis,§ Chuen-Jinn Tsai,‡ and Benjamin Y. H. Liu‡

Particle Technology Laboratory, Mechanical Engineering Department, University of Minnesota, 111 Church Street S. E., Minneapolis, Minnesota 55455, and U.S. Environmental Protection Agency, Atmospheric Research and Exposure Assessment Laboratory, Research Triangle Park, North Carolina 27711

■ A compact coiled denuder has been designed and its performance evaluated both theoretically and experimentally. The design is based on special features of laminar flow in a curved tube, which significantly enhance the mass-transfer Sherwood number governing gas collection at the wall. At 10 standard L/min (slpm) the gas collection efficiency for SO_2, using a sodium carbonate/glycerine wall coating, was measured to be 99.3 ± 0.5%, while losses for particles in the range of 0.02–2.5-μm diameter averaged well under 5%.

Introduction

Diffusion denuders have become increasingly popular for separating reactive gases from particles as a means to measuring their separate concentrations (*1–5*). The ideal denuder is a channel whose inner wall is a sink for a gas and is operated so that the trace reactive gas is collected with 100% efficiency on the wall while 100% of the particles traverse the channel, thus being available for collection on a downstream substrate in an airstream free of the reactive gas. If the gaseous sink is a reactive coating, the gas concentration can be determined by extracting the coating and measuring the amount of chemically transformed gas it contains. Denuders have proved to be particularly valuable in nitrogenous atmospheric chemistry, enabling accurate and artifact-free measurements of particulate nitrate and gaseous nitric and nitrous acids to be made simultaneously (*6*).

The invention of the annular denuder (*7*) significantly increased the practicality of denuders by reducing the required channel length to approximately 20 cm, about an order of magnitude less than that needed for a hollow straight tube denuder. However, since an annular denuder system may use as many as four such units (with coatings for different gases) in series along a common axis, the dimensions of the overall system can be inconvenient. Hence an even more compact denuder design would be desirable.

The denuder design examined in this article is a 1 cm i.d. glass tube bent into a three-turn, 10 cm diameter helical coil, intended to operate at 10 standard L/min (slpm). In the following sections the theoretical and experimental aspects of gas collection efficiency and particle transmission for this design will be presented.

Table I. Heat- and Mass-Transfer Correspondences

heat transfer	P_r	N_u	T	$\dot{q}$
mass transfer	S_c	S_h	C	$\dot{m}$

Theoretical Considerations

Heat- and Mass-Transfer Analogy. Because of the analogy between heat and mass transfer, researchers in these fields have often calculated the rate of heat transfer from mass-transfer data and vice versa. The corresponding parameters that are used in heat- and mass-transfer analogy are listed in Table I.

In Table I, P_r is the Prandtl number, which is defined as ν/α with ν the kinematic viscosity and α the thermal diffusivity; S_c is the Schmidt number, which is defined as ν/D with D the mass diffusivity; N_u is the Nusselt number, which is defined as $h(2a)/\kappa$ with h the heat-transfer coefficient, a the tube radius, and κ the thermal conductivity; S_h is the Sherwood number, which is defined as $k(2a)/D$ with k the mass-transfer coefficient; T is temperature; C is mass concentration; $\dot{q}$ is heat-transfer rate; $\dot{m}$ is mass-transfer rate. In the following analysis, heat-transfer relationships that will be used in the gas collection efficiency calculations are written in the corresponding mass-transfer forms.

Gas Collection Efficiency. The present coiled denuder design is based on the special features of laminar flow in curved pipes. This flow is characterized by secondary flow in any cross-sectional plane normal to the main flow, and an axial velocity profile that is skewed to the outer wall of the pipe due to centrifugal force. Figure 1 shows the secondary flow streamlines for a curved pipe, where the counterrotating vortexes continuously bring fluid in the interior near the pipe wall, with the result that mass- (and heat-)transfer efficiencies are significantly increased relative to the straight pipe case.

The nature of this flow depends on the Dean number D_e and curvature ratio R_o. Curvature ratio R_o is defined as R/a with R the radius of the coil and a the radius of the tube. The Dean number is defined as $D_e = R_e/\sqrt{R_o}$ with R_e the flow Reynolds number. The heat-transfer problem for fully developed flow in curved pipes has been solved analytically (*8–11*). Numerical studies of flow and heat transfer in curved pipes have been conducted (*12–15*). The heat-transfer analysis by Mori and Nakayama et al. (*8–10*) was based on the assumption that the flow can be

† Particle Technology Laboratory Publication no. 679.
‡ University of Minnesota.
§ U.S. Environmental Protection Agency.

0013-936X/90/0924-0307$02.50/0

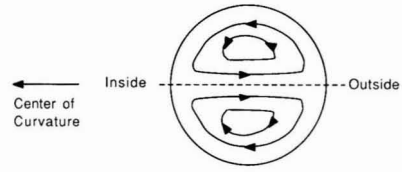

Figure 1. Secondary flow streamlines in the cross-sectional plane of the curved tubes. The axial velocity profile is skewed toward the outside of the tube.

divided into a core region and a boundary layer. This theoretical model was validated by the authors themselves (*8*) and consequently was considered to be the most rigorous for use in the present work.

Although turbulent flow is associated with a larger mass-transfer Sherwood number than laminar flow, larger inertial impaction loss of particles is, unfortunately, also likely with the former. Therefore in the current coiled denuder design, the flow is restricted to the laminar regime.

In a straight pipe, assuming the flow is fully developed and the concentration profile is developing, the mass-transfer efficiency, η (=1 − P, P is penetration), can be calculated as (from eq 8-31 in ref 16)

$$\eta = 1 - P \tag{1a}$$

$$P = \frac{C_{out}}{C_{in}} = \exp\left(-\frac{\pi L D}{Q}\bar{S}_h\right) \tag{1b}$$

where C_{in} is the inlet concentration, C_{out} is the outlet concentration, L is the pipe length, D is the gas diffusivity, Q is the flow rate, and $\bar{S}_h$ is the mean mass-transfer Sherwood number over the pipe length, equal to 3.66 for a fully developed temperature profile with constant wall temperature condition. In a curved pipe, following the suggestion made by Mori and Nakayama (*9*, *10*), the mass-transfer efficiency can also be calculated by using eq 1 if the mean mass-transfer Sherwood number is known.

In the laminar flow regime, Mori and Nakayama (*9*, *10*) showed that for fully developed flow (both velocity and concentration profiles), the mean mass-transfer Sherwood number, $\bar{S}_h$, in a curved pipe can be approximated as

$$\bar{S}_h = \frac{0.864}{\zeta} D_e^{1/2}(1 + 2.35 D_e^{-1/2}) \tag{2}$$

where

$$\zeta = \frac{2}{11}\left[1 + \left(1 + \frac{77}{4}\frac{1}{S_c^2}\right)^{1/2}\right] \quad \text{if } \zeta \le 1 \text{ (or } S_c \ge 1) \tag{3}$$

or

$$\zeta = \frac{1}{5}\left[2 + \left(\frac{10}{S_c^2} - 1\right)^{1/2}\right] \text{ if } \zeta \ge 1 \text{ (or } S_c \le 1) \tag{4}$$

where ζ is the thickness ratio of the concentration boundary layer to the momentum boundary layer.

Equation 2 is based on the assumption of a fully developed concentration boundary layer. At the point of entry, the Sherwood number has its maximum value since the concentration boundary layer is still developing. Figure 2 shows two best fit curves obtained from data of Sparrow and Chrysler (*17*). It shows the normalized Sherwood number S_h/S_h^* (S_h^* is the Sherwood number for a fully developed concentration profile) versus dimensionless tube length L/a at R_e = 5000 and 8200, when the flow can still be considered as laminar since both Reynolds numbers are

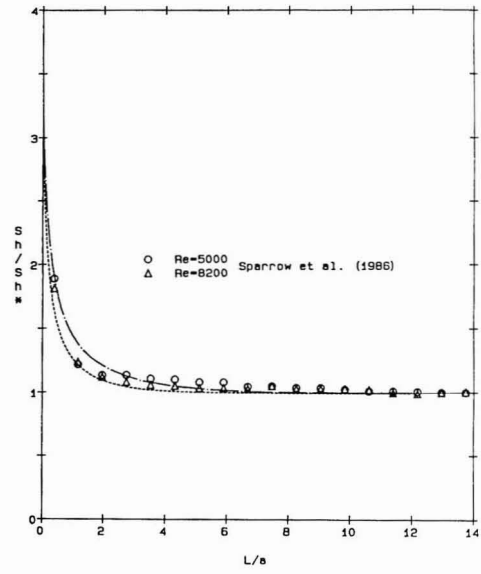

Figure 2. Normalized Sherwood number versus normalized tube length.

lower than the critical value 9900. [From Ito (*18*) the critical Reynolds number is $R_{e,cr} = 2 \times 10^4(R_o)^{-0.32} = 2 \times 10^4(9)^{-0.32} = 9900$. Ito's equation is valid for $R_o \le 860$; when $R_o > 860$, $R_{e,cr}$ approaches 2000–3000. Note that the present Reynolds number is 1407.] It is seen that the normalized Sherwood number quickly approaches unity monotonically as the concentration profile becomes fully developed. This Sherwood number length dependence is similar to the straight pipe case (*16*). The effect of the concentration entry length is to increase the overall mass-transfer efficiency or decrease penetration. To account for this entry length effect, a correction factor f_1, which is always smaller than 1.0, needs to be included in eq 1 as

$$P = \frac{C_{out}}{C_{in}} = f_1 \exp\left(-\frac{\pi L D}{Q}\bar{S}_h\right) \tag{5}$$

Because the dependence of Sherwood number on length is similar for curved and straight pipe flows, factor f_1 can be found by considering the entry length effect in a straight pipe flow, as follows.

In a straight pipe, assuming the flow is hydrodynamically fully developed and the concentration profile is still developing, the penetration can be calculated from the Gormley–Kennedy equation (*19*) as

$$P = 0.819\exp(-11.5\xi) + 0.0975\exp(-70.1\xi) + 0.0325\exp(-179\xi) \quad \text{for } \xi > 0.007 \tag{6}$$

where $\xi = DL/Q$. If ξ is large enough, only the first term in the right-hand side of the above equation is important. The coefficient 11.5 in the exponent is simply the product of π and $\bar{S}_h$, 3.66, which is the Sherwood number for fully developed flow in concentration, in the case of constant (zero) wall concentration. Comparing eq 5 and 6, it is seen that factor f_1 is 0.82 for large ξ. Alternatively, one can take the ratio of penetrations represented by eq 6 and 5 and plot the correction factor f_1 versus tube length as shown in Figure 3 assuming a = 0.5 cm, D = 0.136 cm^2/s, and three different flow rates of 5, 10, and 15 slpm. It is seen that factor f_1 approaches 0.82 when the tube length is greater than 30, 60, and 90 cm at flow rates of 5, 10, and 15 slpm, respectively. Therefore, in the present coiled

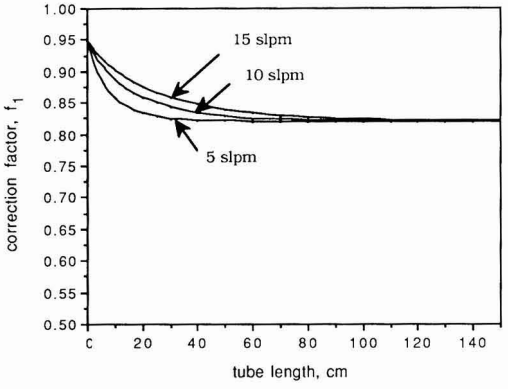

Figure 3. Correction factor f_1 versus tube length at different flow rates.

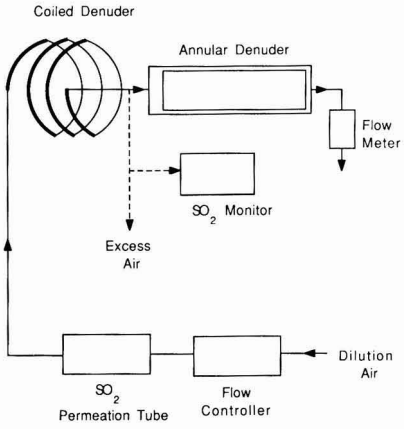

Figure 4. Experimental setup for measuring gas collection efficiency.

denuder design where the nominal flow rate is 10 slpm and the tube length is greater than 60 cm, the gas collection efficiency can be calculated as

$$\eta = 1 - P = 1 - 0.82 \exp\left(-\frac{\pi LD}{Q}\bar{S}_h\right) \qquad (7)$$

where the mean Sherwood number $\bar{S}_h$ can be calculated from eq 2. The present coiled denuder geometry gives a Sherwood number of 21.996, which is ~6 times that of straight pipe, 3.66. Hence, mass-transfer efficiency in coiled tubes is expected to be significantly larger than that in hollow straight tubes.

Particle Loss. Particle loss in any transport system can originate from many different mechanisms such as gravitational settling, diffusion, inertial impaction, and turbulent deposition. A concise review of various particle loss mechanisms in straight pipe flow can be found in ref 20. In a coiled tube, inertial impaction loss is important for particles greater than 1.0 μm in aerodynamic diameter, while diffusion loss is important for submicron particles. Experimental study for particle loss in a 90° bend by Pui et al. (*21*) indicated that inertial impaction loss is negligible when the particle Stokes number is smaller than 0.1. Using the numerical results obtained by Tsai et al. (*15*), an attempt was made to calculate the loss in one 90° bend and multiply it by 12 (the coiled denuder contains 12 90° bends) to obtain the total loss in the coiled denuder. However, since the flow inside the coiled denuder eventually becomes fully developed, the developing flow assumption in the numerical work resulted in an underestimation of inertial impaction loss as compared to the experimental results. On the other hand, a separate numerical study assuming a fully developed profile resulted in an overestimation of inertial impaction loss. This indicates that further numerical study of particle loss in coils would be desirable. For the purpose of the present study, an empirical fit to the inertial impaction loss, Loss_I, was used.

We were similarly unsuccessful in obtaining an analytical solution to diffusion loss, Loss_D, in a coiled denuder. Again, an empirical fit was used. Assuming both Loss_I and Loss_D are small, total particle loss in a coiled denuder can be written as

$$\begin{aligned}\text{loss (\%)} &= [1.0 - (1 - \text{Loss}_D)(1 - \text{Loss}_I)] \times 100 \\ &\approx [\text{Loss}_D + \text{Loss}_I] \times 100 \qquad (8)\end{aligned}$$

In the remainder of this article, we present the experimental characterization of the resulting coiled denuder design, which has achieved the design objectives of both high gas collection efficiency and low particle loss.

Experimental Methods and Results

Gas Collection Efficiency and Capacity. Gas collection efficiency measurements using SO_2 were performed with the experimental arrangement shown in Figure 4. The basis of the measurements was to determine the amounts of SO_2 simultaneously collected in the coiled denuder and in an efficient downstream collector, an annular denuder (University Research Glassware Co., Model 2000-30B). The efficiency can then be calculated from

$$\text{coil efficiency (\%)} = \frac{M_{\text{coil}}}{M_{\text{coil}} + M_{\text{annular}}} \times 100 \qquad (9)$$

where each M is the mass of SO_2 collected on the specified component.

For each measurement set the previously roughened (by sandblasting with no. 100 grain carborundum) interior wall of the coiled denuder was coated with a Na_2CO_3/glycerine solution in a methanol and distilled water mixture, in the manner previously described (*6*). The same coating was applied to the annular denuder. After exposure to the SO_2 gas stream both denuders were extracted (*6*) and the extracts were analyzed for both sulfite and sulfate by ion chromatography. Sulfur dioxide reacts with Na_2CO_3 to form sulfite, but since this gradually oxidizes to sulfate, the total amount of collected SO_2 must be inferred from the concentrations of both sulfur species. Sodium carbonate/glycerine coating solution concentrations of 1%/1%, the "standard" coating, and 5%/5% were both used in separate experiments. SO_2 breakthrough experiments were conducted for both coating solutions, using the alternative arrangement shown by dashed lines in Figure 4, to ensure that SO_2 sampling times for the efficiency measurements were shorter than the time for which coating depletion was first perceptible.

Figure 5 shows a typical breakthrough result. The TECO Model 43 pulsed fluorescence SO_2 analyzer used has a detection limit near 1 ppb, compared with the SO_2 test concentration of ~70 ppb. A breakthrough product of 700 ppb·h, or 1 mg of SO_2, can be inferred from Figure 5. It must be understood that this value is only a lower limit for the device's capacity under typical field conditions. This is because the laboratory measurements happened to be performed at extremely low relative humidity, estimated to be <10%. In general, the capacity of the coiled denuder should be similar to that of the previously mentioned annular denuder, since the wall areas of the two

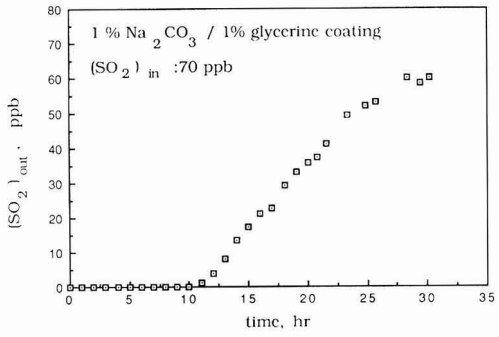

Figure 5. SO_2 breakthrough for coiled denuder.

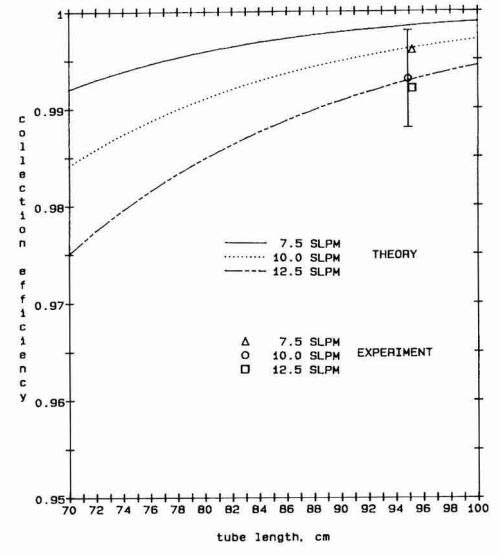

Figure 6. Coiled denuder gas collection efficiency versus tube length at different flow rates.

devices are nearly the same.

From a total of six determinations at 10 slpm the coiled denuder SO_2 gas collection efficiency was found to be 99.3 ± 0.5% (mean ± SD). One measurement each at 7.5 and 12.5 slpm gave efficiencies of 99.6 and 99.2%, respectively. The comparison of theory (eq 7) and experiment shown in Figure 6 indicates resonable agreement. Finally, three runs at 10 slpm were performed with the coiled denuder replaced by a second annular denuder. The annular denuder efficiency was found to be ≥99.9% in all cases, consistent with its use as an efficient downstream collector for the coiled denuder efficiency measurements.

Particle Loss. Particle loss measurement has been performed for particle sizes ranging from 0.015 to 5.4 μm. Results for monodisperse aerosol between 1.0 and 5.4 μm aerodynamic diameter were obtained with a vibrating orifice aerosol generator (TSI Model 3450) operated as part of the experimental system shown in Figure 7a. The monodispersity of the aerosol was monitored by an Aerodynamic Particle Sizer (APS, TSI Model 33). The liquid used in the aerosol generator consisted of oleic acid dissolved in denatured alcohol and containing a small quantity of uranine (1 g/L) as a fluorescent tracer. That is, the amounts of uranine measured on the coiled denuder and downstream filter are proportional to the amounts of particles deposited on these components. The solution

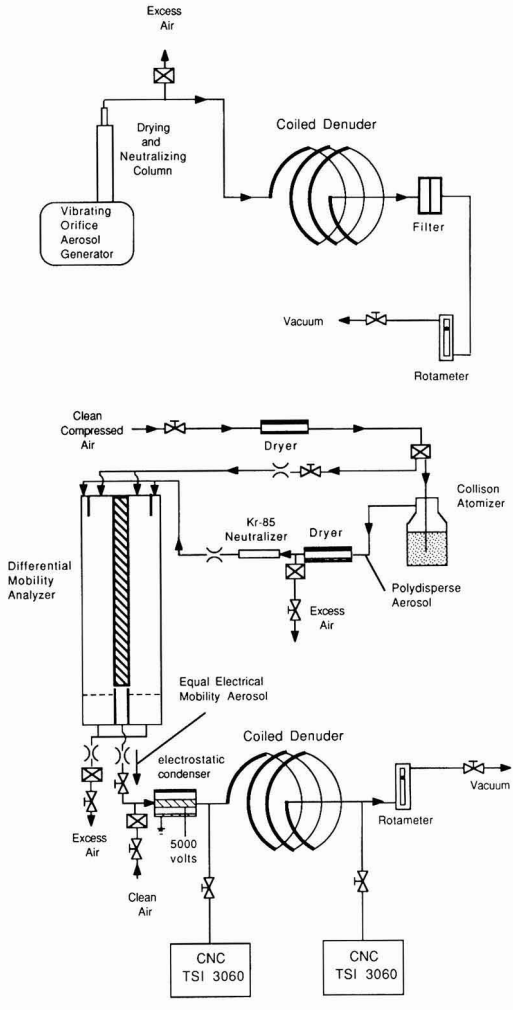

Figure 7. (a) Schematic diagram of particle loss test system, $D_p \geq 1.0$ μm. (b) Schematic diagram of particle loss test system, $D_p < 1.0$ μm. (neutral particles)

used to wash the filter and denuder was 15 or 30 mL of 0.001 N NaOH. The deposited particle mass is proportional to the product of the measured uranine concentration and the amount of washing solution used. The particle loss in the denuder was then calculated from

$$\text{loss (\%)} = \frac{M_{\text{coil}}}{M_{\text{coil}} + M_{\text{filter}}} \times 100 \qquad (10)$$

where M_{coil} and M_{filter} are the deposited particle masses in the coiled denuder and filter, respectively. Particle loss was determined at three different flow rates, 7.5, 10, and 12.5 slpm. The accuracy of the measurements was estimated to be ±1% for particles from 1 to 3 μm and ±3% for particles above 3 μm in aerodynamic diameter.

For submicron particles, the experimental system shown in Figure 7b was used. A Collison atomizer generated polydisperse aerosol by spraying NaCl solution of 0.05, 0.5, or 10% volume concentration. The particles were dried in a diffusion dryer and passed through a ^{85}Kr neutralizer. The polydisperse aerosol was then classified by a differential mobility classifier (DMA, TSI Model 3702). By varying the voltage supplied to the center rod inside the

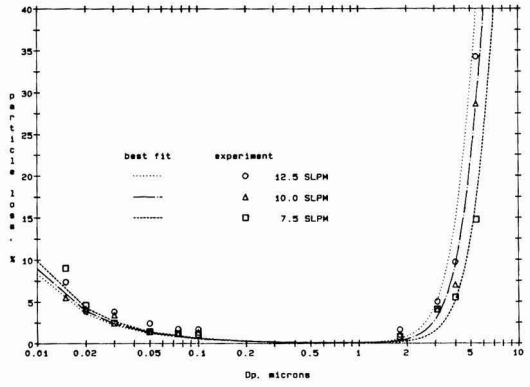

Figure 8. Total particle loss in coiled denuder at three different flow rates (neutral particles).

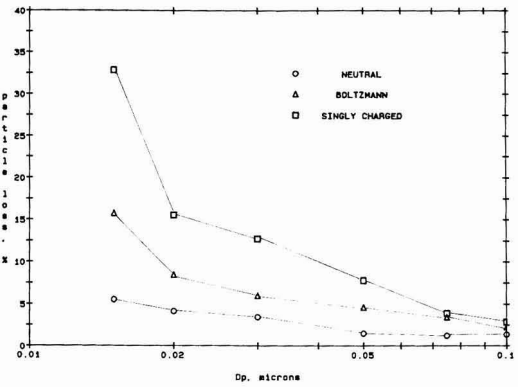

Figure 9. Effect of different charge states of test aerosol on particle loss, 10 slpm.

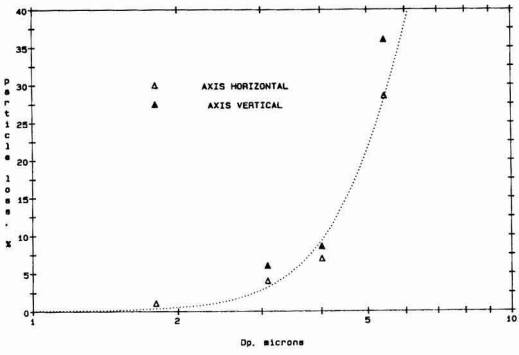

Figure 10. Effect of orientation on particle loss at 10 slpm.

DMA a monodisperse aerosol of equal electric mobility can be generated, as described by Liu and Pui (22). Most of the monodisperse submicron particles emerging from the DMA carry a single elementary charge. To obtain neutral particles for the experiment, this aerosol was passed through an electrostatic condenser to remove all charged particles. Two other tests were also conducted using Boltzmann equilibrium and singly charged aerosols to investigate the effect of electrical charge on particle loss. For the singly charged particle loss test, the aerosol coming out of the DMA was used directly. The Boltzmann equilibrium aerosol was obtained by neutralizing the aerosol before entering the coiled denuder. Downstream (C_{out}) and upstream (C_{in}) aerosol concentrations were measured by condensation nuclei counters (CNC, TSI Model 3060). Particle loss can then be computed as $1 - C_{out}/C_{in}$. The test was conducted at the same three previous flow rates. The accuracy of the particle loss results was estimated to be ±2% for particles greater than 0.02 μm and ±4% for particles less than 0.02 μm.

A fit to the experimental results for particles greater than 1 μm can be expressed in the following form:

$$\text{Loss}_I = 1/(1 + 0.00177St_k - 2.24) \qquad (11)$$

For diffusion loss of submicron particles the conventional Gormley–Kennedy equation for a straight tube was found to underestimate the experimental particle loss in the coiled denuder by a factor of 2–3. By use of a form similar to that for particle loss in straight tube, a fit to the experimental neutral particle loss data for particles smaller than 1 μm resulted in the following form:

$$\text{Loss}_D = 1.83\xi_1^{2/3} - 1.26\xi_1 \qquad (12)$$

where $\xi_1 = (\pi LD/11.5\,Q)\bar{S}_h$. Note for a straight tube, the coefficients of the first and second terms are 5.5 and 3.77, respectively, with ξ_1 replaced by LD/Q (eq 7.29 in ref 23).

Figure 8 shows the experimental total particle losses, including both the inertial impaction and diffusion losses, and those given by eq 8 at 7.5, 10, and 12.5 slpm. Note the diffusion losses refer to neutral particles. Since denuders are generally used with preclassifier inlets having cut points near 2.5 μm, the high losses measured above this particle size are unimportant. The submicron neutral particle loss is also small. At 0.015 μm, the loss is 6 ± 4%, and at 0.1 μm the loss is 2 ± 2%.

The results shown in Figure 8 apply for the test made with neutral particles in the submicron range. The effect of different charge states of test aerosol on submicron particle loss is shown in Figure 9. It is seen that the aerosol charge enhances the loss substantially. The neutral aerosol always has the smallest loss, with increasingly higher losses for Boltzmann equilibrium and singly charged states, respectively. For use of this apparatus in atmospheric sampling, the test results for the Boltzmann equilibrium case are the most relevant. The neutral particle losses were very reproducible, but the Boltzmann and singly charged tests showed considerably day to day variation. This is the reason for emphasizing the neutral particle results in this article. Charges in relative humidity were undoubtedly an important factor in this variation, but we have no comprehensive understanding of the effect.

While extremely low humidity will likely impair the device's operation, due to electrostatic and premature coating depletion effects, very high humidity may also be troublesome: the hygroscopicity of the glycerine in the coating may accumulate so much water that the coating may run off the denuder surfaces. Some control of this can be achieved by decreasing the glycerine content of the coating solution.

The effect of orientation on particle loss was also investigated and is shown in Figure 10 for particles larger than 1 μm. It is seen that the total particle loss is only slightly higher when the coiled denuder axis is vertical, compared to the horizontal case. Hence, it is concluded that the coiled denuder can be operated in any orientation.

The particle test data presented above apply to a smooth uncoated tube. Limited measurements have shown that results for an uncoated sand blasted tube are similar. Extensive measurements (*24*) comparing particle losses for coated versus uncoated *annular* denuders have shown smaller losses for the coated cases, presumably because of

Table II. Coiled Denuder Description

material	glass
tube i.d., cm	1
coil diam, cm	10
no. of turns	3
uncoiled tube length, cm	95
axial length, cm	6
flow rate, slpm	10
Reynolds number	1407
SO_2 collection effic, %	99.3 ± 0.5
neutral particle loss, %	
2.5 μm (St_k = 0.0086)	1 ± 1
1.0 μm	0 ± 1
0.1 μm	2 ± 2
0.015 μm	6 ± 4

a reduction of electrostatic effects from the electrical conductivity of the coating. It can be anticipated that the same will hold for the coiled denuder.

Summary

A 10 slpm coiled denuder has been designed and experimentally characterized. Its geometrical parameters and operating characteristics are summarized in Table II. The gas collection efficiency for SO_2 exceeds 99% and thus is comparable with annular denuder efficiencies. Experiment has shown that the particle loss is small for neutral particles in the size range 0.015–2.5 μm. Particle loss measurements also indicate that the unit can operate equally well in any orientation. The short axial length (6 cm) of the coiled denuder has the advantage that a denuder train of multiple units in series will have a total length that is substantially less than a corresponding train of annular denuders.

Glossary

a	tube radius, cm
C	mass (particle) concentration, g/cm³ (no./cm³)
	C_{out}, outlet concentration; C_{in} inlet concentration
C_c	slip correction factor
c	specific heat at constant pressure, erg/(g K)
D	mass diffusivity, cm²/s
D_e	Dean number, $R_e/\sqrt{R_o}$
D_p	particle diameter, cm
f_1	correction factor
h	heat-transfer coefficient, erg/(s cm² K)
k	mass-transfer coefficient, cm/s
L	tube length, cm
loss	particle loss
	$Loss_I$, inertial impaction loss in coiled denuder, decimal value
	$Loss_D$, diffusion loss in coiled denuder, decimal value
	loss (%), total particle loss, %
M	particle (or SO_2) mass
	M_{coil}, mass collected in coiled denuder
	M_{filter}, mass collected in filter
	$M_{annular}$, mass collected in annular denuder
$\dot{m}$	mass (particle) transfer rate, g/s (no./s)
N_u	Nusselt number, $h(2a)/\kappa$
P	penetration, C_{out}/C_{in}
P_r	Prandtl number, ν/α
Q	volumetric flow rate, cm³/s
$\dot{q}$	heat-transfer rate, erg/s
R	coil radius, cm
R_e	Reynolds number, $\rho\bar{w}(2a)/\mu$
R_o	curvature ratio, R/a
S_c	Schmidt number, ν/D
S_h	Sherwood number, $k(2a)/D$
$\bar{S}_h$	mean Sherwood number
S_h^*	fully developed Sherwood number
St_k	Stokes number, $\bar{w}\tau/a$
T	temperature, K
$\bar{w}$	average axial velocity, cm/s
α	thermal diffusivity, $\kappa/(\rho c)$, cm²/s
η	efficiency, 1 − P
κ	thermal conductivity, erg/(s cm K)
ρ	air density, g/cm³
ρ_p	particle density, g/cm³
μ	air dynamic viscosity, dyn s/cm²
ξ	parameter in eq 6, DL/Q
ν	air kinematic viscosity, μ/ρ, cm²/s
τ	particle relaxation time, $\rho_p D_p^2 C_c/(18\ \mu)$, s
ζ	thickness ratio of concentration to momentum boundary layer

Registry No. Na_2CO_3, 497-19-8; SO_2, 7446-09-5; glycerine, 56-81-5.

Literature Cited

(1) Stevens, R. K.; Dzubay, T. G.; Russwurm, G.; Rickel, D. *Atmos. Environ.* **1978**, *12*, 55.
(2) Forrest, J.; Spandau, D. J.; Tanner, R. L.; Newman, L. *Atmos. Environ.* **1982**, *16*, 1473.
(3) Braman, R. S.; Shelley, T. J.; McClenny, W. A. *Anal. Chem.* **1982**, *54*, 358.
(4) Ferm, M.; Sjödin A. *Atmos. Environ.* **1985**, *19*, 985.
(5) Durham, J. L.; Spiller, L. L.; Ellestad, T. G. *Atmos. Environ.* **1987**, *21*, 589.
(6) Vossler, T. L.; Stevens, R. K.; Paur, R. J.; Baumgardner, R. E.; Bell, J. P. *Atmos. Environ.* **1988**, *22*, 1729.
(7) Possanzini, M.; Febo, A.; Liberti, A. *Atmos. Environ.* **1983**, *17*, 2605.
(8) Mori, Y.; Nakayama, W. *Int. J. Heat Mass Transfer* **1965**, *8*, 67.
(9) Mori, Y.; Nakayama, W. *Int. J. Heat Mass Transfer* **1967**, *10*, 37.
(10) Mori, Y.; Nakayama, W. *Int. J. Heat Mass Transfer* **1967**, *10*, 681.
(11) McConalogue, D. J.; Srivastava, R. S. *Proc. R. Soc. London, A* **1968**, *307*, 37.
(12) Patankar, S. V.; Pratap, V. S.; Spalding, D. B. *J. Fluid Mech.* **1974**, *62*, 539.
(13) Soh, W. Y.; Berger, S. A. *J. Fluid Mech.* **1984**, *148*, 109.
(14) Humphrey, J. A. C.; Iacovides, H.; Launder, B. E. *J. Fluid Mech.* **1985**, *154*, 357.
(15) Tsai, C. J.; Pui, D. Y. H. *Aerosol Sci. Technol.*, in press.
(16) Kays, W. M.; Crawford, M. E. *Convective Heat and Mass Transfer*, 2nd ed.; McGraw-Hill Book Co.: New York, 1980.
(17) Sparrow, E. M.; Chrysler, G. M. *J. Heat Transfer* **1986**, *108*, 40.
(18) Ito, H. *J. Basic Eng.* **1959**, *81D*, 123.
(19) Gormley, P.; Kennedy, M. *Proc. R. Ir. Acad.* **1949**, *52A*, 163.
(20) Liu, B. Y. H.; Pui, D. Y. H.; Rubow, K. L.; Szymanski, W. W. *Ann. Occup. Hyg.* **1985**, *29*, 251.
(21) Pui, D. Y. H.; Romay-Novas, F.; Liu, B. Y. H. *Aerosol Sci. Technol.* **1987**, *7*, 301.
(22) Liu, B. Y. H.; Pui, D. Y. H. *J. Colloid Interface Sci.* **1974**, *47*, 155.
(23) Hinds, W. C. *Aerosol Technology*; John Wiley & Sons: New York, 1982.
(24) Ye, Y.; Tsai, C.-J.; Pui, D. Y. H.; Lewis, C. W. Presented at AAAR 1989 Annual Meeting, Reno, NV; submitted for publication in *Aerosol Sci. Technol.*

Received for review May 11, 1989. Accepted October 24, 1989. This work was supported by the U.S. Environmental Protection Agency under Purchase Order No. 8D1432YASA. Although the research described in this article has been funded by the U.S. EPA, it has not been subjected to Agency review and, therefore, does not necessarily reflect the views of the Agency, and no official endorsement should be inferred. Mention of commercial products does not constitute endorsement by U.S. EPA. We thank Suzanna Browne, John Bell, and Bill Karches for their help in performing the gas collection efficiency measurements.

Environ. Sci. Technol. 1990, 24, 313-315

Atmospheric Reactivity of Gaseous Dimethyl Sulfate

Steven M. Japar,* Timothy J. Wallington, Jean M. Andino, and James C. Ball

Research Staff, Ford Motor Company, Dearborn, Michigan 48121

■ The atmospheric reactivity of dimethyl sulfate (DMS) with a series of atmospheric species has been investigated. Upper limits to the rate constants for the homogeneous gas-phase reactions of DMS with O_3, NH_3, and H_2O have been determined by using FTIR spectroscopy and are $<1.4 \times 10^{-21}$, $<1.5 \times 10^{-21}$, and $<1.1 \times 10^{-23}$ cm^3 molecule^{-1} s^{-1}, respectively. The reactivity of DMS toward OH radicals and Cl atoms has been determined by using relative rate techniques, and the rate constants for those reactions are $<5 \times 10^{-13}$ and $(4.2 \pm 0.5) \times 10^{-13}$ cm^3 molecule^{-1} s^{-1}, respectively. These rate constants correspond to atmospheric lifetimes ranging from >23 days with respect to reaction with OH radicals to >33 years with respect to reaction with ozone. With the possible exception of its reaction with water, for which the calculated lifetime of DMS is >2 days, these results indicate that the atmospheric fate of DMS is not determined by its homogeneous gas-phase reactions with any of the atmospheric species studied.

Introduction

Dimethyl sulfate (DMS) has been shown to be carcinogenic in different animal systems and is considered to be a probable human carcinogen (*1*). Although for alkylating agents DMS is considered a weak carcinogen, it has been extensively studied by the chemical carcinogenesis community in an attempt to understand the reactions of chemical carcinogens (*2*) and has been used specifically as an example of an alkylating agent that reacts via an S_N2 reaction mechanism.

These properties of DMS are noteworthy because DMS has been found in the atmosphere. Specifically, during 1–3 August 1983, Eatough et al. (*3*) measured atmospheric DMS concentrations up to ~4 ppb, with essentially all the material (≥98%) being present in the gas phase. DMS has also been found in particulate matter from coal- and oil-fired power plants (*4*), and in the gas phase in power plant plumes downwind of a number of plants (*4*). In the latter case, it is clear that DMS formation is taking place in the plumes well downwind of the stacks and that a majority of the DMS in the plumes is actually formed in the atmosphere (*5*).

Even though the presence of DMS in the atmosphere is a potential human health concern, there is essentially nothing known about the atmospheric chemistry of DMS, either in regard to its formation or its fate. We report the first systematic study of the atmospheric reactivity of gaseous dimethyl sulfate.

Experimental Section

Experiments were carried out in a system consisting of a Mattson Instruments Inc. Sirius 100 FT-IR spectrometer interfaced to a 140-L, 2-m-long evacuable Pyrex chamber ($S/V = 0.14$ cm^{-1}) described previously (*6*). The Pyrex chamber was surrounded by 24 UV fluorescent lamps (GTE F40BLB). White-type multiple-reflection optics were mounted in the reaction chamber enabling path lengths up to 120 m to be achieved; however, the path length used in the present study was 8 m. The spectrometer was operated at a resolution of 0.25 cm^{-1}. Infrared spectra were typically derived from 8–16 coadded interferograms, which were transformed by using a Masscomp 5500 computer. Reference spectra were acquired by filling the chamber with known concentrations of the appropriate compounds.

In the present work we have used the relative rate technique to investigate the kinetics of the reaction of DMS with Cl atoms and OH radicals in the evacuable chamber. Cl atoms were generated in these experiments from the photolysis of molecular chlorine by the black lights

$$Cl_2 + h\nu \rightarrow 2Cl \quad (1)$$

while OH was formed through the photolysis of methyl nitrite in air (*8*):

$$CH_3ONO + h\nu \rightarrow CH_3O + NO \quad (2)$$

$$CH_3O + O_2 \rightarrow HO_2 + H_2CO \quad (3)$$

$$HO_2 + NO \rightarrow OH + NO_2 \quad (4)$$

Reaction mixtures consisting of a reference organic (methane, ethane, ethene, or cyclohexane) and DMS diluted in synthetic air together with either chlorine or methyl nitrite were introduced into the chamber by expansion of the gases from known volumes and were left to mix for at least 15 min. In the presence of Cl atoms (or OH radicals) there is competition between DMS and the reference organic for the available reactive radicals via reactions 5 and 6, e.g., for Cl atoms. Providing that the

$$Cl + \text{reactant organic} \Rightarrow \text{products} \quad (5)$$

$$Cl + \text{reference organic} \Rightarrow \text{products} \quad (6)$$

reactant and reference organics are lost solely by reactions 5 and 6 and that neither organic is reformed in any process, then it can be shown that

$$\ln \frac{[\text{reactant organic}]_{t_0}}{[\text{reactant organic}]_t} = \frac{k_5}{k_6} \ln \frac{[\text{reference organic}]_{t_0}}{[\text{reference organic}]_t}$$

where $[\text{reactant organic}]_{t_0}$ and $[\text{reference organic}]_{t_0}$ and $[\text{reactant organic}]_t$ and $[\text{reference organic}]_t$ are the concentrations of the reactant and reference organics at times t_0 and t, respectively, and k_5 and k_6 are the rate constants of reactions 5 and 6, respectively.

Methyl nitrite was generated by the dropwise addition of 50% H_2SO_4 to methanol saturated with sodium nitrite (*9*). It was dried by passage through a column of $CaCl_2$, purified by fractional distillation, and stored in the dark at 77 K. Prior to use the purity of the methyl nitrite was checked by FTIR spectroscopy; no observable impurities were detected. O_3 was formed in a stream of O_2, which had passed through a silent discharge, and was introduced directly into the FTIR cell. Cl_2 (Matheson Gas Products, High Purity) and NH_3 (Matheson Gas Products) were used as received. The purity of the DMS (Aldrich Chemical Co.; 99+%) was found to be ≥96% by gas chromatography. The impurities were relatively low-boiling and were minimized by a freeze–thaw degassing procedure on the vacuum line before samples were introduced into the reactor.

0013-936X/90/0924-0313$02.50/0

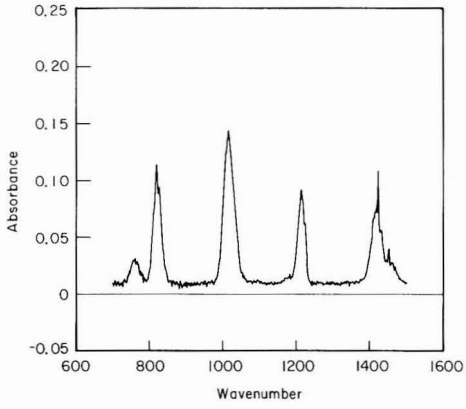

Figure 1. Infrared spectrum of DMS (5.8 mTorr; path length, 7.6 m) in the range from 700 to 1500 cm^{-1}.

Results and Discussion

DMS + Ozone, NH_3, and H_2O. The reactions of DMS with O_3, NH_3, and H_2O were investigated in the evacuable reactor by FTIR spectroscopy. The behavior of DMS was monitored by its characteristic infrared absorption in the 800–1500-cm^{-1} region (Figure 1). In the absence of other reactants DMS concentrations were stable in the reactor for more than 1 h. DMS (5–10 mTorr) was mixed with either O_3 (up to 130 mTorr), NH_3 (up to 240 mTorr), or H_2O (up to 3.7 Torr) and left to stand in the chamber in the dark for 60 min, 30 min, and 4 h, respectively. In all cases no loss of DMS (≤2%) was observed, thereby enabling the assignment of upper limits of $<1.4 \times 10^{-21}$, $<1.5 \times 10^{-21}$, and $<1.1 \times 10^{-23}$ cm^3 $molecule^{-1}$ s^{-1} to the homogeneous gas-phase rate constants for the reaction of DMS with O_3, NH_3, and H_2O, respectively.

DMS + Cl Atoms. In the present work we have used the relative rate technique to investigate the kinetics of the reaction of DMS with Cl atoms. In these experiments, carried out in 700 Torr air, typical DMS concentrations were 5–10 mTorr, the reference organic concentrations were 225 mTorr, and chlorine concentrations were ~1 Torr. The relative rate technique relies on the assumption that both the reactant and reference organics are removed solely by reaction with chlorine atoms. To test this assumption mixtures of chlorine with both organics were prepared and left in the dark. In all cases, reaction of the organic species with chlorine, in the absence of ultraviolet light, was of negligible importance over the typical time periods used in this work. In addition, to test for the possible photolysis of the reactants used in the present work, mixtures of the reactants in synthetic air in the absence of chlorine were irradiated. No photolysis of any of the reactants was observed.

Figure 2 shows plots of ln ($[reactant]_{t_0}/[reactant]_t$) vs ln ($[reference]_{t_0}/[reference]_t$) for DMS with methane and ethane references. As seen from Figure 2, such plots are linear with intercepts at the origin, within two standard deviations (2σ), suggesting that the present work is free from complications due to secondary chemistry. For each system studied, at least two separate gas mixtures were prepared and irradiated to check the experimental reproducibility; in all cases, indistinguishable results were obtained from successive experiments. In the experiments using methane as a reference, significant losses of both DMS and methane were observed. Linear least-squares analysis of the data yields a rate constant ratio, k_5/k_6, for DMS relative to methane of 4.23 ± 0.48. This in turn can

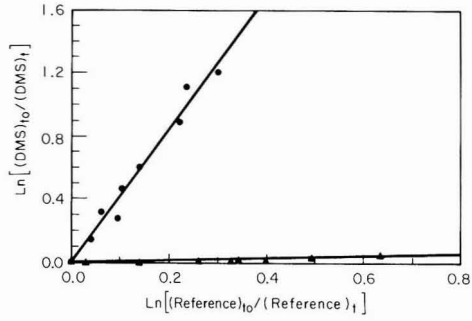

Figure 2. Plot of ln ($[DMS]_{t_0}/[DMS]_t$) vs ln ($[reference)_{t_0}/[reference]_t$) using the two reference organics methane (●) and ethane (▲) in the presence of Cl atoms. The solid lines represent linear least-squares fits to the data.

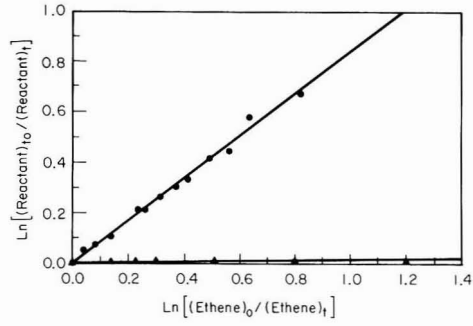

Figure 3. Plot of ln ($[reactant]_{t_0}/[reactant]_t$) vs ln ($[ethene]_{t_0}/[ethene]_t$) for cyclohexane (●) and DMS (▲) in the presence of OH radicals. The solid lines represent linear least-squares fits to the data.

be combined with the literature value of 1.0×10^{-13} cm^3 $molecule^{-1}$ s^{-1} (*10*) for the rate constant for the reaction of Cl atoms with methane to yield a rate constant of (4.2 ± 0.5) × 10^{-13} cm^3 $molecule^{-1}$ s^{-1} for the reaction of Cl atoms with DMS. (Errors quoted represent 2σ from the linear least-squares analysis and do not include any systematic errors due to errors in the reference rate constant.) The results of the experiments using ethane as a reference are consistent with those using methane, although in that case, while the decay of the ethane was appreciable, there was only slight decay noted for the DMS. The data yield a rate constant ratio of 0.07 ± 0.06 and, in combination with the rate constant for the reaction of Cl with ethane, 5.7×10^{-11} cm^3 $molecule^{-1}$ s^{-1} (*10*), indicate an upper limit to the rate constant for the reaction of Cl atoms with DMS of $\leq 4 \times 10^{-12}$ cm^3 $molecule^{-1}$ s^{-1}. Thus, the rate constant for the reaction of Cl with DMS, based on the methane results, is (4.2 ± 0.5) × 10^{-13} cm^3 $molecule^{-1}$ s^{-1}.

DMS + OH. The reactivity of DMS with OH radicals was also investigated by use of the relative rate approach. In these experiments, carried out in 700 Torr air, typical DMS and reference organic concentrations were 5–15 mTorr, while the CH_3ONO concentration was typically 150 mTorr. In all cases, reaction of the organic species with methyl nitrite, in the absence of ultraviolet light, was of negligible importance over the typical time periods used in this work. To test for the possible photolysis of the reactants used in the present work, mixtures of the reactants in synthetic air in the absence of methyl nitrite were irradiated by using the black lamps surrounding the reactor. No photolysis of any of the reactants was observed. Figure 3 shows the relative rate data for cyclohexane and DMS vs ethene as a reference. The plots are linear with

Table I. Atmospheric Reactivity and Calculated Lifetimes of Gaseous Dimethyl Sulfate

reactant	rate constant[a]	DMS lifetime
ozone	$<1.4 \times 10^{-21}$	>33 years
OH	$<5 \times 10^{-13}$	>23 days
Cl	4.2×10^{-13}	8 years
NH_3	$<1.5 \times 10^{-21}$	>8 years
H_2O	$<1.1 \times 10^{-23}$	>2 days

assuming
$[O_3] = 7.5 \times 10^{11}$ cm^{-3}
$[OH] = 1 \times 10^{6}$ cm^{-3}
$[Cl] = 1 \times 10^{4}$ cm^{-3}
$[NH_3] = 2.5 \times 10^{12}$ cm^{-3}
$[H_2O] = 15$ Torr

[a] In cm^3 molecule^{-1} s^{-1}.

intercepts at the origin. Linear least-squares analysis of the data yields a ratio of the OH rate constant for cyclohexane to that for ethene of 0.83 ± 0.04, in excellent agreement with the rate constant ratio 0.86 calculated from the individual rate constants recommended by Atkinson (*11*). This is an excellent demonstration that the relative rate technique for OH radicals can be carried out in the evacuable reactor and serves to validate our experimental apparatus and technique. Figure 3 also shows the data for DMS. In this case, while the ethene decayed appreciably, there is no observable loss of DMS, so that the reactivity of DMS with OH is at least an order or magnitude lower than that for ethene. From the data in Figure 3, an upper limit to the rate constant for the reaction of OH with DMS can be calculated to be $<5 \times 10^{-13}$ cm^3 molecule^{-1} s^{-1}.

Conclusions

The rate constants derived for the reaction of DMS with OH, Cl, NH_3, O_3, and H_2O are summarized in Table I. If these rate constants are combined with estimates (indicated in Table I) of the atmospheric concentrations of the various reactive species, it is possible to derive approximate atmospheric lifetimes for DMS in terms of the homogeneous gas-phase reactions studied in the present work. These lifetimes are also summarized in Table I and are notable in that they indicate lifetimes of greater than 23 days vs OH and greater than 33 years vs O_3. With the exception of the value for water, i.e., >2 days, these lifetimes are quite long, and it would appear that the fate of DMS in urban atmospheres is not controlled by the homogeneous gas-phase reactions investigated in the present work.

There is little in the literature to hint at the fate of DMS in the atmosphere. DMS is only slightly soluble in water (*12*), so that it is unlikely to be efficiently scavenged below clouds by rain. However, it is likely to become incorporated into fog- and cloudwater. In this case it will hydrolyze to monomethyl hydrogen sulfate (and finally to sulfuric acid) and methanol, with a half-life on the order of 30–60 min (*13*, *14*), even at pHs (≤3) typical of acid rain and acid fog. Other reactions in solution are possible, i.e., the alkylation of amines, but little is known about such chemistry in acidified solutions.

Acknowledgments

We would like to thank C. M. Savage and C. A. Gierczak for their assistance in the setup and maintenance of the FTIR system.

Registry No. DMS, 77-78-1; O_3, 10028-15-6; OH, 3352-57-6; Cl, 22537-15-1; NH_3, 7664-41-7; H_2O, 7732-18-5.

Literature Cited

(1) Hoffmann, G. R. *Mutat. Res.* **1980**, *75*, 63–129.
(2) Lawley, P. D. Carcinogenesis by Alkylating Agents. In *Chemical Carcinogens*, 2nd ed.; Searle, E., Ed.; ACS Monograph 182; American Chemical Society: Washington, DC, 1984; pp 326–484.
(3) Eatough, D. J.; White, V. F.; Hansen, L. D.; Eatough, N. L.; Cheney, J. L. *Environ. Sci. Technol.* **1986**, *20*, 867–872.
(4) Eatough, D. J.; Lee, M. L.; Later, D. W.; Richter, B. E.; Eatough, N. L.; Hansen, L. D. *Environ. Sci. Technol.* **1981**, *15*, 1502–1506.
(5) Hansen, L. D.; Eatough, D. J.; Cheney, J. L.; Eatough, N. L. The Formation of Dimethyl Sulfate in Power Plant Plumes. Annual Meeting of the Air Pollution Control Association, New York, June 21–26, 1987; Paper No. 87-96.3.
(6) Wallington, T. J.; Japar, S. M. *J. Atmos. Chem.*, in press.
(7) Wallington, T. J.; Skewes, L. M.; Siegl, W. O.; Wu, C. H.; Japar, S. M. *Int. J. Chem. Kinet.* **1988**, *20*, 867–875.
(8) Atkinson, R.; Carter, W. P. L.; Winer, A. M.; Pitts, J. N., Jr. *J. Air Pollut. Control Assoc.* **1981**, *31*, 1090–1092.
(9) Taylor, W. D.; Allston, T. D.; Moscato, M. J.; Fazekas, G. B.; Kozlowski, R.; Takacs, G. A. *Int. J. Chem. Kinet.* **1980**, *12*, 231–240.
(10) DeMore, W. B.; Molina, M. J.; Sander, S. P.; Golden, D. M.; Hampson, R. F.; Kurylo, M. J.; Howard, C. J.; Ravishankara, A. R. NASA-JPL Publication No. 87-41, 1987.
(11) Atkinson, R. *Chem. Rev.* **1986**, *86*, 69, and references therein.
(12) *Handbook of Chemistry and Physics*; CRC: Cleveland, OH, 1973.
(13) Kaiser, E. T.; Panar, M.; Westheimer, F. H. *J. Am. Chem. Soc.* **1963**, *85*, 602–607.
(14) Robertson, R. E.; Sugamori, S. E. *Can. J. Chem.* **1966**, *44*, 1728–1730.

Received for review February 21, 1989. Revised manuscript received July 31, 1989. Accepted October 30, 1989.

Environ. Sci. Technol. 1990, 24, 316–328

Development of a Thermal Stability Based Ranking of Hazardous Organic Compound Incinerability

Philip H. Taylor,*,† Barry Dellinger,† and C. C. Lee‡

Environmental Sciences Group, University of Dayton Research Institute, Dayton, Ohio 45469-0001, and U.S. Environmental Protection Agency, Office of Research and Development, Office of Environmental Engineering and Technology, Risk Reduction Engineering Laboratory, Thermal Destruction Branch, Cincinnati, Ohio 45268

■ It is believed that emissions from full-scale incinerators can often be related to poor microscale mixing of waste and oxygen. To develop a scientifically defensible ranking of hazardous organic waste incinerability, the temperatures for 99% decomposition for a series of organic compounds were evaluated under constant conditions of elemental waste mixture composition (C:H:Cl molar ratios of 3:3:1), fuel/oxygen equivalence ratio (Φ = 3.0), and gas-phase residence time (t_r = 2.0 s). Theoretically consistent data were obtained for 66 compounds. A thermochemical reaction kinetic analysis indicated that the ranking can be applied to waste/oxygen equivalence ratios greater than 1.0 and H/Cl ratios greater than 1.0. This result suggests that deviations from the ranking may occur under thermal quenching and/or high waste chlorine failure modes. Pilot- and full-scale evaluations of the laboratory-based ranking are currently being conducted.

Introduction

Controlled, high-temperature incineration, in spite of the associated high costs, is a viable organic waste reduction technology (*1*). The current performance requirement states that principal organic hazardous constituents (POHCs) designated in each waste must be destroyed and/or removed to an efficiency of 99.99%. The complexity of hazardous organic waste streams often makes correct POHC selection and demonstration of 99.99% destruction and removal efficiency (DRE) a nontrivial task.

To aid the process of POHC selection, the U.S. EPA has limited the number of hazardous organic compounds to those listed in Appendix VIII of 40 CFR Part 261.3 and ranked these substances by their heat of combustion per unit mass (ΔH_c/g) (*2*). This scale is based on the premise that the lower the heat of combustion, the more difficult the compound is to incinerate. The heat of combustion approach has undergone considerable policy debate and received criticism on theoretical grounds from the scientific community (*3–5*). Results of laboratory- and full-scale studies have indicated that this ranking is not consistent with the relative gas-phase thermal stability of numerous POHCs (*6–9*).

Calculations and experimental observations have shown that the emissions of undestroyed, residual POHCs are kinetically, not thermodynamically controlled, (i.e., thermodynamic equilibrium calculations predict emission rates 3–10 orders of magnitude less than observed) (*3, 10–13*). Thus, under the assumption that heterogeneous reactions are insignificant and mass transport is not rate-limiting, POHC destruction in incinerators is controlled by gas-phase chemical kinetic factors including temperature, reaction atmosphere, and residence time. A numerical model encompassing the exact time, temperature, and reaction atmosphere history of all molecules in an incinerator is necessary to determine absolute POHC destruction efficiency (DE). Detailed chemical kinetic models of the thermal degradation of a few simple chlorinated hydrocarbons (e.g., chloromethane, dichloromethane, trichloroethylene) are under development by several researchers (*14–17*). Computer codes modeling incinerator conditions are also under development (*18*). Nonetheless, a sufficiently detailed understanding of this complex chemical and physical process is not currently possible. However, less information is required to estimate the relative DE (viz., incinerability ranking) of potential POHCs.

Simple conceptual models and more complex computer models indicate that all hazardous compounds entering the flame zone of an incinerator are destroyed and only the small fraction that does not pass through this zone may be emitted from the facility (*19, 20*). Various transient "failure modes" may cause a small fraction of POHCs to circumvent the flame zone (*5, 20*). Once in the postflame zone, thermal decomposition kinetics control the rate of POHC destruction. Even with the simplified hypothesis that postflame thermal decomposition controls the relative emission rates of POHCs, there remain several complex, interdependent kinetic variables. The objective of this study was to develop a self-consistent set of precisely controllable experimental conditions where POHC relative incinerability could be expediently evaluated by using a laboratory-scale thermal instrumentation system.

Our initial necessary assumption was that all POHCs in a given waste stream experienced the same postflame residence time, temperature, and reaction atmosphere. This required that mixtures of POHCs were volatilized at nearly the same rate. Our own calculations (*21*) as well as models and experiments from other laboratories (*22, 23*) have shown that vaporization times for even very large droplets (>500 μm) are still very short compared to the total gas-phase residence time in an incinerator. Thus, the individual components of multicomponent droplets experience essentially identical gas-phase residence times, as initially assumed. Clearly one cannot make this assumption for POHCs injected at different points in an incinerator (e.g., rotary kiln and an afterburner).

The problem was thus reduced to one of developing a set of independent temperatures, residence times, and reaction atmospheres that could be used to effectively predict relative POHC incinerability for a range of operating conditions. It has been previously proposed that the temperature for 99% destruction at 2.0-s residence time is a viable method of determining the relative stability of POHCs (*4, 19*). Other residence times or temperatures may be used to develop such a ranking. However, laboratory-scale flow reactor data have indicated that although absolute POHC DEs are dependent upon time and temperature, relative DEs are insensitive to these parameters (*19*).

The concept of reaction atmosphere may be specifically characterized by four parameters: total reactant concentration, molecular waste composition, elemental waste composition, and waste/oxygen equivalence ratio. Under the partial equilibrium hypothesis, it is assumed that the concentrations of highly reactive species, e.g., OH radicals

† University of Dayton Research Institute.
‡ U.S. Environmental Protection Agency.

0013-936X/90/0924-0316$02.50/0

and H, O, and Cl atoms, achieve equilibrium with each other via fast bimolecular reactions even though the overall system is not at chemical equilibrium (*24*). Since bimolecular pathways involving these reactive species along with unimolecular reactions govern the rate of POHC decomposition, only the elemental composition of the waste feed and waste/oxygen stoichiometry will *critically* affect POHC DE. Laboratory studies have confirmed that oxygen concentration and elemental composition are major variables in determining relative incinerability (*7*, *9*).

In principle, other reactive species including polyatomic radicals (e.g., CH_3) can also react to destroy the feed material. These reactions have been proposed at moderately high temperatures in models of the degradation of simple hydrocarbons (*25*) and chlorohydrocarbons (*15*, *16*). However, at higher temperatures, the concentrations of these "alternate" radicals are generally 1–2 orders of magnitude smaller than OH, H, O, and Cl such that highly improbable radical chain reactions in the long-chain limit are required for appreciable contribution to waste destruction.

Calculations using available kinetic data indicate that the emissions from full-scale incinerators are several orders of magnitude higher than those calculated by using oxidation kinetics and residence times and temperatures near the mean values in the postflame zones of typical incinerators (*5*, *8*, *12*). This result suggests that oxygen-depleted pathways are responsible for most POHC emissions (*8*, *26*, *27*). Even though typical incineration facilities may be operating under a nominally oxygen-rich stoichiometry, poor mixing on the molecular level may result in the creation of oxygen-deficient pockets. Consequently, it is believed that gas-phase thermal stability under oxygen-starved reaction conditions may be an effective predictor of relative POHC DE.

Experimental Approach

Quantitative decomposition of synthetic waste mixtures was measured with the Thermal Decomposition Unit-Gas Chromatographic System. The thermal decomposition unit consisted of a fused-silica tubular reactor in which a gas stream exhibiting a laminar flow pattern was exposed to temperatures as high as 1100 °C for mean residence times of 2.0 s. Reactor design ensured that each molecule experienced a square-wave thermal pulse with a very narrow ($\Delta t/t_\tau = 0.006\,92$), near-Gaussian residence time distribution (*28*, *29*). Heated fused silica transfer lines (250 °C) connected the insertion chamber to the reactor and the reactor to the gas chromatographic analytical system. The analytical function was performed by a Varian Vista 4600 programmed temperature gas chromatograph in conjunction with a CDS 401 computer data station.

For each multicomponent mixture, a constant elemental waste feed composition of C_3H_3Cl was a priori selected on the basis of estimated upper limit C:H:Cl molar ratios of hazardous waste streams subjected to full-scale incineration (~50 wt % Cl). For a large majority of mixtures tested, atom populations were balanced within ±10% of these constraints. For each mixture, a constant experimental condition of waste/oxygen equivalence ratio (Φ = 3.0) and mean residence time (t_τ = 2.0 s) was also a priori selected on the basis of a statistically significant correlation between laboratory-scale flow reactor and full-scale emissions data under oxygen-deficient reaction conditions (*8*). [Fuel/oxygen equivalence ratio (Φ) was defined as (moles of fuel/moles of $O_2)_{actual}$/(moles of fuel/moles of $O_2)_{stoich}$. CO_2, H_2O, HCl, HF, HBr, and NO were assumed to be combustion end products as appropriate for a given waste mixture composition (*30*, *31*).] Calibration tests indicated that a *total* organic mixture reactor concentration of ~1000 ppm would ensure highly reproducible data acquisition within the constraints of the previously defined reaction atmosphere. This was also felt to be a reasonable approximation of the waste concentration in a full-scale incinerator. Concentrations of the individual components varied from ~100 to ~900 ppm. Exposure temperature was thus chosen as the critical independent variable with data gathered over a range of 300–1100 °C.

For the large majority of experiments, condensed-phase samples were prepared by injecting specific amounts of high purity (≥99%) stock liquids and solids into a small borosilicate vial. Liquid samples were then injected into the insertion chamber with a small submicroliter syringe at a nominal rate of ~0.01 μL/s. Flowing dry nitrogen doped with 1000 ± 10 ppm oxygen was used as the carrier gas for these experiments. For experiments involving highly volatile POHCs, gas-phase hazardous organic mixtures were prepared by injecting specific amounts of high-purity (≥99%) stock liquids and gases into a 1-L Pyrex bulb purged with room air. Gaseous samples were then injected into the insertion chamber of the thermal decomposition unit with special gas-tight syringes at a nominal rate of ~1.5 μL/s. Flowing dry nitrogen (≤1 ppm oxygen) was used as the carrier gas for these experiments.

Chromatographic analyses of the reactor effluent were obtained by use of several different fused silica capillary columns, depending on the nature of the samples being evaluated. Typically, the gas chromatography (GC) oven was programmed from −60 to 250 °C at 20 °C/min. Helium was used as the GC carrier gas and a hydrogen flame ionization detector was used for solute detection. Relative retention time indexes were used to monitor the destruction of a given POHC. For each mixture, an internal standard, normally benzene, toluene, or dichloromethane, was used to ensure the accuracy of this approach, especially for experiments where low POHC integrated responses were measured.

Regarding data precision, day-to-day uncertainty in the raw data (integrated response) was generally within ±5% for quantitation runs and for low levels of thermal decomposition (<10%). For high levels of decomposition (>90%), uncertainties ranged from ±10 to ±20%. Thermocouple and flow meter calibrations indicated exposure temperature and residence time uncertainties of less than 1%.

Results

Figure 1 represents an example of the type of thermal stability ranking data obtained with this approach. The relative stability of the individual components of a given mixture was determined by the position of the thermal decomposition profile plotted as fraction remaining (on a logarithmic scale) versus reactor temperature. To quantitate the data, the individual components were ranked by the temperature required for 99% percent destruction for a mean residence time of 2.0 s (T_{99}). Ranking by this method allowed intercomparison of thermal stability results from different mixtures.

During the course of this investigation, 69 multicomponent mixtures were examined. Table I presents a list of 66 compounds for which experimentally and theoretically consistent data were obtained. For comparison, $\Delta H_c/g$ values for each compound evaluated are also presented in Table I. The lack of a relationship between a compound's gas-phase thermal stability and heat of combustion is clearly apparent. Several compounds were reexamined in different mixtures to determine the effect of concentration on T_{99}. As shown in Table II, T_{99} was

Table I. Thermal Stability and Heat of Combustion Indexes for Experimentally Evaluated POHCs

POHC	T_{99}	ΔH_c/g
hydrogen cyanide	>1150	N/A[a]
benzene	~1150	10.03
naphthalene	1070	9.62
acetonitrile	1000	7.37
chlorobenzene	990	6.60
acrylonitrile	985	5.57
2-chloronaphthalene	975	7.37
1,2-dichlorobenzene	970	4.57
1,3-dichlorobenzene	960	4.57
1,3,5-trichlorobenzene	955	3.40
1,2,4-trichlorobenzene	955	3.40
1,2,3,5-tetrachlorobenzene	955	2.61
chloromethane	950	3.25
1,2,4,5-tetrachlorobenzene	950	2.61
bromomethane	935	1.70
pentachlorobenzene	935	2.05
hexachlorobenzene	935	1.79
toluene	895	10.14
tetrachloroethene	890	1.19
trichloroethene	865	1.74
1,1-dichloroethene	860	2.70
1,2-dichloroethene	825	3.00
dichloromethane	815	1.70
methacrylonitrile	815	8.55
pyridine	785	7.83
1,1-dichloropropene	780	3.44
1,2,2-trichloro-1,1,2-trifluoroethane	780	N/A[a]
difluorodichloromethane	775	0.22
acetophenone	775	8.26
trichlorofluoromethane	775	0.11
ethyl cyanide	770	4.57
hexachlorobutadiene	765	2.12
dimethyl phthalate	765	5.74
acetyl chloride	765	2.77
p-cresol	745	8.18
benzenethiol	725	8.43
isobutyl alcohol	715	7.62
crotonaldehyde	710	7.73
3-chloropropene	695	N/A[a]
1,1,2,2-tetrachloroethane	690	1.39
benzyl chloride	685	6.18
dibromomethane	685	0.50
1,2-dichloroethane	680	3.00
1,4-dioxane	660	6.41
nitrobenzene	655	5.50
3-chloropropionitrile	655	4.50
methyl ethyl ketone	650	8.07
tetrachloromethane	645	0.24
chlorodifluoromethane	645	N/A[a]
hexachlorocyclohexane	645	1.12
dichlorofluoromethane	640	N/A[a]
pentachloroethane	640	0.53
1,1,2-trichloroethane	635	1.99
trichloromethane	625	0.75
1,2,3-trichloropropane	625	2.81
benzal chloride	625	N/A[a]
bis(2-chloroethyl) ether	615	3.38
1,1-dichloroethane	610	3.00
tribromomethane	585	0.13
hexachloroethane	580	0.46
2-chloroethyl vinyl ether	565	5.19
1,1,1,2-tetrachloroethane	560	1.39
1,1,1-trichloroethane	545	1.99
hexachloropropene	505	0.70
n-butyl benzyl phthalate	415	N/A[a]
di-*n*-octyl phthalate	380	N/A[a]

[a] N/A, heat of combustion data unavailable for this compound.

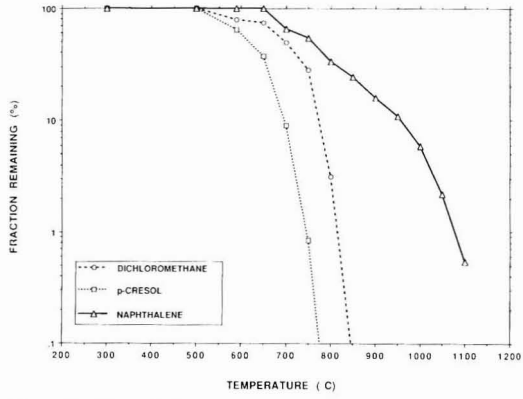

Figure 1. Thermal decomposition curves for a three-component hazardous organic compound mixture. Elemental composition, C_3-$H_{3.6}Cl_{1.7}O_{0.01}$; $\Phi = 2.9$; $t_r = 2.0$ s.

Table II. Effect of POHC Concentration on T_{99}

POHC	concn, ppm	T_{99}
acetonitrile	95	980
	155	1000
acrylonitrile	210	950
	615	935
benzene	455	~1150
	360	~1150
benzyl chloride	665	690
	310	685
	435	690
chlorobenzene	760	980
	260	950
chloromethane	160	950
	315	950
1,3-dichlorobenzene	355	1000
	590	960
1,1-dichloroethene	175	880
	655	860
1,2-dichloroethene	265	835
	655	840
dichloromethane	780	815
	580	810
	540	810
	275	815
	95	800
methyl ethyl ketone	165	650
	200	650
	95	650
tetrachloroethene	570	905
	335	880
tetrachloromethane	60	670
	100	645
	335	645
toluene	590	895
	240	920
	410	900
	595	890
	665	900
trichloroethene	165	860
	410	865
trichloromethane	200	635
	450	625

relatively insensitive to large variations in individual component concentration.

A priori, it is reasonable to expect that the kinetic behavior of many of the compounds tested is not first order in parent concentration. This may at first seem to contradict our experimental results. However, we must remember that each compound was studied in a multicomponent mixture of constant total concentration and elemental composition. Our results indicate that the invariant composition of the high-temperature radical pool derived from these mixtures controls the decomposition of each compound. The complexity of pure compound

decomposition kinetics is thus dampened. This is the same result as one might expect in a full-scale incinerator where concentrations of POHCs in the waste feed vary from <100 to ~10 000 ppm.

The results of this experimental study and prior studies reported in the literature in conjunction with thermochemical reaction kinetic theory (*32*) have been used to develop an incinerability ranking (*33*) of 320 POHCs. The incinerability ranking is presented in Appendix I. The subsequent paragraphs present a generalized evaluation of the ranking.

The incinerability ranking may be divided into three stability families defined by the type of mechanism that generally dominates compound decomposition. The first family, which includes the most stable 77 compounds on the list, may be characterized by bimolecular decomposition processes, which are believed to dominate decomposition. Compounds in this class include hydrogen cyanide, benzene, naphthalene, 2-chloronaphthalene, short-chain aliphatic nitriles, chlorinated benzenes, monosubstituted halomethanes, chlorinated ethylenes, and toluenes. Of the three stability families, this group of compounds is the most difficult to assess theoretically due to the lack of high-temperature bimolecular reaction rate data and the multiplicity of reaction pathways. Emphasis was thus placed on accurate experimental measurements with 24 of the compounds in this class experimentally evaluated.

For a large majority of these compounds, degradation is likely dominated by H atom methathesis and Cl atom displacement reactions. The relative stability of the hydrogen-containing chlorinated ethylenes is consistent with H atom metathesis. Tetrachloroethylene, however, cannot decompose by this pathway. Besides C–Cl bond fission, Cl atom displacement by H atoms is the only available route. Preliminary studies of the rates of displacement versus metathesis for other organic compounds at 1000 °C indicate the former to be somewhat slower (*27*). This is consistent with the greater stability of C_2Cl_4 as compared to the other chlorinated ethylenes (see Table I). The displacement mechanism has been further verified by the identification of trichloroethylene as a major product in the thermal decomposition of a multicomponent mixture containing C_2Cl_4 (*34*). The chlorinated benzenes represent another class of stable POHCs that are believed to decompose largely by Cl displacement reactions under oxygen-starved reaction conditions (*27*).

Hydrogen cyanide is of particular interest due to its extreme stability. Abstraction of H by Cl would appear to be the dominant destruction mechanism, although still very slow due to the strength of the H–CN bond (125 kcal/mol) (*35*). Re-formation of HCN is also highly probable due to the extreme stability of the CN radical, which can recombine with available H atoms. This reformation behavior was observed in laboratory experiments above temperatures of 1050 °C.

The second family division, which includes compound 78 through compound 125, may be characterized by decomposition dominated by mixed unimolecular and bimolecular processes. Compounds within this class include halogen-saturated chlorofluorocarbons (CFCs), oxygenated compounds, chlorinated propylenes, cresol, pyridine, hexachlorobutadiene, ethyl cyanide, etc. The decomposition of CFCs, hexachlorobutadiene, and the oxygenated compounds is consistent with dominant unimolecular mechanisms involving bond fission or concerted molecular elimination. In addition to these unimolecular processes, H atom metathesis and Cl displacement contribute to the decomposition of pyridine, cresol, chlorinated propylenes, dimethyl phthalate, and acetyl chloride. Seventeen of the compounds in this class have been experimentally evaluated.

The third family division, which includes all compounds below compound 125, may be characterized by decomposition dominated by unimolecular processes. Compounds within this class include CFCs, halogenated alkanes, nitrobenzenes, chlorinated toluene derivatives, ketones, esters, ethers, phthalates, etc. The decomposition of α-chlorinated toluene derivatives, nitrobenzene, and tetrachloromethane are believed to be dominated by bond fission (*36*). Documented concerted molecular elimination processes include four-center HCl and HBr elimination for halogenated alkanes and hydrogen-containing CFCs, H_2O elimination for certain ethers, and six-center elimination for long-chain alkylated phthalates (*32*). Twenty-five of the compounds in this class have been experimentally evaluated.

Discussion

The complexity of incineration and chemical reaction kinetics makes it essentially impossible for a single incinerability ranking to apply to every operating scenario. In this section, a reaction kinetic analysis is conducted to determine the effect of changes in reaction atmosphere on the ranking, i.e., to determine the range of conditions for which the ranking may be considered appropriate. For approximately 65% of the 320 compounds ranked, thermal decomposition is postulated to occur by unimolecular processes that are largely independent of reaction atmosphere. (Our data were generated at atmospheric pressure as is typical of full-scale incinerators. Thus, possible pressure-related "falloff" effects would not appear to be the cause for any special concern.) The remaining 35%, which undergo bimolecular thermal decomposition processes, were targeted in this analysis.

Comparison to Theory. To develop a theoretical thermal decomposition curve, a kinetic expression similar to that used by other researchers (*3*) incorporating all known reaction pathways for chemical transformation of the POHC was derived:

$$-\ln f_r = \sum_i tA_i \exp(-E_i/RT) + \sum_j tR_j\lambda_j A_j \exp(-E_j/RT) \quad (1)$$

where f_r is the fraction remaining, A_i the preexponential factor for unimolecular reaction (1/s), A_j the preexponential factor for bimolecular reaction (cm^3/molecule·s), E_i the activation energy for unimolecular reaction (cal/mol), E_j the activation energy for bimolecular reaction (cal/mol), $R_j(T)$ the temperature-dependent radical concentration (molecule/cm^3), λ_j the chain length for radical j, defined as number of POHC molecules destroyed divided by the steady-state population of radical j, T the reaction temperature (K), R the ideal gas constant (cal/mol·K), and t the gas-phase residence time (s).

In the evaluation of eq 1, a major consideration is the estimation of the radical concentration at elevated temperatures. We are currently invoking the partial equilibrium hypothesis (*24*, *30*) to estimate these radical concentrations. We justify this approach on the basis of general agreement (factor of 2) between reactive species concentrations from experimental flame measurements and equilibrium calculations under fuel-rich conditions (*37–40*). A similar result is expected in our reactor (and incinerators) due to the atmospheric pressure conditions, which promote fast termolecular reaction, and fuel-rich nature, which prevents radical overshoot of equilibrium.

Table III. Kinetic Analysis Arrhenius Rate Parameters

model compd	k, s^{-1} (bond homolysis)	k, s^{-1} (HCl elimination)	k, cm^3/molecule·s (H, Cl atom abstrctn)	k, cm^3/molecule·s (CH_3 displace.)
$CHCl_3$	$1.6 \times 10^{16} \exp[-77000/RT]^a$	$2.0 \times 10^{14} \exp[-54500/RT]^d$	$1.0 \times 10^{-11} \exp[-3300/RT]^{e,h}$	
CH_2Cl_2	$2.6 \times 10^{16} \exp[-79400/RT]^a$	$7.1 \times 10^{13} \exp[-70000/RT]^a$	$4.2 \times 10^{-11} \exp[-3000/RT]^{e,h}$	
CH_3Cl	$2.5 \times 10^{15} \exp[-82200/RT]^a$		$5.3 \times 10^{-11} \exp[-3300/RT]^{e,h}$	
$C_6H_5CH_3$	$8.0 \times 10^{16} \exp[-90800/RT]^b$		$7.6 \times 10^{-18} T^2 \exp[22/RT]^{f,i}$	$2.0 \times 10^{-10} \exp[-5122/RT]^g$
			$2.0 \times 10^{-10} \exp[-8222/RT]^{g,j}$	
C_6H_6	$2.0 \times 10^{17} \exp[-118000/RT]^c$		$3.3 \times 10^{-18} T^2 \exp[-684/RT]^{f,i}$	
			$6.1 \times 10^{-11} \exp[-7948/RT]^{g,j}$	

[a] High pressure limit Arrhenius parameters derived from transition-state theory (*32*). [b] High pressure limit Arrhenius parameters ($C_6H_5CH_3 \rightarrow C_6H_5CH_2 + H$) obtained from ref 45. [c] High pressure limit Arrhenius parameters obtained from ref 46. [d] High pressure limit Arrhenius parameters obtained from ref 42. [e] Arrhenius parameters obtained from ref 43. [f] Arrhenius parameters obtained from ref 44. [g] Arrhenius parameters obtained from ref 27. [h] Arrhenius coefficients reflect Cl abstraction by H and H abstraction by H and Cl; equal rate coefficients for all three metathesis reactions have been employed. [i] Arrhenius coefficients reflect H abstraction by Cl. [j] Arrhenius coefficients reflect H abstraction by H.

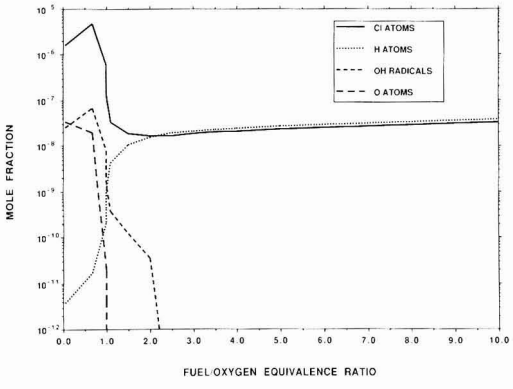

Figure 2. Equilibrium reactive species concentrations at 1273 K as a function of waste/oxygen equivalence ratio. Organic mixture elemental composition, C_3H_3Cl.

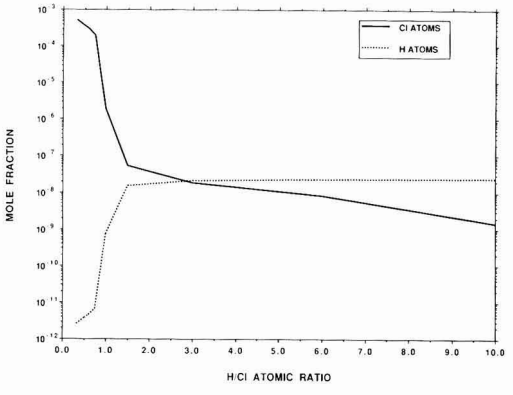

Figure 3. Equilibrium reactive species concentrations at 1273 K as a function of H/Cl atomic ratio. $\Phi = 3.0$.

Subsequent paragraphs demonstrate that this approach does appear to adequately predict reactive species concentrations, resulting in agreement between experimental and theoretical thermal decomposition curves for compounds suspected of undergoing bimolecular thermal decomposition.

Figure 2 presents equilibrium radical concentrations (at 1000 °C) as a function of waste/oxygen equivalence ratio for an elemental waste composition of C_3H_3Cl. Figure 3 depicts equilibrium radical concentrations (at 1000 °C) as a function of H/Cl atomic ratio for a waste/oxygen equivalence ratio of 3.0. The data in Figure 2 indicate that OH radicals and O and Cl atoms are in highest concentration under oxygen-rich ($\Phi \leq 1.0$) conditions while H and Cl atoms are in highest concentration under fuel-rich ($\Phi > 1.0$) conditions. For a fuel-rich stoichiometry ($\Phi = 3.0$), the data in Figure 3 indicated that the Cl atom concentration became equal to or greater than the H atom concentration for H/Cl atomic ratios of <3.0. For larger H/Cl atomic ratios (up to H/Cl of 10.0), the H atom concentration gradually increased while the Cl atom concentration steadily decreased. On the basis of these equilibrium calculations, under the conditions of this study, Cl atoms and H atoms were the reactive species in greatest concentration (typical concentrations ranged from 2×10^9 cm^{-3} at 800 °C to 5×10^{11} cm^{-3} at 1100 °C).

Equation 1 was used to generate theoretical curves for comparison to experimental decomposition curves for five POHCs for which generally reliable kinetic data were available. The thermal stabilities of these compounds ranged from moderately fragile to very stable with kinetic pathways ranging from unimolecular to mixed unimolecular and bimolecular processes. These model compounds included trichloromethane, dichloromethane, chloromethane, toluene, and benzene. Table III presents a summary of the Arrhenius parameters used for the model compounds in this analysis. Transition-state theory (*32*) and unimolecular QRRK calculations (*41*) were employed to provide reasonable estimates of rate parameters where experimental data were unavailable.

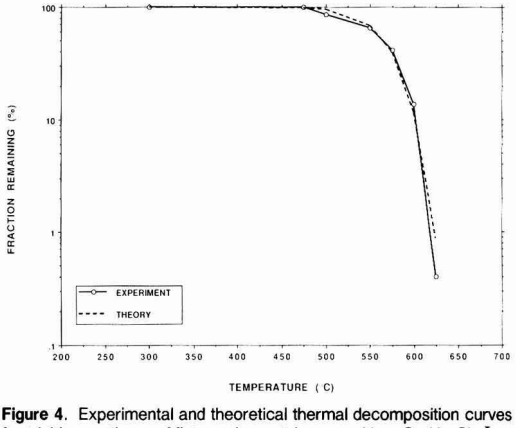

Figure 4. Experimental and theoretical thermal decomposition curves for trichloromethane. Mixture elemental composition, $C_{2.7}H_{3.3}Cl$; $\Phi = 3.0$; $t_r = 2.0$ s.

The decomposition of trichloromethane (see Figure 4) is largely unimolecular in nature. The dominant reaction is concerted three-center HCl elimination with Arrhenius rate parameters recently measured (*42*). C–Cl bond fission

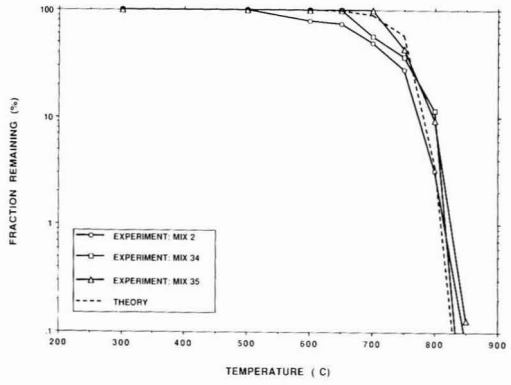

Figure 5. Experimental and theoretical thermal decomposition curves for dichloromethane. Mix 2: elemental composition, C_3H_4Cl; $\Phi = 3.0$. Mix 34: elemental composition, $C_3H_{3.5}Cl$; $\Phi = 3.2$. Mix 35: elemental composition, $C_3H_4Cl_{0.4}$; $\Phi = 2.9$; $t_r = 2.0$ s.

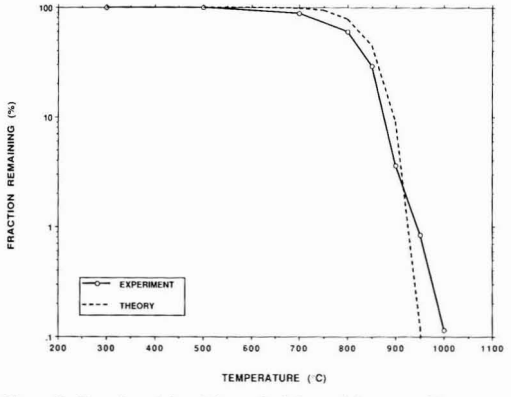

Figure 6. Experimental and theoretical thermal decomposition curves for chloromethane. Mixture elemental composition, $C_{3.1}H_4Cl_{1.3}$; $\Phi = 3.0$; $t_r = 2.0$ s.

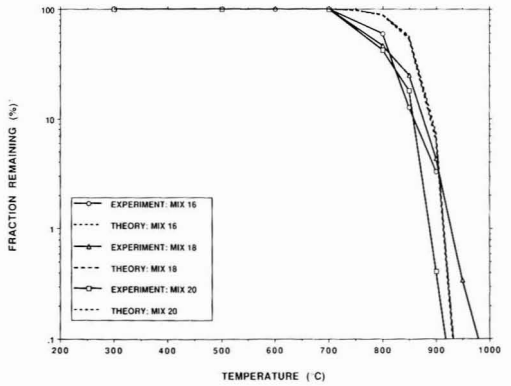

Figure 7. Experimental and theoretical thermal decomposition curves for toluene. Mix 16: elemental composition, $C_3H_{3.3}Cl_{1.1}$; $\Phi = 3.4$. Mix 18: elemental composition, $C_{3.3}H_3Cl_{0.4}$; $\Phi = 3.0$. Mix 20: elemental composition, $C_{3.7}H_4Cl$; $\Phi = 2.7$; $t_r = 2.0$ s.

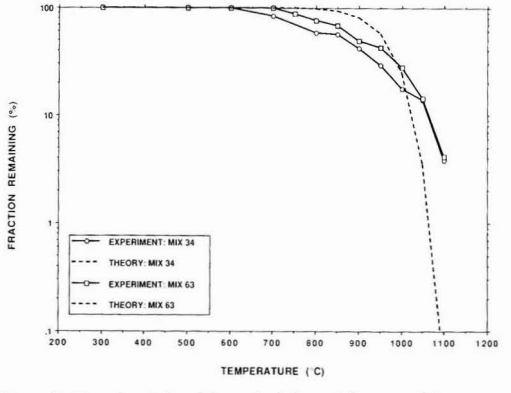

Figure 8. Experimental and theoretical thermal decomposition curves for benzene. Mix 34: elemental composition, $C_3H_{3.5}Cl$; $\Phi = 3.0$. Mix 63: elemental composition, C_3H_4Cl; $\Phi = 3.0$; $t_r = 2.0$ s.

is insignificant at these temperatures and H and Cl atom methathesis is negligible due to the low H and Cl atom concentrations. The excellent agreement between theory and experiment at the 1% remaining level (within 5 °C) indicated that a single unimolecular pathway adequately accounted for the thermal decomposition behavior of this compound. The decomposition of dichloromethane (see Figure 5) is also largely unimolecular in nature. The dominant reactions are three-center HCl elimination and C–Cl bond fission. H and Cl atom metathesis reactions represented minor contributions at higher temperatures (>800 °C). The good agreement between theory and experiment at the 1% remaining level (within 10 °C) indicated that inclusion of these two unimolecular reaction channels adequately accounted for the thermal decomposition behavior of this compound.

The remaining compounds, chloromethane, toluene, and benzene, decompose largely through bimolecular reaction pathways. For chloromethane and benzene (see Figures 6 and 8), H abstraction by Cl atoms makes the largest contribution, with H abstraction by H (and Cl abstraction by H for CH_3Cl) also significant. For toluene (see Figure 7), H atom metathesis by Cl atoms and CH_3 displacement by H atoms dominate. For all three compounds, the experimental curves indicated reaction commencing at ~100 °C lower temperatures, probably due to concentrations of reactives species greater than predicted by the equilibrium code. However, for high levels of POHC decomposition (1–10% remaining), the experimental and theoretical curves tend to converge with agreement at the 1% remaining level within 10 and 30 °C for chloromethane and toluene, respectively. For benzene, at the ~10% remaining level, the theoretical and experimental curves intersected, with the experimental data demonstrating greater stability at higher temperatures. The extrapolated discprepancy between theory and experiment is estimated to be ~50 °C at the 1% remaining level. POHC re-formation reactions excluded in the kinetic relation may be responsible for the larger discrepancy observed for this compound. The agreement between theory and experiment was fairly good for chloromethane ($\Delta T \leq 50$ °C for levels of destruction greater than 10%). This suggests that H atom metathesis by CH_3 radicals does not significantly effect the T_{99} of this compound under the conditions of this study.

We believe the stability of the atoms and diatomic radicals at elevated temperatures is the key to the success of our simple model. Potentially reactive organic (e.g., CH_3, C_2H_3, CCl_3) and inorganic (e.g., ClO) radicals are not stable enough above 750–800 °C to significantly contribute to the destruction of the waste. Indeed, a kinetic sensitivity analysis of a chemical kinetic model for fuel-rich C_2HCl_3 combustion demonstrated that unimolecular HCl elimination and H metathesis by Cl dominate fuel con-

Table IV. ΔT_{99} as a Function of Waste Feed Concentration (Radical Concentration) for Five Model Compounds[a]

A/A_0	R/R_0	$CHCl_3$	CH_2Cl_2	$C_6H_5CH_3$	CH_3Cl	C_6H_6
1.1	1.02	<-1	<-1	<-1	<-1	-5
1.3	1.06	<-1	<-1	<-1	-2	-14
1.5	1.10	<-1	<-1	-1	-3	-23
2.0	1.20	<-1	<-1	-1	-6	-46
3.0	1.40	<-1	<-1	-3	-12	-88

[a] In this analysis, we have assumed that the additional radical concentration (R/R_0) abstracts a H atom from the model compound at the same rate as a Cl atom. The relationship between waste feed concentration (A/A_0) and radical concentration was determined from a series of equilibrium calculations for nominal incinerability mixtures at 1000 °C.

sumption above 750 °C while H metathesis by OCl and C_2Cl_3 are significant destruction pathways at lower temperatures (*15*).

Effect of Varying Waste Feed Rate and Radical Chains. On the basis of the known complexity of hydrocarbon and chlorinated hydrocarbon reaction systems (*47, 14–17*) it may seem fortuitous that such a simple kinetic model can predict the thermal decomposition behavior of such a wide range of species. We acknowledge the need for detailed chemical kinetic mechanisms to predict the thermal decomposition behavior of a given species over wide ranges of experimental conditions. However, the goal of this kinetic analysis was simply the prediction of T_{99}s for one experimental condition.

Using eq 1, we have iteratively calculated the effect of increases in the waste feed concentration on T_{99} for the five model compounds. As shown in Table IV, results indicate that acceptably small decreases in T_{99} (<20 °C) were observed for all compounds for a factor of 2 increase in waste feed rate and acceptably small decreases were observed for all compounds except benzene for a factor of 3 increase in waste feed concentration (~40% increase in radical concentration). For chloroform and dichloromethane, the insensitivity of T_{99} on waste feed concentration is consistent with mechanisms dominated by molecular elimination reactions. The variance in T_{99} for the other compounds is due to the relative contributions of bimolecular radical attack versus unimolecular reaction.

In principle, radical chain reactions can increase the effect of varying radical concentration. Significant chain lengths ($\lambda > 2$) are not expected under incineration conditions due to termination by the formation of stable H_2 and HCl molecules. Polymerization reactions may have longer chain lengths but these reactions are not likely to contribute to POHC destruction in the H- and Cl-rich environment of an incinerator. Both pseudoequilibrium and kinetic calculations indicate that other readily formed polyatomic radicals (e.g., CH_3, CCl_3) that can participate in short chains are in concentrations lower by a factor of 10–100 than H and Cl. Thus, chain lengths for these species would have to be on the order of 10–100 before they would contribute to POHC destruction, which is highly unlikely. Our calculations indicate that chains of $\lambda \leq 2$ produce shifts in T_{99} of equal or lesser magnitude than the effect of changing the radical concentration of up to a factor of 2.

The above analysis indicates that exceptional compounds that are resistant to unimolecular reaction and exhibit large shifts in T_{99} with small increases in radical concentration do exist (e.g., C_6H_6). However, since the stability of all compounds undergoing bimolecular decomposition will shift in the same direction as the radical concentration is varied, changes in their *relative* T_{99} values

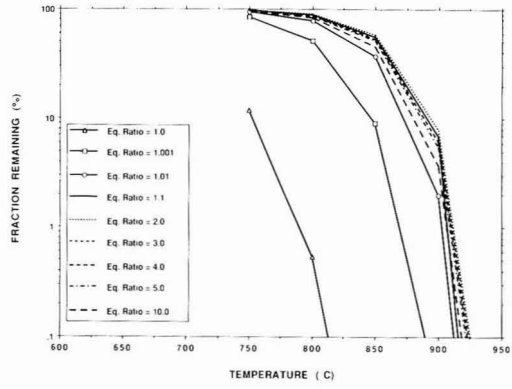

Figure 9. Sensitivity of toluene thermal decomposition behavior as a function of waste/oxygen equivalence ratio. Mixture elemental composition, C_3H_3Cl; t_r = 2.0 s.

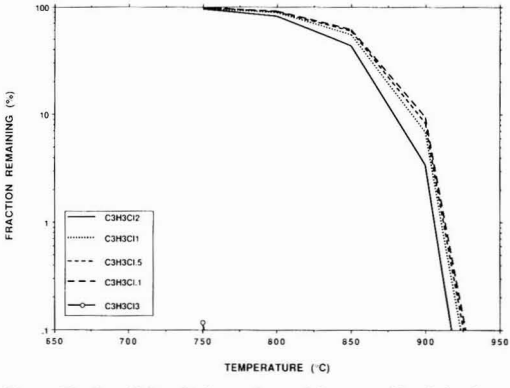

Figure 10. Sensitivity of toluene thermal decomposition behavior as a function of organic mixture Cl atom population. Φ = 3.0; t_r = 2.0 s.

will be suppressed. Since compounds at the top of the ranking decompose predominantly via bimolecular reactions, changes in their relative incinerability are expected to be minimal. Only as we descend through the ranking to where different compounds decompose by bimolecular versus unimolecular pathways will the ranking be expected to exhibit some variance. However, in this regime unimolecular decomposition reactions are available for compounds dominated by bimolecular pathways at nominal conditions. Thus, changes in T_{99} are again expected to be minimal.

Effect of Varying Equivalence Ratio and Waste Feed Composition. Toluene was selected as the model compound for further analysis, as this compound decomposes by numerous bimolecular reactions that are sensitive to changes in reaction atmosphere. We have analyzed the effect of reaction atmosphere by varying the fuel/oxygen stoichiometry ($0.05 < \Phi < 10.0$) for nominal values of mixture elemental composition and by varying mixture elemental composition ($0.33 < H/Cl < 30.0$) for nominal values of fuel/oxygen stoichiometry. Figure 9 presents the results of the sensitivity analysis for variation of waste/oxygen equivalence ratio while Figure 10 presents the results in relation to a variation of Cl and H atom populations, respectively.

Inspection of Figure 9 indicates that for waste/oxygen equivalence ratios ranging from 2.0 to 5.0, there is no significant difference (±10 °C) in T_{99}. As one decreases this parameter to 10.0, a small decrease in T_{99} was ob-

served. A shift in this parameter to 1.0 produced a ~130 °C decrease in T_{99}. Simulations were also conducted for fuel-lean equivalence ratios of 0.67 and 0.05, respectively. The large Cl, O, and OH concentrations (see Figure 2) for these stoichiometries resulted in greater than 99% DE at a temperature of 750 °C. Experimentally evaluated indexes were obtained by fuel/oxygen stoichiometries ranging ±20% of the nominal value (Φ = 3.0). This analysis indicates that the T_{99}s generated in laboratory experiments are clearly intercomparable with relative uncertainties of less than ±10 °C.

In Figure 10, inspection of the toluene decomposition curve indicated that a factor of 10 increase in H/Cl ratio (for a constant C/H ratio) produced only a ~5 °C change T_{99}. However, a factor of 2 decrease in H/Cl ratio decreased T_{99} by ~10 °C, with a factor of 3 decrease in H/Cl ratio dramatically shifting the stability ranking to much lower temperatures. As shown in Figure 3, the dramatic decrease in toluene thermal stability is due to the Cl atom concentration reaching a threshold value where its rate of attack becomes greater than the rate of H atom attack. Flow reactor mixture experiments for benzene, toluene, and naphthalene with very high Cl atom populations have demonstrated this effect. Experimentally evaluated indexes have been obtained for H and Cl atom populations within a factor of 2 of nominal values. This analysis indicates the T_{99}s are clearly intercomparable with relative uncertainties of less than ±10 °C.

The effects of reaction atmosphere on toluene stability may be interpreted on the basis of the concentration and reactivity of OH radicals and Cl, O, and H atoms as a function of these widely varying reaction atmospheres. For nominal elemental compositions under oxidative reactive atmospheres, the concentration of highly reactive OH radicals and Cl atoms becomes kinetically significant at relatively low temperatures, thus promoting rapid thermal destruction. For nominal oxygen-starved fuel/oxygen stoichiometries, the effects of H/Cl ratio may be interpreted on the basis of the relative reactivities of these elemental species when involved in H atom metathesis reactions. Although the kinetic data base for Cl atom attack is very limited, results indicate that Cl atoms rival and in some instances surpass the reactivity of OH radicals, with H atoms much less reactive at temperatures of 800–1100 °C (*25*). These differences in reactivity are such that toluene exhibits a nearly identical thermal behavior for organic mixture elemental compositions of $C_3H_{10}Cl$ and C_3H_3Cl. The somewhat surprising result as one increases the fuel/oxygen stoichiometry from oxygen-starved to completely pyrolytic conditions is due to a subtle increase in the Cl and H atom concentration, countering the effects of a rapidly decreasing OH concentration.

Summary

A thermochemical reaction kinetic based "sensitivity" analysis of the ranking has produced several significant findings. In relation to the laboratory-scale flow reactor experiments, results indicated that 66 thermal stability rankings obtained over the slight variations in reaction atmosphere are intercomparable. This is especially important for the ~110 Appendix VIII compounds whose decomposition is likely dominated by bimolecular reaction. The results of this analysis also indicated that experimental variations in fuel/oxygen stoichiometry and H/Cl atomic ratio were not sufficiently large to produce significant changes in decomposition mechanisms for a given class of hazardous organic compounds.

In relation to full-scale incineration conditions, an analysis of fuel/oxygen stoichiometry indicated that a pyrolytic based ranking applies to fuel-rich stoichiometries ($\Phi > 1.0$) and an oxidative based ranking applies to stoichiometric and fuel-lean stoichiometries ($\Phi \leq 1.0$). A similar analysis of the effect of H/Cl atomic ratio of the waste feed indicated that a high-Cl ranking applies to H/Cl ratios equal to or less than 1.0 and a low-Cl ranking applies to H/Cl ratios greater than 1.0. Thus, the incinerability ranking developed may be further classified as a pyrolytic, low-Cl based ranking.

This ranking would appear to be appropriate for most full-scale incineration conditions, although exceptions must certainly exist. Full-scale incinerators nominally operate at postflame temperatures of ≥1000 °C and residence times of ≥2.0 s. For these conditions, our simple kinetic model and other kinetic calculations indicate that, for gaseous pockets of $\Phi \leq 1.0$, very little material escapes undestroyed and there is little contribution to the emissions. However, short residence time or low-temperature oxidative pathways where POHC destruction is incomplete cannot be ruled out, and an oxidative ranking would dominate under temporal or thermal incinerator failure mode conditions. The kinetic analysis also indicated that very low H/Cl ratios (≤1.0) were required for a significant change in the incinerability ranking. It would seem that H/Cl ratios of ≤1.0 are very unlikely in an incinerator and the validity of the ranking developed here would be maintained. One could argue that high-chlorine pockets of gas may escape from the flame zone due to their difficulty in burning.

The rates of bimolecular reactions are extremely sensitive to changes in reactive species concentration and composition. Thus, a change in the relative ranking of incinerability is likely when the *local* radical concentrations in full-scale systems are outside of the waste/oxygen equivalence ratio and H/Cl ranges discussed above. On the basis of our analysis, one would expect a general contraction of the ranking with increases in oxygen and Cl concentration as nearly all compounds suspected of undergoing bimolecular decomposition would exhibit substantially lower thermal stability.

In conclusion, to cover all possible conditions, it would be desirable to develop both oxidative and pyrolytic rankings. However, pilot- and full-scale comparisons are currently being conducted to determine if the pyrolytic, low-Cl ranking approach presented here is sufficient to accurately predict the relative incinerability of hazardous organic compounds.

Acknowledgments

We acknowledge S. Stelmac of the U.S. EPA's Office of Solid Waste for her support and input concerning the practical application of the ranking. We also thank W. Tsang and S. Heneghan for their helpful discussions regarding pyrolytic thermal decomposition mechanisms for aromatic and chlorinated aromatic hydrocarbons and W. Rubey, J. Graham, and R. Striebich for their review of the experimental design. Last, but not least, we owe special thanks to J. Kasner for assisting in the STANJAN equilibrium and unimolecular QRRK calculations.

Appendix I. Thermal Stability Ranking of Hazardous Organic Compounds

Principal Organic Hazardous Constituent[a]	Rank
cyanogen [ethanedinitrile]	1
hydrogen cyanide [hydrocyanic acid]	2
benzene	3
sulfur hexafluoride[b]	4
naphthalene	5

Footnotes: [a]Boldface print indicates compound thermal stability is experimentally evaluated; ranking based on UDRI experimental data coupled with reaction kinetic theory. Italicized print indicates compound thermal stability is ranked on the basis of literature experimental data coupled with reaction kinetic theory. [b]This compound is not currently on the U.S. EPA Appendix VIII list. [c]N.O.S. listing; ranking is based on either UDRI or literature ex-

perimental data coupled with reaction kinetic theory.

Literature Cited

(1) Oppelt, E. T. *JAPCA* **1987**, *37*, 558.
(2) *Guidance Manual for Hazardous Waste Incinerator Permits*; Prepared by Mitre Corp. for the U.S. EPA Office of Solid Waste and Emergency Response, Washington, DC, 1983; pp 2.16–2.26, NTIS PB84-100577.
(3) Tsang, W.; Shaub, W. Chemical Processes in the Incineration of Hazardous Wastes. In *Detoxification of Hazardous Waste*; Exner, J., Ed.; Ann Arbor Science: Ann Arbor, MI, 1982; pp 41–59.
(4) Lee, K. C.; Morgan, N.; Hansen, J. L.; Whipple, G. M. Revised Model for the Prediction of the Time–Temperature Requirements for Thermal Destruction of Dilute Organic Vapors and its Usage for Predicting Compound Incinerability. *Proceedings of the Seventy-Fifth Air Pollution Control Association Meeting*; New Orleans, LA, 1982; Paper 82-5.3.
(5) Dellinger, B.; Rubey, W. A.; Hall, D. L.; Graham, J. L. *Hazard. Waste Hazard. Mater.* **1986**, *3*, 139.
(6) Trenholm, A.; Lee, C. C. Analysis of PIC and Total Mass Emissions from an Incinerator. *Proceedings of the Twelfth Annual Research Symposium on Land Disposal, Remedial Action, Incineration, and Treatment of Hazardous Waste*; EPA/600/9-86/022; U.S. EPA: Cincinnati, OH, 1986; pp 376–381.
(7) Graham, J. L.; Hall, D. L.; Dellinger, B. *Environ. Sci. Technol.* **1986**, *20*, 703.
(8) Dellinger, B.; Graham, M.; Tirey, D. *Hazard. Waste Hazard. Mater.* **1986**, *3*, 293.
(9) Taylor, P. H.; Dellinger, B. *Environ. Sci. Technol.* **1988**, *22*, 438.
(10) Trenholm, A.; Gorman, P.; Jungelaus, G. *Performance Evaluation of Full-Scale Incineration*; EPA-600/2-84-181 a–e; U.S. EPA: Cincinnati, OH, 1984; Vols. I–V.
(11) Chang, D. P. Y.; Sorbo, N. W.; Law, C. K.; Steeper, R. R.; Richards, M. K.; Huffman, G. L. Relationships between Laboratory and Pilot-Scale Combustion of Some Chlorinated Hydrocarbons. *Proceedings of the AIChE National Meeting*; Denver, CO, 1988.
(12) Hart, J. H. The Use of Combustion Modelling in Permitting of Hazardous Waste Incinerators. *Proceedings of the Third Annual National Symposium on the Incineration of Industrial Wastes*; San Diego, CA, 1989; Paper No. 15.
(13) Yang, M.; Karra, S. B.; Senkan, S. M. *Hazard. Waste Hazard. Mater.* **1987**, *4*, 55.
(14) Chang, W. D.; Karra, S. B.; Senkan, S. M. *Combust. Sci. Technol.* **1987**, *49*, 107.
(15) Chang, W. D.; Senkan, S. M. *Environ. Sci. Technol.* **1989**, *23*, 442.
(16) Weissman, M.; Benson, S. W. *Int. J. Chem. Kinet.* **1984**, *16*, 307.
(17) Senser, D. W.; Cundy, V. A.; Morse, J. S. *Combust. Sci. Technol.* **1986**, *51*, 209.
(18) Clark, W. D.; LaFond, J. F.; Moyeda, D. K.; Richter, W. F.; Seeker, W. R.; Lee, C. C. Engineering Analysis of Hazardous Waste Incineration: Failure Mode Analysis for Two Pilot-Scale Incinerators. In *Incinerating Hazardous Wastes*; Freeman, H. M., Ed.; Technomic Publishing: Lancaster, PA, 1988; pp 349–356.
(19) Dellinger, B.; Torres, J.; Rubey, W. A.; Hall, D. L.; Graham, J. L.; Carnes, R. A. *Hazard. Waste Hazard. Mater.* **1984**, *1*, 137.
(20) Clark, W. D.; Seeker, W. R.; Lee, C. C. Engineering Analysis of Hazardous Waste Incineration: Energy and Mass Balance. In *Incinerating Hazardous Wastes*; Freeman, H. M., Ed.; Technomic Publishing: Lancaster, PA, 1988; pp 357–364.
(21) Graham, M. D.; Taylor, P. H.; Dellinger, B. A Model Study of Vaporization and Thermal Oxidation of a Multicomponent Hazardous Waste Droplet. *Proceedings of the Eastern States Section—Combustion Institute Meeting*; San Juan, Puerto Rico, 1986; Paper 57-1.
(22) Bergen, N. E.; Flatbush, E. K.; Dwyer, H. A. Unsteady Processes in Droplet Combustion: Application to Hazardous Waste Incineration. *Proceedings of the International Flame Research Committee Symposium on the Incineration of Hazardous, Municipal, and Other Wastes*, Palm Springs, CA, 1987.
(23) Sorbo, N. W.; Steeper, R. R.; Law, C. K.; Chang, D. P. y. An Experimental Investigation of the Incineration and Incinerability of Chlorinated Alkane Droplets. *Twenty-Second International Symposium on Combustion*, The Combustion Institute, in press.
(24) Glassman, I. *Combustion*; Academic Press: New York, 1977; p 225.
(25) Westbrook, C. K.; Dryer, F. L. *Prog. Energy Combust. Sci.* **1984**, *10*, 1.
(26) Tsang, W. Fundamental Aspects of Key Issues in Hazardous Waste Incineration. ASME Publication 86-WA/HT-27, 1986.
(27) Tsang, W. High-Temperature Chemical and Thermal Stability of Chlorinated Benzenes. *Proceedings of the International Flame Research Committee Symposium on the Incineration of Hazardous, Municipal, and Other Wastes*, Palm Springs, CA, 1987.
(28) Rubey, W. A. *Design Considerations for a Thermal Decomposition Analytical System*; EPA-600/2-80-098; U.S. Environmental Protection Agency: Cincinnati, OH, 1980.
(29) Rubey, W. A.; Carnes, R. A. *Rev. Sci. Instrum.* **1985**, *56*, 1795.
(30) Reynolds, W. C. *STANJAN Equilibrium Program, Version 3.3*; Department of Mechanical Engineering, Stanford University: Stanford, CA, 1986.
(31) Senkan, S. M. Combustion Characteristics of Chlorinated Hydrocarbons. In *Detoxification of Hazardous Wastes*; Exner, J., Ed.; Ann Arbor Science: Ann Arbor, MI, 1982; p 63.
(32) Benson, S. W. *Thermochemical Kinetics*, 2nd ed.; Wiley and Sons: New York, 1976.
(33) *Guidance on Setting Permit Conditions and Reporting Trial Burn Results*; Hazardous Waste Incineration Guidance Series; EPA/625/6-89/019; Prepared by Acurex Corp. for the U.S. EPA, Risk Reduction Engineering Laboratory and Center for Environmental Research Information, Office of Research and Development, Cincinnati, OH, 1989; Vol. II, pp 105–123.
(34) Dellinger, B.; Taylor, P. H.; Tirey, D. A. High Temperature Pyrolysis of C_2 Chlorocarbons. *Proceedings of the 198th National Meeting of the American Chemical Society, Symposium on Incineration*, Division of Fuel Chemistry, Miami Beach, FL, 1989.
(35) McMillen, D. F.; Golden, D. M. *Annu. Rev. Chem.* **1982**, *33*, 493.
(36) Benson, S. W.; O'Neal, H. E. Kinetic Data on Gas-Phase Unimolecular Reactions; NSRDS-NBS 21; U.S. Government Printing Office: Washington, DC, 1970.
(37) Biordi, J. C.; Lazzara, C. P.; Papp, J. F. *Sixteenth Symp. (Int.) on Combustion*; The Combustion Institute, 1976; p 1097.
(38) Drake, M. C.; Pitz, R. W.; Lapp, M.; Fenimore, C. P.; Lucht, R. P.; Sweeney, D. W.; Laurendeau, N. M. *Twentieth Symp. (Int.) on Combustion*; The Combustion Institute, 1984; p 327.
(39) Correa, S. M.; Drake, M. C.; Pitz, R. W.; Shyy, W. *Twentieth Symp. (Int.) on Combustion*; The Combustion Institute, 1984; p 337.
(40) Stepowski, D.; Labbaci, K.; Borghi, R. *Twenty-First Symp. (Int.) on Combustion*; The Combustion Institute, 1986; p 1561.
(41) Dean, A. M. *J. Phys. Chem.* **1985**, *89*, 4600.
(42) Schug, K. P.; Wagner, H. Gg.; Zabel, F. *Ber. Bensenges, Phys. Chem.* **1979**, *83*, 167.
(43) Kondratiev, V. N. *Rate Constants of Gas-Phase Reactions*; NSRDS COM-72-10014; National Institute of Standards and Technology: Washington, DC, 1972.
(44) Atkinson, R. A. *Chem. Rev.* **1986**, *86*, 69.
(45) Astholz, D. C.; Durant, J.; Troe, J. *Eighteenth Symp. (Int.) on Combustion*; The Combustion Institute, 1981; p 885.
(46) Kiefer, J. H.; Mizerka, L. J.; Patel, M. R.; Wei, H.-C. *J. Phys. Chem.* **1985**, *89*, 2013.

(47) Westbrook, C. K.; Dryer, F. L. *Prog. Energy Combust. Sci.* **1984**, *10*, 1.

Received for review December 28, 1988. Revised manuscript received August 28, 1989. Accepted October 27, 1989. This work was performed under the partial sponsorship of the U.S. EPA Risk Reduction Engineering Laboratory under Cooperative Agreement CR-813938. Although this research was funded by the U.S. EPA, it has not been subjected to Agency review and therefore does not necessarily reflect the views of the Agency and no official endorsement should be inferred.

Use of Humic Acid Solution To Remove Organic Contaminants from Hydrogeologic Systems

Abdul S. Abdul,* Thomas L. Gibson, and Devi N. Rai

Environmental Science Department, General Motors Research Laboratories, Warren, Michigan 48090

■ Experiments were carried out to evaluate the effectiveness of a 29 mg/L solution of humic acid to enhance the removal of six aromatic hydrocarbons (benzene, toluene, *p*-xylene, ethyltoluene, *sec*-butylbenzene, and tetramethylbenzene) from a sandy material. None of the compounds were completely removed from the material. Nonetheless, the compounds with the highest water solubility, benzene and toluene, were removed effectively; less than 1 mass % was retained with use of either the humic acid solution or water. For the less soluble organic compounds, removal was more difficult and was enhanced by the humic acid solution compared to water. Mass percent retained with humic acid was as follows: *p*-xylene, 1.4% (24% less than water); 3-ethyltoluene, 6.4% (40% less); *sec*-butylbenzene, 39% (14% less); and tetramethylbenzene, 43% (14% less). The positive effect of humic acid on the removal of these organics may arise from the aggregation of the humic acid molecules to form membranes and/or micelles, having hydrophilic exteriors and hydrophobic interiors. Partitioning of the hydrophobic organics from the bulk solution into the hydrophobic interior of these humic acid structures can account for their enhanced removal from the sandy material.

Introduction

Spills, leaks, or subsurface disposal of industrial solvents and petroleum products is known to have contaminated soil and groundwater systems with organic compounds including aromatic, chlorinated, and polycyclic aromatic hydrocarbons. Much is now known about the relative mobility of these chemicals through hydrogeologic systems; however, technologies to remediate contaminated sites are still under development.

The migration of nonpolar organic contaminants (NPOC) having low water solubility through hydrogeologic systems depends on the fraction of organic carbon (f_{oc}) of the hydrogeologic material and the water solubility (S) or the octanol-water partition coefficient (K_{ow}) of the NPOC (*1–4*). Their rate of migration decreases as the values of f_{oc} and K_{ow} increase (as K_{ow} increases S decreases); thus, NPOC having low water solubility are expected to migrate slowly through hydrogeologic systems and could be contained close to the source. Results from several studies have demonstrated that the removal of NPOC from soil and aquifer systems is resistant to water washing (*5–8*). Further, remediation based only on pumping is likely to be a lengthy and expensive task (*9*).

Humic acid (HA) solution may enhance the removal of NPOC from soil and aquifer systems because dissolved humic acid was previously found to increase the apparent water solubility of NPOC (*9–18*). The increase in solubility in an aqueous system containing dissolved humic acid can be described by eq 1 (*17*):

$$S_w^* = S_w (1 + C_{ha}K_{ha}) \quad (1)$$

where, S_w^* and S_w are the solubilities of the NPOC in the humic acid solution and in pure water, respectively. C_{ha} is the concentration of the humic acid (g/mL of water) and K_{ha} is the partition coefficient of the compound between the humic acid and water.

Humic acid, which is a component of soil organic matter, is made up of structural units including carboxylic, hydroxylic, phenolic, and aliphatic groups stabilized into aggregates. These structural units could take several structural forms, such as vesicle, membrane, and micelle (*16*). The membranes and micelles are characterized by hydrophilic exteriors and hydrophobic interiors. Wershaw (*16*) and Chiou et al. (*17*) proposed that the partitioning of hydrophobic contaminants to the hydrophobic interior of humic acid membranes or micelles could explain the apparent increase in the water solubility of NPOC.

Because NPOC are primarily bound to the organic carbon of soil and aquifer materials (*19, 2*) and dissolved humic acid increases the apparent water solubility of NPOC (*10, 14*), the migration of NPOC through soil and aquifer systems can be accelerated or retarded according to their partition coefficients (K_p) relative to the K_p of the humic acid. The objective of this study was to evaluate the effectiveness of a dissolved humic acid to accelerate the removal of six NPOC (benzene, toluene, *p*-xylene, ethyltoluene, *sec*-butylbenzene, and tetramethylbenzene) from a sandy-aquifer material.

Materials and Methods

Materials. The uncontaminated aquifer material selected for this study was obtained from the water table region of a shallow-perched aquifer. The material was air-dried and sieved, using a mechanical shaker to collect the 125–250-μm grain-size range. This aquifer material is a medium-fine sandy mixture of 91% sand, 8% silt, and 1% clay, and it has an average f_{oc} value of 0.006.

Benzene, toluene, *p*-xylene, 3-ethyltoluene, *sec*-butylbenzene, 1,2,4,5-tetramethylbenzene (>99% purity), and the humic acid sodium salt (technical grade, lot 042687) used in the experiments were from Aldrich Chemical Co., Milwaukee, WI. Also, ACS reagent-grade sodium chloride and potassium persulfate (J. T. Baker Chemical Co., Phillipsburg, NJ) and ACS reagent-grade sodium azide, sodium carbonate, sodium bicarbonate, sulfuric acid, and HPLC-grade acetonitrile and water (Fisher Scientific, Fairlawn, NJ) were used.

A 50 mg/L sodium chloride solution was prepared in organic-free deionized water (Milli-Q system, Millipore, Inc.) for use in determining the volume of the pore space in the column. A 2% potassium persulfate aqueous solution was prepared for the total organic carbon (TOC) an-

 0013-936X/90/0924-0328$02.50/0

Table I. Aqueous Solubilities of the Six NPOC and Their Equilibrium Concentrations within the Columns at the End of the Adsorption Phase

compound	water sol, mg/L	log K_{ow}	equilibrium conditions: mg/L, column 1	mg/L, column 2	mass of NPOC, μg, column 1	mass of NPOC, μg, column 2	K_d, mL/g
benzene	1800	2.13	47.0	41.0	7797.7	6802.2	0.47
toluene	535	2.65	26.0	23.2	5534.4	4938.4	0.61
p-xylene	150	3.18	10.0	9.6	3670.2	3488.5	1.04
3-ethyltoluene	40		2.3	2.2	1270.5	1215.2	1.58
sec-butylbenzene	17.6		0.7	0.57	748.0	609.1	3.06
1,2,4,5-tetramethylbenzene	3.5	4.72	0.24	0.22	289.2	258.4	3.42

alyzer. A potassium hydrogen phthalate solution (4250 mg/L equivalent to 2000 mg/L carbon) was used to calibrate the TOC analyzer. For ion chromatography, a 0.75 mM $NaHCO_3$/2 mM Na_2CO_3 buffer and 0.025 N H_2SO_4 were prepared in deionized water. The humic acid solution was prepared by dissolving 4000 mg of its sodium salt in 250 mL of deionized water. The solution was stirred for 30 min and centrifuged at 1000 relative centrifugal force for 25 min, and the supernatant was filtered through a precombusted 0.45-μm glass-fiber filter paper (Gelman Sciences Inc., Ann Arbor, MI). The organic carbon content of this stock solution was measured and the concentration was calculated as milligrams of organic carbon per liter (1760 mg/L). Further dilutions to the required concentration of humic acid were then prepared in deionized water. An aqueous solution of six aromatic hydrocarbons (see Table I for concentrations) was prepared by the slow addition, using a syringe pump and flow of 0.15 mL/min, of their methanolic solution (2 mL) to 4 L of deionized water continuously stirred in a closed reservoir (*20*).

Column Packing. Columns were constructed from 7.6 cm (i.d.) by 10 cm (long) Pyrex glass tubes, and stainless steel distributor plates, supporting plates, screens, and ports (Figure 1). To minimize adsorption of the NPOC by the system, all connecting tubes, fittings, nuts, and stopcocks were made of Teflon. Each column was slowly packed by pouring a continuous thin stream of sand while tapping the side of the column to achieve a uniform porous medium. The bed of sand in each column was 5.6 cm thick (349 g) and had the following physical properties: saturated hydraulic conductivity, $\simeq 10^{-2}$ cm/s; porosity, 0.42; bulk density, 1.37. The air in the pore spaces of the sand bed was displaced by flushing with CO_2 gas (at ~10 psi), which is water soluble, through each column for 10 min. This step was carried out to reduce the extent of entrapped air in the column. The columns were then slowly saturated with water containing 0.25 mg/L sodium azide, to inhibit microbial processes. A variable-speed, cassette-type peristaltic pump (Manostat Co., New York) was used to pump the solution from a 1-gal amber glass bottle through the columns. Glass sample vials (4, 8, and 16 mL) with screw- or crimp-top caps having Telfon-lined septa were used for the collection of samples.

Adsorption Procedure. The compounds dissolved in water were pumped at 1.0 mL/min into the column (flux, 0.022 cm/min; average linear velocity, 0.052 cm/min) via the inlet port at the base of the column (Figure 1). The effluent samples were collected in vials filled to the top with a minimum headspace. Except for a needle-point vent in its cap, each sample vial formed a closed loop with the column. Samples were immediately refrigerated for subsequent analysis. Results of prepared aqueous samples of the NPOC (controls having minimum headspace), which were stored and handled in a manner similar to the experimental samples, did not show any measurable loss of the NPOC from solution. To keep track of the total

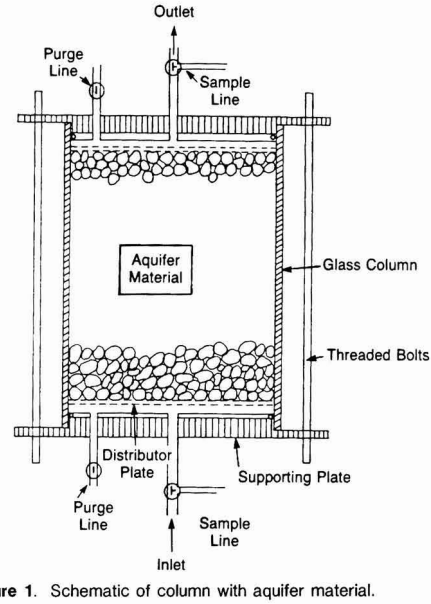

Figure 1. Schematic of column with aquifer material.

volume of solution passed through the columns, the time was recorded at the beginning and end of each sample collection, and the flow rate was checked several times during the experiment. When adsorption equilibrium was reached (equal inlet and outlet concentrations), the inlet and outlet stopcocks were closed, and the pump was shut off for 5–10 min to prepare for the desorption phase.

Desorption Procedure. In preparation for a desorption experiment, the inlet solution was changed to either water or humic acid and all tubing attached to the inlet end of each column was replaced. The desorbing solution was then pumped at 1.0 mL/min through the column material. The same method was adopted for sample collection as described in the adsorption procedure.

Analytical Procedures. The organic carbon content of the aquifer material was determined with an automatic carbon analyzer (Coulometrics, Inc., Wheat Ridge, CO) (*2*). Total organic carbon (TOC) of the humic acid in aqueous samples was determined with a Dohrmann/Xertex DC-80 analyzer. In this analyzer, TOC is measured by ultraviolet-promoted persulfate oxidation followed by infrared detection of CO_2. The chloride ion concentration for the pore volume study was measured on a Dionex ion chromatograph (Dionex Corporation, Sunnyvale, CA). Elution of chloride was accomplished by using carbonate/bicarbonate buffer at a flow rate of 2.3 mL/min on the 3 by 500 mm anion separator and 6 by 250 mm anion suppressor columns; the response was measured by a conductivity detector. The concentrations of aromatic hy-

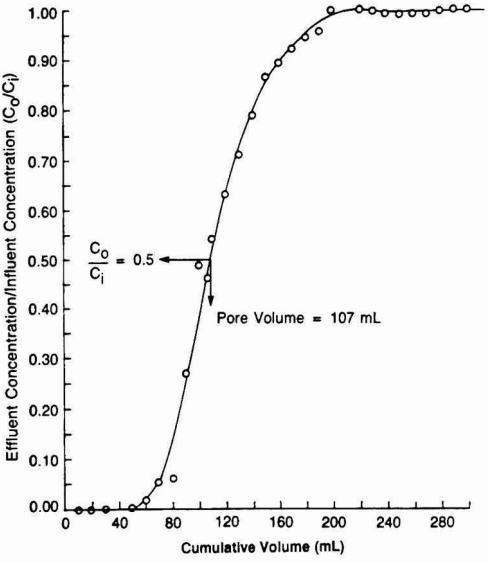

Figure 2. Adsorption breakthrough curve for chloride migration through the column.

drocarbons in the influent and effluent samples were measured by HPLC (*20*) using a Varian 5020 liquid chromatograph, Zorbax ODS column [25 cm by 4.6 mm (i.d.), Du Pont Co.], and Kratos Spectroflow 757 UV detector fitted with a 12-μL flow cell of 8-mm path length. Aqueous samples (25 μL) were directly injected on the column and eluted with acetonitrile and water (80 and 20%, v/v, respectively). The absorbance of the aromatic compounds was measured at 205-nm wavelength, and their concentrations were determined by comparison of peak areas with standard solutions.

Experiments

Pore Volume Determination. Each column was flushed with a 50 mg/L sodium chloride solution for 5 h, and the effluent samples were collected and analyzed by ion chromatography for chloride ion concentrations. The volume of solution needed to cause the effluent concentration of chloride to reach 50% of the influent solution is a measure of 1 pore volume (Figure 2).

Adsorption of Aromatic Hydrocarbons. An aqueous solution of the six aromatic hydrocarbons was introduced from a closed-feed reservoir (maintained under slight positive N_2 pressure, $\simeq$1 psi) to the bottom of both columns (adsorption procedure) for 42 h. The influent and effluent samples were collected and analyzed for the aromatic hydrocarbons by HPLC.

Desorption of Aromatic Hydrocarbons. The adsorbed aromatic hydrocarbons were subsequently eluted from one column with deionized water and from the other column by a 29 mg/L aqueous solution of humic acid. The effluent samples were also analyzed for aromatic hydrocarbons.

Adsorption/Desorption of Humic Acid. A separate experiment was conducted to study the adsorption and desorption of the humic acid. A 29 mg/L solution of humic acid was pumped through one column for 9 h (adsorption procedure), and the adsorbed humic acid was then washed from the column material with water (desorption procedure) for 48 h. The aqueous samples were analyzed for TOC.

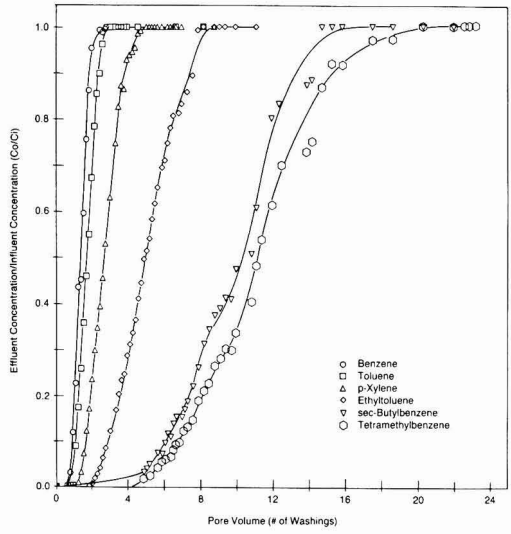

Figure 3. Adsorption breakthrough curves for the migration of the six NPOC through the column.

Results and Discussion

Breakthrough Experiments. Figure 3 shows adsorption breakthrough curves (effluent concentration/influent concentration versus pore volume) for the migration of each NPOC through one of the two columns. The results from the other column are similar. These results are summarized in Table I, which also includes properties of the six NPOC. In general, the breakthrough curves were symmetrical about the 0.5 relative concentration point, and the retardation of the NPOC and the spread in the curves increased as the water solubility of the NPOC decreased. The good symmetry of the curves about the 0.5 relative concentration point indicates that the columns were uniformly packed and that sorption equilibrium was achieved.

The mass of each of the NPOC adsorbed in each of the two columns was determined from the area above the breakthrough curve and the equilibrium breakthrough concentration. These results are included in Table I. The equilibrium concentration for each compound adsorbed in column 1 was higher than that in column 2. As such, the mass of each compound in column 1 (ranging from 7.7977 mg of benzene to 0.2892 mg of tetramethylbenzene) was slightly higher than that in column 2 (ranging from 6.8022 mg of benzene to 0.2584 mg of tetramethylbenzene).

The value of K_p (partition coefficient) for each compound in each column was determined from eq 2, where

$$K_p = \frac{(m_i - m_0)/m_s}{C_0} \tag{2}$$

m_i is the total mass of each NPOC entering column (g), m_0 the total mass of each NPOC leaving column (g), m_s the mass of aquifer material in column (g), and C_0 the equilibrium breakthrough concentration of NPOC (g/mL). As expected, the two values of K_p for each compound, one for each column, are equal. Consistent with the results from previous studies (*3*, *18*), the value of K_p increases as the aqueous solubility of the compound decreases or as its K_{ow} increases.

Decontamination Experiments. The decontamination results from the two columns are shown in Figure 4 as percent mass of each NPOC retained in the columns versus pore volume. The percent mass retained for each

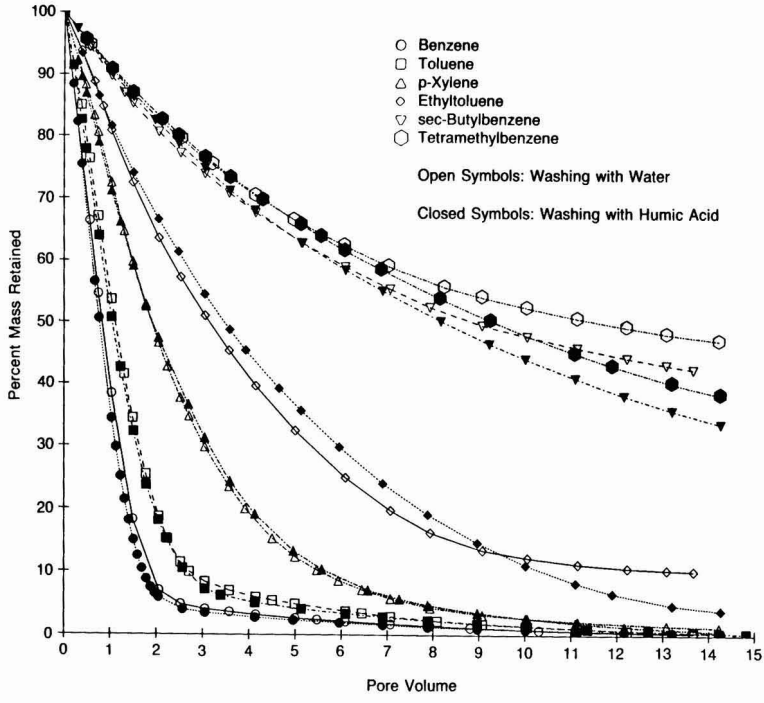

Figure 4. Percent mass of the six NPOC retained by the aquifer material during washing with water and humic acid.

Table II. Mass Percent of Each NPOC Remaining in the Columns after Washing with either Water or the Humic Acid Solution (HA)

	2 pore vol		4 pore vol		8 pore vol		12 pore vol	
compound	water	HA	water	HA	water	HA	water	HA
benzene	8.19	6.26	3.25	2.78	1.41	1.21	0.50	0.57
toluene	10.14	19.21	6.20	5.23	2.29	2.21	0.79	0.83
p-xylene	48.07	48.45	19.37	20.38	4.25	4.58	1.84	1.40
3-ethyltoluene	64.53	67.27	41.22	44.97	16.06	18.64	10.75	6.44
sec-butylbenzene	81.07	82.27	68.48	68.84	52.46	51.01	44.73	38.69
1,2,4,5-tetramethylbenzene	82.97	83.62	71.10	71.34	56.50	54.50	49.65	42.9

NPOC was determined from the total mass retained by the column material during the adsorption experiment (Table I) and the mass removed during any given period of washing. The results in Figure 4 are summarized in Table II for 2, 4, 8, and 12 pore volumes.

All the results show a similar trend of decreasing mass of NPOC, which approached zero asymptotically. As the water solubility of the NPOC decreased, each one was more resistant to being washed from the column material by either water or the solution of humic acid. However, washing with either water or humic acid solution was about equally effective in removing benzene or toluene from the aquifer material. These results could be explained by the lower value of K_p for the humic acid than of benzene or toluene. This observation will be discussed after the results for the other four NPOC are presented.

The results from the two columns for *p*-xylene, ethyltoluene, *sec*-butylbenzene, and tetramethylbenzene show that during the early stages of the experiments, water was more effective than the humic acid solution in washing these compounds from the aquifer material (Figure 4 and Table II). However, as washing continued, the humic acid solution became increasingly more effective in removing these NPOC from the aquifer material. This is illustrated by the crossover of the curves for water and humic acid

Table III. Partition of Each NPOC between the Sand and Solution in Each Column after 12 Pore Volumes

	aq concn, mg/L			K_p		
compound	water (S)	HA (S^*)	S^*/S	water, mL/g	K_p^* (HA), mL/g	K_p/K_p^*
benzene	0.094	0.082	0.87	1.19	1.35	0.88
toluene	0.130	0.116	0.89	0.96	1.01	0.95
p-xylene	0.110	0.154	1.40	1.76	0.91	1.93
3-ethyltoluene	0.058	0.200	3.45	6.75	1.12	6.03
sec-butylbenzene	0.099	0.144	1.45	9.68	4.69	2.06
1,2,4,5-tetramethylbenzene	0.036	0.057	1.58	11.41	5.57	2.05

washing. The crossover is earliest for the least water soluble NPOC. Specifically, the enhanced washing by the humic acid solution started earlier for the least water soluble or the most hydrophobic NPOC. This is consistent with previous findings that macromolecules in solution caused a larger increase in the relative mobility of the more hydrophobic compounds (*21*). Results for the partitioning of each NPOC between the solid phase and solution phase, after washing with either 12 pore volumes of water or humic acid solution, are shown in Table III. These results were calculated by using eq 2 and assuming sorption

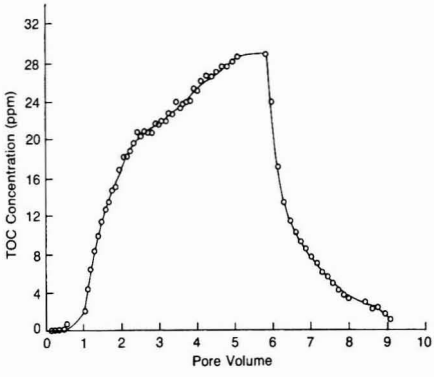

Figure 5. Adsorption/desorption breakthrough curves for humic acid and the aquifer material.

equilibrium conditions existed in the columns. The ratios (S^*/S) of the aqueous concentrations of each NPOC in the presence and absence of the humic acid and (K_p/K_p^*) of its partition coefficients in the absence and presence of the humic acid are included in Table III. The ratios for 3-ethyltoluene are higher than expected; however, it should be noted that after an 8 pore volume washing the S^*/S and K_p/K_p^* values for 3-ethyltoluene were 1.23 and 1.12, respectively. The results in Table III clearly show the effect of the humic acid in enhancing the removal of the compounds (except benzene or toluene) from the column material. These results cannot be adequately described by simple two-phase partitioning relations such as that expressed by eq 1. The composition, concentration, and sorption of the humic acid, the water solubility or K_{ow} of the compound, and the composition of the aquifer material may collectively contribute to the observed enhancing effect of the humic acid.

To better understand the results from washing with the solution of humic acid, consider the results in Figure 5 for the adsorption/desorption of the humic acid by the aquifer material. The results in Figure 5 were obtained from a separate column experiment by following the procedures outlined under Materials and Methods. The adsorption and desorption curves are similar in shape to those previously presented for the six NPOC. Equilibrium adsorption of the humic acid, from a solution of 29 mg/L humic acid, at a flow rate of 1 mL/min, was reached after 5.5 pore volumes of the solution had passed through the column. In addition, the value of K_p for the humic acid as determined from the adsorption curve and by using eq 2 is 0.71 mL/g.

Comparing the values of K_p for the six NPOC with that for the humic acid shows that the K_p for the humic acid is greater than that for benzene or toluene, but smaller than those for the other four NPOC. In that the humic acid solution did not significantly influence the removal of benzene and toluene through the aquifer material, it seems that its mobility through the aquifer material, relative to that of the NPOC, is an important factor in enhancing the removal of the NPOC from the column material.

The results may reflect the outcome of several mechanisms. At the start of the decontamination experiment with humic acid, desorption of NPOC and adsorption of the humic acid will commence. The introduction of humic acid to the column could, therefore, increase the mass of organic matter in the bulk solution and also on the aquifer material in the column. If there is competition between the NPOC and the humic acid for adsorption sites on the aquifer material, this could lead to enhanced removal of the NPOC. This process of competitive sorption is not expected to be significant because of the dilute concentrations of the NPOC and the humic acid used in the study. In contrast, the adsorbed humic acid will increase the organic carbon content on the solid phase and could further influence the partitioning of the NPOC from the aqueous phase.

At the same time, the increase in organic matter in the aqueous phase could enhance the removal of the NPOC from the aquifer material. The mechanism for this enhanced removal may be explained by considering the humic acid models presented by Wershaw (*16*), who proposed that the structural units of humic acid are arranged into membranes and/or micelles having hydrophobic interiors and hydrophilic exteriors. An example of this arrangement is a humic acid aggregate in the form of a micelle having carboxyl and/or hydoxyl groups on the exterior and alkyl groups in the interior. By this model the hydrophobic NPOC became trapped within the hydrophobic interior of the humic acid and were carried along in the bulk solution with the humic acid micelle or membrane.

This induced competition for the NPOC between the solid aqueous phases, as the humic acid is partitioning between these phases is evident in the crossover of the water and humic acid solution curves shown in Figure 4. The effectiveness of the humic acid solution became significant only after the adsorption capacity of the aquifer material for the humic acid was reached (after ~5.5 pore volumes; see Figure 5).

Conclusion

The results from this study indicate that a solution of 29 mg/L humic acid is more effective than water in removing the more hydrophobic NPOC from the aquifer material used in the experiments. However, the absolute effectiveness of humic acid solution to decontaminate hydrogeologic systems contaminated with NPOC cannot be completely assessed from our current findings. The hydrophobicity of the humic acid, the pH of the pore water, and soil/aquifer organic carbon content are three parameters that can significantly influence the effectiveness of a humic acid solution in a decontamination scheme.

The injection of any liquid into the subsurface, even with good intent, must be subjected to very careful scrutiny. Although humic acid occurs naturally in soils, the potential environmental impact from further addition of humic acid to the subsurface will need to be carefully considered.

Registry No. Benzene, 71-43-2; toluene, 108-88-3; *p*-xylene, 106-42-3; 3-ethyltoluene, 620-14-4; *sec*-butylbenzene, 135-98-8; 1,2,4,5-tetramethylbenzene, 95-93-2.

Literature Cited

(1) Schwarzenbach, R. P.; Westall, J. *Environ. Sci. Technol.* **1981**, *15*, 1360.
(2) Abdul, A. S.; Gibson, T. L.; Rai, D. N. The effect of organic carbon on the adsorption of fluorene by aquifer materials. *Hazard. Waste Hazard. Mater.* **1986**, *3*(4), 429.
(3) Abdul, A. S.; Gibson, T. L.; Rai, D. N. Statistical correlations for predicting the partition coefficient for nonpolar organic contaminants between aquifer organic carbon and water. *Hazard. Waste Hazard. Mater.* **1987**, *4*(3), 211.
(4) Swoboda, A. R.; Thomas, G. W. Movement of parathion in soil columns. *J. Agric. Food Chem.* **1968**, *16*, 923.
(5) Rao, P. S. C.; Davidson, J. M. Adsorption and movement of selected pesticides at high concentrations in soils. *Water Res.* **1979**, *13*, 375.
(6) Rogers, R. D.; McFarlane, J. C.; Cross, A. J. *Environ. Sci. Technol.* **1980**, *14*, 457.

(7) Abdul, A. S.; Gibson, T. L. Adsorption-desorption of polycyclic aromatic hydrocarbons by two hydrogeologic materials. *Hazard. Waste Hazard. Mater.* **1986**, *3*(2), 125.
(8) Mackay, M. D.; Roberts, P. V.; Cherry, J. A. Transport of organic contaminants in groundwater. *Environ. Sci. Technol.* **1983**, *19*, 384.
(9) Wershaw, R. L.; Burcar, P. J.; Goldberg, M. C. Interaction of pesticides with natural organic material. *Environ. Sci. Technol.* **1969**, *3*, 271.
(10) Ballard, T. M. Role of humic carrier substances in DDT movement through forest soil. *Soil Sci. Soc. Am. Proc.* **1971**, *35*, 146.
(11) Matsuda, K.; Schnitzer, M. *Bull. Environ. Contam. Toxicol.* **1973**, *6*, 200.
(12) Porrier, M. A.; Bordelon, B. R.; Laseter, J. L. *Environ. Sci. Technol.* **1972**, *6*, 1033.
(13) Boehm, P. D.; Quinn, J. G. *Geochim. Cosmochim. Acta* **1973**, *37*, 2459.
(14) Hassett, J. P.; Anderson, M. A. Association of hydrophobic organic compounds with dissolved organic matter in aquatic systems. *Environ. Sci. Technol.* **1979**, *13*, 1526.
(15) Carter, C. W.; Suffet, I. H. Binding of DDT to dissolved humic materials. *Environ. Sci. Technol.* **1982**, *16*, 735.
(16) Wershaw, R. L. A new model for humic materials and their interactions with hydrophobic organic chemicals in soil-water sediment-water systems. *J. Contam. Hydrol.* **1986**, *1*, 29.
(17) Chiou, C. T.; Malcolm, R. L.; Brinton, T. I.; Kile, D. E. Water solubility enhancement of some organic pollutants and pesticides by dissolved humic and fulvic acids. *Environ. Sci. Technol.* **1986**, *20*, 502.
(18) Chiou, C. T.; Kile, D. E.; Brinton, T. I.; Malcolm, R. L.; Leenheer, J. A.; McCarthy, P. A comparison of water solubility enhancements of organic solutes by aquatic humic materials and commercial humic acids. *Environ. Sci. Technol.* **1987**, *21*, 1231.
(19) Chiou, C. T.; Porter, P. E.; Schmeddling, D. W. Partition equilibria of nonionic organic compounds between soil organic matter and water. *Environ. Sci. Technol.* **1983**, *17*, 227.
(20) Gibson, T. L.; Abdul, A. S.; Rai, D. N. Measurement of toxic organic contaminants in groundwater studies by high-performance liquid chromatography. *Hydrol. Sci. Technol.* **1986**, 2, 61.
(21) Enfield, C. G.; Bengtsson, G. Macromolecular transport of hydrophobic contaminants in aqueous environment. *Ground Water* **1988**, *26*, 64.

Received for review January 30, 1989. Revised manuscript recceived September 1, 1989. Accepted October 27, 1989.

Determination of Sulfite and Thiosulfate in Aqueous Samples Including Anoxic Seawater by Liquid Chromatography after Derivatization with 2,2′-Dithiobis(5-nitropyridine)

Appathural Valravamurthy[†] and Kenneth Mopper*

Division of Marine and Atmospheric Chemistry, Rosenstiel School of Marine and Atmospheric Science, University of Miami, 4600 Rickenbacker Causeway, Miami, Florida 33149-1098

■ 2,2′-Dithiobis(5-nitropyridine) (DTNP) is used to determine sulfite and thiosulfate in aqueous samples by high-performance liquid chromatography and UV detection. Derivatization was performed at pH 6 for 5 min. An ion-pairing agent, tetrabutylammonium hydrogen sulfate (TBAHS) was used to optimize separation on a reversed-phase (C_{18}) microbore column. The DTNP derivatives can be quantitatively extracted from aqueous samples on Sep-Pak C_{18} cartridges, a technique that has proven useful for field sampling as well as manifold sample concentration. The cartridge-adsorbed DTNP derivatives appear to be stable at 0–5 °C for at least 2 weeks and, therefore, can be stored for HPLC analysis at a later date. For aqueous samples the detection limits for thiosulfate and sulfite are about 60 and 80 nM, respectively, and can be decreased further by using the C_{18} cartridge enrichment technique. The precision of the method is about ±5% in the 0.2–5-μM range. Application of this method is illustrated for Black Sea water samples.

Introduction

The determination of sulfite and thiosulfate at trace concentrations in aqueous solutions is important in a variety of applications. Widely used methods for sulfite determination include the Monier–Williams method (*1*) and the West and Gaeke colorimetric method (*2*). Urban's colorimetric method (*3*) was commonly used for thiosulfate determination. The Monier–Williams method for sulfite is time consuming and involves titration of sulfur dioxide released on HCl treatment of samples. The colorimetric methods also have limitations including sensitivity, precision, convenience of use, and interference by other compounds. For example, in Urban's spectrophotometric method for thiosulfate, sulfide causes a positive interference and must be removed by stripping with nitrogen at low pH. A method was recently described for sulfite using ion chromatography with electrochemical detection (*4*). A similar method also has been used for the determination of thiosulfate (*5*). However, ion chromatographic methods are not appropriate for determination of trace constituents in ionic media such as seawater. The polarographic technique of Luther et al. (*19*) appears to be better suited for this application. Dasgupta and Yang recently described a fluorometric flow injection method for sulfite based on *N*-acrydinylmaleimide derivatization (*6*). Sulfite was also determined by flow injection and spectrometry based on reaction with Ellman's reagent, 5,5′-dithiobis(2-nitrobenzoic acid) (DTNB) (*7*), as well as by using a sulfite oxidase enzyme electrode (*8*).

Here we describe a high-performance liquid chromatographic (HPLC) method for the determination of sulfite and thiosulfate in aqueous samples. The present method involves precolumn derivatization with 2,2′-dithiobis(5-nitropyridine) (DTNP) for reversed-phase separation and UV detection. The derivatization involves a simple displacement reaction, resulting in a new disulfide derivative and 2-mercapto-5-nitropyridine.

[†]Present address: Environmental Chemistry Division, Department of Applied Science, Brookhaven National Laboratory, Upton, NY 11973.

0013-936X/90/0924-0333$02.50/0

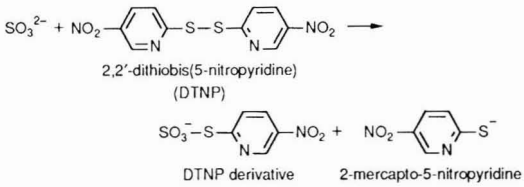

DTNP was previously used for the spectrophotometric determination of thiols in biological samples (*9*, *10*). This reagent was found superior to the structurally analogous Ellman's reagent in sensitivity as well as reactivity over a wide pH range (*10*).

As opposed to other methods, the DTNP method lends itself well to field work. Samples can be derivatized with DTNP and extracted on reversed-phase C_{18} Sep-Pak cartridges in the field. The cartridge-adsorbed DTNP derivatives appear to be stable at 0–5 °C for at least 2 weeks and can be stored for HPLC analysis at a later date. Sep-Pak cartridge extraction also enables manifold decrease in detection limit; because the DTNP derivatives can be enriched from a large sample volume. This method has been used in a cruise to the Black Sea, and the results are presented here.

Experimental Section

Apparatus. A reversed-phase C_{18} microbore column (150 mm × 2.0 mm) containing Hypersil ODS, 5-μm packing (Keystone Scientific, State College, PA), was used to obtain HPLC separations. A microbore guard column (Upchurch Scientific, Oak Harbour, WA) packed with 5-μm Spherisorb ODS-2 preceded the analytical column. The HPLC instrument consisted of a gradient system (Gilson Medical Electronics, Middleton, WI) with two single-piston pumps (Model 302, 5.SC), a manometric module (Model 802B), and a UV detector (Model 116) with a 2-μL flow cell. The detection wavelength was 320 nm. A static, 9-μL mixer (Lee Co., Westbrook, CT) was used as the gradient mixer. Gilson's 714 HPLC System Controller software (version 1.2) loaded in an IBM PC/AT was used as the system controller. A Rheodyne (Berkeley, CA) 7125 injector with a 20-μL external loop was used for sample introduction. To minimize extracolumn dispersion in the connecting tubing, precut stainless steel tubing with 0.13-mm (0.005in.) i.d. was used for connections between the mixer and the detector, whereas 0.51-mm (0.020in.)-i.d. tubing was used from the pump to the mixer. Absorption spectra of the DTNP derivatives were obtained with a Hewlett-Packard (HP) Model 1040A diode array detector interfaced to a HP 9000 Series computer module.

Chemicals. Milli-Q-grade water (Millipore Corp., Bedford, MA) and HPLC-grade solvents (Burdick and Jackson, Muskegon, MI) were used in the preparation of reagent solutions, standards, and mobile phases. The derivatization agent, 2,2′-dithiobis(5-nitropyridine) (DTNP) and organic thiols were obtained from Aldrich Chemical Co. (Milwaukee, WI). Sodium thiosulfate and anhydrous sodium sulfite (Mallinckrodt Chemicals) were used for standards. Tetrabutylammonium hydrogen sulfate (purity, >99%) was from Fluka Chemical Co. (Ronkonkoma, NY). HPLC-grade sodium acetate was obtained from J. T. Baker Chemical Co. (Phillipsburg, NJ).

Standards. Both Milli-Q water and filtered seawater (from open ocean) used in the preparation of standards were sparged with nitrogen prior to use in order to minimize oxidation. Primary standards in the range of 20–50 mM were made in Milli-Q water and discarded after a day's use. Working standards were made by appropriate dilution of primary standards just prior to analysis.

Derivatization. Standards in the 0.1–5 μM range (made in Milli-Q water or filtered seawater) were derivatized by addition of 50 μL of DTNP solution (a 2 mM solution in acetonitrile) and 50 μL of a sodium acetate buffer (0.2 M) of pH 6 to 1-mL solutions of standards. The mixture was allowed to react for 5 min at ambient temperature prior to injection. For samples containing high levels of sulfide (e.g., sediment pore waters), it was necessary to add the reagent in more than 2-fold excess of the sulfide concentration, because DTNP also reacts with sulfide as well as with sulfite and thiosulfate. We routinely used a 10 mM DTNP solution in acetonitrile for derivatization of samples. When DTNP is present in excess, it precipitates in the aqueous reaction mixture. This precipitate was removed by centrifugation prior to HPLC injection.

Sep-Pak C_{18} Cartridge Extraction. Sep-Pak C_{18} cartridges were obtained from Waters Associates (Milford, MA). Prior to use, the cartridges were rinsed with ~5 mL of methanol, 5 mL of Milli-Q water, and 5 mL of a pH 6 buffer solution containing 20 mM sodium acetate and 10 mM tetrabutylammonium hydrogen sulfate. The final rinse with tetrabutylammonium solution is necessary because sulfite and thiosulfate derivatives are negatively charged species and therefore require ion-pair formation for quantitative adsorption on the hydrophobic C_{18} stationary phase. The sample was loaded onto the cartridge at a flow rate of 3–4 mL/per min. After the sample was passed through, the cartridge was rinsed with ~3–5 mL of water and subsequently nitrogen was blown through. The adsorbed derivatives were eluted from the Sep-Pak cartridge with 1 mL of methanol and mixed with an equal volume of water prior to HPLC analysis. Sep-Paks are reusable at least 3 times.

HPLC Conditions. HPLC separations were performed by gradient elution using a flow rate of 100 or 200 μL/min. The column temperature was ambient. The stronger eluent (B) was acetonitrile, and the weaker eluent (A) was an aqueous solution containing 0.05 M sodium acetate and 7.5 mM tetrabutylammonium hydrogen sulfate (TBAHS) in Milli-Q water. Eluent A was adjusted to pH 3.5 ± 0.05 with 6 N HCl. On start-up, the eluents were degassed by combined application of evacuation and sonication; during analysis helium was sparged through the eluents. Gradient elution was required in order to separate sulfite and thiosulfate derivatives from those of organic thiols. The gradient typically used was as follows: isocratic at 10% B for 1 min; 10% B to 34% B in 8 min; 34% B to 55% B in 14 min; 55% B to 100% B in 5 min; isocratic at 100% B for 2 min; back to 10% B in 2 min; at this point the next sample was injected.

Results and Discussion

The absorption spectra of DTNP derivatives of sulfite and thiosulfate, as well as some thiols, were obtained by using the diode array detector, as the peaks eluted in an HPLC run. The spectra of the different derivatives were identical, with absorption maxima in the region of 315–320 nm (Figure 1); therefore the detection wavelength was set at 320 nm.

The effect of pH on derivatization was studied with buffer solutions made to 0.2 M by use of sodium acetate for pH 5 and 6, sodium phosphate for pH 7 and 8, and sodium borate for pH 9. The time required for completion of reaction of sulfite and thiosulfate with DTNP was examined at these pH values by varying the time from 2 min to 1 h prior to injection into the chromatograph. A 1-mL aliquot of a 1 μM standard in seawater was derivatized at

Emerging Developments in Environmental Science

ENVIRONMENTAL SCIENCE & TECHNOLOGY

Enter your own monthly subscription to ES&T and be among the first to get the most authoritative technical and scientific information on environmental issues.

☐ **YES! I want my own one-year subscription to ENVIRONMENTAL SCIENCE & TECHNOLOGY at the rate checked below:**

1990 Published Monthly	U.S.	Canada & Mexico	Europe	All Other Countries
ACS members:	☐ $ 36	☐ $ 50	☐ $ 65	☐ $ 72
Nonmembers Personal	☐ $ 67	☐ $ 81	☐ $ 96	☐ $103
Nonmembers-Institutional	☐ $276	☐ $290	☐ $305	☐ $312

☐ Payment Enclosed (Payable to American Chemical Society)
☐ Bill Me ☐ Bill Company
Charge my ☐ ViSA/MasterCard
☐ Diners Club/Carte Blanche

Card No. _____

Expires _____ Signature _____

Name _____

Title _____ Employer _____
Address ☐ Home
☐ Business _____

City, State, Zip _____

Employer's Business: ☐ Manufacturing ☐ Academic ☐ Government
☐ Other _____

Member rates are for personal use only.
Subscriptions outside the U.S., Canada, and Mexico are delivered via air service.
Foreign payment must be made in U.S. currency by international money order, UNESCO coupons, or U.S. bank draft. Orders accepted through your subscription agency. For nonmember rates in Japan, contact Maruzen Co., Ltd. Please allow 45 days for your first copy to be mailed.

Redeem until December 31, 1990.

680 **MAIL THIS POSTAGE-PAID CARD TODAY!** 5454J

(800) 227-5558 (U.S. only)

NO POSTAGE
NECESSARY
IF MAILED
IN THE
UNITED STATES

BUSINESS REPLY MAIL

FIRST CLASS PERMIT NO. 10094 WASHINGTON, D.C.

POSTAGE WILL BE PAID BY ADDRESSEE

American Chemical Society
Marketing Communications Department
1155 Sixteenth Street, N.W.
Washington, D.C. 20077-5768

(800) 227-5558 (U.S. only)

NO POSTAGE
NECESSARY
IF MAILED
IN THE
UNITED STATES

BUSINESS REPLY MAIL

FIRST CLASS PERMIT NO. 10094 WASHINGTON, D.C.

POSTAGE WILL BE PAID BY ADDRESSEE

American Chemical Society
Marketing Communications Department
1155 Sixteenth Street, N.W.
Washington, D.C. 20077-5768

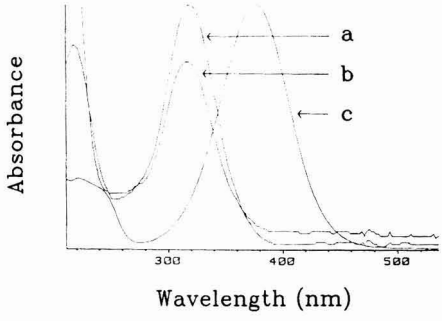

Figure 1. Absorption spectra of (a) DTNP–thiosulfite derivative, (b) DTNP–sulfite derivative, and (c) 2-mercapto-5-nitropyridine (byproduct of derivatization).

Table I. Relative Recovery of Thiosulfate with Derivatization Time at Two Different Reaction pHs for a 1 μM Standard in Seawater

time, min	recovery, % pH 6	recovery, % pH 8	time, min	recovery, % pH 6	recovery, % pH 8
2	98	98	30	96	92
5	100	100	60	94	76
10	96	100	180	73	36

ambient temperature with 50 μL of DTNP (2 mM) and 50 μL of the appropriate buffer. At all pH values the maximum in peak area was attained after 2 min, indicating that the reaction was completed within 2 min. The sulfite derivative was found to be stable for at least 1 day, but the thiosulfate derivative began to break down slowly after a few minutes at room temperature. Furthermore, the thiosulfate derivative appeared to break down more rapidly at high than at low pH values (Table I). Therefore, we carried out derivatization at pH 6 for 5 min routinely. Although we did not perform a separate study of the breakdown reaction, we did observe an increase in sulfite concentration with the decrease in thiosulfate level, which suggests that sulfite derivative is one of the products in the breakdown of the thiosulfate derivative. Since DTNP is nearly insoluble in water, addition of it in excess causes the appearance of a precipitate or cloudiness in the reaction mixture. However, the derivatives of sulfite and thiosulfate remain in solution in aqueous medium because of their ionic character. DTNP derivatives of hydrophilic thiols are also water soluble. Derivatization with increasing amounts of the reagent showed no significant variation in recoveries of sulfite or thiosulfate. This indicates that sulfite and thiosulfate derivatives are not removed from the aqueous phase with the reagent when it precipitates. Comparison of derivatization of standards in seawater with that in Milli-Q water did not indicate any interference by salts and organic compounds present in seawater.

Sep-Pak (C_{18}) Extraction. DTNP derivatives of sulfite and thiosulfate are strongly retained on Sep-Pak C_{18} cartridges treated with tetrabutylammonium solution. We routinely extracted up to 20 mL of reacted samples through each Sep-Pak. The derivatives were not detected in the Sep-Pak eluate, confirming that they were extracted with high efficiency by the cartridge. The adsorbed derivatives were eluted with methanol, and 1 mL was found enough for quantitative elution. The methanol extract was mixed with an equal volume of water prior to injection in order to facilitate sample focusing at the top of the reversed-phase column. Alternatively, the methanol extract can be evaporated to dryness and reconstituted in 200 μL of 20% aqueous methanol, which results in a 100-fold sample concentration.

Table II. Stability of DTNP Derivatives of Sulfite and Thiosulfate on Sep-Pak at 5 °C

time, days	recovery, % sulfide	recovery, % thiosulfate	time, days	recovery, % sulfide	recovery, % thiosulfate
1	98	96	8	93	92
3	97	89	11	100	92
6	97	96	14	93	91

Table III. Stability of DTNP Derivatives of Sulfite and Thiosulfate on Sep-Pak at Room Temperature (25 ± 1 °C)[a]

time, days	recovery, % sulfite	recovery, % thiosulfate	time, days	recovery, % sulfite	recovery, % thiosulfate
1	98	92	6	104	48
2	97	93	8	112	53
4	97	80			

[a] Note: an increase in sulfite recovery with a decreasing thiosulfate concentration suggests the sulfite derivative as one of the breakdown products of the thiosulfate derivative.

We examined the stability of the derivatives on Sep-Pak C_{18} cartridges. The cartridges were stored at 5 ± 1 °C and analyzed over a period of 2 weeks. As shown in Table II, both sulfite and thiosulfate derivatives appear to be stable on Sep-Pak cartridges during the storage period. However, at ambient temperatures, the cartridge-adsorbed derivatives appear to be stable for less than a week (Table III).

Optimization of Chromatographic Separation. Natural waters from anoxic environments (e.g., sediment pore waters, Black Sea) invariably contain organic thiols, along with sulfite and thiosulfate. Since thiols also form derivatives with DTNP, we optimized the separation of sulfite and thiosulfate derivatives from those of common hydrophilic thiols. The following thiols, which are known to occur in anoxic environments (*11*, *12*), were included for optimization: cysteine, glutathione, mercaptoacetic acid, 2-mercaptoethanesulfonic acid (coenzyme M), 2-mercaptoethanol, 2-mercaptopropionic acid, 3-mercaptopropionic acid, monothioglycerol, and thiomalic acid. The best chromatographic separation was obtained by using both ion-pairing agent (7.5 mM tetrabutylammonium hydrogen sulfate, TBAHS) and low pH of 3.50 ± 0.05 in the aqueous phase (Figure 2). The overall selectivity was better with acetonitrile than with methanol. The 20-μL injection volume did not affect the efficiency of HPLC separation noticeably, although it was too large for a microbore system. For the system with a column of 2 mm i.d. and 15 cm length used in this study, the maximum sample volume to avoid dispersion in the injector was 2 μL based on Katz's derivation (*13*). The efficiency of sample focusing at the top of the column, as a result of the reversed-phase effect, has probably offset the dispersion effect in the injector.

Precision, Linearity, and Detection Limit. Sulfite and thiosulfate standards were spiked into 20 mL of seawater at 0.25–5 μM concentration range and were subjected to the analytical procedure described here, including the Sep-Pak extraction step. The methanol eluate, however, was diluted to the original volume (20 mL) with water prior to injection. Recoveries for sulfite and thiosulfate were ~98–99%, with relative standard deviation less than ±5% (Table IV). For aqueous samples, excluding Sep-Pak cartridge enrichment, the detection limits for thiosulfate and sulfite are about 60 and 80 nM, respectively, which correspond to a signal-to-noise ratio of 2 at 0.01 AUFS detector sensitivity, 20-μL injection volume, and a 100-μL

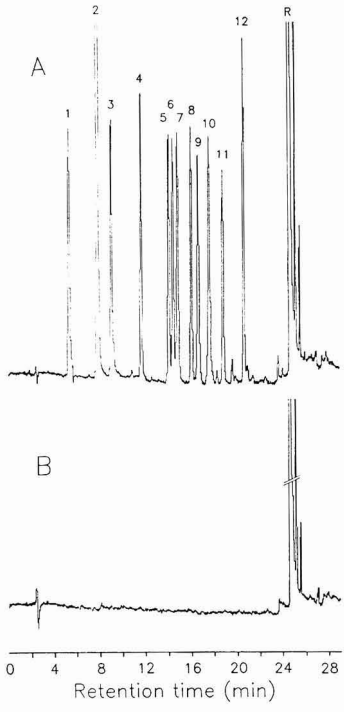

Figure 2. (A) Chromatogram of DTNP derivatives of 1 μM standards at 0.03 AUFS; derivatization and chromatographic parameters as in the text: (1) cysteine; (2) 2-mercapto-5-nitropyridine; (3) glutathione; (4) monothioglycerol; (5) thiomalic acid; (6) mercaptoacetic acid; (7) 2-mercaptoethanol; (8) coenzyme M (2-mercaptoethanesulfonic acid); (9) 2-mercaptopropionic acid; (10) 3-mercaptopropionic acid; (11) sulfite; (12) thiosulfate; (R) DTNP (reagent). (B) reagent blank.

Table IV. Recovery of Sulfite and Thiosulfate from Spiked Seawater[a]

species	concn range, μM	av rec (X), %	n	RSD (s/X)
sulfite	0.25–5.0	98	7	4.4
thiosulfate	0.25–5.0	99	7	4.2

[a] n, number of determinations; RSD, relative standard deviation; s, standard deviation.

solvent flow rate. The detection limit can be readily decreased, by using the Sep-Pak enrichment technique with which we obtained ~10-fold reduction using 20-mL samples. Calibration of standards in the 0.2–10 μM range showed excellent linearity of response (correlation coefficient, r, ~0.999) (Figure 3).

Application to Samples. The method described here was used to measure sulfite and thiosulfate concentrations in Black Sea waters in July 1988. Derivatization with DTNP was carried out within 30 s after sampling from the air-tight GO-FLO bottles (General Oceanics, Miami, FL). About 20-mL aliquots of derivatized samples were extracted on Sep-Paks and stored in tightly closed vials at ~4 °C until HPLC analysis. Figure 4 shows a typical chromatogram obtained with the Black Sea water samples. Depth profiles of both sulfite and thiosulfate are given in Figure 5 for a sampling location at 43°06′ N and 34°00′ E. Both sulfite and thiosulfate concentrations increase with depth, a trend similar to that of hydrogen sulfide. If chemical oxidation of hydrogen sulfide by air is the major mechanism for the formation of sulfite and thiosulfate,

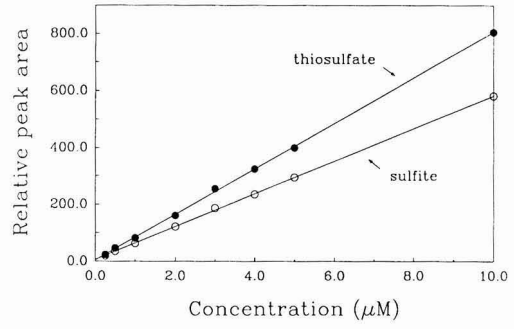

Figure 3. Standard curves of sulfite and thiosulfate.

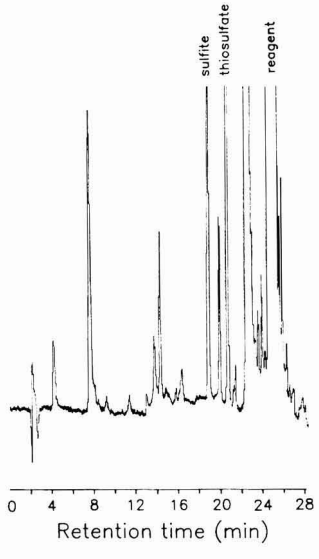

Figure 4. Typical chromatogram obtained with the Black Sea water samples.

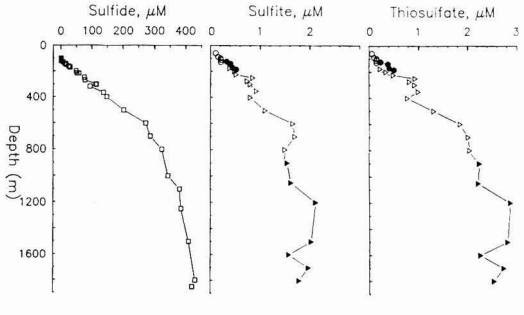

Figure 5. Depth profiles of sulfide, sulfite, and thiosulfate in the Black Sea for a sampling location around latitude 43°06′ N and longitude 34°00′ E. Symbols used in the sulfite and thiosulfate profiles reflect different casts. (F. J. Millero is acknowledged for the sulfide data.)

maxima of these species should have been found near the oxic/anoxic interface, which is around 80-m depth. The relatively low concentrations of sulfite and thiosulfate near the surface suggest that other factors, such as bacterial activities, may be important in controlling their distribution, and that both sulfite and thiosulfate are turned over rapidly in these waters.

The reasons for the gradual increase in concentrations of sulfite and thiosulfate with depth (down to ~2000 m) are not clear. It is possible that some sulfite could have formed by air oxidation of sulfide during sampling, since there was a brief exposure to air (<30 s) just prior to derivatization. However, from kinetic considerations, this brief exposure was not likely to have given rise to the observed high concentrations in the deep samples (*14*). Furthermore, the sulfite depth profile closely parallels that of thiosulfate, which has a much slower formation rate than that of sulfite during air oxidation of sulfide in Black Sea water (*14*). An earlier work reported more than 20 μM concentrations of thiosulfate in the Black Sea waters deeper than ~300 m and attributed bacterial processes for its formation (*15*). The similarity of sulfite and thiosulfate profiles to that of sulfide suggests a common origin of these species in bacterial sulfate reduction. In fact, studies by Millet using radiolabeled sulfate revealed that sulfite was formed as an intermediate in the conversion of sulfate to sulfide (*16*). Since sulfite as well as thiosulfate are also formed as intermediates in the oxidation of sulfide to sulfate (*17*, *18*), it is likely that the reverse reactions occur during sulfate reduction. Our results imply that both sulfite and thiosulfate are probably intermediates in bacterial sulfate reduction.

Acknowledgments

We thank F. J. Millero and B. F. Taylor for valuable discussions during the study. Assistance given by R. J. Sikorski in setting up the microbore HPLC system is acknowledged.

Registry No. DTNP, 2127-10-8; sulfite, 14265-45-3; thiosulfate, 14383-50-7; water, 7732-18-5.

Literature Cited

(1) *Fed. Regist.* **1986**, *51* (*131*), 25012–25021.
(2) West, P. W.; Gaeke, G. C. *Anal. Chem.* **1956**, *28*, 1816–1819.
(3) Urban, P. J. *Z. Anal. Chem.* **1961**, *179*, 415–426.
(4) Kim, H. J.; Kim, Y. K. *J. Food Sci.* **1986**, *51*, 1360–1361.
(5) Weiss, J.; Gobl, M. *Fresenius Z. Anal. Chem.* **1985**, *320*, 439–444.
(6) Dasgupta, P. K.; Yang, H. C. *Anal. Chem.* **1986**, *58*, 2839–2844.
(7) Brown, D. S.; Jenke, D. R. *Analyst (London)* **1987**, *112*, 899–902.
(8) Smith, V. J. *Anal. Chem.* **1987**, *59*, 2256–2259.
(9) Grassetti, D. R.; Murray, J. F., Jr. *J. Chromatogr.* **1969**, *41*, 121–123.
(10) Swaditat, A.; Tsen, C. C. *Anal. Biochem.* **1972**, *45*, 349–356.
(11) Mopper, K.; Taylor, B. F. In *Organic Marine Chemistry*; Sohn, M. L., Ed.; ACS Symposium Series 305; American Chemical Society: Washington, DC, 1986; pp 324–339.
(12) Shea, D.; Maccrehan, W. A. *Sci. Total Environ.* **1988**, *73*, 135–141.
(13) Katz, E. D. In *Small Bore Liquid Chromatography Columns: Their Properties and Uses, Chemical Analysis*; Scott, R. P. W., Ed.; Wiley-Interscience: New York, 1984; pp 23–58.
(14) Millero, F. J. University of Miami, Miami, FL, personal communication, 1988.
(15) Tuttle, J. H.; Jannasch, H. W. *Mar. Biol.* **1973**, *20*, 64–70.
(16) Millet, J. C. *R. Hebd. Seances Acad. Sci.* **1955**, *240*, 253–255.
(17) Cline, J. D.; Richards, F. A. *Environ. Sci. Technol.* **1969**, *3*, 838–843.
(18) O'Brien, D. J.; Birkner, F. G. *Environ. Sci. Technol.* **1977**, *11*, 1114–1120.
(19) Luther, G. W.; Giblin, A. E.; Varsolona, R. *Limnol. Oceanogr.* **1985**, *30*, 727–736.

Received for review December 19, 1988. Accepted October 24, 1989. This work was supported by the Office of Naval Research Grant 0014-84-K-0733 and by the National Science Foundation Grants OCE 8516020 and 8613940.

Interaction of Metals and Protons with Algae. 2. Ion Exchange in Adsorption and Metal Displacement by Protons

Ray H. Crist, J. Robert Martin, Paul W. Guptill, and Jill M. Eslinger

Messiah College, Grantham, Pennsylvania 17027

DeLanson R. Crist*

Department of Chemistry, Georgetown University, Washington, DC 20057

■ Adsorption of Sr on *Vaucheria* released an equivalent amount of Ca and Mg, indicating that metal adsorption by alkali and alkaline-earth metals is an ion-exchange phenomenon based on electrostatic interactions. Release of protons when Cu was adsorbed demonstrated additional covalent bonding for this transition metal. Protonated ethylenediamine is adsorbed both as a cation similar to metals and as a neutral species, indicating the presence of additional bonding sites. When the pH of an algal suspension is decreased, Ca and Mg are released equivalent to the amount of proton uptake, which occurred in fast (<50 s) and slow (2 h) processes. Kinetic evidence suggests that the slow process represents rate-determining diffusion of Ca through a dense-phase structure of the alga.

Introduction

Recently reported applications of metal–algae interactions include the use of algae as biosorbents for recovery of metals from industrial solutions (*1*), either to sequester toxic metals (*2*) or to recover precious metals (*2–5*). In some cases, concentration factors of $>10^6$ have been reported (*6*). Such adsorption of metals may lead to use of algae in wastewater treatment (*5*), and algae have been proposed as monitoring organisms for Cu and Hg in estuaries (*7*). The environmental impact of algae in these and other areas have been reviewed recently (*8*). Also, enhanced sensitivity in analytical methods has been achieved by using algae for preconcentration of metals at very low concentrations (*9*) or on a modified electrode for Cu (*10*).

It would be useful in such applications involving metals to understand the nature of their interaction with algae. Electrostatic attractions occur with some metals (Ca, Na) (*11*, *12*), covalent-type bonding with others (Cu) (*11–14*),

0013-936X/90/0924-0337$02.50/0

and redox reactions with certain noble metals (Au) (*4*, *15*).

Anions such as carboxylate groups of pectin, the polymer of galacturonic acid, are the most likely sites for electrostatic bonding. These substances, found in *Oedogonium* (*16*) and *Nautilis flexilis* (*17*, *18*), have pK_a values consistent with our adsorption results (*11*, *12*). Algae collected from limestone springs where Ca and Mg are ca. 1×10^{-4} M would thus contain these ions, and in fact the metal contents of a *Vaucheria* sample were 442 and 156 μmol/g of alga for Ca and Mg, respectively. We also observed that positive-charged complex ions of metals are adsorbed (*19*), as expected for electrostatic attraction to an anionic surface.

When the pH of an algal suspension is decreased, we found (*12*) that two types of proton uptake processes occur, a rapid one due to neutralization of the carboxylate sites, and a slow process, which occurs over several hours.

We now report our results on the stoichiometry of metal adsorption/displacement as well as adsorption of a neutral amine. Also, rate studies will be presented that clarify the nature of the slow proton uptake by identifying it more completely with metal release from algal dense-phase sites.

Materials and Methods

Algae were collected from limestone springs and stored at 0 °C as described previously (*12*). Species used were *Vaucheria* sp., *Rhizoclonium* sp., and *Tribonema* sp. Unless otherwise stated, an algal mass was separated from solutions by gravity filtration through a 16–20 mesh screen.

An algal preparation was made by finely cutting to facilitate mixing a sample, suspension in deionized, distilled water, and removal of contaminants from solution by filtration. This process was repeated four times before making a final suspension. The actual amount of alga was determined at the end of an experiment by filtration, drying to constant weight at 80 °C, and expressing all procedures and results in terms of dry weight of alga. For metal adsorption studies, the dried sample was ashed and the metal determined by atomic absorption (AA) on an acid solution (*12*) with a Perkin-Elmer Model 2380 instrument. In all equilibration studies concentrations were determined from triplicate experiments. In all rate studies, kinetic runs were carried out in triplicates.

Proton Displacement of Metals. To a suspension of 0.05–0.10 g of the alga in 50 mL of water was added 0.10 M HCl to bring $[H^+]$ to the desired level (<20–100 s), where it was maintained by successive additions of acid. These $[H^+]$ levels were 1.0×10^{-4}, 3.0×10^{-4}, 6.0×10^{-4}, and 10.0×10^{-4} M corresponding to pH values of 4.00, 3.52, 3.22, and 3.00, respectively. Initial proton uptake in obtaining the desired pH is rapid (<50 s). First-order rate constants for the subsequent slow uptake (1–3 h) were calculated from acid addition–time data when the fast reaction was over (ca. 100 s). A smooth curve was drawn through 5–10 data points of V_t, the total mL of 0.10 M HCl added to time t, vs t. Values of k_H were calculated in the standard manner (*20*) from $k_H = 1/t \ln (V_\infty - V_0)/(V_\infty - V_t)$, as described in Table I for data of Figure 1, and averaged, $n \geq 4$.

For Ca,Mg release on proton uptake, ca. 0.35 g of *Vaucheria* in 100 mL was filtered and the suspension remade several times until the Ca,Mg in solution was $<1.0 \times 10^{-5}$ M. HCl (0.10 M) was added to bring the solution to pH 4, where it was held by successive additions of acid. At various times a 1-mL aliquot was removed through a 10-mm glass tube with the end covered by cloth mesh and this aqueous solution analyzed for Ca,Mg by AA.

Rate of Ca Removal by EDTA. *Vaucheria* (0.05 g) was suspended in 50 mL of water and the pH adjusted to 7.0. To this suspension was added 50 mL of 0.01 M EDTA, also at pH 7. Aliquots of 1.0 mL were withdrawn at various times after 50 s and Ca(aq) determined by atomic adsorption (AA). Runs were also carried out at pH 8.0 and 9.0.

Table I. Rate Constants[a] for Proton Uptake by *Vaucheria* at pH 4.0 and 25 °C[b]

addition–time data		fast and slow processes[c]		slow process only[d]		
time, s	0.10 M HCl added, V_t, mL	$V_\infty - V_t$, mL	k_H, s^{-1}	time, s	$V_\infty - V_t$, mL	k_H, s^{-1}
0						
200	1.38	0.92	45.8	0	0.92	
400	1.50	0.80	26.4	200	0.80	6.9
800	1.67	0.63	16.2	600	0.63	6.3
1600	1.93	0.37	11.4	1400	0.37	6.5
3200	2.18	0.12	9.2	3000	0.12	6.8
∞	2.30					
						$\langle 6.62 \pm 0.22 \rangle$

[a] Calculated from $k_H = 1/t \ln (V_\infty - V_0)/(V_\infty - V_t)$. [b] Solution was that described in Figure 1. [c] $V_\infty = 2.30$, $V_0 = 0$. [d] Values of k_H were calculated from data starting at $t = 200$ s. Thus, $V_\infty = 2.30$, but $V_0 = 1.38$, and the time at 200 s is taken as $t = 0$ s.

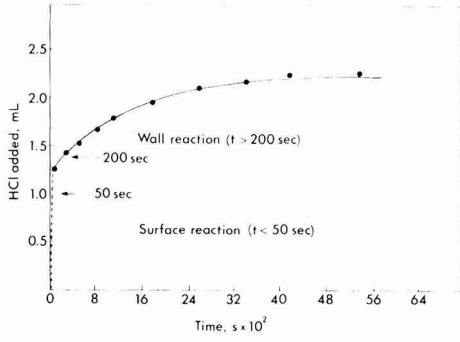

Figure 1. Rate of proton update by *Vaucheria* at pH 4.0. HCl (0.10 M) was added to a suspension of 0.33 g in 100 mL to bring the pH to 4.0, where it was held by making successive additions. The y axis is the total amount of HCl added up to time t. There were clearly two types of proton uptake processes: a fast one in the first 50 s and a slow one after 200 s, which followed good first-order kinetics (see Table I, "slow process only").

Metal and Proton Displacement by Metal Adsorption. In order to obtain the most self-consistent data in this type of study, the *same algal sample* was exposed to increasing amounts of the substance to be adsorbed. The algal sample was first *slowly* brought to the desired pH with HCl, allowing time for Ca and Mg equilibration, and metals released by this pH adjustment were then washed from the alga, which was resuspended in water at the same pH before beginning an adsorption study.

For the Sr study, an algal sample of 0.6–1.0 g was suspended in 200 mL of water. After stabilization at pH 7.0 (ca. 60 min), the algal mass was separated from the Ca,-Mg-containing supernatant liquid, resuspended in distilled water, and restabilized to pH 7.0. A 10-mL aliquot was removed and filtered and the algal mass retured to the suspension. Residual Ca,Mg was analyzed by AA of a 1-mL aliquot of the filtrate. Then 1 mL of water was added to the filtrate (to conserve volume) as well as 0.2 mL of 1 M Sr. This filtrate, now containing Sr, was slowly added to the suspension while 0.01 M acid or base was added (<0.03 mL) is necessary to maintain pH constant at 7.0. After a few minutes, 10 mL of the suspension was removed and the algal mass filtered, pressed with absor-

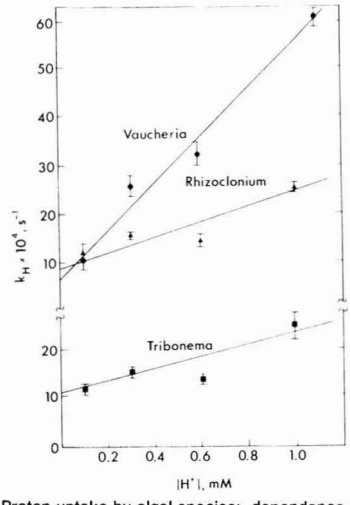

Figure 2. Proton uptake by algal species: dependence of first-order rate constants on $[H^+]$. HCl was added to the algal suspension to give a definite $[H^+]$ (taking <50 s) and held there by successive additions. Rate constants were determined after completion of the initial fast surface reaction (ca. 100 s). Triplicate runs were made for each $[H^+]$ at 25 °C.

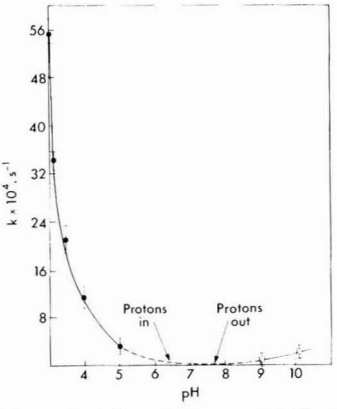

Figure 3. Rate constants for proton transport in *Vaucheria* vs pH: uptake by alga at pHs <7.0 (●); release from alga for pHs >7.0 (□). For the experiments at pHs >7, 0.2 g of the alga in 100 mL was filtered, washed, and then resuspended, all at the pH being studied. The amount of NaOH (0.05 M) added to keep the pH constant gave the measure of protons out. The suspension was under argon to avoid CO_2 interference. Runs were made in duplicate.

bent paper to remove residual solution, and then dried to constant weight before Sr analysis by AA (*12*). A 1-mL sample was removed from the filtrate for Ca,Mg analysis, and it was replaced with 1 mL of water. After addition of 0.2 mL of 1 M Sr to the filtrate, the filtrate was returned to the suspension. This process of Ca,Mg determination and addition of Sr was repeated four times with 0.4 mL of 1 M Sr, resulting in solutions 1, 2, 4, 6, 8, and 10 mM in Sr in the original suspension. Data at pH 4.5 were obtained in a similar way, except that a shorter time (30 min) was required for pH stabilization.

For Cu adsorption, the amount adsorbed and Ca,Mg released for various Cu concentrations was determined by use of the identical amounts and procedure as above for pH 4.5. Unlike Sr, Cu also displaces H^+, but this amount was better determined in a separate experiment. Successive additions of 0.2, 0.2, 0.4, 0.4, 0.4 and 0.4 mL of a 0.10 M Cu solution to ~0.10 g of the alga in 20 mL were made, corresponding to 1, 2, 4, 6, 8, and 10 mM Cu. The amount of 0.05 M NaOH needed to keep the pH constant for each addition gave the amount of H^+ released by that concentration of Cu. The dry weight of alga was obtained from the filtered material after all additions were made.

Adsorptions and Displacement of Ethylenediamine (en). Successive amounts of 1.0 M en were added to *Vaucheria*, with all solutions at the desired pH, by the procedure used for Sr, and displaced Ca,Mg were determined as before at pH 6.0 and 9.7 in separate experiments. The adsorbed en for various [en] was determined in a separate experiment. To six beakers containing 10 mL of 1, 2, 3, 4, and 6 mM en solutions at pH 6.0 was added ^{14}C-labeled en solution in sufficient amount to give 300–600 counts/min for a 200-μL sample. A 200-μL sample was removed from each for an initial ^{14}C count by a scintillation counter (Searle, Isocap/300). A 0.03–0.05-g algal sample, taken from a stirred suspension stabilized at pH 6.0, was added to each beaker. The alga was separated by filtration and a ^{14}C count made on the filtrate. Adsorbed en was calculated from the difference of these two counts. The separated alga was dried well with paper and split, one portion for dry weight and the other for en extraction by Sr, which was accomplished by grinding in a mortar with 10 mL of 0.10 M Sr. After filtration, the labeled en displaced by Sr was determined by counting. All experiments were in triplicate.

Table II. Exchange of Protons and Divalent Cations

	sample						
	1	2	3	4	5	6	7
time, s	150	310	550	1040	1500	2546	4000
HCl adsorbed, μmol	152	183	195	207	215	225	232
Ca,Mg released, μmol	81	94	101	103	103	113	119
H/Ca,Mg, mol/mol	1.88	1.95	1.93	2.00	2.09	1.99	1.95

Results

Proton Uptake. The data for proton uptake by *Vaucheria* are presented in Figures 1–3 and Table I. In Figure 1 are given the milliliters of 0.10 M HCl vs time for bringing the pH of the algal suspension to 4.0 and for holding it until the uptake was complete. The initial rate is much faster than shown because some 30 s were taken to bring the pH to 4.0 in order to avoid local low pHs. A first-order rate constant was first calculated for the whole process, but there was a wide variation in k_H values (see Table I, "fast and slow processes"). The latter part of the curve was explored by considering data starting from 200 s. As shown by the uniformity of k_H (Table I, "slow process only"), this part of the process follows first-order kinetics.

Variations of k_H (slow process only) with H^+ concentration is shown in Figure 2 for several species over a 10-fold range, 0.1–1.0 mM (pH 4–3). The data indicate that the uptake rate is linear with $[H^+]$, as would be expected. A wide profile of k_H vs $[H^+]$ is shown in Figure 3 where the pH scale is used to accommodate the range of H^+ from 10^{-3} to 10^{-10} M. Above pH 7 the proton activities are such as to cause an efflux into the aqueous medium. An Ar or N_2 blanket was used above pH 7 to avoid complications with CO_2.

The Ca,Mg released on proton uptake at pH 4 are shown in Table II. The average amount of H^+ adsorbed per Ca,Mg released is 1.97 ± 0.46. In two additional experiments, the ratios were 1.98 ± 0.06 and 1.88 ± 0.12. Thus, the stoichiometry of the process is 1Ca,Mg released per $2H^+$ adsorbed. The fact that this result obtains, within

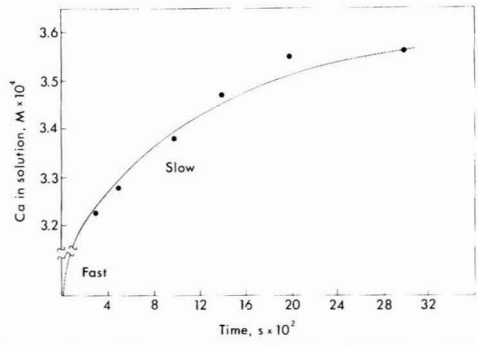

Figure 4. Rate of Ca removal from *Vaucheria* by EDTA at pH 9. A 0.137-g sample was suspended in 100 mL of 0.005 M EDTA. A 1-mL aliquot was removed at times 100–3000 s for Ca analysis by AA. This method avoided correction for sample removal since the relationship of the system components was not changed. Values of k_{Ca} were calculated from data starting at t = 300 s. When the time at 300 s is taken as 0 s, $[Ca]_0$ is thus 3.21×10^{-4} M; $[Ca]_\infty$ is 3.56×10^{-4} M.

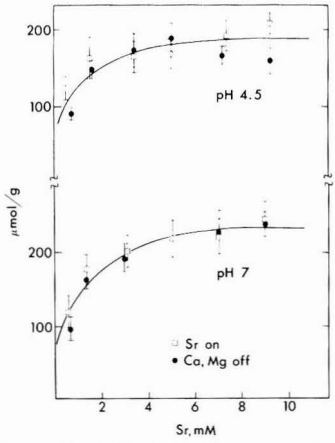

Figure 5. Sr adsorption by *Vaucheria* with accompanying displacement of Ca,Mg at two pH values: Sr on (□); Ca,Mg off (●). Sr was added to the algal suspension to give 0.001–0.010 M solutions. The sample was analyzed for Sr and the solution for Ca,Mg. For duplicate runs the average deviation was ca. ±15 μmol/g for Sr and for Ca,Mg.

experimental error, *for each time* shows that the rate of Ca,Mg off is twice the rate of H^+ adsorbed. This requires that on an equivalence basis the *rate constant for Ca,Mg release is the same as that for proton uptake.*

Rate of Ca Removal by EDTA. The appearance of Ca in a solution containing 0.005 M EDTA and *Vaucheria* occurred in fast and slow processes as indicated in Figure 4. In less than 100 s ~87% of the total change occurred, i.e., from 0 to ca. 3.2×10^{-4} M, and then in a slow process, this concentration increased to 3.56×10^{-4} M. First-order rate constants ($10^4 k_{Ca}$, s^{-1}) for the slow process for various pHs are as follows: pH 7, 11.0 ± 0.5; pH 8, 9.6 ± 1.4; pH 9, 9.5 ± 1.4, where k_{Ca} did not change significantly when [EDTA] was increased to 0.01–0.02 M.

Adsorption on *Vaucheria*. Adsorptions of Sr on *Vaucheria* at pH 4.5 and 7 are shown in Figure 5, where additions of Sr caused no noticeable pH changes. The amount of Ca,Mg released was essentially the same as for the Sr adsorbed.

Data for the Cu–Ca,Mg–H system at pH 4.5 are shown in Figure 6. Higher pH values were not used because of $Cu(OH)_2$ precipitation. In contrast to the case for Sr, the amount of Ca,Mg displaced is much less than the amount

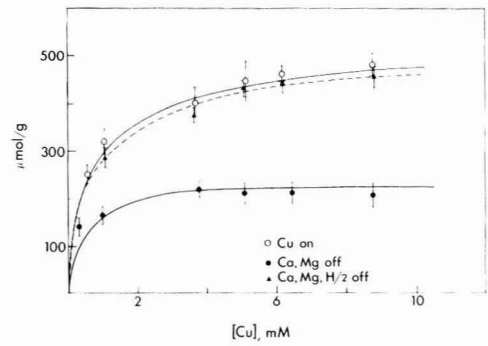

Figure 6. Cu adsorption by *Vaucheria* at pH 4.5 with displacement of Ca,Mg,H: Cu on (O); Ca,Mg off (●); dashed line for the sum of Ca,Mg and H/2 displaced (▲). Cu was added to the algal suspension to give 0.001–0.010 M solutions. The sample was analyzed for Cu and the solution for Ca,Mg. Displacement of H was obtained by adding Cu and NaOH together, keeping the pH constant. For duplicate runs the average deviation was ±25 μmol/g for Cu and ±19 μmol/g for Ca,Mg.

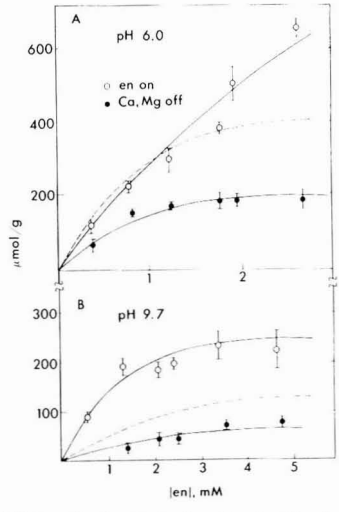

Figure 7. Ethylenediamine (en) adsorption by *Vaucheria* with displacement of Ca,Mg at pH 6.0 (curve A) and 9.7 (curve B): en on (O); Ca,Mg off (●); dashed line for twice the amount of Ca,Mg off. The alga was put in 10 mL of various en solutions containing [^{14}C]en. Adsorbed en was determined by ^{14}C count of the solution before and after addition of alga. Ca,Mg displaced was determined in a separate experiment with unlabeled en. Duplicate runs were made for each [en].

of Cu adsorbed. This is because Cu also displaces H^+, and when half the amount of H^+ released is included with Ca,Mg, the sum of displaced "divalent" material equals Cu adsorbed (dashed line in Figure 6).

Adsorptions of en at pH 6.0 and 9.7 are shown in Figure 7, as well as the amounts of Ca,Mg displaced, which are considerably less at each [en]. For comparison, dashed lines are also shown that are twice the amounts of Ca,Mg displaced to indicate what adsorption was expected for a monovalent cation. Adsorbed en was displaced by Sr, as evidenced by the fact that 60–80% of the en adsorbed at pH 6.0 was found in the combined filtrates of two extractions with 0.1 M Sr.

Discussion

Proton Uptake. The overall stoichiometry (fast surface reaction and slow process) of proton uptake was that 1

divalent metal (Ca or Mg) was released when 2 protons were adsorbed. Measurements at times that included the *slow process* showed that the rate constant for proton uptake was the same as that for Ca release to the solutions. The slow process is one that presumably involves processes within the cell wall. Since the mobility of H^+ is considerably greater than that of Ca, one can conclude that the rate-determining process is diffusion of Ca through dense-phase algal material into the aqueous layer.

The linear dependence of k_H on $[H^+]$ for each alga (Figure 2) can be expressed by the relationship $k_H = k_0 + k'[H^+]$ in the pH 3–4 range. Values of these constants for the three algae were

alga	$10^4 k_0$, s^{-1}	$10^4 k'$, M^{-1} s^{-1}
Rhizoclonium	9.0 ± 2.9	1.61 ± 0.48
Tribonema	11.3 ± 3.0	1.20 ± 0.49
Vaucheria	6.1 ± 5.0	4.97 ± 0.83

The large variation in k' for the various algal species could be due to different diffusion rates of Ca through different dense-phase structures of the various algal species. Such factors as porosity, chemical composition, or other aspects of the microstructure of cell walls may be important. This interpretation is similar to the conclusions of recent electrochemical results with polymer-coated electrodes (*21*, *22*) for which electron transfer was limited by transport of charge-compensating counterions through the polymer to the electrode. Further interpretation of the data must await more detailed structural studies.

The "intercept" rate constant k_0 was further investigated by carrying out runs at much lower $[H^+]$. In the entire acid range of the expanded pH profile (Figure 3), it seems reasonable to assume that the driving force for proton uptake results from an activity difference

$$a_H(aq) > a_H(alga)$$

This difference produces a chemical potential for proton uptake, which can occur, however, only with the compensating transfer of positive ions (Ca as observed for pH 3–4) out of the alga. In basic solutions (pH 9–10 in Figure 3), since these activities are reversed, protons move out of the alga, presumably with an in-flow of Na, Ca, and Mg.

Activity differences can also explain the efflux of Ca when alga is placed in an EDTA-containing solution at pH 8. In this case

$$a_{Ca}(alga) > a_{Ca}(aq)$$

since $[Ca^{2+}]$ is only ca. 10^{-10} M under these conditions. Presumably, this process was accomplished by a proton uptake from water or EDTA, since the k_{Ca} values were essentially independent of pH from pH 7 to 9. This uptake would not be observed as a change in pH, however, due to proton release by the reaction

$$HL^{3-} + Ca^{2+} \rightarrow CaL^{2-} + H^+$$

where HL^{3-} is the most abundant EDTA species (98%) at pH 8. No Na uptake was found in many attempts.

Adsorption as a Displacement Reaction. Sr was taken as a model for electrostatic bonding, which would be expected for alkali and alkaline-earth metals. Charge conservation was maintained in the adsorption process, with amounts of Ca,Mg displaced equal to the amount of Sr adsorbed. Thus, adsorption can be viewed primarily as an ion-exchange equlibrium of an cation character on the anionic algal surface.

With Cu^{2+} which is known for its strong covalent-bonding properties, adsorption released not only Ca,Mg but also H^+. Again, charge was conserved when H^+ released is included (Figure 6, dashed line). A probable explanation for this release is complex formation of Cu with adjacent algal ammonium (*13*) or carboxylic acid groups, which can be represented by the reactions

$$Alg\text{-}(NH_3)_2^{2+} + Cu^{2+} \rightarrow [Alg\text{-}(NH_2)_2Cu]^{2+} + 2H^+$$

$$Alg\text{-}(CO_2H)_2 + Cu^{2+} \rightarrow [Alg\text{-}(CO_2)_2Cu] + 2H^+$$

Some combination of these reactions, as long as the 2:1 H/Cu stoichiometry is maintained, is also possible, and the resulting complex would be analogous to the EDTA–Cu complex and the inorganic colloid–transition-metal complexes described in a recent review article (*23*). Other reactions are possible also, e.g., ones involving sulfhydryl groups.

Electrostatic bonding (displacement of Sr) and covalent bonding (proton release) by Cu as deduced in our previous work (*12*) is consistent with the two-site model of Van Cutsem (*13*, *14*) for Cu adsorption to the cell wall of *Nautilis flexilis*. From ESR measurements, the high-affinity-type site was proposed to be more covalent.

Adsorption of en at pH 6, where it exists 98% as protonated species, fits the pattern expected from metal behavior: its adsorption is accompanied by release of Ca,Mg, and adsorbed en was displaced by added Sr. Both results are consistent with the adsorption of en as a cationic species. At higher pH, where en is unprotonated, its adsorption is still high (*19*) and would have to involve other types of bonding.

Conclusions

The present results are fully consistent with our previous model (*12*) for proton uptake and metal adsorption on algae: (1) a negative-charged surface, which exhibits fast proton uptake and adsorption of cations by electrostatic and, for Cu, covalent bonding, and (2) slow proton uptake by dense-phase algal material, which could be the same as on the surface.

The slow proton uptake process, by its stoichiometry and rate constant relationship to Ca released, appears to represent a rate-determining diffusion of Ca through a dense-phase structure of the alga. The different rate constants for various algal species could be due to such factors as porosity, chemical composition, or other aspects of the microstructure of cell walls.

The stoichiometry of Sr adsorption by *Vaucheria* with an equivalent amount of Ca,Mg released now identifies adsorption phenomena as an ion-exchange process for alkali and alkaline-earth metals. The Langmuir adsorption constants previously reported thus represent exchange reactions. Furthermore, the proton release and stoichiometry of Cu adsorption shows clearly the added covalent bonding of Cu as deduced previously from its unusual y_m value (*12*), leaching experiments (*11*), and ESR studies (*13*, *14*).

Acknowledgments

We wish to acknowledge the many helpful discussions with Dr. Karl Oberholser during the course of this study. Also, the data on amine adsorption were obtained with the help of Jeffrey Kramer, Joseph Miller, Richard Shetzline, and Matthew Whitestone. We are grateful to Dr. I. Stankovic for making the algae available.

Registry No. Sr, 7440-24-6; Cu, 7440-50-8; Mg, 7439-95-4; Ca, 7440-70-2; H^+, 12408-02-5; ethylenediamine, 107-15-3.

Literature Cited

(1) Kuyucak, N.; Volesky, B. *Biotechnol. Lett.* **1988**, *10*, 137–142.

(2) Mann, H.; Fyfe, W. S.; Kerrich, R. *Toxic. Assess.* **1988**, *3*, 1-16.
(3) Kuyucak, N.; Volesky, B. *Precious Met., Proc. Int. Precious Met. Inst. Conf., 10th* **1986**, 211-216.
(4) Greene, B.; Hosea, M.; McPherson, R.; Henzl, M.; Alexander, M. D.; Darnall, D. W. *Environ. Sci. Technol.* **1986**, *20*, 627-632.
(5) Darnall, D. W.; Greene, B.; Henzl, M. T.; Hosea, J. M.; McPherson, R. A.; Sneddon, J.; Alexander, M. D. *Environ. Sci. Technol.* **1986**, *20*, 206-208.
(6) Mann, H.; Tazaki, K.; Fyfe, W. S.; Beveridge, T. J.; Humphrey, R. *Chem. Geol.* **1987**, *63*, 39-43.
(7) Seeliger, U.; Cordazzo, C. *Environ. Pollut., Ser. A* **1982**, *29*, 197-206.
(8) Lembi, C. A., Waaland, J. R., Eds. *Algae and Human Affairs*; Cambridge University Press: New York, 1988.
(9) Mahan, C. A.; Majidi, V.; Holcombe, J. A. *Anal. Chem.* **1989**, *61*, 624-627, and references therein.
(10) Gardea-Torresdey, J.; Darnall, D.; Wang, J. *Anal. Chem.* **1988**, *60*, 72-76.
(11) Crist, R. H.; Oberholser, K.; Shank, N.; Nguyen, M. *Environ. Sci. Technol.* **1981**, *15*, 1212-1217.
(12) Crist, R. H.; Oberholser, K.; Schwartz, D.; Marzoff, J.; Ryder, D.; Crist, D. R. *Environ. Sci. Technol.* **1988**, *22*, 755-760.
(13) Van Cutsem, P.; Gillet, C. *Plant Soil* **1981**, *62*, 367-375.
(14) Van Cutsem, P.; Mestdagh, M. M.; Rouxhet, P. G.; Gillet, C. *React. Polym., Ion Exch., Sorbents* **1984**, *2*, 31-35.
(15) Watkins, J. W., II; Elder, R. C.; Greene, B.; Darnall, D. W. *Inorg. Chem.* **1987**, *26*, 1147-1151.
(16) Pearlmutter, N. L.; Lembi, C. A. *J. Phycol.* **1980**, *16*, 602-616.
(17) Van Cutsem, P.; Gillet, C. *Plant Physiol.* **1983**, *73*, 865-867.
(18) Van Cutsem, P.; Gillet, C. *J. Exp. Bot.* **1982**, *33*, 847-853.
(19) Van Wagoner, J.; Martin, L.; Helphrey, J. D.; Myers, R.; Hess, G. D.; Crist, R. H. *Proc. Pa. Acad. Sci.* **1985**, *59*, 147-150.
(20) Frost, A. A.; Pearson, R. G. *Kinetics and Mechanism*, 2nd ed.; Wiley: New York, 1961; p 29.
(21) Kahl, J. L.; Faulkner, L. R.; Dwarakanath, K.; Tachikawa, H. *J. Am. Chem. Soc.* **1986**, *108*, 5434-5440.
(22) Kaufman, F. B.; Schroeder, A. H.; Engler, E. M.; Kramer, S. R.; Chambers, J. Q. *J. Am. Chem. Soc.* **1980**, *102*, 483-488.
(23) Honeyman, B. D.; Santschi, P. H. *Environ. Sci. Technol.* **1988**, *22*, 862-871.

Received for review September 1, 1988. Revised manuscript received August 17, 1989. Accepted September 12, 1989. We are grateful to The J. Howard Pew Freedom Trust of The Glenmede Trust for funding the atomic adsorption instrument.

Concentrations and Fluxes of Polycyclic Aromatic Hydrocarbons and Polychlorinated Biphenyls across the Air–Water Interface of Lake Superior

Joel E. Baker[†] and Steven J. Eisenreich*

Environmental Engineering Sciences, Department of Civil and Mineral Engineering, The University of Minnesota, Minneapolis, Minnesota 55455

■ Concentrations of polycyclic aromatic hydrocarbons (PAHs) and polychlorinated biphenyls (PCBs) were measured in the atmosphere and surface waters of Lake Superior to estimate the direction and magnitude of their fluxes across the air–water interface. Atmospheric PAH concentrations ($\sum$[PAH] = 3.8 ± 1.7 mg/m^3, 13 PAHs) were typical of levels found in continental background air. Atmospheric PCB concentrations (x = 1.2 ng/m^3) have remained relatively constant over the Great Lakes during the past 10 years despite lower PCB loadings. PCB congener fugacity gradients suggest PCB volatilization from Lake Superior's surface waters in August 1986. Mean volatilization fluxes of total PCBs (19 ng/m^2·day) are similar to estimates of gross atmospheric deposition to the lake, supporting the hypothesis of nonequilibrium, steady-state PCB exchange across the air–water interface. PAH fluxes could not be calculated due to uncertainties in PAH Henry's law constants.

Introduction

Chemical exchange across the air–water interface is one of the major processes that controls concentrations and residence times of synthetic organic chemicals in natural waters. Hydrophobic organic chemicals (HOCs) such as chlorinated pesticides, polychlorinated biphenyls (PCBs), and polycyclic aromatic hydrocarbons (PAHs) are transported long distances in the atmosphere and enter surface waters via wet and dry deposition. Atmospheric fluxes often dominate HOC inputs to remote lakes and the oceans (*1–8*). Once in surface waters, dissolved HOCs may revolatilize and the *net* HOC flux across the air–water interface is the difference between gross deposition and volatilization. Mackay et al. (*9*) described exchange of HOCs across the air–water interface as intense episodic inputs from the atmosphere during precipitation events followed by slow but prolonged volatilization during dry periods.

Historically, the atmosphere has been a source of anthropogenic compounds to surface waters and the net flux has been from the atmosphere to large lakes and the oceans. More recently, decreased production and emissions of many HOCs have resulted in lower levels of these compounds in the environment (e.g., ref 10). If the atmosphere has responded more rapidly to these decreases than have surface waters, HOC gradients across the air–water interface may have reversed and large water bodies may currently be sources of organic contaminants to the atmosphere. Wet atmospheric deposition of HOCs has been measured at several locations in North America (*3, 4, 6, 10–17*). Rates of diffusive exchange (e.g., volatilization or absorption) across the air–water interface may be modeled as a first-order mass-transfer process if the concentration gradient (or fugacity gradient) and the compound-specific mass-transfer coefficient for specific environmental conditions are known. In this study, concentrations of PCB congeners and selected PAHs were measured in the atmosphere and surface waters. A fugacity-based model was employed to estimate the direction and magnitude of exchange. Our goals are not only to compare the magnitude of these air–water exchanges to those of other transport processes (e.g., wet and dry atmospheric deposition, sedimentation), but also to illustrate the uncertainties in calculating exchange of semivolatile organic compounds

[†]Current address: Chesapeake Biological Laboratory, Center for Environmental and Estuarine Studies, The University of Maryland System, Box 38, Solomons, MD 20688.

0013-936X/90/0924-0342$02.50/0

Table I. Comparison of Mass Concentration- and Fugacity-Based Calculations of Air–Water Exchange (after Mackay et al., ref 9)[a]

parameter	mass concn	fugacity	conversion
dissolved concn	C_d (ng/L)	f_W (Pa)	$f_W = [10^{-6}/MW]C_d/Z_w$
gas-phase concn	C_g (ng/m^3)	f_A (Pa)	$f_A = [10^{-9}/MW]C_g/Z_A$
equilibrium condition	$C_g/C_d = 10^3H/RT$	$f_W/f_A = \alpha = 1$	$\alpha = 10^3[C_d/Z_w]/[C_g/Z_A] = 10^3\ HC_d/[RTC_g]$
mass-transfer coeff	K_{OL} (m/day)	D_{AW} (mol/(m^2·day·Pa))	$D_{AW} = K_{OL}/H$
flux (ng/m^2·day)[b]	$N = K_{OL}[10^3C_d - C_gRT/H]$	$N = 10^9MWD_{AW}[f_W - f_A]$	

[a] 101 325 Pa = 1 atm; MW, molecular weight (g/mol); Z_d, Z_g, fugacity capacity of water and gas, respectively (mol/(Pa·m^3)); H, Henry's law constant (Pa·m^3/mol); R, gas constant (Pa·m^3/(mol·K)); T, absolute temperature (K). [b] In this convention, positive J values represent fluxes from water to air (i.e., volatilization).

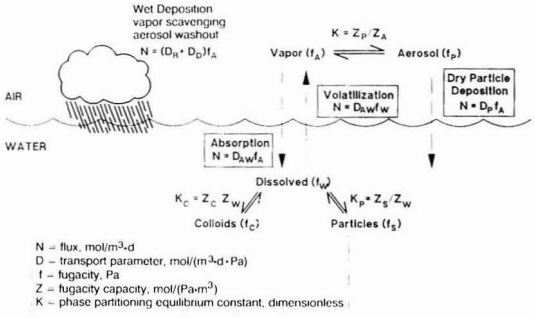

Figure 1. Fugacity-based model of the exchange of semivolatile hydrophobic organic contaminants across the air–water interface (after Mackay et al., ref 9).

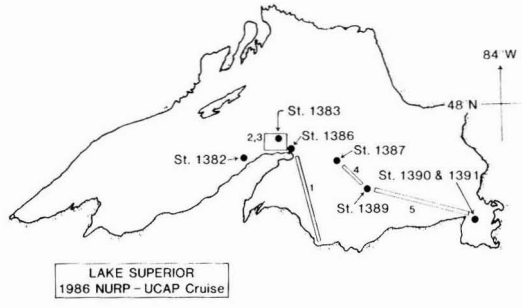

Figure 2. Sampling locations for air and water samples during the August 1986 Lake Superior cruise of the R/V Seward Johnson. Water samples were collected at six stations and five air samples were collected in transit between stations.

across the air–water interface.

Fugacity-Based Model of Air–Water Exchange. Equations describing diffusive chemical exchange across the air–water interface developed from the Whitman two-film resistance model (*18*) have been employed to calculate oxygen-transfer rates (e.g., refs 19 and 20) as well as fluxes of trace gases from the atmosphere to the ocean (*21*). Later, this analysis was extended to include higher molecular weight chlorinated compounds, including PCBs (*22–24*). These models have been extensively reviewed (*1*, *24*, *25*) and only the salient features are presented here. Passive transfer across the air–water interface is driven by the concentration or fugacity gradient at a rate proportional to the compound-specific mass-transfer coefficient (Figure 1). Although contaminant concentrations are usually expressed as weight per unit volume (e.g., ng/L) or weight per unit weight (e.g., ng/g), mass transfer between environmental compartments is more easily formalized when concentrations are expressed as chemical fugacities (*26*). In this paper, concentrations of PCBs and PAHs are reported in mass per unit volume units for comparison with other data and as fugacities for calculating fluxes across the interface. Although we use the fugacity approach, resulting fluxes are equivalent to those calculated by using mass-based concentrations.

As demonstrated by the mass-transport equations in Table I, fluxes across the air–water interface are calculated as the difference between the chemical concentrations or fugacities in the atmospheric gas and aqueous dissolved phases. Because HOCs occur in many physical–chemical forms in the atmosphere and in surface waters, the fugacity gradient is difficult to measure directly. HOCs in the atmosphere are distributed between the gas and aerosol phases and aerosols must be separated prior to measurement of gas-phase HOC concentrations. This separation may be accomplished by drawing air through a glass fiber filter and a gas-collecting adsorbent if sampling artifacts (e.g., HOC desorption from aerosols collected on the filter, adsorption of HOC vapors on the filter) are avoided (*27*). HOCs partition between the dissolved phase and the milieu of natural particles present in surface waters. Because only dissolved HOCs are directly available for exchange across the air–water interface, it is critical to isolate dissolved HOCs from surface waters. The presence of HOC-binding colloids that cannot be separated by conventional filtration or centrifugation make this separation difficult (*28*, *29*). Previous estimates indicate that less than half of the PCBs in Great Lakes surface waters are in the true dissolved phase (*29*). The fraction of HOCs associated with colloids is greater for more hydrophobic compounds. Speciation of HOCs in air and water must be considered when estimating the fugacity gradient and resulting fluxes across the air–water interface.

Experimental Section

Air and water samples were collected from central and eastern Lake Superior between 4 and 10 August 1986 (Figure 2). Details of sampling and analytical procedures employed in this study are described in detail by Baker and Eisenreich (*30*) and are briefly summarized here. Aerosol and gas-phase samples were collected by drawing 300–800 m^3 of air through a glass fiber filter and a polyurethane foam plug at a rate of 0.5 m^3/min. Surface waters were filtered through a glass fiber filter and drawn through a column containing Amberlite XAD-2 resin (*31*).

Air and water samples were analyzed for 14 PAHs and 35 PCB congeners by methods described elsewhere (*30*, *32*). Polyurethane foam (air) or XAD-2 (water) adsorbents were extracted by sequential 48-h extractions in methanol and dichloromethane in a Soxhlet apparatus. After the methanol was removed by partitioning with water, the dichloromethane extract was concentrated to 3 mL and switched to hexane in a Kudurna–Danish evaporator and further concentrated to 1 mL under a purified N_2 stream. PAHs were quantified in the concentrated extract by gas

Table II. Concentrations of Polychlorinated Biphenyl Congeners in the Atmosphere and Surface Waters of Lake Superior, August 1986

	IUPAC	vapor[c]		dissolved[d]	
	no.	av ± SD	N	av ± SD	N
2,4′	8	NA[a]		73.1 ± 52.6	2
2,2′,3	16*, 32[b]	133.4 ± 49.2	5	21.4 ± 9.7	5
2,2′,4	17	165.2 ± 60.4	5	22.6 ± 13.4	5
2,2′,5	18	74.8 ± 30.7	5	33.8 ± 15.5	5
2,3,4′	22	136.9 ± 42.4	5	12.0 ± 11.0	5
2,4,4′	28	134.4 ± 46.0	5	34.6 ± 30.2	5
2,4′,5	31	89.9 ± 33.4	5	46.8 ± 30.6	5
2′,3,4	33	47.0 ± 18.5	5	27.3 ± 24.5	5
3,4,4′	37, 42	19.6 ± 7.3	5	22.2 ± 18.5	5
2,2′,3,4	41, 64	14.4 ± 5.5	5	12.1 ± 6.4	4
2,2′,3,5′	44	28.0 ± 10.8	5	12.9 ± 7.4	5
2,2′,4,4′	47*, 48[b]	19.8 ± 8.2	5	6.8	1
2,2′,4,5′	49	25.0 ± 8.7	5	11.6 ± 3.4	2
2,3,4,4′	60*, 56[b]	17.8 ± 11.5	5	14.6 ± 9.7	5
2,3′,4,4′	66	38.7 ± 17.9	5	32.1 ± 20.0	5
2,3′,4′,5	70	53.8 ± 24.1	5	34.8 ± 24.6	5
2,4,4′,5	74	15.5 ± 8.1	5	12.3 ± 7.9	5
2,2′,3,3′,4	82	46.1 ± 22.3	5	2.9 ± 0.2	2
2,2′,3′,4,5	97	9.6 ± 4.9	5	4.6 ± 2.4	4
2,2′,4,4′,5	99	5.9 ± 2.8	5	6.1 ± 2.5	5
2,2′,4,5,5′	101	15.4 ± 6.4	5	27.3 ± 10.4	5
2,3,3′,4′,6	110	2.9 ± 1.5	5	20.7 ± 10.4	4
2,3′,4,4′,5	118*, 108[b]	15.3 ± 8.6	5	21.9 ± 11.0	4
2,2′,3,4,4′,5′	138	17.5 ± 7.3	5	14.3 ± 10.3	5
2,2′,3,4,5,5′	141	14.6 ± 7.2	5	5.4 ± 4.3	4
2,2′,3,4,5′,6	144	10.5 ± 5.2	5	16.1 ± 9.4	4
2,2′,3,4′,5,5′	146	2.3 ± 0.9	5	16.5 ± 13.2	4
2,2′,3,3′,5,5′	153	14.3 ± 7.7	5	8.4 ± 5.8	2
2,2′,3,3′,4,5,6′	174	4.8 ± 2.9	5	2.1 ± 2.8	2
2,2′,3,3′,4,5′,6	175	1.3 ± 0.7	5	12.4 ± 8.4	5
2,2′,3,4,4′,5,5′	180	4.1 ± 1.2	5	23.1 ± 23.7	5
2,2′,3,4,5,5′,6	185	4.7	1	9.9 ± 7.4	4
2,2′,3,4′,5,5′,6	187*, 159[b]	3.8 ± 2.6	5	3.3 ± 1.9	5
2,2′,3,3′,4,4′,5′,6	196	1.3 ± 1.1	5	3.1 ± 3.2	5
2,2′,3,3′,4′,5,5′,6	201	1.4 ± 0.4	5	3.6 ± 3.5	5
total PCB (sum of 35 congeners)		1250 ± 478	5	547 ± 366	5

[a] NA, not analyzed. [b] Chromatographically unresolved; asterisk denotes dominant congener. [c] Concentrations in pg/m^3. [d] Concentrations in pg/L.

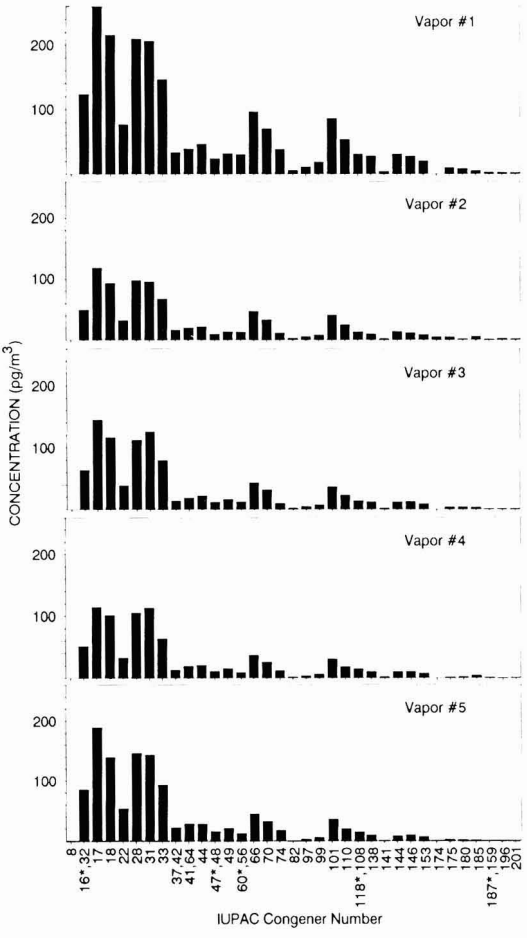

Figure 3. Concentrations of PCB congeners in five vapor samples collected over Lake Superior. Congeners are arranged in increasing IUPAC systematic number as in Table II.

chromatography/mass selective detection (GC–MSD). The extract was then fractionated by elution from a 13-g Florisil column (1.25% deactivated) with 50 mL of hexane. The eluent was concentrated to <1 mL and analyzed for PCB congeners by using gas chromatography with electron capture detection.

PAHs were quantified by high-resolution capillary gas chromatography (HRGC) with a Hewlett-Packard 5880 GC and a HP5970 mass selective detector operated in selected-ion mode. A series of perdeuterated PAHs were used as internal standards to quantify PAHs by isotopic dilution. Chrysene and triphenylene were not chromatographically resolved and their combined concentrations are reported. PCB congeners were analyzed by HRGC using a HP 5840A gas chromatography apparatus equipped with an electron capture detector. The method of ref 33 was used to identify and quantify congeners and a modification employing internal standards was used to analyze the water samples (*30*).

The recovery of mirex added to aerosol, gas-phase, and water samples as a surrogate prior to extraction was 106% ± 20%, 132% ± 8%, and 83% ± 16%, respectively. Recovery of PAHs and PCBs from spiked sediments using these procedures averaged 87.8% (range, 64–120%) and 86.4% (range, 65–120%), respectively. The PUF plugs used to collect gas-phase samples exhibited nonzero blanks for PCBs, contributing between 17% and 35% of PCBs measured in the five samples. All gas-phase and aerosol concentrations have been corrected for blank levels while water samples, which had insignificant blank levels, have not been corrected.

Results and Discussion

Concentrations of PCBs and PAHs. Atmospheric gas and surface water dissolved concentrations of PCB congeners are summarized in Table II. Total PCB concentrations (t-PCB is the sum 35 congeners) in the five gas samples average 1.20 ± 0.46 ng/m^3, in close agreement with concentrations measured during summer months over northern Wisconsin (0.96 ± 0.51 ng/m^3; ref 34) but lower than those over Isle Royale (3.2 ± 1.1 ng/m^3; D. L. Swackhamer, personal communication). Background t-PCB concentrations in air over North America are relatively constant at ≈1 ng/m^3 and levels decrease to 0.01–0.7 ng/m^3 over the open ocean and the Arctic Ocean (Table III). Insufficient air was sampled to detect PCBs in any aerosol samples collected in this study. The more volatile tri- and tetrachlorobiphenyl congeners dominate PCB distributions of the atmospheric gas phase (Figure 3). These PCB patterns are similar to those of filtered surface water, suggesting these compounds are dynamically cycling between the atmosphere and surface waters (*30*).

Table III. Total PCB Concentrations in Air (ng/m³)

	av	range	ref
Great Lakes Basin			
Lake Superior			
1978	1.5	0.9–3.5	35
1979	0.9	0.4–1.4	35
1980	1.0	0.1–0.6	35
1981	0.3	0.1–0.6	35
1983	3.2	1.5–5.2	recalcd from 6
1986	1.2	0.9–2.0	*a*
Lake Michigan (1977)	1.0	0.5–1.5	49
N. Wisconsin (1984)			
summer	0.96	0.60–1.82	34
winter	0.1		34
Turkey Lakes, ON	1.3		58
other continental			
Arizona (1974)		0.02–0.41	59
Kansas (1974)		0.03	59
NW Territories (1974)		0.002–0.07	59
Chesapeake Bay (1973)		1.0–2.0	60
College Station, TX (1979)		0.11–0.48	4,5
Bloomington, IN (1987–1988)	2.7–4.4	0.4–20	61
marine/remote			
Grand Banks (1973)		0.05–0.16	62
Georges Banks (1973)		0.58–1.6	62
Bermuda (1973)		0.15–0.5	62
Bermuda (1973)		0.19–0.66	60
Bermuda (1974)		0.08–0.48	60
N. Atlantic		0.01	63
N. Atlantic (1977–1979)		0.69	4,5
Arctic (1986–1987)		0.017	64
Enewetak Atoll (1979)		0.05	4,5

[a] This study.

Atmospheric levels of total PCBs over the Great Lakes have remained relatively constant near 1 ng/m³ during the past 10 years (Figure 4, Table III) despite decreased water column concentrations and estimated PCB loadings (*8*, *10*, *32*, *35*). Atmospheric PCB levels may be buffered by dynamic seasonal exchange with surface waters, vegetation, soils, and other aquatic and terrestrial contaminant reservoirs. Constant air concentrations coupled with decreasing surface water concentrations suggest that the PCB gradient across the air–water interface has shifted in favor of transfer from water to air.

Concentrations of PAHs in five gas and aerosol samples collected over Lake Superior in August 1986 are shown in Figures 5 and 6 and summarized in Table IV. Total PAH (sum of 13 PAHs) concentrations ranged from 2.5 to 6.3 ng/m³ and averaged 3.9 ± 1.7 ng/m³. The gas phase is dominated by the more volatile PAHs fluorene, phenanthrene, fluoranthene, and pyrene, while aerosols are relatively enriched in higher molecular weight PAHs. Absolute and relative PAH concentrations in the gas phase are

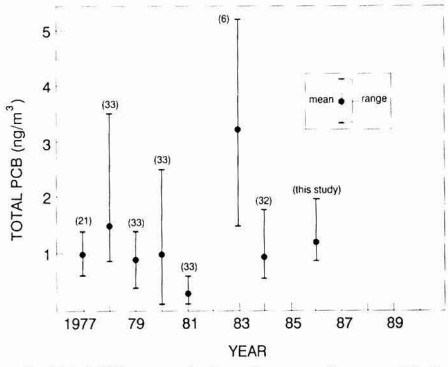

Figure 4. Total PCB concentrations (range and average) in the atmosphere over the Great Lakes, 1977–1986. Data for 1983 recalculated from ref 6.

constant among the five samples, indicating the air mass over Lake Superior was horizontally well mixed with respect to these compounds during the 7-day cruise. Levels of aerosol-associated PAHs did not vary with the exception of ideno[1,2,3-*cd*]pyrene and benzo[*ghi*]perylene, which were higher in samples collected north of the Keweenaw Peninsula (samples 2 and 3, Figure 6). Total PAH concentrations measured in this study agree well with those measured during the summer of 1983 over Isle Royale (*3*) and are lower than levels over Lake Michigan in the mid-1970s (*36*). The sums of seven PAHs measured in all three studies were 6.8, 2.7, and 3.4 ng/m³ over Lake Michigan, Isle Royale, and Lake Superior, respectively. Airborne concentrations of benzo[*a*]pyrene and benzo[*ghi*]perylene were about 1000-fold higher in the Lake Michigan study, while air over Lake Superior and Isle Royale contained 4 times more phenanthrene. These differences may indicate spatial or temporal variations in atmospheric PAH burdens or result from different sampling and analytical procedures. PAH levels on aerosols over Lake Superior are less than those on aerosols collected over the Niagara River (*37*) and aerosols sampled throughout the year at several locations in Scandinavia (*38*), suggesting that PAH concentrations in the relatively clean air over the upper Great Lakes represent continental background levels.

Gas–Aerosol Distributions of PAHs. The distribution of hydrophobic organic contaminants between gas and aerosol phases depends upon the subcooled liquid vapor pressure ($p_l°$, Pa), the surface area concentration of aerosol (S_T, cm²/cm³), and the ambient temperature (*27*, *39–41*). Because aerosol washout by precipitation is much more

Table IV. Concentrations of Polycyclic Aromatic Hydrocarbons in the Atmosphere and Surface Waters of Lake Superior

	aerosol		gas phase			dissolved	
	av ± SD	*N*	av ± SD	*N*	% aerosol range	av ± SD	*N*
fluorene	0.8 ± 0.5	4	449.1 ± 266.2	5	0.0–0.4	0.63 ± 0.17	5
phenanthrene	12.2 ± 3.6	5	2650.5 ± 1043.2	5	0.3–0.7	3.49 ± 1.71	5
fluoranthene	5.8 ± 3.4	5	174.8 ± 126.9	5	1.2–8.2	0.35 ± 0.07	5
pyrene	12.4 ± 6.6	5	332.4 ± 142.8	5	1.7–9.5	0.28 ± 0.11	5
benz[*a*]anthracene	13.8 ± 7.6	5	110.9 ± 216.7	5	2.3–67	0.16 ± 0.15	5
chrysene/triphenylene	17.7 ± 5.0	5	48.1 ± 32.3	5	16–48	0.37 ± 0.21	5
benzo[*b*]fluoranthene	9.8 ± 3.6	5	13.0 ± 9.4	5	35–57	0.07 ± 0.10	5
benzo[*k*]fluoranthene	8.4 ± 4.1	5	12.3 ± 7.9	5	34–52	0.02 ± 0.01	5
benzo[*e*]pyrene	NA[a]		6.3 ± 4.0	5		0.06 ± 0.09	5
benzo[*a*]pyrene	3.8 ± 1.3	5	1.2 ± 1.2	3	72–100	0.39 ± 0.18	5
indeno[1,2,3-*cd*]pyrene	16.8 ± 15.0	5	1.3 ± 0.7	3	77–100	ND[b] (<0.03)	5
dibenz[*a,h*]anthracene	ND[b]		ND			ND[b] (<0.03)	5
benzo[*ghi*]perylene	13.1 ± 8.0	5	8.3 ± 6.1	2	32–100	ND[b] (<0.05)	5

[a] NA, not analyzed. [b] ND, not detected. [c] Concentrations in pg/m³. [d] Concentrations in ng/L.

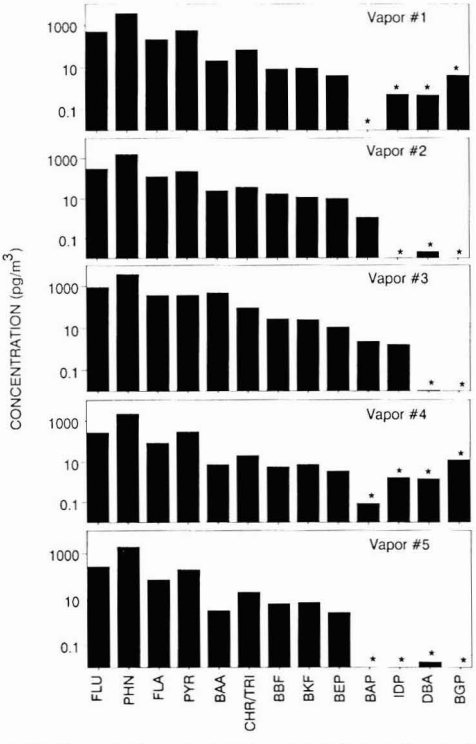

Figure 5. Concentrations of polycyclic aromatic hydrocarbons in five vapor samples collected over Lake Superior. Asterisks indicate compounds that were not detected above the detection limits shown.

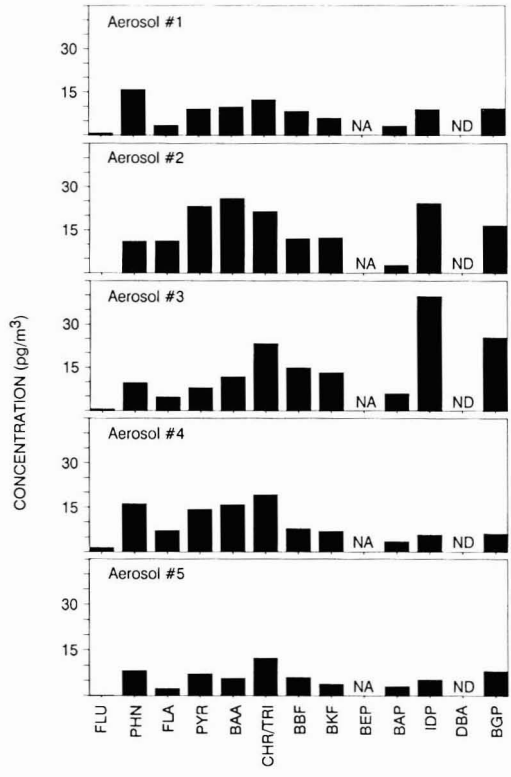

Figure 6. Concentrations of polycyclic aromatic hydrocarbons in five aerosol samples collected over Lake Superior (NA, not analyzed; ND, not detected).

efficient than vapor scavenging for these chemicals (*15, 42*), the gas–aerosol distribution exerts a major control on the rate of HOC deposition from the atmosphere. Junge (*39*) modeled HOC speciation in the atmosphere as a linear, reversible partitioning between gas and aerosols:

$$\varphi = cS_T/(p_1^\circ + cS_T) \quad (1)$$

where φ is the aerosol-associated fraction, c is a compound-specific constant, which depends on molecular weight, surface concentration required for a monolayer coverage, and the difference between heats of desorption and vaporization (*41*), and S_T is the surface area aerosol concentration. Junge (*39*) assumed c was invariant and equal to 1.7×10^{-4} atm·cm (17.2 Pa·cm). From laboratory data of Bidleman and Foreman (*43*) and field data of Bidleman et al. (*44*) and Yamasaki et al. (*40*), Pankow (*41*) calculated values for c of 13.2 Pa·cm and 17.2 Pa·cm for PAHs and organochlorines, respectively. S_T ranges from 4×10^{-7} cm^2/cm^3 in clean continental background air to 10^{-5} cm^2/cm^3 in urban areas (*45*).

In this study, the distribution of PAHs between the aerosol and gas phases was estimated from concentrations collected on the filter (F) and adsorbent foam plug (A), respectively. As predicted by eq 1, the fraction of PAHs assocated with aerosols over Lake Superior varies inversely with vapor pressure (Table IV). In Figure 7, observed PAH φ values for PAH are plotted against subcooled liquid vapor pressures (p_1°) at 25 °C (*46*). The vapor–aerosol distribution predicted by eq 1 using values of c and S_T typical of remote atmospheres is also shown in Figure 7. Compounds with vapor pressures greater than 10^{-2} Pa such as fluorene and phenanthrene occur almost exclusively in the gas phase. Conversely, higher molecular weight PAHs, including indeno[1,2,3-*cd*]pyrene and benzo[*ghi*]perylene

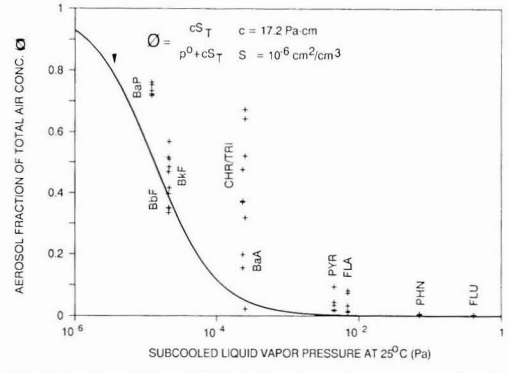

Figure 7. Speciation of PAHs in the atmosphere versus subcooled liquid vapor pressure. Solid line represents the fraction of total air concentration that is associated with aerosol according to Junge's model for typical remote atmospheres (ref 39).

($p_1^\circ < 10^{-6}$ Pa), are predominantly associated with aerosols and are near detection limits in our gas samples. Dibenz[*a,h*]anthracene was not detected in any aerosol or gas sample. Equation 1 is extremely sensitive to the product of c and S_T, and the gas–aerosol distributions of compounds with vapor pressures between 10^{-6} and 10^{-2} Pa are predicted to be variable. The range in φ observed for benz[*a*]anthracene, chrysene/triphenylene, and the benzofluoranthenes may result from subtle changes in aerosol concentration (S_T), temperature, or the energetics of partitioning between sample collections. These PAHs with intermediate vapor pressures may be useful as sensitive

probes of gas–aerosol partitioning.

High molecular weight PAHs exist in the atmosphere almost exclusively associated with aerosols and enter surface waters through dry deposition and aerosol scavenging by precipitation. Once deposited, particle-bound PAHs may not rapidly equilibrate with the dissolved phase and are therefore not likely to volatilize. Hindered release of high molecular weight PAHs from particles may result from slow desorption kinetics and diffusion from within the interior of the particles. Conversely, PAHs such as phenanthrene occur primarily in the atmospheric gas and aqueous dissolved phases and are available for active exchange across the air–water interface.

Although PCB congeners were not detected on aerosols collected over Lake Superior in this study, their concentrations may be estimated from their gas concentrations and the relationship between vapor pressure and gas–aerosol partitioning for organochlorines developed by Bidleman and Foreman (*43*). Subcooled liquid vapor pressures of PCB congeners at 20 °C were interpolated from values at 15 and 25 °C reported by Burkhard et al. (*47*). The ratio of gas to aerosol concentrations for each congener was calculated by the equation

$$\log [A(\mathrm{TSP})/F] = 0.765 (\log p_L^\circ) + 7.26 \qquad (2)$$

where A is the gas (adsorbent-retained) PCB concentration (ng/m^3), TSP is the total suspended particulate matter concentration (μg/m^3), and F is the aerosol (filter-retained) PCB concentration (ng/μg; ref 43). The aerosol concentration was calculated from this ratio and the average gas-phase congener concentration over Lake Superior in 1986. Assuming TSP concentrations of 10 μg/m^3 (*48*), estimated t-PCB aerosol concentrations over Lake Superior are 1.7×10^{-3} ng/m^3 or 0.17 μg/g, approximately half of the t-PCB detection limit in this study. This aerosol concentration is significantly less than measured levels over Lake Michigan of 3–4 μg/g (*11*, *49*). These calculated aerosol PCB concentrations are very sensitive to the chosen vapor pressures and are only order of magnitude estimates. Calculated PCB aerosol concentrations are relatively constant among chlorine homologue groups, with di- and trichlorobiphenyl concentrations supported by relatively high gas-phase levels and the higher chlorinated congener concentrations resulting from their lower vapor pressures (Figure 8).

PCB and PAH Fugacity Gradients across the Air–Water Interface. Simultaneous collection of atmospheric gas and filtered water permits HOC fugacity gradients across the air–water interface to be estimated. In this analysis, samples collected 10 m above and 5–10 m below the interface are assumed to reflect concentrations very near the air–water boundary. Temperature profiles in the epilimnion of Lake Superior indicate that the upper 15 m were well mixed during sampling. In these calculations, an interface temperature of 15 °C was chosen as an intermediate value between measured air and water temperatures (10–24 °C and ≈10 °C, respectively).

PCB and PAH fugacities in the gas and dissolved phases were calculated from measured concentrations and estimated fugacity capacities (Z values) by using the equations in Table I. The fugacity capacity of the vapor phase is compound-independent and equal to $1/RT$, or 4.18×10^{-4} mol/(m^3·Pa) at 15 °C (*26*). Aqueous Z values equal the reciprocal of the Henry's law constants. In this analysis, PCB Henry's law constants reported by Burkhard et al. (*47*) are used. These values were predicted from the ratio of the liquid (or subcooled liquid) vapor pressure and aqueous solubility for each congener, which in turn were estimated from correlations with Gibbs' free energy of

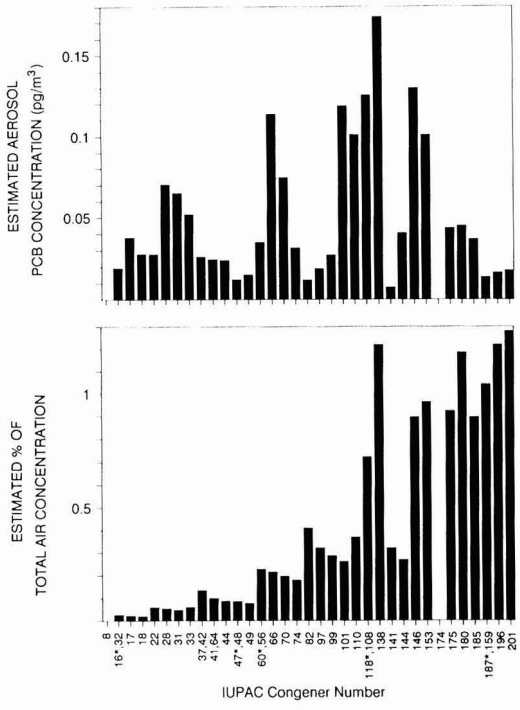

Figure 8. Calculated PCB aerosol concentrations and the percentage of the total atmospheric burden that is associated with aerosols. See calculation in text.

vaporation and solubilization, respectively. Burkhard et al. (*47*) estimated the error in their PCB Henry's law constants to be a factor of 5.

Directly measured Henry's law constants are not available for many PAHs, and the aqueous phase Z values in Table V were calculated from Henry's law constants, which were estimated as follows. *Solid-phase* aqueous solubilities at 25 °C (*50*) were converted to subcooled liquid solubilities by the integrated Clausius–Clapeyron equation, an enthalpy of fusion of 13.5 cal/(deg·mol) (*51*), and PAH melting points (*52*). Henry's law constants at 25 °C were then calculated for PAHs as the ratio of the liquid-phase vapor pressures (*46*) and the subcooled liquid aqueous solubilities calculated above. Finally, Henry's law constants at 25 °C were corrected to 15 °C by using a relationship that describes the temperature dependence of PCB of Henry's law constants (*53*):

$$\ln H = 18.53 - 7868/T \qquad (3)$$

where T is the absolute temperature (K). To correct the PAH values to 15 °C, we used the slope of eq 3 and determined compound-specific intercepts from the 25 °C values. Henry's law constants decrease by a factor of 2 between 25 and 15 °C.

Aqueous PCB and PAH fugacities and the resulting air–water exchange rates depend directly on Henry's law constants, and the overall accuracy of these calculations may be limited by uncertainties in these values. At this point, Henry's law constants for PAHs are no better than order of magnitude estimates and it is difficult to calculate with confidence the direction and magnitude of PAH air–water exchange.

The fugacity gradient is expressed as α, the ratio of HOC fugacities in the aqueous dissolved and atmospheric gas phases. With this convention, values of α greater than 1

Table V. Henry's Law Constants, Fugacity Capacities, and Air–Water Mass-Transfer Coefficients of PAHs and PCBs

	H(15 °C), Pa·m³/mol	Z_w, mol/m³·Pa	K_{OL}, m/day (×1000)	D_{AW}, mol/(m²·day·Pa) (×1000)
fluorene	1.863	0.5	37.73	20.3
phenanthrene	0.691	1.4	19.34	28.0
fluoranthene	0.134	7.5	4.58	34.2
pyrene	0.125	8.0	4.28	34.3
benz[*a*]anthracene	0.092	10.9	3.19	34.7
chrysene/triphenylene	0.037	26.7	1.33	35.5
benzo[*b*]fluoranthene	0.054	18.6	1.90	35.3
benzo[*k*]fluoranthene	0.111	9.0	3.84	34.5
benzo[*e*]pyrene	0.007	136.4	0.26	36.0
benzo[*a*]pyrene	0.009	106.3	0.34	35.9
indeno[1,2,3-*cd*]pyrene	0.001	673.0	0.05	36.1
dibenz[*a*,*h*]anthracene		2558.3	0.01	36.1
benzo[*ghi*]perylene	0.001	1950.6	0.02	36.1

PCB congener	IUPAC no.	H(15 °C), Pa·m³/mol	Z_w, mol/m³·Pa	K_{OL}, m/day (×1000)	D_{AW}, mol/(m²·day·Pa) (×1000)
2,4′	8	11.0	0.091	71	6.4
2,2′,3	16*, 32[a]	15.3	0.065	75	4.9
2,2′,4	17	22.8	0.044	78	3.4
2,2′,5	18	25.4	0.039	79	3.1
2,3,4′	22	6.5	0.15	63	9.7
2,4,4′	28	9.6	0.10	69	7.2
2,4′,5	31	10.7	0.093	71	6.6
2′,3,4	33	7.1	0.14	65	9.1
3,4,4′	37, 42	3.0	0.34	48	16
2,2′,3,4	41, 64	9.8	0.10	69	7.1
2,2′,3,5′	44	13.6	0.074	73	5.4
2,2′,4,4′	47*, 48[a]	17.6	0.057	76	4.3
2,2′,4,5′	49	19.8	0.051	77	3.9
2,3,4,4′	60*, 56[a]	4.1	0.24	54	13
2,3′,4,4′	66	5.4	0.18	60	11
2,3′,4′,5	70	6.1	0.16	62	10
2,4,4′,5	74	6.9	0.14	64	9.3
2,2′,3,3′,4	82	4.8	0.21	58	12
2,2′,3′,4,5	97	8.0	0.12	67	8.3
2,2′,4,4′,5	99	11.4	0.087	71	6.2
2,2′,4,5,5′	101	12.9	0.078	73	5.7
2,3,3′,4′,6	110	6.6	0.15	63	9.6
2,3′,4,4′,5	118*, 108[a]	3.5	0.29	51	15
2,2′,3,4,4′,5′	138	4.1	0.25	54	13
2,2′,3,4,5,5′	141	23.9	0.042	79	3.3
2,2′,3,4,5′,6	144	38.5	0.026	81	2.1
2,2′,3,4′,5,5′	146	6.9	0.15	64	9.3
2,2′,3,3′,5,5′	153	6.6	0.15	63	9.6
2,2′,3,3′,4,5,6′	174	28.8	0.035	80	2.8
2,2′,3,3′,4,5′,6	175	18.3	0.055	76	4.2
2,2′,3,4,4′,5,5′	180	11.1	0.090	71	6.4
2,2′,3,4,5,5′,6	185	17.0	0.059	76	4.4
2,2′,3,4′,5,5′,6	187*, 159[a]	15.5	0.065	75	4.8
2,2′,3,3′,4,4′,5′,6	196	26.3	0.038	79	3.0
2,2′,3,3′,4′,5,5′,6	201	23.5	0.043	78	3.3

[a] Chromatographically unresolved; asterisk denotes dominant congener.

indicate transfer from the water to the atmosphere (i.e., volatilization) and values of <1 denote absorption of HOC gases into surface waters. Fugacities in the two phases are equal at equilibrium (α = 1), and there is no net gas transfer between phases. Fugacity ratios were calculated for six pairs of gas and water samples (Table VI). Two air samples collected on consecutive days within several kilometers of Copper Harbor, MI (2 and 3) are paired with one surface water sample (site 1383) to evaluate the short-term temporal variability in air–water partitioning. Similarly, two water samples collected 55 km apart on consecutive days (site 1387 and site 1389) are paired with an air sample collected during transit between these stations (4) to examine spatial variability.

Fugacity ratios of the PCB congeners are variable but are generally ≥1 (Figure 9). Many α values for PCB congeners observed off the Keweenaw Peninsula (sample pair 1, Table VI) are less than 1, indicating a flux from the atmosphere to the water at this site. In contrast, the steepest PCB gradient from water to air (i.e., largest α values) occurred in the central basin of the lake (sample pair 4, Table VI). Although the fugacity ratio of an individual PCB congener varied 10-fold among sample pairings, α values are relatively constant for the tri-, tetra-, and pentachlorobiphenyls (Figure 9). PCB solubility and vapor pressure covary with increasing congener molecular

Table VI. Samples Pairings for Air–Water Distribution Calculations

air–water pair	gas-phase sample[a]	water sample[a]	air–water pair	gas-phase sample[a]	water sample[a]
1	1	1382	4	4	1387
2	2	1383	5	4	1389
3	3	1383	6	5	1391

[a] See Figure 2.

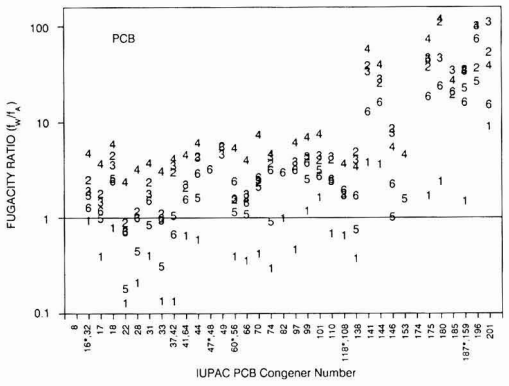

Figure 9. Ratio of PCB congener dissolved and gas-phase fugacities. A ratio of 1 is the equilibrium condition. Numbers refer to the sample pairings in Table VI.

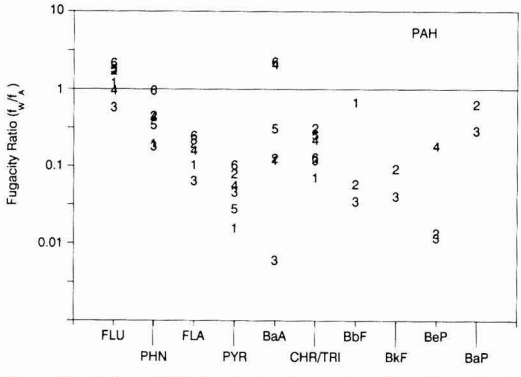

Figure 10. Ratio of PAH dissolved and gas-phase fugacities. A ratio of 1 is the equilibrium condition. Numbers refer to the sample pairings in Table VI.

weight, resulting in Henry's law constants that are relatively invariant among the congeners (*47*, *54*). Higher values of α for hexa-, hepta-, and octachlorobiphenyls indicate either that these congeners are furthest from equilibrium or that measurements have over- or underestimated their dissolved and gas concentrations, respectively (see below).

Fugacity ratios of 10 PAHs range from ≈0.01 to 2 and most values are less that 1, suggesting diffusive PAH fluxes from the atmosphere to surface waters (Figure 10). Due to the large uncertainties in Henry's law constants for PAHs, however, we cannot say with confidence that PAH α values were different from 1. Thus, estimates of PAH fluxes across the air–water interface are not possible.

Measured PCB fugacity ratios greater than 1 agree with the steady-state, nonequilibrium model describing air–water exchange of hydrophobic substances proposed by Mackay et al. (*9*). Diffusive gas exchange can occur in both directions (i.e., absorption and volatilization) while advective wet and dry deposition transports HOCs only from the atmosphere to surface waters. Precipitation events increase dissolved HOC concentrations, resulting in fugacity ratios of >1. During interceding dry periods, HOCs volatilize and α values approach 1. According to this model, volatilization during dry, warm periods is the slow, prolonged response to intense, episodic advective inputs from the atmosphere.

Fluxes of PCBs across the Air–Water Interface. Mass fluxes of PCBs across the air–water interface were estimated from the difference in the aqueous dissolved and atmospheric gas-phase fugacities (Table I). The overall mass-transfer coefficient (D_{AW}, mol/(m²·day·Pa) for each compound was derived from resistances to transfer through the gas and liquid films (k_g and k_l; m/day), respectively.

$$1/D_{AW} = 1/k_l Z_W + 1/k_g Z_A \quad (4)$$

D_{AW} was calculated for each compound by using H values at 15 °C and values of k_l and k_g of 0.086 and 86.4 m/day estimated from semiempirical equations derived by Mackay and Yeun (*25*). These values of k_l and k_g are for calm conditions and thus represent minimum values. Calculated still air mass-transfer coefficients average 0.007 mol/(m²·day·Pa) for PCB congeners (Table V). These values are approximately one-half to one-tenth of those calculated from models (e.g., ref 25) or estimated from mass balance modeling (*3*, *6*), perhaps because enhanced transfer resulting from wind-induced turbulence was not considered. Wind speeds during sample collection ranged from 2 to 11 m/s and averaged 5 m/s. Values of D_{AW} and fluxes at 5 m/s are approximately 7.5 times greater than still air values (Table VII).

Table VII. Fluxes of PCBs into and from Lake Superior Surface Waters

	ng/m²·day	ref
volatilization	19 (still air)	this study
	141 (5 m/s wind)	this study
	15	7[a]
	23	6[b]
	63	8
deposition	18	
wet	10	8
dry	8	8
sediment accum[c]	5.0	*d*
	2.7–54	35

[a] Lake Michigan. [b] Siskiwit Lake, Isle Royale, Lake Superior. [c] Net accumulation rate in upper 0.5 cm of open lake cores. [d] Baker and Eisenreich, unpublished data, 1989.

Calculated fluxes of PCB congeners across the air–water interface are shown in Figure 11. Four of the six sample pairs have PCB gradients that support volatilization, and the total PCB flux from the water averages 19 ± 24 ng/m²·day. Relatively high gas-phase concentrations of tri- and tetrachlorobiphenyls result in fluxes from the air to the water in sample pair 1. Most congeners are near equilibrium in sample pair 5 due to relatively low PCB concentrations in surface water at station 1389. It is unclear whether the significant difference in fluxes between nearby stations 1387 and 1389 (sample pairs 4 and 5, Figure 11) on consecutive days is real. Given the rapid mixing and advection of air over the lake, small-scale variations in HOC concentrations in surface waters would not be conserved in the overlying air mass.

The largest uncertainty in these flux calculations results from the strong dependence of the equilibrium and mass-transport parameters on environmental conditions, specifically wind speed and temperature. Estimates of annual HOC fluxes across the air–water interface require data on the variations of k_l, k_g, and α throughout the year and on the temperature dependence of Henry's law constants. In addition, ice cover, which effectively limits air–water exchange, must be considered in northern lakes. Volatilization fluxes calculated in this study strictly apply to summer conditions and cannot be directly extrapolated to annual rates.

An additional difficulty in calculating HOC fugacity gradients across the air–water interface is that HOCs complexed by colloids in surface waters are not directly

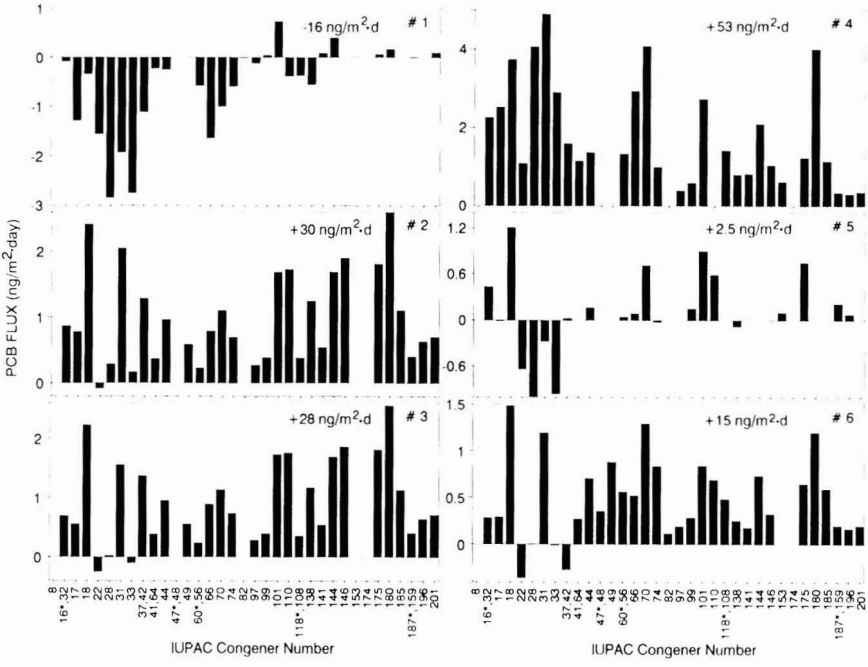

Figure 11. Fluxes of PCB congeners across the air–water interface calculated from the fugacity gradients of the six sampling pairings in Table VI. Positive and negative fluxes represent volatilization and absorption, respectively.

available for exchange across the air–water interface. Baker et al. (*29*) estimated that ≈35% of nonfilterable PCB congeners in Lake Superior water are associated with organic colloids, with the extent of binding proportional to congener hydrophobicity. The "dissolved" HOC concentrations used to calculate aqueous fugacities may overestimate the actual dissolved concentrations because colloidal-bound HOCs were included in the analysis (*29*):

$$f_d(\text{calc}) = [10^{-6}/\text{MW}]\ (C_d + C_c)/Z_w \qquad (5)$$

where f_d is the calculated fugacity based on the total HOC concentration in the filtrate, and C_c is the mass concentration of HOC bound by nonfilterable colloids. The HOC distribution between dissolved and colloidal phases is described by an equilibrium binding constant K_c (L/kg):

$$K_c = 10^6 C_c/[C_d(\text{DOC})] \qquad (6)$$

In this analysis, we assume that dissolved organic carbon (DOC, mg of C/L) is a surrogate measure of colloid concentration in lake water (*28*, *29*, *55*, *56*), use an average value of 2 mg of C/L for Lake Superior (*30*), and estimate K_c from octanol–water partition coefficients (K_{ow}, ref 57). Combining eqs 5 and 6 demonstrates that aqueous fugacities calculated with measured nofilterable HOC concentrations are overestimated by a factor $(1 + K_c(\text{DOC}))$. Colloid binding increases in importance for PCB congeners as their molecular weight, chlorine number, and K_{ow} increases. As shown in Figure 12, correcting for colloid binding decreases fluxes of the most soluble species only slightly (<10%) but exerts a relatively larger influence on the more hydrophobic compounds. In most cases, however, the corrected fugacity gradient is still significant, indicating that although consideration of colloid binding decreases the PCB gradient, there remains a volatilization flux for many of the compounds in this study.

Previous investigations have employed a mass balance strategy to estimate PCB volatilization rates from Siskiwit

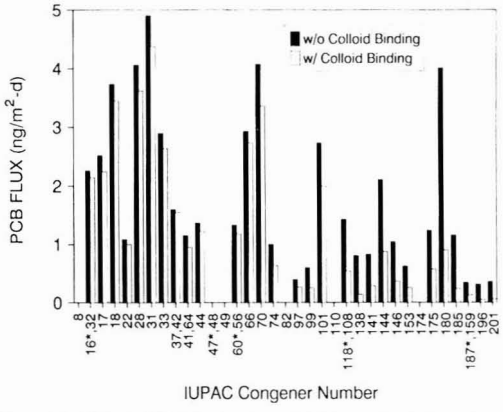

Figure 12. Effect of PCB binding by colloidal organic matter on estimated fluxes across the air water interface for sample pair 4 (Table VI). Open bars represent the flux that results when a fraction of PCBs in surface waters is complexed by dissolved organic carbon (2 mg of C/L).

Lake, Isle Royale (*6*), and the Great Lakes (*7*, *8*). Volatilization rates calculated in the present study are similar to but generally lower than those earlier estimates (Table VII). Mass balance derived volatilization rates are yearly averages while fluxes calculated here cover a short period during the summer, and differences in rates may be due to higher fluxes at other times. Also, the mass-transfer coefficients used in this study are conservative and thus the fluxes may have been underestimated. HOC fluxes calculated from measured fugacity gradients are more direct and, therefore, are likely to be more accurate than estimates from mass balances.

To place calculated PCB volatilzation fluxes in perspective, they are compared to rates of other transport processes in Table VII. Volatilization rates are greater

than net rates of burial in bottom sediments. Given the uncertainties in the fluxes in Table VII, rates of PCB volatilization are quite close to estimates of current gross atmospheric deposition, suggesting that the lake is near steady state with respect to atmospheric exchange and emphasizing the importance of degassing in the overall PCB budget of the Great Lakes. Volatilization rates were determined over a short period while atmospheric deposition and sediment accumulation rates are averaged over at least 1 year, and further work is required to assess the seasonality of HOC fluxes across the air–water interface. These flux calculations indicate that the Great Lakes may currently be a source of PCBs to the atmosphere.

Conclusions

Modeling exchange of hydrophobic organic contaminants across the air–water interface requires measurements of both compound-specific equilibrium and mass-transfer parameters (i.e., Z and D_{AW}) as well as estimates of the fugacity gradient across the boundary. Although improved measurements of Henry's law constants and mass-transfer coefficients have refined these calculations, there exists a need to measure the fugacity gradient under a variety of environmental conditions to accurately quantify this important contaminant pathway. In this study, the fugacity gradient has been approximated by simultaneously measuring organic contaminant concentrations in the atmospheric gas phase and in surface water. Despite limitations inherent to this approach (e.g., association of HOCs in surface waters by colloidal organic matter, poor temporal and spatial resolution), these data indicate that Lake Superior is degassing organic contaminants during the summer months. Due to lower mass-transfer coefficients and Henry's law constants at lower temperatures, HOC fluxes across the air–water interface likely decrease and may change direction during fall, winter, and spring. Volatilization fluxes are similar to estimated gross atmospheric deposition rates, suggesting that exchange across the air–water interface is near steady state. These findings are consistent with the description of Mackay et al. (*9*) of intense HOC fluxes to the lake during precipitation events followed by prolonged but lower volatilization during dry periods. Understanding of HOC gas exchange across the air–water interface of large lakes is practically limited by (1) the difficulty in directly measuring HOC fugacities in surface waters, (2) the lack of field-measured concentration gradients and fluxes under a variety of environmental conditions, and (3) limited data on the temperature dependences of Henry's law constants and mass-transfer coefficients. Further efforts are required to develop and validate methodologies that directly measure HOC fluxes across the air–water interface.

Acknowledgments

We thank T. Bidleman (University of South Carolina) and D. Mackay (University of Toronto) for their insightful reviews of this manuscript. We also thank R. Hites (Indiana University) for lending us the air sampler used in this work. The assistance of the captain and crew of the R/V Seward Johnson during our cruises and S. Ugargol and R. Holzknecht in the laboratory is much appreciated. The NOAA National Undersea Research Program at the Univerisity of Connecticut—Avery Point provided ship time and related services for this work and F. Younger (Chesapeake Biological Laboratory) prepared the graphics.

Registry No. PCB-8, 34883-43-7; PCB-16, 38444-78-9; PCB-32, 38444-77-8; PCB-17, 37680-66-3; PCB-18, 37680-65-2; PCB-22, 38444-85-8; PCB-28, 7012-37-5; PCB-31, 16606-02-3; PCB-33, 38444-86-9; PCB-37, 38444-90-5; PCB-42, 36559-22-5; PCB-41, 52663-59-9; PCB-64, 52663-58-8; PCB-44, 41464-39-5; PCB-47, 2437-79-8; PCB-48, 70362-47-9; PCB-49, 41464-40-8; PCB-60, 33025-41-1; PCB-56, 41464-43-1; PCB-66, 32598-10-0; PCB-70, 32598-11-1; PCB-74, 32690-93-0; PCB-82, 52663-62-4; PCB-97, 41464-51-1; PCB-99, 38380-01-7; PCB-101, 37680-73-2; PCB-110, 38380-03-9; PCB-118, 31508-00-6; PCB-108, 70362-41-3; PCB-138, 35065-28-2; PCB-141, 52712-04-6; PCB-144, 68194-14-9; PCB-146, 51908-16-8; PCB-153, 35065-27-1; PCB-174, 38411-25-5; PCB-175, 40186-70-7; PCB-180, 35065-29-3; PCB-185, 52712-05-7; PCB-187, 52663-68-0; PCB-159, 39635-35-3; PCB-196, 42740-50-1; PCB-201, 40186-71-8; fluorene, 86-73-7; phenanthrene, 85-01-8; fluoranthene, 206-44-0; pyrene, 129-00-0; benz[*a*]anthracene, 56-55-3; chrysene/triphenylene, 218-01-9; benzo[*b*]fluoranthene, 205-99-2; benzo[*k*]fluoranthene, 207-08-9; benzo[*e*]pyrene, 192-97-2; benzo[*a*]pyrene, 50-32-8; indeno[1,2,3-*cd*]pyrene, 193-39-5; dibenz[*a*,*h*]anthracene, 53-70-3; benzo[*ghi*]perylene, 191-24-2; triphenylene, 217-59-4.

Literature Cited

(1) Eisenreich, S. J.; Looney, B. B.; Thornton, J. D. *Environ. Sci. Technol.* **1981**, *15*, 30–38.
(2) Czuczwa, J. M.; McVeety, B. D.; Hites, R. A. *Science* **1984**, *226*, 568–569.
(3) McVeety, B. D.; Hites, R. A. *Atmos. Environ.* **1988**, *22*, 511–536.
(4) Atlas, E. L.; Giam, C. S. *Science* **1981**, *211*, 163.
(5) Atlas, E. L.; Giam, C. S. *Water, Air, Soil Pollut.* **1988**, *38*, 19–36.
(6) Swackhamer, D. L.; McVeety, B. M.; Hites, R. A. *Environ. Sci. Technol.* **1988**, *22*, 664–672.
(7) Swackhamer, D. L.; Armstrong, D. E. *Environ. Sci. Technol.* **1986**, *20*, 879–883.
(8) Strachan, W. M. J.; Eisenreich, S. J. *Mass Balancing of Chemical Pollutants in the Great Lakes; The Role of Atmospheric Deposition*, International Joint Commission Report: Windsor, Ontatio Region Office, 1988.
(9) Mackay, D.; Paterson, S.; Schroeder, W. H. *Environ. Sci. Technol.* **1986**, *20*, 810–816.
(10) Rapaport, R. A.; Eisenreich, S. J. *Environ. Sci. Technol.* **1988**, *22*, 931–941.
(11) Murphy, T. J.; Rzeszutko, C. P. *J. Great Lakes Res.* **1977**, *3*, 305–312.
(12) Strachan, W. M. J.; Huneault, H. J. *J. Great Lakes Res.* **1979**, *5*, 61–68.
(13) Strachan, W. M. J. *Environ. Toxicol. Chem.* **1985**, *4*, 677–683.
(14) Ligocki, M. P.; Leuenberger, C.; Pankow, J. F. *Atmos. Environ.* **1985**, *19*, 1609–1617.
(15) Ligocki, M. P.; Leuenberger, C.; Pankow, J. F. *Atmos. Environ.* **1985**, *19*, 1619–1626.
(16) Ligocki, M. P.; Pankow, J. F. *Environ. Sci. Technol.* **1989**, *23*, 75–83.
(17) Eisenreich, S. J.; Franz, T. P.; Swanson, M. B. *Atmos. Environ.*, in press.
(18) Whitman, W. G. *Chem. Metall. Eng.* **1923**, *23*, 146.
(19) O'Connor, D. J. *J. Environ. Eng. (N.Y.)* **1983**, *109*, 731–752.
(20) Brutsaert, W.; Jirka, G. H. *Gas Transfer at Water Surfaces*; D. Reidel Publishing Co.: Dordrecht, The Netherlands, 1984.
(21) Liss, P. S.; Slater, P. G. *Nature (London)* **1974**, *247*, 181–184.
(22) Mackay, D.; Leinonen, P. J. *Environ. Sci. Technol.* **1975**, *9*, 1178–1180.
(23) Doskey, P. V.; Andren, A. W. *Environ. Sci. Technol.* **1981**, *15*, 705–711.
(24) Andren, A. W. In *Physical Behavior of PCBs in the Great Lakes*; Mackay, D., Patersen, S., Eisenreich, S. J., Simmons, M. S., Eds.; Ann Arbor Science Publishers: Ann Arbor, MI, 1983; pp 127–140.
(25) Mackay, D.; Yuen, A. T. K. *Environ. Sci. Technol.* **1983**, *17*, 211–216.
(26) Mackay, D. *Environ. Sci. Technol.* **1979**, *13*, 1218–1223.
(27) Bidleman, T. F. *Environ. Sci. Technol.* **1988**, *22*, 361–367.
(28) Gschwend, P. M.; Wu, S.-C. *Environ. Sci. Technol.* **1985**, *19*, 90–96.

(29) Baker, J. E.; Capel, P. D.; Eisenreich, S. J. *Environ. Sci. Technol.* **1986**, *20*, 1136–1143.
(30) Baker, J. E.; Eisenreich, S. J. *J. Great Lakes Res.* **1989**, *15*, 84–103.
(31) Baker, J. E.; Eisenreich, S. J.; Johnson, T. C.; Halfman, B. M. *Environ. Sci. Technol.* **1985**, *19*, 854–861.
(32) Capel, P. D.; Eisenreich, S. J. *J. Great Lakes Res.* **1985**, *11*, 447–461.
(33) Capel, P. D.; Rapaport, R. A.; Eisenreich, S. J.; Looney, B. B. *Chemosphere* **1985**, *14*, 439–450.
(34) Manchester-Neesvig, J.; Andren, A. W. *Environ. Sci. Technol.* **1989**, *23*, 1138–1148.
(35) Eisenreich, S. J. In *Sources and Fates of Aquatic Pollutants*; Hites, R. A., Eisenreich, S. J., Eds.; Advances In *Chemistry* 216; American Chemical Society: Washington, DC, 1987; pp 393–469.
(36) Andren, A. W.; Strand, J. W. In *Physical Behavior of PCBs in the Great Lakes*; Mackay, D., Patersen, S., Eisenreich, S. J., Simmons, M. S., Eds.; Ann Arbor Science Publishers: Ann Arbor, MI, 1981; pp 459–479.
(37) Hoff, R. M.; Chan, K. W. *Environ. Sci. Technol.* **1987**, *21*, 556–561.
(38) Bjorseth, A.; Lunde, G.; Lindskog, A. *Atmos. Environ.* **1979**, *13*, 45–53.
(39) Junge, C. E. In *Fate of Pollutants in the Air and Water Environments*; Suffett, I. H., Ed.; Advances in Environmental Science and Technology; J. Wiley & Sons: New York, 1977; p 7–25.
(40) Yamasaki, H.; Kuwata, K.; Miyamoto, H. *Environ. Sci. Technol.* **1982**, *16*, 189–194.
(41) Pankow, J. F. *Atmos. Environ.* **1987**, *21*, 2275–2283.
(42) Duinker, J. C.; Bouchertall, F. *Environ. Sci. Technol.* **1989**, *23*, 57–62.
(43) Bidleman, T. F.; Foreman, W. T. In *Sources and Fates of Aquatic Pollutants*; Hites, R. A., Eisenreich, S. J., Eds.; Advances in Chemistry 216; American Chemical Society: Washington, DC, 1987; pp 27–56.
(44) Bidleman, T. F.; Billings, W. N.; Foreman, W. T. *Environ. Sci. Technol.* **1986**, *20*, 1038–1043.
(45) Whitby, K. T. *Atmos. Environ.* **1978**, *12*, 135–159.
(46) Yamaskai, H.; Kuwata, K.; Kuge, Y. *Nippon Kagaku Kaishi* **1984**, *8*, 1324–1329; *Chem. Abstr.* **1984**, *101*, 156747p.
(47) Burkard, L. P.; Andren, A. W.; Armstrong, D. E. *Environ. Sci. Technol.* **1985**, *19*, 500–507.
(48) Hollod, G. J. Ph.D. Thesis, Univesity of Minnesota, Minneapolis, 1979.
(49) Doskey, P. V.; Andren, A. W. *J. Great Lakes Res.* **1981**, *7*, 15.
(50) Pearlman, R. S.; Yalkowsky, S. H.; Banergee, S. J. *Phys. Chem. Ref. Data* **1984**, *13*, 555–562.
(51) Yalkowsky, S. H. *Ind. Eng. Chem. Fundam.* **1979**, *18*, 108–111.
(52) Weast, R. F., Ed. *Handbook of Chemistry and Physics*, 63rd ed.; The Chemical Rubber Co.: Cleveland, OH, 1982–1983.
(53) Tateya, S.; Tanabe, S.; Tatsukawa, R. In *Toxic Contamination in Large Lakes*; Schmidtke, N. W., Ed.; 1988; Vol. III, pp 237–281.
(54) Dunnivant, F. M.; Coates, J. T.; Elzerman, A. W. *Environ. Sci. Technol.* **1988**, *22*, 448–453.
(55) Brownawell, B. J.; Farrington, J. W. *Geochim. Cosmochim. Acta* **1986**, *50*, 157–169.
(56) Capel, P. D.; Eisenreich, S. J. In *Influence of Aquatic Humic Substances on Fate and Treatment of Pollutants*; MacCarthy, P., Suffet, I. H., Eds.; Advances in Chemistry 219; American Chemical Society: Washington, DC, p 1.
(57) Schwarzenbach, R. P.; Westall, J. *Environ. Sci. Technol.* **1981**, *15*, 1360–1367.
(58) Johnson, N. D.; Lane, D. A.; Schroeder, W. J.; Strachan, W. M. J. Presented at the Third Chemical Congress of North America, Toronto, Ontario, Canada, June 5–10, 1988.
(59) Bidleman, T. F.; Rice, C. P.; Olney, C. E. In *Marine Pollutant Transfer*; Windon, H. L., Duce, R. A., Eds.; Lexington Books: Lexington, MA, 1977; pp 323–351.
(60) Bidleman, T. F.; Olney, C. E. *Science* **1974**, *183*, 516–518.
(61) Hermanson, M.; Hites, R. A. *Environ. Sci. Technol.* **1989**, *23*, 1253–1258.
(62) Harvey, G. R.; Steinhauer, W. G. *Atmos. Environ.* **1974**, *8*, 777–782.
(63) Atlas, E. L.; Schauffer, S. Presented at the Third Chemical Congress of North America, Toronto, Ontario, Canada, June 5–10, 1988.
(64) Bidleman, T. F.; Patton, G. W.; Hinkely, D. A.; Walla, M. D.; Hargrave, B. T. Presented at the Third Chemical Congress of North America, Toronto, Ontario, Canada, June 5–10, 1988.

Received for review April 17, 1989. Revised manuscript received August 17, 1989. Accepted November 15, 1989. This work is the result of research sponsored by the Minnesota Sea Grant College Program supported by the NOAA Office of Sea Grant, Department of Commerce, under Grant No. NA-85-AA-D-SG136, Journal Reprint No. 246. The U.S. Government is authorized to reproduce and distribute reprints or government purposes, not withstanding any copyright notation that may appear hereon.

Environ. Sci. Technol. 1990, 24, 353-357

Distribution of Several Organophosphorus Insecticides and Their Oxygen Analogues in a Foggy Atmosphere

Dwight E. Glotfelty,*,† Michael S. Majewski,‡ and James N. Seiber‡

U.S. Department of Agriculture, Agricultural Research Service, Environmental Chemistry Laboratory, Beltsville Agricultural Research Center, Beltsville, Maryland 20705, and Department of Environmental Toxicology, University of California, Davis, California 95616

■ We measured the distribution of four organophosphorus insecticides (diazinon, parathion, chlorpyrifos, and methidathion) between the droplet and air phases during six fog events. We also measured the distribution of their oxon transformation products, which result from the oxidative conversion of the parent organophoshorothioate to the corresponding organophosphate. We found up to 60 μg/L for the total of the four parent insecticides, and up to 75 μg/L for the total of their oxons in the fogwater. In agreement with earlier studies, nearly all the compounds exhibited aqueous-phase concentrations much higher than would be expected from measured vapor concentrations and Henry's law. Even though high concentrations and high enrichments were found in the aqueous phase, for most of the compounds the largest proportion was present in the interstitial air phase, either as vapor or adsorbed to aerosol particles. Only very small amounts (<1%) of any of the compounds were found associated with particles within the fog droplets.

Introduction

The processes whereby pesticides enter the atmosphere are well-known: by application drift during spraying operations, by wind erosion of soil or formulation particles, or by postapplication volatilization (*1*). Once in the atmosphere, pesticides are carried away from the treated area, and regional or even global-scale transport is known to occur. The redeposition of the chemical to the surface, either by washout with precipitation or by direct uptake of airborne particles and vapor, leads to widespread, low-level environmental contamination.

The association of an airborne pesticide with atmospheric moisture is a key process controlling its residence time and cycling in the atmosphere. This association is usually expressed as a washout coefficient, the ratio of concentration in rain to concentration in air. The washout coefficient of vapor-phase pesticides is usually assumed to be equal to the reciprocal of K_{AW}, the dimensionless Henry's law constant (*2*). Washout coefficients have been measured for a number of pesticides and other organic xenobiotics (*3–6*). These washout coefficients are frequently found to be very different from K_{AW}^{-1}, and various interpretations have been offered to explain these findings. For example, non-Henry's law behavior is frequently assumed to arise because pesticides in the atmosphere associate with aerosol particles. The washout of particulate-bound pesticides will not be described by Henry's law, which is valid only for vapor-phase species in equilibrium with an ideal solution. The extent of association of pesticides with particles is rarely known with any degree of certainty, so that measured washout coefficients have commonly been used to infer the ambient atmospheric vapor/particle distribution.

We believe there may be several potential problems with the way the washout coefficients are measured and interpreted. For example, air samples are taken at ground level while rain forms aloft. Do air and rain samples collected in the normal fashion actually represent the same air mass? Are local-source interferences and nonequilibrium processes possible? Finally, is it safe to assume that a pesticide forms an ideal solution in rain? If it does not, then it is incorrect to apply Henry's law to the distribution. These potential problems argue for a more direct approach to experimentally verifying whether the distribution of pesticides with atmospheric moisture conforms with Henry's law coefficients based on vapor pressure and solubility data.

Glotfelty et al. reported on the occurrence and distribution of pesticides in fog (*7*). They found a variety of pesticides present in fog that was sampled in the Central Valley of California, and in the vicinity of Beltsville, MD. The measured concentrations in fogwater were found to be 2 orders of magnitude or more higher than is commonly found in rain. The measured air/water distribution coefficients indicated an apparent increased solubility of the pesticides in fogwater, compared to the theoretical air/water distribution derived from Henry's law based on vapor pressure and solubility. The pesticide content of the fog droplets was as much as several thousand fold higher than expected from the measured interstitial vapor-phase concentration.

The present study was undertaken to obtain in-depth information about the distribution of pesticides in a foggy atmosphere. It was conducted at one of the Central Valley sampling sites from the earlier study and focused on four of the most prominent pesticides identified in that study: diazinon, parathion, chloropyrifos, and methidathion. Their structures are given in Figure 1. In the environment, each of the parent insecticides can undergo a thion-to-oxon conversion

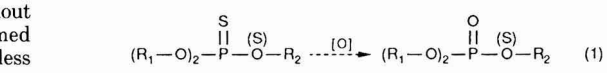

$$(R_1\text{—}O)_2\text{—}P\text{—}O\text{—}R_2 \xrightarrow{[O]} (R_1\text{—}O)_2\text{—}P\text{—}O\text{—}R_2 \quad (1)$$

[The (S) in (1) represents methidathion, which is a phosphorodithioate.] We examined the behavior of both the parent pesticides and their oxon transformation products. The two groups of chemicals provide good examples for study because their thion–oxon pairs are structurally similar, yet the oxons exhibit much greater water solubility, and, thus, lower Henry's law constants (Table I). (We were unable to locate reliable vapor pressure, solubility, and Henry's law constant data for diazoxon, chloropyrifos oxon, and methidathion oxon.)

Experimental Section

Fog and Air Sampling. The experiment was performed at the Kearney Agricultural Research Center (KAC) of the University of California, located near Parlier, CA. One sample (1.11.86) was taken of low stratus clouds along Hills Valley Road, in the foothills of the Sierra Nevada Mountains, ~50 km east of Parlier, and at an approximate elevation of 500 m. The area of the Central

† U.S. Department of Agriculture.
‡ University of California.

0013-936X/90/0924-0353$02.50/0

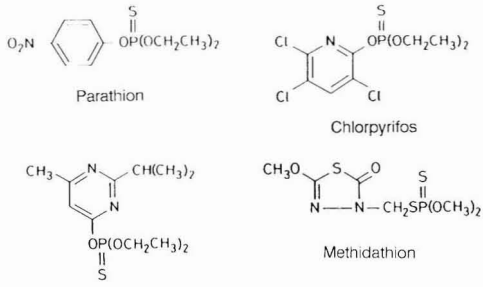

Figure 1. Structures of the insecticides included in the study.

Table I. Vapor Pressures, Water Solubilities, and Dimensionless Henry's Law Constants for the Pesticides in the Study[h]

compound	water sol, mg/L	vapor pressure mPa	Henry's law constant ($\times 10^{-6}$)
diazinon	38[a]	8[a]	4.6[b]
parathion	15[a]	0.6[a]	3.5[c]
chlorpyrifos	0.3[a]	1.5[a]	170[c]
methidathion	240[d]	0.13[d]	0.07[e]
paraoxon	3640[f]	8.8[g]	0.25[e]

[a] Reference 13. [b] Reference 14. [c] Reference 15. [d] Reference 16. [e] Calculated from the ratio of vapor pressure to water solubility. [f] Reference 17. [g] Reference 18. [h] We were unable to find vapor pressure, solubility, and Henry's law constant data for diazoxon, chlorpyrifos oxon, and methidathion oxon.

Valley surrounding KAC is dominated by fruit, nut (primarily almonds), and citrus orchards. Winter dormant sprays containing the four subject organophosphorus insecticides are applied to the deciduous orchards mainly in January, which coincides with the rather frequent occurrence of dense, radiation-type fogs (Tule fog) in the valley. The study was conducted in mid-January 1986. The times and dates of sample collection are given in Table II.

Fogwater was collected with a high-volume fog sampler described in detail elsewhere (*8*). It is a rotating screen device, 50-cm diameter, in which four layers of stainless-steel screen are rotated around a central axis at 720 rpm. Fogwater obtained from droplets impacting on the screen is centrifuged to the periphery, collected in a slotted aluminum tube, and drained into a collection vessel. A large fan pulls air through the device at a sampling rate of ~160 m^3/min. This sampling rate typically allows 1 L of fogwater to be collected in 1–2 h, depending on the liquid water content of the fog. The sampler was dismantled and thoroughly cleaned by water wash and acetone rinse before the start of the experiment.

Air was sampled by means of a high-volume dichotomous sampler that is described in detail elsewhere (*8*). This sampler provided a sample of the interstitial vapor- and particle-phase pesticides by eliminating fog droplets of >8 μm through the large particle orifice of the device. Fog droplets of <8 μm, unactivated (dry) aerosol particles, and vapor passed first through a precombusted (400 °C overnight) glass-fiber filter (GFF), which removed particulate material and then through a 7.5 cm diameter × 7.5 cm deep bed of porous polyurethane foam (PUF), which trapped the pesticide vapors. The PUF plugs were cleaned by an established method (*9*).

Sample Extraction and Fractionation. Fogwater samples were filtered as soon as possible after collection (usually no more than 1 h) by using a Buchner funnel and a double layer of clean glass-fiber filter (Whatman 934-AH), fortified with 20 g/L Na_2SO_4 (cleaned by overnight baking at 400 °C) and then extracted three times with dichloromethane (DCM) in accord with an established multiresidue procedure (*10*). The volume of DCM used for each extraction was one-tenth that of the water sample. The DCM extracts were concentrated to a small volume with a Kuderna-Danish (KD) evaporative concentrator equipped with a three-ball Snyder column. In the final stages of solvent evaporation, the DCM was exchanged for benzene.

Table II. Temperatures, Liquid Water Contents, Total Organic Carbon Contents, and pH of Fog Samples Collected near Parlier, CA, January 1986

date	time	T, °C	liq water content, g/m^3	total organic C, mg/L	pH
1/8–9	2220–0355	ND[a]	0.069	44	7.0
1/9	1710–2310	8.0–8.5	0.052	42	5.5
1/10	2334–0534	7.0–8.5	0.080	43	5.4
1/11[b]	0958–1330	5.5–7.5	0.034	38	5.5
1/12	0015–0910	5.0	0.024	55	6.0
1/12–13	2106–0300	1.5–3.0	0.060	41	5.8

[a] ND, no data. [b] Hills Valley Road site.

The GFF containing the particles filtered from the fogwater were extracted with DCM for 12 h (12 cycles/h) in a Soxhlet apparatus under subdued light. The DCM extract was then concentrated to a small volume and exchanged for benzene.

The PUF plugs and dichotomous air sampler GFF were extracted with 1:1 hexane/acetone (HA) for 6 h in a Soxhlet apparatus. The HA extracts were then also concentrated to a small volume and exchanged for benzene.

The concentrated extracts from all the sample media were fractionated by silica gel HPLC using a hexane to methyl *tert*-butyl ether gradient following a procedure reported in detail elsewhere (*11*). Four fractions of increasing polarity were obtained: fraction 1 contained chlorpyrifos; fraction 2 contained parathion, diazinon, and methidathion; fraction 3 contained chlorpyrifos oxon and ~30% of the methidathion oxon; fraction 4 contained the remaining methidathion oxon, plus paraoxon and diazoxon. Each fraction was concentrated to a small volume and exchanged for benzene in a KD concentrator receiver tube equipped with a three-ball micro-Synder column.

Gas Chromatographic Analysis. The pesticides and their oxons were analyzed with an Hewlett-Packard 5890A gas chromatograph equipped with an HP 19256A flame photometric detector operated in the P mode. A 30 m × 0.322 mm i.d. DB 1^+ (0.25-μm film thickness) fused-silica capillary column was used (J&W Scientific). The column temperature was programmed from 120 to 210 °C at 15 °C/min, with no initial delay. The detector and inlet temperatures were 220 and 250 °C, respectively. The injector split ratio was 7.0:1. The carrier gas was ultra-high purity H_2 (Air Products and Chemicals, Inc.). At 160 kPa inlet pressure the linear gas velocity was 105 cm/s (7.3 mL/min). The detector gas flow rates (mL/min) were as follows: H_2, 81; air, 70; and N_2, 28. Peaks were integrated by an HP 3393A integrator.

Chlorpyrifos and parathion are difficult to separate on the DB 1^+ column. In order to verify the separation of these two compounds by the HPLC fractionation method, the gas chromatograph was operated closer to optimum conditions for increased resolution. The inlet pressure was lowered to 82 kPa, resulting in a linear gas velocity of 55 cm/s (3.8 mL/min), and the column temperature was

Table III. Concentrations (μg/L) of Selected Organophosphorus Insecticides and Their Oxon Transformation Products in Fog Samples Collected near Parlier, CA, January 1986

compound	dates					
	1/8–9	1/9	1/10	1/11[a]	1/12	1/12–13
diazinon	2.4	7.5	7.1	0.31	13	18
parathion	3.6	31	30	2.7	39	23
chlorpyrifos	0.39	4.6	5.5	1.2	3.9	7.7
methidathion	0.12	2.3	0.92	0.093	4.8	1.9
diazoxon	0.79	0.42	2.6	2.2	28	6.8
paraoxon	0.072	6.3	4.2	3.1	34	2.8
chlorpyrifos oxon	0.14	3.2	1.6	<0.06	5.6	1.2
methidathion oxon	0.2	2.3	1.3	0.2	7.3	1.5

[a] Hills Valley Road site.

programmed from 120 to 210 °C at 5 °C/min following a 1-min initial hold. Under these conditions, nearly base-line resolution was obtained, and we were able to verify that the HPLC separation of chlorpyrifos and parathion was complete.

Results and Discussion

Table III shows the concentrations of the compounds that were dissolved in the fog for the six events sampled. ("Dissolved" is an operational term for the material in the fogwater that passed through the double layer of glass-fiber filter.) Parathion was greater than 20 μg/L in four of the events and was as high as nearly 40 μg/L on 1.12.86. Oxons of all four compounds were found in nearly all the fog events. Paraoxon concentration was greater than 34 μg/L on 1.12.86, and in general it was the most prominent oxon.

Pesticide concentrations were lowest in the low stratus cloud sample obtained on Hills Valley Road on 1.11.86. This is reasonable because this location was some distance from any treated areas. Even though the concentrations were lower in this sample, the pesticide content was not that much different from the samples taken at KAC. This suggests that the pesticides in the study were well mixed throughout the atmosphere in the Central Valley.

When concentrations in the water phase are compared to the concentrations in the interstitial vapor phase, the resulting air/water distribution coefficient indicates substantial aqueous-phase enrichment for several of the pesticides. We define the enrichment factor to be K_{AW}/D, where K_{AW} is the Henry's law constant, and D is the measured air/water distribution coefficient. Aqueous-phase enrichments of pesticides in fog of up to several thousand fold were previously reported (*7*). In the earlier study, the enrichments appeared to be a function of K_{AW}, but may have arisen from surface-active or solubility-enhancing components in the fog.

Enrichment factors for the five events in the present study for which both air and water data are available are shown in Table IV. The enrichments are variable, with the smallest enrichments occuring in the 1.8–9.86 sample, and the largest occurring in the 1.12–13.86 sample. Diazinon enrichment varied from 6 to 160 in these two samples. Only methidation failed to show a consistent aqueous-phase enrichment. In fact, in two of the samples, 1.8–9.86 and 1.11.86, there was an apparent deficit of methidation in the aqueous phase.

It is not immediately obvious why the enrichment factors should be different for the various fog events. Only small enrichment factors were found for the 1.8–9.86 and 1.11.86 samples. The 1.9.86 and 1.12.86 samples showed intermediate enrichments, and enrichments in the 1.12–13.86 sample were high. This ordering of the fog

Table IV. Aqueous-Phase Enrichment Factors (K_{AW}/D) for the Distribution of Pesticides between Fogwater and Air

compound	date					mean
	1/8–9	1/9	1/11[a]	1/12	1/12–13	
diazinon	6	59	14	50	160	58
parathion	4	12	5	18	29	14
chlorpyrifos	7	55	35	40	74	42
methidathion	0.06	3	0.02	1.4	2.3	1.4
paraoxon	2.1	15	10	48	>69	>19

[a] Hills Valley Road site.

events was the same for each pesticide and transformation product, except for methidathion. It can be seen by comparing Table II to Table IV that this order does not correspond to either liquid water content or total organic carbon content of the fog. It is interesting to note that the ordering of the fog events for methidathion would be similar to the other pesticides if the calculated value of K_{AW} were for some reason ~2 orders of magnitude too low. Since K_{AW} for methidathion was not measured directly but was calculated from vapor pressure and solubility (Table I), an error in the reported values of either of these properties would cause an error in K_{AW}.

Temperature effects may explain part of the discrepancy between K_{AW} and the measured air/water distribution in fog. The latent heat of solution is less than the latent heat of vaporization, which implies that vapor pressure will increase more rapidly than solubility with temperature. Consequently, K_{AW} should increase with increasing temperature. Unfortunately, heats of solution and vaporization of pesticides are not generally available. For many organic compounds, K_{AW} is reported to increase a factor of 2 for each 10 °C rise in temperature (*5*). Since most of the values for K_{AW} in Table I were determined near 25 °C, while the fog samples were collected in the temperature range of 1.5–8.5 °C (Table II), the discrepancy between K_{AW} and D may be a factor of 2- to 4-fold smaller than reported in Table IV. More research on the effects of temperature on K_{AW} for pesticides is needed.

Thus we see that, in agreement with the earlier study, the pesticides are present in the fog droplets, frequently in high (μg/L) concentrations, and that substantial aqueous-phase enrichments occur for several of the pesticides and their oxons. During most of the fog events in the present study, plant leaves became saturated to the point of dripping with captured fog moisture. In fact, it is generally the case that most of the moisture in fog will migrate to the ground surface during the event, particularly if the wind is blowing (*12*). On 1.12.86 this moisture contained ~40 μg/L parathion as well as substantial concentrations of a number of other compounds. Therefore, some contamination of vegetation and other surfaces with fogborne pesticides could occur.

Distribution in a Foggy Atmosphere. When fog forms, pesticides in the atmosphere will redistribute to accommodate the liquid phase. This redistribution will involve at least four phases: vapor, particles in the air, water, and particles suspended in the water. (Other phases may, in fact, be present, such as surface films or colloids associated with the droplet.) Figure 2 shows this distribution for parathion in the foggy atmosphere on 1.12.86. The total concentration of parathion in the atmosphere was 9.4 ng/m^3. (The concentration represented by the liquid droplets was calculated from the liquid water content of the fog, 0.024 g/m^3, and the parathion concentration in the fog liquid.) Of the 9.4 ng/m^3, 78% (7.3 ng/m^3) was in the vapor phase. Only 10% (0.9 ng/m^3) was dis-

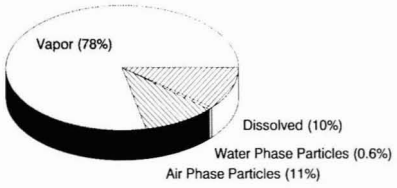

Figure 2. Distribution of parathion in the foggy atmosphere near Parlier, CA, on January 12, 1986.

Table V. Distribution of Pesticides in the Foggy Atmosphere at Parlier, CA, January 12, 1986

compound	total concn, ng/m³	percent of total			
		air phase		water phase	
		vapor	part.	dissol	part.
diazinon	1.6	76.1	3.7	19.8	0.4
parathion	9.4	78.5	10.9	9.9	0.6
chlorpyrifos	17.4	94.3	4.6	0.5	0.5
methidathion	0.45	57.5	16.8	25.4	0.3
diazoxon	0.82	13.4	4.9	81.7	0.02
paraoxon	2.3	7.8	56.7	35.5	0.09
methidathion oxon	0.84	<7.1	78.6	20.8	0.1

solved in the fog droplet, even though the concentration in the droplet was 39 μg/L and the enrichment factor was 18. Up to 11% (1.0 ng/m³) appeared to be attached to aerosol particles. Some of the pesticide on the dichotomous air sampler GFF could have arisen from vapor adsorption, or from the capture of small fog droplets not removed in the large particle orifice of the sampler, so that this represents an upper limit figure. Finally, only 0.6% of the parathion was attached to solids filterable from the fogwater.

Table V shows the distribution of six other compounds in the foggy atmosphere on 1.12.86. Chlorpyrifos is almost exclusively in the vapor phase (94%), even though its concentration in the droplets was 3.9 μg/L, and its enrichment factor was 40. Methidathion, paraoxon, diazoxon, and methidathion oxon were present to a greater extent in the water phase, in keeping with their lower vapor pressure and higher water solubilities. Chlorpyrifos oxon distribution could not be determined because measurable amounts were found only in the water phase.

Table VI summarizes the distributions for five compounds in the five events for which air samples were taken. The ranges for the distributions are large. For example, the average proportion of diazinon in the vapor phase was 57%, but this ranged from 25 to 83%. The largest portion of all the pesticides occurred in the air phase, either vapor or "aerosol particle". The contribution from solids suspended in the fog droplets was small (<1.0%) in every case.

Oxons. The presence of oxons in fog is of interest because of their toxicity and the evidence they provide of transformations of the organophosphorus insecticides in the atmosphere. Table VII shows the oxon to thion ratios for the six fog events sampled. The highest oxon to thion ratio (except for chlorpyrifos) occurred at the Hills Valley Road site on 1.11.86. This was a sample of low stratus clouds collected under daylight conditions. The high oxon proportion in this sample may have resulted from sunlight-driven photochemical oxidations. (All of the KAC samples were collected after dark.) On the other hand, the high ratios at the Hills Valley Road site may merely reflect longer residence time and thus more conversion in the atmosphere, because the sampling location was remote from treated areas. The question of the source and rates of formation of these compounds in the atmosphere needs

Table VI. Means and Ranges of the Distribution of Pesticides between Air and Droplet Phases during Five Fog Events Sampled near Parlier, CA, January 1986

compound		percent of total			
		air phase		water phase	
		vapor	part.	dissol	part.
diazinon	mean	56	19	24	0.5
	range	25–83	3–40	6–51	0.03–1
parathion	mean	67	27	10	0.6
	range	34–85	11–48	4–18	0.05–1.4
chloropyrifos	mean	89	12	1	0.8
	range	70–97	4–27	0.3–1.8	0.07–1.6
methidathion	mean	54	23	27	0.6
	range	17–87	6–52	0.8–71	<0.01–2.5
paraoxon	mean	20	51	42	0.2
	range	<3–44	43–57	3–75	0.07–0.3
diazoxon[a]	mean	57		41	<0.3
	range	13–81		19–82	

[a] Only three samples; generally below the limit of detection on both air-phase and water-phase particles.

Table VII. Oxon to Thion Ratios For Several Organophosphorus Insecticides in Fogwater Collected near Parlier, CA, January 1986

date	parent pesticide			
	diazinon	parathion	chlorpyrifos	methidathion
1/8–9	0.33	0.02	0.36	1.7
1/9	0.056	0.2	0.7	1.0
1/10	0.36	0.14	0.29	1.4
1/11[a]	7.1	1.2	<0.05	2.2
1/12	2.2	0.88	1.4	1.5
1/12–13	0.37	0.12	0.16	0.79

[a] Hills Valley Road site.

to be addressed in future research.

Conclusions. The distributions of four organophosphorus insecticides and their oxon transformation products were determined during six fog events near Parlier, CA. All four insecticides and their oxons were found. Parathion was the most abundant compound in the collected fogwater, followed in order by diazinon, chlorpyrifos, and methidathion. The concentrations of diazoxon and paraoxon were about equal in fog, and lesser amounts of the oxons of methidathion and chlorpyrifos were found. The highest concentrations were found in the 1.12.86 event, which had >60 ppb for the sum of the parent insectides and 75 ppb for the sum of their oxons. In this sample, parathion concentration in the fogwater was 39 ppb and paraoxon was 34 ppb.

The oxon to thion ratio in the fogwater was generally <1, except for the low stratus cloud sample collected on Hills Valley Road during the morning of 1.11.86 and for the 1.12–13.86 event at KAC. We believe the source of the oxons to be atmospheric oxidation, especially during daylight hours, followed by uptake into the fog when it forms. Further research on this point is needed.

In agreement with earlier studies, we found that the concentration in the water phase was much greater than would be expected from the vapor-phase concentration and Henry's law. The aqueous-phase enrichment factor (EF) was calculated for five compounds. The order of enrichment, based on averages found for five events, was diazinon > chlorpyrifos > paraoxon = parathion > methidathion. The EF varied between events, being small (EF = 1–10) for two events, intermediate (EF = 10–50) for two events, and large (EF up to 160) for the 1.12–13.86 event. The EF for all five compounds went up and down together from one event to another. The only compound that failed to

show an EF consistently greater than 1 was methidathion. For this compound, K_{AW} was estimated from literature values of vapor pressure and solubility and may have been in error. Temperature effects play an important but poorly known role in the air/water distribution of pesticides and may reduce the measured EF by a factor of 2–4 in the present experiment.

Even though there were high concentrations and high EF for the water phase, the largest proportion of all the compounds in all events was in the interstitial air phase, either vapor or adsorbed to aerosol particles. The distribution between air and droplet phases for each pesticide covered a broad range from one event to the next. The proportion associated with droplet-phase particles was small, averaging <1% for all the compounds.

Information about air/water distribution of pesticides in fog is perhaps not relevant to cloud processes, where liquid water contents may be as much as a factor of 10 greater than was found in the fog events reported here. The data for the low stratus cloud sample obtained on Hills Valley road suggest that the air/water distribution in clouds may not follow Henry's law, but we would not attempt to extrapolate this meager data to a more general case. Studies similar to ours of the air/water distribution in clouds are needed.

Registry No. Diazinon, 333-41-5; parathion, 56-38-2; chlorpyrifos, 2921-88-2; methidathion, 950-37-8; diazoxon, 962-58-3; paraoxon, 311-45-5; chlorpyrifos oxon, 5598-15-2; methidathion oxon, 39856-16-1.

Literature Cited

(1) Taylor, A. W.; Glotfelty, D. E. In *Environmental Chemistry of Herbicides*; Grover, R., Ed.; CRC Press: Boca Raton, FL, 1988; Vol. 1, pp 89–129.
(2) Hales, J. M. *Atmos. Environ.* **1972**, *6*, 635–659.
(3) Bidleman, T. F.; Christensen, E. J. *J. Geophys. Res.* **1979**, *84(C12)*, 7857.
(4) Eisenreich, S. J.; Looney, B. B.; Thornton, J. D. *Environ. Sci. Technol.* **1981**, *15*, 30–38.
(5) Ligocki, M. P.; Leuenberger, C.; Pankow, J. F. *Atmos. Environ.* **1985**, *19*, 1609–1617.
(6) Harder, H. W.; Christensen, E. C.; Matthews, J. R.; Bidleman, T. F. *Estuaries* **1980**, *3*, 142–147.
(7) Glotfelty, D. E.; Seiber, J. N.; Liljedahl, L. A. *Nature* **1987**, *325*, 602–605.
(8) Glotfelty, D. E.; Seiber, J. N.; Liljedahl, L. A. In *Proceedings, 1986 EPA/APCA Symposum on Measurement of Toxic Air Pollutants*; U.S. EPA/Air Pollution Control Association, 1986; pp 168–175.
(9) Bidleman, T. F.; Olney, C. E. *Bull. Environ. Contam. Toxicol.* **1974**, *11*, 442.
(10) Thompson, J. F.; Reid, S. J.; Kantor, E. J. *Arch. Environ. Contam. Toxicol.* **1977**, *6*, 143–157.
(11) Wehner, T. A.; Woodrow, J. E.; Kim, Y.-H.; Seiber, J. N. In *Identification and Analysis of Organic Pollutants in Air*; Keith, L. H., Ed.; Butterworths: Boston, MA, 1984; pp 273–290.
(12) Barrie, L. A.; Schemenauer, R. S. *Water, Air, Soil Pollut.* **1986**, *30*, 91–104.
(13) Suntio, L. R.; Shiu, W. Y.; Makay, D.; Seiber, J. N.; Glotfelty, D. E. *Rev. Environ. Contam. Toxicol.* **1988**, *103*, 1–59.
(14) Fendinger, N. J.; Glotfelty, D. E. *Environ. Sci. Technol.* **1988**, *22*, 1289–1293.
(15) Fendinger, N. J.; Glotfelty, D. E. *Environ. Toxicol. Chem.* **1990**, *9*, 6.
(16) Worthing, C. R. *The Pesticide Manual*, 6th ed.; British Crop Protection Council: Croyden, England, 1979.
(17) Bowman, B. T.; Sans, W. W. *J. Environ. Sci. Health* **1979**, *B14*, 625–634.
(18) Williams, E. F. *Ind. Eng. Chem.* **1951**, *43*, 950.

Received for review June 29, 1989. Accepted October 20, 1989.

Assessment of Fecal Sterols and Ketones as Indicators of Urban Sewage Inputs to Coastal Waters

Joan O. Grimalt,* Pilar Fernández, Josep M. Bayona, and Joan Albaigés

Department of Environmental Chemistry (CID—CSIC), Jordi Girona, 18, 08034-Barcelona, Spain

■ The sterol and sterone compositions of aquatic samples, namely, water particulates and sediments, collected in urban polluted and pristine areas have been investigated for the assessment of steroid components as chemical markers of urban sewage contamination. The results have shown that the occurrence of coprostanol [5β(*H*)-cholestan-3β-ol] cannot by itself be unambiguously attributed to fecal matter inputs. However, these contributions can be positively identified when the relative concentrations of this sterol and the related 5β(*H*)-cholestan-3-one (coprostanone) are higher than their corresponding 5α epimers. In this respect, coprostanone provides a useful complementary parameter for urban sewage monitoring, especially in cases of moderate to low pollution.

Introduction

5β(*H*)-cholestan-3β-ol (coprostanol) (IV) (Figure 1) has been used as an indicator of sewage pollution in coastal areas (*1–11*). This is based on the occurrence of coprostanol in human feces resulting from the biohydrogenation of cholesterol (I) by the intestinal microflora (*12–15*). The transformation mechanism involves the intermediary formation of cholest-4-en-3-one (II) and 5β(*H*)-cholestan-3-one (III) (*12–14*).

The use of this compound for sewage monitoring, including the effects of sewage treatment on sterol composition, has been reviewed by Walker et al. (*16*) and Vivian (*17*). The limits of detection and quantitation for this sterol in bulk water samples have recently been evaluated by Eganhouse et al. (*11*). However, more information about environmental stability and, particularly, source specificity is needed for its general acceptance as a sewage indicator.

In this respect, the rapid decay of coprostanol in aerobic water systems is known (*16*). In anoxic sediments, long-term stability has been assumed on the basis of the fate of 5α(*H*)-cholestan-3β-ol (*4*) and results from experiments using artificial sediments (*18*).

On the other hand, diagenetic degradation of sterols in anoxic environments gives rise to 5α(*H*) and 5β(*H*) stanols (*19–23*), the latter being potential markers of oxic–anoxic

0013-936X/90/0924-0357$02.50/0

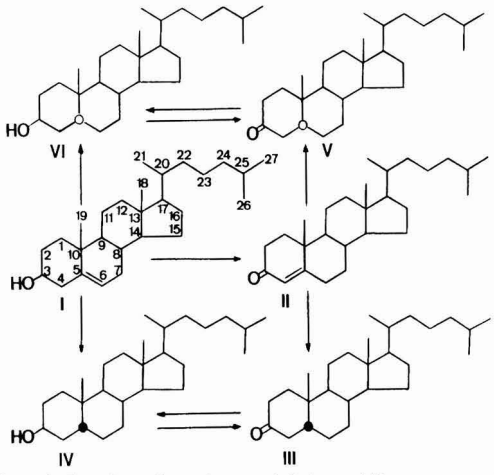

Figure 1. Transformation pathways of cholesterol (I) to coprostanol (IV) and cholestanol (VI).

environmental depositional conditions (*24*). Radiolabeled incubations have also demonstrated the interconversion of stanols and stanones in anoxic sediments (*25*). The significance of these transformations for the use of coprostanol for sewage monitoring is still to be addressed. Moreover, the results of an annual study in Bedford Basin showed that the temporal variation of coprostanol in water particulates was identical with that of the rest of natural phytosterols (*26*), thus questioning the specificity of this sterol as an urban sewage indicator.

All these aspects compel a reassessment of coprostanol as a sewage marker and the investigation of the usefulness of other steroids present in aquatic samples for the recognition of sewage contamination. Since both 5β(*H*) stanols and stanones are generated in the intestinal (*12–14*) and sedimentary (*19–23*) processes of sterol reduction, and both steroid functionalities are found in sewage (*6*) and urban polluted waters (*27*), these two types of components, including their 5α(*H*) and 5β(*H*) isomers, must be considered. Accordingly, we have selected a group of contemporary samples representing well-defined situations in terms of sewage pollution or anoxic depositional environments for the analysis of the stanone and sterol composition.

Experimental Section

Sampling. A detailed description of the water sampling system is given elsewhere (*28*). In summary, it encompasses a priming circuit, a noncontaminating Teflon impeller pump (Jupiter, Fluorocarbon Corp.), and a 142 mm diameter stainless steel filter holder. Flow rates and water volumes were monitored with a turbine flowmeter and a totalizer. All connection tubing was made of $^3/_4$-in. Teflon pipe and was externally protected with stainless steel coil. Water particulate samples were collected on a kiln-fired (350 °C) glass fiber filter (rated pore size 0.5 μm). Collection of particles larger than 1 mm was prevented by placing a stainless steel grid at the inlet of the pumping tube.

Prior to sampling, 50 L of distilled water was pumped through the plumbing system and the tubing was additionally rinsed with organic solvents. Volumes between 10 and 100 L were collected for each sample at a flow rate of ~500 mL/min. Filters were changed whenever rates dropped below 50% of normal. Filters were wrapped in solvent-rinsed aluminum foil, sealed in Teflon bags, and frozen immediately after filtration until analysis.

Surface sediments were taken by gravity coring and kept at −20 °C for storage. Before analysis the upper 3 cm was cut, freeze-dried, and sieved through 250-μm sieves.

Steroid Isolation and Fractionation. Filters were torn into 1-cm^2 pieces with stainless steel tweezers before extraction. These as well as the homogenized sediments (~30 g) were extracted with 150 mL of (2:1) methylene chloride–methanol for 36 h in a Soxhlet apparatus. The extract was vacuum evaporated to 2 mL, hydrolyzed overnight with 35 mL of 6% KOH–MeOH, and further extracted with *n*-hexane (3 × 30 mL) to recover the neutral fraction. These neutrals were fractionated by column chromatography according to previously established methods (*29*). A column filled with 8 g each of 5% water-deactivated alumina (70–230 mesh, Merck) (top) and silica (70–230 mesh, Merck) (bottom) was used. The following fractions were collected: (I) 20 mL of *n*-hexane, (II) 20 mL of 10% methylene chloride in *n*-hexane, (III) 40 mL of 20% methylene chloride in *n*-hexane, (IV) 40 mL of 25% *n*-hexane in methylene chloride, (V) 20 mL of 5% methanol in methylene chloride (stanone fraction), and (VI) 40 mL of 10% methanol in methylene chloride (sterol fraction). This latter fraction was derivatized prior to instrumental analysis with bis(trimethylsilyl)trifluoroacetamide.

Instrumental Analysis. Gas chromatography (GC) was performed with a Carlo Erba FTV 4160 GC instrument, equipped with a flame ionization detector and a splitless injector. A column of 25 m × 0.25 mm i.d. coated with SE-54 was used (film thickness 0.15 μm). Hydrogen was the carrier gas (50 cm/s). The temperature was programmed from 60 to 300 °C at 6 °C/min. Injector and detector temperatures were, respectively, 300 and 330 °C. The injection was in the splitless mode (solvent, isooctane; hot needle technique) keeping the split valve closed for 35 s.

Selected fractions were analyzed by gas chromatography–mass spectrometry using a Hewlett-Packard 5995 instrument coupled to an HP 300 data system. The chromatographic conditions were the same as described above except that helium was used as carrier gas. Data were acquired in a scanning range of m/z 50–550 at 1 s/decade. Mass spectrometry temperatures were as follows: transfer line, 300 °C; ion source, 200 °C; analyzer, 230 °C.

Quantitation. Stanones were quantified by comparison with an external standard of synthesized 5α(*H*)- and 5β(*H*)-cholestan-3-one. Sterols were quantitatively determined with reference to an external standard containing coprostanol, 5α(*H*)-cholestan-3β-ol, and 24-ethylcholest-5-en-3β-ol (Aldrich-Chemie, F.R.G.). Samples and standards were repeatedly injected until less than 5% dispersion was observed in the measured areas.

Results and Discussion

The aquatic samples considered in this study are listed in Table I. They consist of particulates collected from a sewage outfall (W1), in coastal areas receiving urban inputs (W2–6), and in uncontaminated waters overlying anoxic sediments (W7–9). Sediment samples from both contaminated (S1–9) and pristine environments (S10–12) have also been included. Samples S1–7 were collected at a progressive distance from the effluent dumping site where water particulates W1 were obtained. A representative series of model cases results from these examples. It must be indicated, however, that among uncontaminated areas only those containing significant coprostanol levels have been considered.

Table I. Description of the Samples Considered in This Study

code	description	location	sewage load	TOC, %
water particulates				
W1	effluent from an urban sewage treatment plant	Barcelona (NE Spain)	sewage sample	
W2	~2 km offshore marine water	Barcelona	high	
W3–6	river water[a]	Ebre River (NE Spain)	variable	
W7–9	estuarine waters[a] overlying anoxic sediments	Alfacs Bay Ebre Delta	absent	
sediments				
S1–7	sediments around a sewage dumping site[b]	Barcelona	high	0.5–8
S8–9	sediments from a heavily polluted bay	Havana Bay (Cuba)	high	3–5
S10–11	anoxic marsh sediments	Guadalquivir Delta (SW Spain)	remote area	3.5–9
S12	coastal evaporite system	Santa Pola (SE Spain)	remote area	3–3.5

[a] Collected between August 1986 and May 1987. [b] Ordered according to distance from the point of discharge, 0–3 km.

Table II. Steroid Concentrations ($\mu g/L$)[b] for Diverse Water Particulates (Sample Description in Table I)

	steroid	samples								
		W1	W2	W3	W4	W5	W6	W7	W8	W9
1	5β-cholestan-3β-ol	630	0.29	0.50	0.35	0.26	0.14	0.014	0.012	0.006
2	5β-cholestan-3α-ol	5	0.005	0.03	0.02	0.02	0.02	nd	nd	nd
3	cholest-5-en-3β-ol	300	0.21	0.99	0.50	0.56	0.16	0.094	0.25	0.070
4	5α-cholestan-3β-ol	10	0.04	0.24	0.10	0.09	0.05	0.030	0.055	0.034
5	24-ethyl-5β-cholestan-3β-ol	100	0.10	0.24[a]	0.17[a]	0.16[a]	0.05[a]	nd	nd	nd
6	24-ethylcholest-5-en-3β-ol	50	0.054	0.78	0.77	0.34	0.19	0.10	0.16	0.013
7	24-ethyl-5α-cholestan-3β-ol	20	0.017	0.08	0.10	0.04	0.02	0.14	0.097	0.043
8	5β-cholestan-3-one	280	0.21	0.35	0.32	0.20	0.12	0.090	0.012	0.050
9	5α-cholestan-3-one	nd	0.016	0.040	0.081	0.040	0.035	0.27	0.042	0.140
10	24-ethyl-5β-cholestan-3-one	40	0.060	0.23	0.10	0.12	0.050	nd	nd	nd
11	24-ethyl-5α-cholestan-3-one	nd	0.005	0.029	0.017	0.01	nd	0.81	0.009	0.28

[a] Semiquantitative value. [b] nd, not detected.

Table III. Steroid Concentrations ($\mu g/g$)[b] for Diverse Sediments (Sample Description in Table I)

	steroid	samples											
		S1	S2	S3	S4	S5	S6	S7	S8	S9	S10	S11	S12
1	5β-cholestan-3β-ol	390	45	34	24	15	1.3	1.0	1.1	0.41	2.0	3.5	1.0
2	5β-cholestan-3α-ol	5	2	1.5	1	0.5	0.1	0.08	0.1	0.04	0.6	1.0	0.05
3	cholest-5-en-3β-ol	80	10	9	20	12	1.0	0.5	3.2	1.0	11	15	25
4	5α-cholestan-3β-ol	16	7	4	3	3	0.4	0.25	0.68	0.55	12	17	17
5	24-ethyl-5β-cholestan-3β-ol	70	15	12	7	8	0.8	0.6	0.35	0.35	1.9[a]	3.2[a]	0.8[a]
6	24-ethylcholest-5-en-3β-ol	30	5	3	2.5	1.5	1.0	0.15	2.1	1.3	10	22	19
7	24-ethyl-5α-cholestan-3β-ol	4	3	1.3	0.8	5	0.3	0.35	0.36	0.69	11	25	6.4
8	5β-cholestan-3-one	120	17	14	6.6	6.0	0.8	0.7	0.84	1.3	nd	nd	3.0
9	5α-cholestan-3-one	5	0.8	2	0.7	0.4	0.2	0.12	0.06	0.1	nd	nd	20
10	24-ethyl-5β-cholestan-3-one	17	4	3	3	2	0.3	0.14	1.2	1.9	nd	nd	0.5
11	24-ethyl-5α-cholestan-3-one	nd	0.8	nd	nd	0.4	nd	0.04	nd	nd	nd	nd	5.1
	distance to dumping site, km	0.05	0.7	1.0	1.8	2.0	2.5	3.0					

[a] Semiquantitative value. [b] nd, not detected.

Representative chromatograms of the sterol and sterone fractions are displayed in Figure 2. Tables II and III report the corresponding concentrations. Only the steroids involved in the above described reduction processes of C_{27} or C_{29} Δ^5 sterols have been included.

Sterols. The coprostanol contents in the sewage sample (W1) and the associated sediment (S1), as well as in the polluted waters (W2–6) and sediments (S2–9), are comparable to those reported in the literature for areas affected by urban sewage discharges (*2*, *6*, *7*, *27*). The coprostanol distribution of samples S1–7 is consistent with their progressive distance from the sewage source.

Coprostanol concentration differences of 1 order of magnitude are observed between particulates corresponding to polluted (W2–6) and unpolluted (W7–9) waters. However, coprostanol is present in all cases. Furthermore, the concentrations in the former group are of the same order of magnitude as those found in Bedford Basin, where a direct relation of coprostanol and sewage contamination was questioned (*26*). On the other hand, a clear differentiation between sewage-polluted and pristine sediments cannot be established from their coprostanol contents. Samples S6–9 (urban influence) and S10–12 (pristine) contain about the same levels of coprostanol (~0.41–3.5 $\mu g/g$). In this respect, concentrations as low as 0.1 $\mu g/g$ have still been attributed to sewage pollution (*8*, *9*). All these aspects illustrate the need for a "qualitative criterion" indicating whether or not a determined level of coprostanol in coastal areas may be representative of fecal pollution.

As shown in Figure 2 and Tables II and III the amounts of epicoprostanol [5β(*H*)-cholestan-3α-ol] were in all cases very low with respect to the concentration of the 3β isomer. This sterol is particularly abundant in urban waste waters treated in sludge digestors (*6*). 24-Ethyl-5β-cholestan-3β-ol was difficult to quantify because of coelution with other sterols. GC–MS examination of samples W7–9 showed no detectable amounts of this sterol (<1 ng/L).

Although coprostanol is present in all samples, strong contrasts are observed in terms of the 5β and 5α stanol

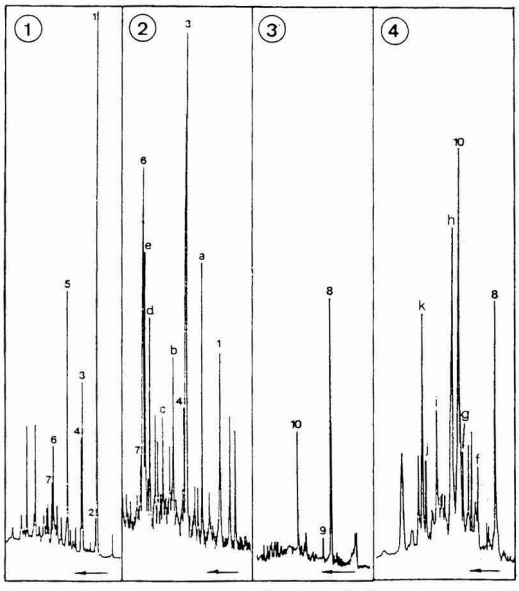

Figure 2. Gas chromatograms of the sterol (1, 2) and sterone (3, 4) fractions of samples S2 (1, 3) and S8 (2, 4). Identification of numbered peaks as in Tables II and III. Lettered peaks as follows: (a) cholesta-5,22(*E*)-dien-3β-ol; (b) 24-methylcholesta-5,22(*E*)-dien-3β-ol; (c) 24-methylcholest-5-en-3β-ol; (d) 24-ethylcholest-5,22(*E*)-dien-3β-ol; (e) C_{29} 4-methylstanol; (f) 22,29,30-trisnorhopan-21-one; (g) taraxer-14-en-3-one; (h) olean-12-en-3-one; (i) urs-12-en-3-one; (j) friedelan-3-one; (k) hopanone.

isomer ratios (see Figure 2 and Table II). In one group of particulate samples (W1–6, coprostanol concentration of >0.1 μg/L) the 5β isomer predominates [5β/(5β + 5α) ratio ranging between 0.96 and 0.68], whereas in the other (W7–9, coprostanol concentration of <0.2 μg/L) the 5α-(*H*)-cholestan-3β-ol is predominant [5β/(5β + 5α) ratio ranging between 0.32 and 0.15]. The ratios in sediment samples S1–7 (0.96–0.76) also show a clear predominance of the 5β isomer which, as observed for the water particulates, corresponds to a situation of urban sewage pollution (see Figure 3). Indeed, the composition of the sewage particulates and sediment S-1 is characterized by the higher predominance of 5β isomers. Finally, sediments S10–12 (remote areas) display the lowest ratios of the whole series (0.05–0.17), thus enabling their classification as nonpolluted samples.

As it is known, the 5α stanols are thermodynamically more stable than their 5β epimers (*30*). Accordingly, the sedimentary reduction processes of Δ^5 sterols give rise to stanol mixtures in which the 5α isomers predominate (*19, 21–24, 31*) (see Figure 4). These processes are influenced by microbial communities, especially in recent environments. In this respect, experiments in which microbial assemblages, obtained by enrichment from marine sediments, were allowed to grow in anaerobic media containing radiolabeled cholesterol as the sole source of carbon and energy have provided nearly equal concentrations of 5α- and 5β(*H*)-cholestan-3β-ol (*20*). In contrast, 5β stanols have been observed to be preferentially produced in incubation experiments where radiolabeled cholesterol was introduced in a sewage sludge (*19*).

All these aspects indicate that not only the occurrence of coprostanol but the 5β/(5β + 5α) ratio is needed for the elucidation of either urban sewage contributions or natural reduction processes of Δ^5 sterols in the sedimentary environment. As illustrated in Figures 3 and 4, lower 5β/(5β + 5α) ratios correspond to lower coprostanol content. Sample grouping between urban polluted and uncontaminated samples is therefore observed from both parameters. This is especially significant for the sediment samples considered in this study because no clear coprostanol threshold is found between polluted and nonpolluted samples. The differentiation between these two kinds of samples is obtained from the 5β/(5β + 5α) ratio. As indicated above, values between 0.7 and 1 are characteristic of urban polluted samples whereas ratios in the order of 0.1–0.3 correspond to sediments collected in remote areas. The specific depositional conditions corresponding to the samples showing intermediate ratios (0.6–0.4; S8–9) will be discussed below.

The above discussed significance of the 5β/(5β + 5α) ratio can be essentially supported for the 5β and 5α isomers of both cholestan-3β-ol and 24-ethylcholestan-3β-ol. In this sense, the contrast observed between samples W1–6 and W7–9 is reinforced when the 5β/(5β + 5α) ratio is calculated for the C_{29} homologues, because in the second case no 5β(*H*)-24-ethylcholestan-3β-ol was found (see Table II). However, the quantitation of the 24-ethylstanols, especially the 5β(*H*) isomer, is more difficult than that of the C_{27} homologues due to problems of peak resolution.

However, besides these problems of chromatographic overlapping, other interfering processes may restrict the range of application of these criteria. Diverse aerobic organisms, including some phytoplankton, zooplankton, and macrophyte species, biosynthesize 5α(*H*)-cholestan-3β-ol (*31–35*). Their presence in the waters may therefore

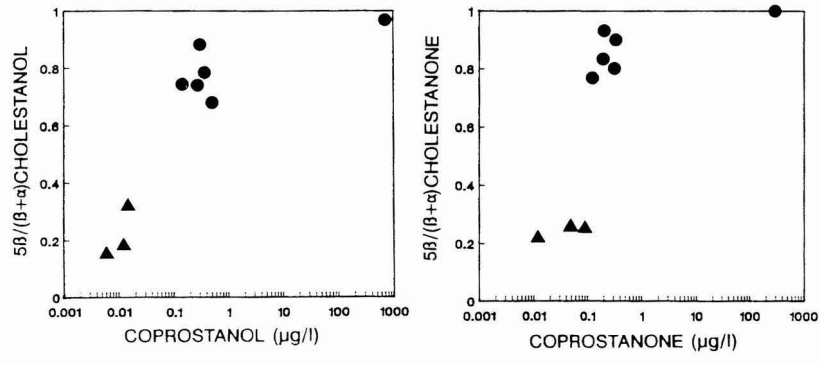

Figure 3. Cross-representation of the coprostanol and coprostanone concentrations and their corresponding C_5 epimeric ratios for the water particulate samples (● and ▲ samples collected, respectively, at urban polluted and remote areas).

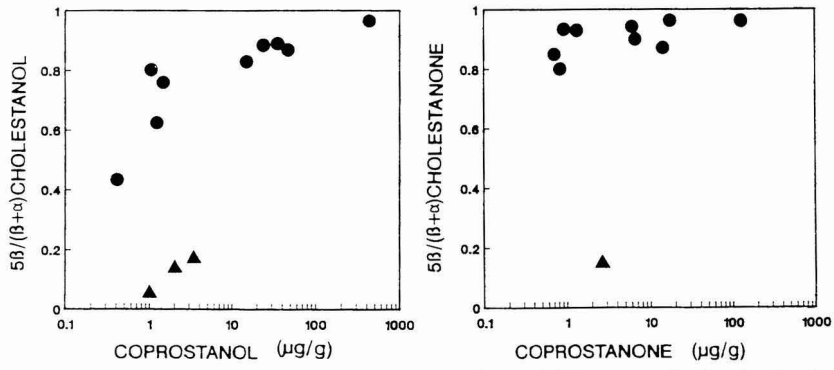

Figure 4. Cross-representation of the coprostanol and coprostanone concentrations and their corresponding C_5 epimeric ratios for the sediment samples (symbols as in Figure 3).

modify the $5\beta/(5\beta + 5\alpha)$ stanol ratio, especially in cases of high productivity.

In this respect, the intermediate $5\beta/(5\beta + 5\alpha)$ cholestan-3β-ol ratios of S8–9 samples merit a particular consideration. In fact, they represent an interesting example of the recognition of sewage pollution in an area of high algal productivity. A detailed description of this enclosed system is given elsewhere (*36*). In short, among other wastes, Havana Bay receives $\sim 2 \times 10^5$ m^3/day of untreated urban waters, which results in a constant high level of fecal pollution (total coliforms, $\sim 6.5 \times 10^4$/100 mL; fecal coliforms, $\sim 5 \times 10^4$/100 mL). In association with the anthropogenic discharges, an important flow of nutrients is also introduced. This gives rise to high algal growth (average chlorophyll *a* concentration, 45 mg/m^3) and to the enhancement of diverse microbial degradation processes occurring in both the water column and sediments (*36*).

Accordingly, the sedimentary sterol composition (see Figure 2) is dominated by algal contributions, namely, diatoms and dinoflagellates. The important proportion of a C_{24} 4-methylsterol (predominant in sample S9) likely reflects the extensive growth of a dinoflagellate *Gymnodinium spendens*, which is responsible for the "red tides" currently observed in some areas of the bay. The occurrence of cholesta-5,22(*E*)-dien-3β-ol, 24-methylcholest-5-en-3β-ol, and 24-methylcholest-5,22(*E*)-dien-3β-ol is related to algal and zooplankton contributions (e.g., *Oitona nana* and *Oikopleura dioica*).

The "sewage sterol pattern", including coprostanol and 24-ethyl-5β(*H*)-cholestan-3β-ol, is also well represented. However, the dominance of phytosterols precludes the use of the $5\beta/(5\beta + 5\alpha)$ sterol ratios for confirmation because an important proportion of 5α(H) stanols is likely contributed from algal species (*21*, *31*, *33*). This situation can be clarified if the ketone fraction is considered.

Sterones. The presence of coprostanone in urban sewage has already been reported (*6*), although to the best of our knowledge, it has not been considered in detail for sewage monitoring (*27*). The sterone composition of water particulates and sediments polluted with fecal matter is essentially constituted of C_{27} and C_{29} 5β(*H*)-cholestan-3-ones (see Figure 2). In fact, similar distribution trends for coprostanol and coprostanone are observed in the set of samples considered here, so that larger concentrations of these sterones apparently correspond to a higher degree of sewage pollution, although some differences can be recognized.

When the C_{27} 5β(*H*) sterone/sterol ratio is considered (Tables II and III), a significant decrease with increased pollution is evidenced. This is clearly observed in samples W1–2 and S1–7, although the composition of samples W3–6 and S6–7 suggests that an equilibrium between these two components is reached after an initial decay. In fact, the rapid decay of coprostanol under the influence of aerobic bacteria is well documented (*16*, *18*). On the other hand, radiolabeling experiments have demonstrated that interconversion between stanols and stanones may also occur (*25*) (see Figure 4). In any case, the present data illustrate the significance of coprostanone for a comprehensive characterization of urban sewage inputs in coastal waters.

However, coprostanone is also present in uncontaminated waters (*37*) and sediments (*21–23*) (see samples W7–9 and S12), thus raising the question whether another criterion for the correlation of this component with sewage pollution can be established. Again, the 5β(*H*)/5α(*H*) epimeric ratio may provide some information.

As with that observed for the stanols, 5α(*H*)-cholestan-3-one predominates in anoxic depositional environments (*21–23*, *33*) as a consequence of the microbial and/or diagenetic reduction of Δ^5 sterols. Diverse experiments involving microbial reduction of sterols (*38*, *39*) have also shown that 5α(*H*)-cholestan-3-one is preferentially produced. In contrast, intestinal bacteria give rise to 5β-(*H*)-cholestan-3-one due to their stereospecific mechanism of Δ^5 sterol biohydrogenation (*12*, *13*, *15*, *40*).

In agreement with these observations, samples W1–6 and S1–9 display $5\beta/(5\beta + 5\alpha)$ cholestan-3-one ratios ranging between 1 and 0.77 whereas 5α(*H*)-cholestan-3-one clearly predominates in samples W7–9 ($5\beta/5\beta + 5\alpha$) ratio between 0.22 and 0.26) and S12 (C_5 epimeric ratio, 0.15) (see Figures 3 and 4). This is especially significant for samples S8–9 (ratio 0.93) where, as indicated in the previous section, the intermediate values of the $5\beta/(5\beta + 5\alpha)$ cholestan-3β-ol ratio did not allow a definite assessment of the urban sewage pollution.

The above results illustrate that the cholestan-3-one ratio is less affected than the corresponding cholestan-3β-ol ratio by interferences from direct biogenic contributions (namely algal). Thus, in contrast to C_{27} sterols, sterone contributions from algal organisms are very minor so that the $5\beta/(5\beta + 5\alpha)$ ratio is very little affected. In the case of the highly eutrophic bay (S8–9), besides 5β(*H*) C_{27}–C_{29} cholestan-3-ones, taraxer-14-en-3-one, olean-12-en-3-one, urs-12-en-3-one, friedelan-3-one, and some hopanones, representing vascular plant and microbial sources, were identified (Figure 2). In some sediments (S10–11), the absence of coprostanone represents another feature of differentiation. However, as shown in the coastal evaporite

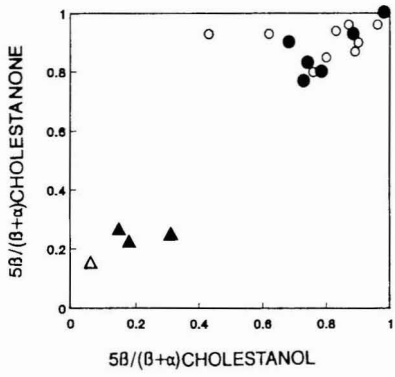

Figure 5. Cross-representation of the $5\beta/(5\beta + 5\alpha)$ isomeric ratios of cholestan-3β-ol and cholestan-3-one (● and ▲ water particulate samples collected at urban polluted and remote areas, respectively. △ and ○ sediment samples from unpolluted and sewage-contaminated areas).

system, coprostanone may also be found in sediments from pristine areas, which requires the use of the $5\beta/(5\beta + 5\alpha)$ ratio for sewage pollution identification.

When the $5\beta/(5\beta + 5\alpha)$ cholestanone ratio is calculated for the C_{29} homologues, even more distinct differences are observed between sewage-polluted and nonpolluted samples (see for instance samples W1–6 and W7–9 in Tables II and III). However, as has been indicated for the 24-ethylcholestan-3β-ols, the quantitation of C_{29} cholestan-3-ones may often pose analytical difficulties.

A joint evaluation of the C_{27} two epimeric ratios is represented in Figure 5 for the water particulate and sediment samples. As can be observed, the relative composition of the 5α and 5β isomers of either cholestan-3β-ol or cholestan-3-one affords a clear differentiation between sewage-polluted and unpolluted samples. Cross-representation of both ratios affords an even better classification.

Conclusions

The occurrence of coprostanol in coastal environments cannot be unambiguously attributed to urban sewage pollution. The relative composition of the C_5 epimers of cholestan-3β-ol and cholestan-3-one, the main intermediate steroid products involved in the sedimentary and intestinal processes of cholest-5-en-3β-ol reduction, must be considered. Thus, fecal matter can be positively identified in water particulates and sediments containing a higher proportion of 5β vs 5α isomers of these two components $[5\alpha/(5\beta + 5\alpha) > 0.7]$.

On the other hand, the strong decrease of coprostanol vs coprostanone found in moderately polluted samples (characteristic coprostanol concentration on the order of micrograms per gram or below) indicates that coprostanone should also be quantitatively determined for sewage monitoring. In this respect, it has been observed that the $5\beta/(5\beta + 5\alpha)$ cholestan-3β-ol ratio is modified by direct inputs of 5α(*H*)-cholestan-3β-ol in cases of high algal productivity. The usefulness of that ratio is precluded in these situations. However, the $5\beta/(5\beta + 5\alpha)$ cholestan-3-one ratio is not significantly affected, affording an alternative parameter for the reliable identification of sewage pollution in this type of depositional environment.

Registry No. 5β-Cholestan-3β-ol, 360-68-9; 5β-cholestan-3α-ol, 516-92-7; cholest-5-en-3β-ol, 57-88-5; 5α-cholestan-3β-ol, 80-97-7; 24-ethyl-5β-cholestan-3β-ol, 33947-19-2; 24-ethylcholest-5-en-3β-ol, 19044-06-5; 24-ethyl-5α-cholestan-3β-ol, 19044-02-1; 5β-cholestan-3-one, 601-53-6; 5α-cholestan-3-one, 566-88-1; 24-ethyl-5β-cholestan-3-one, 83603-22-9; 24-ethyl-5α-cholestan-3-one, 81571-54-2.

Literature Cited

(1) Wun, C. K.; Walker, R. W.; Litsky, W. *Water Res.* **1976**, *10*, 955–959.
(2) Goodfellow, R. M.; Cardoso, J.; Eglinton, G.; Dawson, J. P.; Best, G. A. *Mar. Pollut. Bull.* **1977**, *8*, 272–276.
(3) Hatcher, P. G.; Keister, L. E.; McGillivary, P. A. *Bull. Environ. Contam. Toxicol.* **1977**, *17*, 491–498.
(4) Hatcher, P. G.; McGillivary, P. A. *Environ. Sci. Technol.* **1979**, *13*, 1225–1229.
(5) McCalley, D. V.; Cooke, M.; Nickless, G. *Bull. Environ. Contam. Toxicol.* **1980**, *25*, 374–381.
(6) McCalley, D. V.; Cooke, M.; Nickless, G. *Water Res.* **1981**, *15*, 1019–1025.
(7) Wade, T. L.; Oertel, G. F.; Brown, R. C. *Can. J. Fish. Aquat. Sci.* **1983**, *40*, 34–40.
(8) Brown, R. C.; Wade, T. L. *Water Res.* **1984**, *18*, 621–632.
(9) Pierce, R. H.; Brown, R. C. *Bull. Environ. Contam. Toxicol.* **1984**, *32*, 75–79.
(10) Readman, J. W.; Preston, M. R.; Mantoura, R. F. C. *Mar. Pollut. Bull.* **1986**, *17*, 298–308.
(11) Eganhouse, R. P.; Olaguer, D. P.; Gould, B. R.; Phinney, C. S. *Mar. Environ. Res.* **1988**, *25*, 1–22.
(12) Bjorkhem, I.; Gustafsson, J. A.; Wrange, O. *Eur. J. Biochem.* **1973**, *37*, 143–147.
(13) Eyssen, H. J.; Parmentier, G. G.; Compernolle, F. C.; de Pauw, G.; Piessens-Denef, M. *Eur. J. Biochem.* **1973**, *36*, 411–421.
(14) Parmentier, G.; Eyssen, H. *Biochim. Biophys. Acta* **1974**, *348*, 279–284.
(15) Rosenfeld, R. S.; Fukushima, D. K.; Hellman, L.; Gallagher, T. F. *J. Biol. Chem.* **1954**, *211*, 301–311.
(16) Walker, R. W.; Wun, Ch.; K. Litsky, W. *CRC Crit. Rev. Environ. Control* **1982**, *12*, 91–112.
(17) Vivian, C. M. G. *Sci. Total Environ.* **1986**, *53*, 5–40.
(18) Bartlett, P. D. *Mar. Pollut. Bull.* **1987**, *18*, 27–29.
(19) Gaskell, S. J.; Eglinton, G. *Nature* **1975**, *254*, 209–211.
(20) Taylor, C. D.; Smith, S. O.; Gagosian, R. B. *Geochim. Cosmochim. Acta* **1981**, *45*, 2161–2168.
(21) Robinson, N.; Cranwell, P. A.; Finley, R. J.; Eglinton, G. *Org. Geochem.* **1984**, *6*, 143–152.
(22) Boudou, J. P.; Trichet, J.; Robinson, N.; Brassell, S. C. *Org. Geochem.* **1986**, *10*, 705–709.
(23) Robinson, N.; Cranwell, P. A.; Eglinton, G.; Brassell, S. C.; Sharp, C. L.; Gophen, M.; Pollingher, U. *Org. Geochem.* **1986**, *10*, 733–742.
(24) Nishimura, M. *Geochim. Cosmochim. Acta* **1982**, *46*, 423–432.
(25) Edmunds, K. L. H.; Brassell, S. C.; Eglinton, G. In *Advances in Organic Geochemistry 1979*; Douglas, A. G., Maxwell, J. R., Eds.; Pergamon: Oxford, 1980; pp 427–434.
(26) Pocklington, R.; Leonard, J. D.; Crewe, N. F. *Oceanolog. Acta* **1987**, *10*, 83–89.
(27) Dougan, J.; Tan, L. *J. Chromatogr.* **1973**, *86*, 107–116.
(28) Gomez-Belinchón, J. I.; Grimalt, J. O.; Albaigés, J. *Environ. Sci. Technol.* **1988**, *22*, 677–685.
(29) Aceves, M.; Grimalt, J. O.; Albaigés, J.; Broto, F.; Comellas, L.; Gassiot, M. *J. Chromatogr.* **1988**, *436*, 503–509.
(30) van Graas, G.; Baas, J. M. A.; van de Graaf, B.; de Leeuw, J. W. *Geochim. Cosmochim. Acta* **1982**, *46*, 2399–2402.
(31) Nishimura, M.; Koyama, T. *Geochim. Cosmochim. Acta* **1977**, *41*, 379–385.
(32) Smith, A. G.; Goodfellow, R.; Goad, L. J. *Biochem. J.* **1972**, *128*, 1371–1372.
(33) Nishimura, M.; Koyama, T. *Chem. Geol.* **1976**, *17*, 229–239.
(34) Robinson, N.; Eglinton, G.; Brassell, S. C.; Cranwell, P. A. *Nature* **1984**, *308*, 439–441.
(35) Grimalt, J.; Albaigés, J. *Mar. Geol.*, in press.
(36) Ramos, I.; Fuentes, M.; Mederos, R.; Grimalt, J. O.; Albaigés, J. *Mar. Pollut. Bull.* **1989**, *20*, 262–268.

(37) Gagosian, R.; Smith, S. O.; Nigrelli, G. E. *Geochim. Cosmochim. Acta* **1982**, *46*, 1163-1172.
(38) Lefebvre, G.; Germain, P.; Schneider, F. *Bull. Soc. Chim. Fr.* **1980**, *1-2*, II-96-II-97.
(39) Stohs, S. J.; Haggerty, J. A. *Phytochemistry* **1973**, *12*, 2869-2872.
(40) Fauve, A.; Kergomard, A. *Tetrahedron* **1981**, *37*, 899-901.

Received for review March 20, 1989. Accepted November 9, 1989. Financial support from EROS-2000 Project is gratefully acknowledged. We thank J. I. Gomez-Belinchon, R. Llop, and M. Valls for technical assistance.

Oxidation of Aniline and Other Primary Aromatic Amines by Manganese Dioxide

Shonali Laha and Richard G. Luthy*

Department of Civil Engineering, Carnegie Mellon University, Pittsburgh, Pennsylvania 15213

■ This investigation evaluated the redox reaction between a manganese dioxide, δ-MnO_2, and anilines and other aromatic reductants in aqueous suspensions at pH values ranging from 3.7 to 6.5. The reaction with manganese dioxide may represent a pathway for transformation of aniline and other primary aromatic amines in acidic mineralogical and soil/water environments in the absence of oxygen and substantial microbial activity. The reaction rate with aniline is pH-dependent, increasing with decreasing pH, and first order with respect to δ-MnO_2 and organic solute. Aniline and *p*-toluidine are demonstrated to be 2-equiv reductants, as is believed to be the case for the other aromatic solutes considered in this study, including the substituted anilines, and hydroquinone and catechol and their alkyl substituents. Ring-bound nitrogen-containing aromatic solutes (methylimidazole, quinoline, and 5,5-dimethylhydantoin) were unreactive with manganese dioxide at pH 6.4. The order of the reactivity of para-substituted anilines was methoxy $\gg$ methyl > chloro > carboxy $\gg$ nitro; the relative reactivity of these compounds correlated with the solute's half-wave potential and Hammett constant. The principal oxidation products of aniline and *p*-toluidine with manganese dioxide at pH 4 were azobenzene and 4,4′-dimethylazobenzene, respectively, which agreed with a postulated oxidative-coupling reaction mechanism. The abiotic redox reactions of primary aromatic amines and azo compounds may result in various respective oxidative-coupling and reductive-decoupling reactions. These processes may be significant with regard to the persistance and transformation of these classes of organic contaminants in environmental systems.

Introduction

The purpose of this investigation was to assess the rate of the redox reaction between a manganese dioxide, δ-MnO_2(s), and various aromatic reductants including several nitrogen-containing compounds. The initial rate and order of the reaction with respect to the reductant was determined as well as the effects of manganese dioxide concentration and pH. The principal reaction products, under acidic conditions, resulting from the oxidation of aniline and *p*-toluidine were determined.

In natural waters, Mn(III) and Mn(IV) are usually present in the form of sparingly soluble oxides and hydroxides, whereas Mn(II) is the soluble phase. In soil/sediment environments, manganese oxide is believed to be among the strongest oxidizing agents that may be encountered in the absence of molecular oxygen. Manganese oxide can be reduced and dissolved by organic compounds, increasing the mobility of manganese and its availability to organisms (*1*, *2*). These oxidative processes involving manganese oxides may constitute an important abiotic degradative pathway for organic compounds in subsurface environments. Earlier studies by Stone and Morgan (*2*) demonstrated some features of the reductive dissolution reaction between manganese oxide and organic solutes and some of the factors that influence the rate of the reaction. Stone (*3*) considered the reductive dissolution of manganese(III/IV) oxides by substituted phenols. Those investigations were performed with various manganese oxide suspensions, one of which was primarily the mineral-phase feitknechtite, β-MnOOH(s), with some amount of manganite, γ-MnOOH(s). In this study, a hydrous manganese dioxide suspension was prepared according to Murray (*4*), for which his stoichiometric and X-ray diffraction analyses indicated that this synthetic manganese dioxide is structurally similar to the naturally occurring mineral birnessite, δ-MnO_2(s).

The organic reductants investigated in this study were aniline and various substituted anilines, hydroquinone and catechol and some of their alkyl substituents, and several ring-substituted nitrogen-containing aromatics. Figure 1 shows the structures of the compounds discussed in this study. Anilines and other aromatic amines may originate as environmental contaminants from the use of pesticides and herbicides, as well as from chemical manufacturing residues, and from byproducts of energy technologies. Along with phenol, aniline is listed as a high-priority compound in the study of pollutants from coal-conversion process wastes (*5*). Aniline residues are formed in the soil as a result of microbial and plant metabolism of phenylurea, acylanilide, phenylcarbamate, and nitroaniline herbicides (*6*). Chlorinated anilines such as 2,4,5-trichloroaniline, 4-chloroaniline, 3,4-dichloroaniline, and 2,6-diethylaniline may be released as degradation products and intermediates of various phenylurea and phenylcarbamate pesticides (*7*, *36*). Aniline derivatives occur as intermediates in dye-stuff manufacture and this constitutes another possible source of environmental aniline contamination. A number of substituted anilines may be carcinogenic (*8*). Aniline and toluidine, i.e., methylaniline, and other aromatic amines are generally toxic and can induce various adverse physiological responses (*8*, *9*). For these reasons it is of considerable interest to explore the physical, chemical, and microbial transformations that may alter the toxicity, mobility, and bioavailability of aniline and related compounds in the environment.

Aniline and other aromatic amines are subject to complex environmental transformations. Lyons, Katz, and Bartha (*6*, *10*, *11*) performed studies on the microbial pathways for aniline elimination from aquatic environments, from which they concluded that biodegradation may be the most significant mechanism for the removal of aniline from pond water. Hwang and Lee (*7*) concluded that photochemical processes were primarily responsible for mineralization of 2,4,5-trichloroaniline in surface water

0013-936X/90/0924-0363$02.50/0

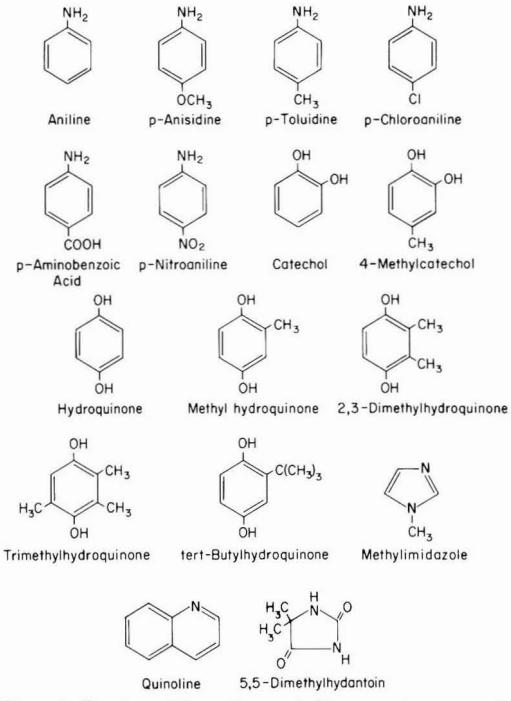

Figure 1. Structure of the anilines and other aromatic compounds employed in this study.

from an eutrophic lake. Zepp and Schlotzhauer (*12*) showed that the photolytic degradation of aniline is enhanced in the presence of algae.

The principal degradative processes for aniline and other primary aromatic amines in subsurface environments are either microbially induced reactions or abiotic degradation processes through redox reaction with soil constituents, for which the oxidative degradation of aniline by manganese dioxide is reported here.

Materials and Methods

The inorganic reagents were analytical grade (Fisher Chemicals) and the organic compounds were used as received (purity >99%, Aldrich). All stock solutions of organic substrates were used within 24 h to minimize the possibility of degradation by photolysis or oxidation by oxygen. Deionized water was used in the experiments and all glassware was soaked in 1:5 HNO_3/water and thoroughly rinsed with deionized water prior to use. Other reagent solutions were also made up in acid-cleaned glassware with deionized water; these solutions were discarded within 2 or 3 days to prevent microbial activity. Reagents and reaction solutions were foil-wrapped, and the more reactive nitrogen aromatics were maintained under inert atmosphere.

Preparation of Oxide Suspension. The preparation of approximately 0.01 M δ-MnO_2(s) was performed as described by Murray (*4*). Murray's analysis of the manganese dioxide produced by his method indicated it to be structurally similar to the naturally occurring mineral birnessite, with a surface area of 263 ± 5 m^2/g by the BET method and a maximum pH (zpc) of 2.4 by extrapolating electrophoretic mobilities. The manganese dioxide used in this study may be similar to that described by Murray, as the same method of preparation was employed. The procedures for preparation of the manganese dioxide were as follows: 1. Combine 40 mL of 0.1 M $KMnO_4$ and 80 mL of 0.1 M NaOH with stirring; adjust volume to 500 mL. 2. Add 60 mL of 0.1 M $MnCl_2$. 3. Allow δ-MnO_2 suspension to settle out. 4. Decant supernatant; wash oxide several times and adjust to 1-L volume with water having the same ionic strength and buffer as to be utilized in the experiments.

The reactivity of a manganese oxide suspension may change with time (*1*, *2*). To account for the effect of aging, all suspensions were used 24 h after preparation.

Tests with Catechols and Hydroquinones. Hydroquinone, methylhydroquinone, 2,3-dimethylhydroquinone, trimethylhydroquinone, *tert*-butylhydroquinone, catechol, and 4-methylcatechol were evaluated in dissolution reactions with manganese dioxide. The reaction rate was monitored by increase in Mn(II) with atomic adsorption spectrometry (Perkin-Elmer Model 703). The reaction was performed with continuous stirring under nitrogen purge with no oxygen. Samples of 5 mL were withdrawn by syringe at predetermined time intervals and expressed through a syringe-tight membrane filter (0.22 μm pore, 1-in. diameter; Millipore Millex-GS). It was verified that the filtration procedure stopped the reaction. The aliquots were acidified with 4 N HNO_3 and analyzed for dissolved manganese, $[Mn(II)]_{diss}$. Where the reaction proceeded very fast, the reacting solutions were flash mixed in a beaker, and samples were withdrawn by syringe immediately and then filtered. The reaction time included the residence time in the syringe, and filtration marked the end of the time interval. The minimum reaction interval by this procedure was about 12–15 s, which represents a practical limit of such a technique.

The $[Mn(II)]_{diss}$ is an operational definition of dissolved manganese as employed earlier in Stone and Morgan's work (*1*). It is that amount of manganese not retained by the membrane filter; and an increase in manganese beyond any that may be present in a reaction blank is taken to mean soluble manganese, Mn(II).

The pH of the reaction mixture was maintained at 6.4–6.5 for these tests with a 0.01 M sodium bicarbonate buffer. Ionic strength was kept at 0.1 M $NaNO_3$. Blanks were prepared without organic solute to assess any changes in oxide and Mn(II) concentrations due to reasons other than reductive dissolution by reaction with the organic solute. The Mn(II) reported represents net manganese oxide dissolved, accounting for any manganese that may pass the filter initially. Thus, a value of zero is taken for the initial concentration of Mn(II) produced by reaction. Generally blanks were found not to have significant dissolved manganese. Initial reaction rates were determined from the slope of the manganese dissolution curve by using the first few data points for which the reactant concentrations did not change significantly.

Tests with Aniline and Substituted Anilines. The test protocols were similar to those for the hydroquinones, but in addition to evaluating the reaction rate by increase in Mn(II), the organic concentration was also monitored by use of high-pressure liquid chromtographic (HPLC) techniques. Tests were performed at pH 4 with an acetate buffer as well as at pH 6 with a bicarbonate buffer. Chromatographic analyses were performed with a Perkin-Elmer Series 3 liquid chromatograph equipped with a Rheodyne 7105 injector and a Perkin-Elmer LC-15 UV detector at wavelength 254 nm. The column used was a 15-cm Supelco LC-PAH column with a particle size of 5 μm. The solvent used was 50:50 acetonitrile/water, at a flow rate of 1 mL/min. Injection volumes were between 4 and 9 μL. Where higher concentrations of reactants were

used the buffer concentration was also increased, e.g., 0.1 M acetate for 0.005 M reactants at pH 4, and 0.1 M bicarbonate for pH values of 6. Samples were withdrawn at predetermined time intervals by syringe and then filtered (0.2-μm pore, Millipore Millex-FG Teflon filters) into 5-mL vials that were sealed, covered with foil, and refrigerated until analyzed by HPLC techniques. Representative aqueous stock solutions of organics were analyzed both before and after filtration to ensure lack of organic adsorption on the Teflon filters. Reaction blanks were also studied to observe any change in aniline concentration in the absence of both oxygen and δ-MnO_2. Aniline degradation was negligible under such conditions in the time period of the experiment.

Peak areas for the organic analysis from HPLC determinations were divided by the quantity injected to yield response factors from which calibration curves were constructed with known solute concentrations. Graphs of solute concentration remaining versus time were plotted and the initial slopes were used to determine the initial reaction rates.

Identification of Reaction Products. The principal reaction products for aniline and *p*-toluidine were determined by GC–MS techniques. These samples were prepared for reaction by mixing 0.01 M organic and 0.01 M δ-MnO_2(s), at pH 4 with 0.1 M acetate buffer and 0.1 M $NaNO_3$ ionic strength, in a separatory flask. The flask was shaken intermittently in a gentle manner to ensure proper mixing. L-Ascorbic acid (1 M) was added to stop the reaction by dissolving the remaining manganese oxide (*1*). The dissolution of residual manganese oxide also provided for release of any adsorbed reaction products. The pH of the mixture was then adjusted to 12 by the addition of sodium hydroxide pellets, and the organic compounds were extracted with methylene chloride by shaking vigorously for 10 min, allowing the CH_2Cl_2 to separate, and withdrawing through a Teflon stopcock. The methylene chloride extract was concentrated by use of a Kuderna–Danish evaporator concentrator to volatilize the solvent. In these tests filtration was avoided in the event that a reaction product may have been retained on the filters.

The concentrated extract was injected into a 5985 Hewlet-Packard gas chromatograph–mass spectrophotometer with a 25 m × 0.2 mm SB-Smectic column. The injection temperature was 280 °C, the carrier gas helium at 1 mL/min, the ionization potential 70 eV, and the voltage 2400 V. The program was 1 min at 40 °C, 40–220 °C at 20 °C/min and 220–280 °C at 4 °C/min. The mass spectra indexes used were obtained from the literature (*13, 14*). Standards were also run under the same conditions to confirm the identity of the reactants and major products. The confirmation was done by matching the chromatographic retention time and comparing the principal mass ion distribution of standards and samples with those reported in the compendia of mass spectra.

Stock solutions of aniline and *p*-toluidine were analyzed by GC–MS to ensure purity and the absence of possible degradation products. Control samples having organic solute and buffer, but no δ-MnO_2(s), were carried through the mixing and extraction procedure, including the addition of ascorbic acid to verify the lack of reaction products and to demonstrate that identified organic products were present as a result of redox reaction with δ-MnO_2(s), rather than as a spurious experimental artifact.

Additional Tests. Rate tests were performed with the following ring-substituted nitrogen-containing organic compounds: methylimidazole, quinoline, and 5,5-dimethylhydantoin. The pH was maintained at 6–6.4 and the reaction was monitored by the concentration of dissolved manganese (using atomic absorption spectrometry techniques) over a period of days.

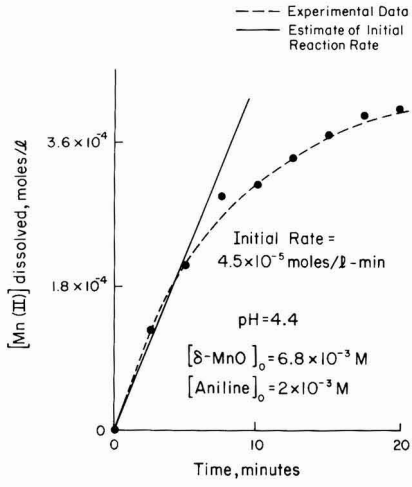

Figure 2. Reductive dissolution of manganese dioxide by aniline at pH 4.4.

Results

Initial Reaction Rates with Aniline. Rate tests were performed to evaluate the dissolution of manganese dioxide by several nitrogen-containing aromatic compounds. The compounds considered were aniline, *p*-anisidine, quinoline, methylimidazole, and 5,5-dimethylhydantoin. The objective was to observe the rate of dissolution of manganese dioxide by representative nitrogen-containing aromatics in order to identify those compounds that are reactive with manganese dioxide. The reaction was monitored by increase in the concentration of dissolved manganese.

At pH 6.4 and millimolar concentrations of organic and oxide, dissolution of δ-MnO_2(s) by methylimidazole was extremely slow, and unambiguous results were not obtained over 1 month. Similarly, quinoline and 5,5-dimethylhydantoin did not exhibit significant dissolution rates under these test conditions.

The initial rate with aniline and δ-MnO_2(s) was relatively slow at a pH value of 6.5, and the reaction rate increased with decreasing pH. Figure 2 shows that at pH 4.4 dissolution of manganese dioxide by aniline gave an initial reaction rate of 4.5×10^{-5} mol/L·min expressed in terms of rate of dissolution of manganese, and that the reaction appeared to proceed at a slower rate after ~20 min. Subsequent experiments with aniline were monitored by determining the concentration of aniline remaining in solution with HPLC techniques, for which a typical result gave an initial reaction rate of 8×10^{-5} mol/L·min expressed in terms of consumption of aniline for test conditions similar to those shown in Figure 2, except for a small proportional increase in the initial aniline concentration. The similarity of the initial reaction rates under comparable test conditions as given by either manganese dissolution or consumption of aniline, in conjunction with identification of aniline reaction products as discussed later, suggests an equivalent stoichiometry in the reduction of aniline by manganese dioxide. An analogous conclusion regarding stoichiometry was obtained by Stone and Morgan (*1, 2*) for the case of reductive dissolution of β-MnOOH(s) by hydroquinone, which was applied in their work for the case of 15 aromatic and 12 aliphatic com-

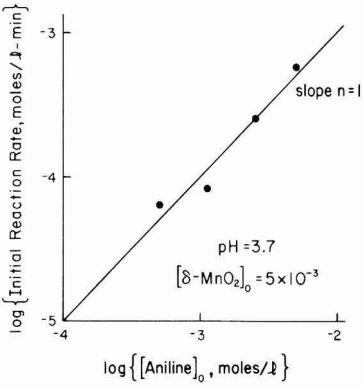

Figure 3. Estimation of the order of initial reaction rate with respect to aniline concentration for oxidation of aniline by manganese dioxide.

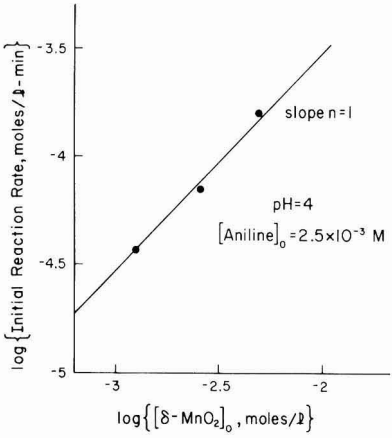

Figure 4. Estimation of the order of initial reaction rate with respect to manganese dioxide concentration for reduction of δ-MnO_2 by aniline.

pounds behaving as 2-equiv reductants with manganese oxide. A similar inference regarding the compounds reacting as 2-equiv reductants was used in this study to assess the rate of the reaction for δ-MnO_2(s) with aniline and substituted anilines, as well as for catechols and hydroquinones. Hence, the amount of organic compounds remaining could be expressed in terms of dissolution of manganese:

$$[\text{organic}]_t = [\text{organic}]_0 - [\text{Mn(II)}]_t \qquad (1)$$

where $[\text{organic}]_t$ represents the molar concentration of organic solute at time t, and $[\text{Mn(II)}]_t$ represents the difference in molar concentration of dissolved manganese between the reaction mixture and blanks at time t. While subsequent identification of principal reaction products in acidic samples suggests that aniline and *p*-toluidine are primarily 2-equiv reductants, additional work is needed to determine if the anilines are exactly 2-equiv reductants under various conditions.

Reaction Order with Aniline. The reaction kinetics of aniline and manganese dioxide were investigated to determine the order of the reaction with respect to the initial organic solute and oxide concentrations and the dependence of the initial reaction rate on the pH of the reaction mixture.

The order of the initial reaction rate with respect to aniline was evaluated by tests in which the oxide concentration was employed at a relatively high value of 5×10^{-3} M, while maintaining constant pH and buffer strengths through comparative tests and varying the aniline concentration by an order of magnitude from 0.5×10^{-3} to 5×10^{-3} M. In this approach, the initial reaction rate is computed over the first few time increments of the reaction, for which it may be assumed that the change in concentration of the reactants is negligible. The results shown in Figure 3 demonstrate that the reaction rate is first order with respect to aniline.

Similarly, the order of the reaction with respect to δ-MnO_2(s) was determined by varying the initial oxide concentration from 1.25×10^{-3} to 5×10^{-3} M, while maintaining the initial aniline concentration at 2.5×10^{-3} M and pH at 4. Figure 4 indicates that the reaction order with respect to manganese dioxide concentration is approximately unity.

The effect of pH on the initial reaction rate was determined at six different pH values from 4.0 to 6.5 at an initial aniline concentration of 2×10^{-3} M and an initial manganese oxide concentration, $[\delta\text{-}MnO_2]_0$, of 5×10^{-3} M. The results are shown in Figure 5, from which it is seen

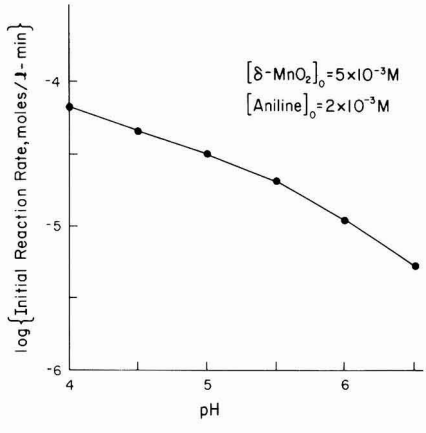

Figure 5. Effect of pH on the initial reaction rate for oxidation/reduction reaction between aniline and manganese dioxide.

that pH has a marked effect on reaction rate with the rate decreasing by an order of magnitude over this pH range. The reaction order is not constant with respect to pH, increasing from ~0.3 at pH 4 to ~0.6 at pH 6.5. Although pH values generally encountered in natural systems are higher, a pH of 4 was chosen in subsequent tests to assess reaction products and to evaluate the effect of substituents on the reaction rate of anilines. This was done for purposes of experimental convenience because of the ease of generation of data in a short period of time; also the blank values were negligible the shorter the reaction time considered. It is appreciated, however, that the reaction rate may diminish substantially at higher pH, as suggested by data in Figure 5.

Substituent Effect and Reaction Order for Hydroquinone and Catechol. Hydroquinines and catechols are benzyl compounds with two hydroxy substituents, at para and ortho positions, respectively. A study of the dissolution of manganese was performed with hydroquinone, catechol, and several alkyl substituents: methylhydroquinone, 2,3-dimethylhydroquinone, trimethylhydroquinone, *tert*-butylhydroquinone, and 4-methylcatechol. The initial concentrations of the organic solutes were varied from 0.5×10^{-3} to 5.0×10^{-3} M.

δ-MnO_2 was used in these tests at $(1.7\text{–}2.3) \times 10^{-3}$ M concentration with pH maintained at 6.5 by using 0.01 M

Table I. Initial Reaction Rates for Hydroquinone and Alkyl-Substituted Hydroquinones at pH 6.5

init concn, mol/L			init reaction rate,[a] mol/L·min			
$[\delta\text{-}MnO_2]_0$	$[organic]_0$	HQ	methyl-HQ	2,3-dimethyl-HQ	*tert*-butyl-HQ	trimethyl-HQ
1.7×10^{-3}	0.5×10^{-3}	2.4×10^{-4}	2.1×10^{-4}	2.0×10^{-4}	1.6×10^{-4}	1.4×10^{-4}
1.7×10^{-3}	1.5×10^{-3}	1.5×10^{-3}	1.4×10^{-3}	5.2×10^{-4}	5.2×10^{-4}	4.4×10^{-4}
2.3×10^{-3}	2.5×10^{-3}	1.5×10^{-3}	2.0×10^{-3}	1.0×10^{-3}	1.0×10^{-3}	5.9×10^{-4}
1.9×10^{-3}	5.0×10^{-3}	2.3×10^{-3}	2.2×10^{-3}	1.9×10^{-3}	1.9×10^{-3}	1.8×10^{-3}

[a] HQ, hydroquinone.

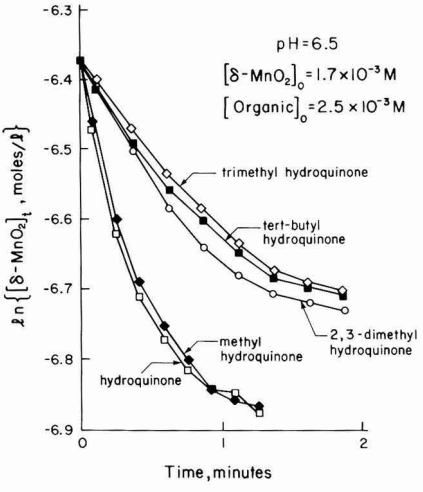

Figure 6. Reductive dissolution of manganese dioxide by hydroquinone and alkylsubstituted hydroquinones at pH 6.5.

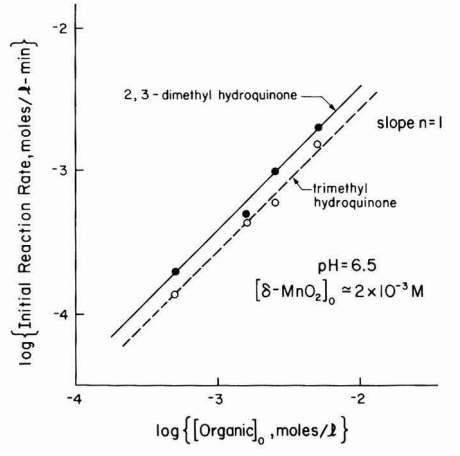

Figure 7. Estimation of the order of the redox reaction with respect to 2,3-dimethylhydroquinone and trimethylhydroquinone for reduction of manganese dioxide.

$NaHCO_3$ buffer. Dissolution of δ-MnO_2 was measured over time. The results were expressed as the natural logarithm of the oxide remaining in the reaction mixture versus time since the start of the reaction, for which a typical set of results obtained for the hydroquinones is shown in Figure 6. These data indicate that the reaction may slow with time, and thus only the initial reaction rates were considered for comparison, as summarized in Table I.

It is observed that reaction rate increases with the initial concentration of organic reductant, and results shown in Figure 7 for dimethylhydroquinone and trimethylhydroquinone indicate that the reaction order with respect to initial organic loading is close to unity. This is consistent with the data presented in Table I, for which the initial reaction rates for the hydroquinones increase by approximately an order of magnitude as initial organic concentration increases from 5×10^{-4} to 5×10^{-3} M. Methylhydroquinone and hydroquinone are the most reactive among the five compounds. However, the substituent effect on reaction rate for the hydroquinones is not particularly significant. As the reaction proceeds, the data in Figure 6 show deviation from linearity, suggesting that the reaction processes are more complex than implied by comparison of first-order initial reaction rates.

Results in Table II show the initial reaction rates for catechol and 4-methylcatechol. The initial reaction rates are in the range of those observed for the hydroquinones. As with the hydroquinones, it was observed that the dissolution reaction with catechol was rapid, with the reaction slowing appreciably after 2 min for these test conditions. The initial reaction rates increase for 4-methylcatechol in proportion to the organic concentration. However, at a concentration of 5×10^{-3} M organic the reaction rate for both catechol and 4-methylcatechol is no different from

Table II. Initial Reaction Rates for Catechol and 4-Methylcatechol at pH 6.4

init concn, mol/L		init reaction rate, mol/L·min	
$[\delta\text{-}MnO_2]_0$	$[organic]_0$	catechol	4-methylcatechol
1.7×10^{-3}	0.5×10^{-3}	1.0×10^{-3}	4.5×10^{-4}
1.9×10^{-3}	1.5×10^{-3}	1.5×10^{-3}	1.7×10^{-3}
1.7×10^{-3}	2.5×10^{-3}	2.6×10^{-3}	2.7×10^{-3}
2.3×10^{-3}	5.0×10^{-3}	2.7×10^{-3}	2.7×10^{-3}

that at organic concentration 2.5×10^{-3} M. Stone (*3*) reported similar behavior for the case of *p*-methylphenol and manganese(III/IV) oxide in which the reaction rate begins to level out as the pH is decreased below 5.0. This is explained through a reaction scheme in which precursor complex formation and electron transfer are rate-limiting steps and electron back-transfer is negligible. In that case, the reaction rate resembles a transition from pseudo first order to zero order with respect to the concentration of the organic compound. In Stone's work it was explained that, at lower concentrations of *p*-methylphenol, the reaction rate increases linearly with organic concentration, but as the concentration of the organic compound increases, a point is reached where the oxide surface is saturated with organic compound and electron transfer becomes rate limiting, and the reaction rate remains unaffected by higher concentrations of organic. In this study the results for catechol and 4-methylcatechol indicate that as the initial concentration of the organic solute increases beyond the initial concentration of δ-MnO_2, the proportionality between reaction rate and organic concentration no longer holds, probably through a change in rate-limiting mechanism as suggested by Stone (*3*).

The formation of Mn(II)–organic complexes was not investigated. Stability constants reported for catechol by

Table III. Initial Reaction Rates for Aniline and Substituted Anilines in the Presence of δ-MnO_2

compound	$E_{1/2}$,[a] V	Hammett[b] const	$[organic]_0$, mol/L	$[MnO_2]_0$, mol/L	pH	init rate, mol/L·min	k_{exp}, L/mol·min
p-anisidine	0.393	−0.78	6.2×10^{-5}	3.3×10^{-5}	4.4	6.5×10^{-4}	32000
p-toluidine	0.537	−0.31	2×10^{-3}	2.5×10^{-3}	4	1.2×10^{-3}	240
aniline	0.625		2.5×10^{-3}	5×10^{-3}	4	1.3×10^{-4}	10.4
p-chloroaniline	0.675	0.11	5×10^{-3}	5×10^{-3}	4	1.1×10^{-3}	44
aminobenzoic acid	0.794	0.42	5×10^{-3}	5×10^{-3}	4	3.1×10^{-3}	3.44
p-nitroaniline	0.935	0.79	2×10^{-3}	5×10^{-3}	4	$\sim 1 \times 10^{-7}$	~0.01

[a] $E_{1/2}$ values from Suatoni et al. (*18*). [b] σ^+ values from March (*21*).

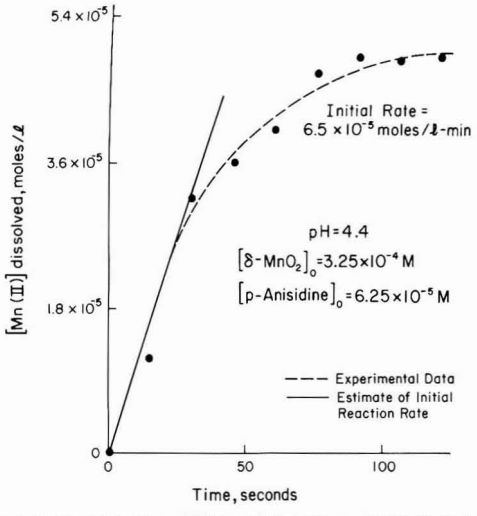

Figure 8. Reaction of *p*-anisidine and manganese dioxide at pH 4.4.

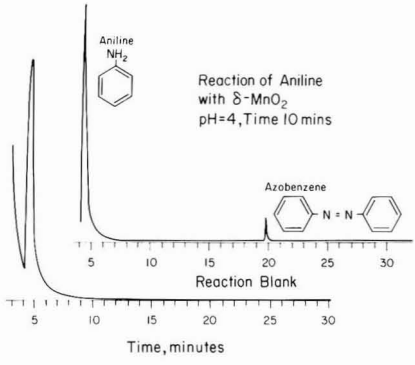

Figure 9. Chromatogram from GC–MS analysis for identification of reaction product for 10-min redox reaction of aniline and manganese dioxide.

Sillen and Martell (*37*), e.g., log $K_1 = 7.52$, suggest that Mn(II)–organic complex formation in the aqueous phase may have an effect on the reaction mechanism and rate. Smith and Martell (*38*) reported no stability constants for Mn(II) with aniline, *p*-toluidine, or *p*-anisidine. However, reported log K values are small for Cd(II) with aniline (log $K = 0.1$), *p*-toluidine (log $K = 0.26$), and *p*-anisidine (log $K = 0.45$), and by inference, complexation of the anilines with Mn(II) may be insignificant in comparison to catechol.

Substituent Effect for Aniline. The initial reaction rate was evaluated for various substituents of aniline: *p*-anisidine (i.e., *p*-methoxyaniline), *p*-toluidine (i.e., *p*-methylaniline), *p*-nitroaniline, 4-aminobenzoic acid, and *p*-chloroaniline. These tests were performed at pH 4 with acetate buffer. An initial oxide concentration of 5×10^{-3} M was employed except for the tests with *p*-toluidine and *p*-anisidine, for which $[\delta\text{-}MnO_2]_0 = 2.5 \times 10^{-3}$ and 3.25×10^{-4} M, respectively. The organic solute concentration was $(2\text{–}5) \times 10^{-3}$ M, except for tests with *p*-anisidine, for which it was 6.25×10^{-5} M. *p*-Anisidine dissolved manganese oxide so rapidly that it was not possible to measure the dissolution rate at millimolar concentrations of both oxide and organic. Figure 8 shows a test result for increase in Mn(II) for *p*-anisidine where the initial concentrations of organic and δ-MnO_2 are 6.25×10^{-5} and 3.25×10^{-4} M, respectively. In this case the reaction was complete in ~2 min, as the amount of manganese dissolved approached the stoichiometric amount of *p*-anisidine. For the tests with the other compounds, the rate was substantially slower and the course of the reaction was assessed by disappearance of reductant.

Table III summarizes the initial reaction rates of the various substituted anilines. The experimental rate constants, k_{exp}, are also presented in the table. The rate constants were computed as

$$k_{exp} = (\text{initial reaction rate})/[\delta\text{-}MnO_2]_0[organic]_0 \quad (2)$$

where psuedo-first-order dependence has been assumed with respect to both organic compound and manganese dioxide for the initial reaction rate as discussed earlier.

p-Nitroaniline was found to be particularly unreactive; after a reaction period of 12 h there was only ~5% disappearance of the compound at pH 4. As with *p*-anisidine, *p*-toluidine reacted readily with visible color production; the oxide suspension became wine-red on addition of organic, and dissolution was pronounced. *p*-Chloroaniline and *4*-aminobenzoic acid also reacted rapidly with visible color changes, the product being a deep peach for the former and orange for the latter.

Reaction Products. The identity of the reaction products was investigated for the reductive dissolution of manganese dioxide by aniline and *p*-toluidine. A set of tests with aniline was conducted by mixing 5 mL of 10^{-2} M aniline with 5 mL of 10^{-2} M δ-MnO_2 in acetate buffer at pH 4 in a centrifuge tube. The reaction was stopped at 10 min by the addition of 30 mL of 0.05 M L-ascorbic acid, which dissolved the remaining oxide suspension immediately. Aside from stopping the reaction, the purpose of this step was to release any reaction product that may have adsorbed on unreacted manganese dioxide and to prevent problems of solids separation and emulsification during subsequent extraction of the reaction mixture. The extraction was performed by adjusting the pH of the reaction solution to 12 with sodium hydroxide and extracting with 10 mL of methylene chloride for 10 min with vigorous shaking. The extract was concentrated by a factor of 13 and the concentrated extract was analyzed by GC–MS procedures. A typical chromatographic result is presented in Figure 9, which shows the presence of aniline at retention time 4.3 min and azobenzene at retention time 19.8

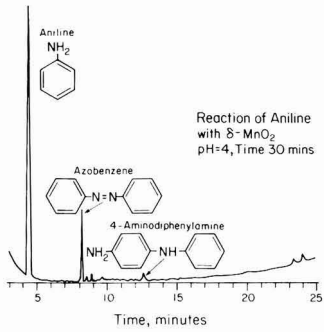

Figure 10. Chromatogram from GC–MS analysis for identification of reaction products for 30-min reaction of aniline and manganese dioxide showing azobenzene as the principal product with various minor products including 4-aminodiphenylamine.

min. The chromatogram shows no apparent reaction products other than azobenzene. Sample blanks were prepared for analysis in the same manner with the omission of the manganese dioxide, in which the manganese suspension volume was replaced by distilled water. Figure 9 also shows the chromatogram for the reaction blank, which indicates that sample manipulation and preparation for analysis, including the addition of ascorbic acid, resulted in no reaction product formation, confirming that the azobenzene is a product of the reaction of aniline with manganese dioxide, rather than being attributable to other degradative processes or impurities in the aniline.

Figure 10 shows a chromatogram of products for reaction of δ-MnO_2 and aniline at equimolar concentrations of 5×10^{-3} in a separatory flask in which the reaction was allowed to proceed for 30 min prior to analysis. In this test, larger volumes (100 mL) of reactants were used so that the subsequent extract would result in a greater concentration factor. In this case of the longer reaction time, azobenzene was still the principal reaction product, although a number of minor species were apparent also. *p*-Aminodiphenylamine was identified as one of the minor reaction products.

Azobenzene was confirmed by comparison of retention time and spectral intensities of an analytical standard. Figure 11 shows an inset of mass spectra for the reaction products corresponding to Figures 9 and 10 compared with a mass spectrum of an azobenzene standard. The four largest intensities for the azobenzene standard are m/z 77, 182, 105, and 152, which agree with the spectral displays for the identification of the compound as reaction product and which are listed as intense peaks in mass spectra indexes (*13*, *14*).

Figure 12 shows a chromatogram of reaction products for 5×10^{-3} equimolar concentrations of *p*-toluidine and δ-MnO_2 for a 10-min reaction time at pH 4. The predominant reaction product is clearly 4,4′-dimethylazobenzene, although several unidentified species were also present as minor reaction products. GC–MS determination of 4,4′-dimethylazobenzene was confirmed with an analytical standard by comparison of the chromatographic retention times and the largest spectral intensities, i.e., mass ion distribution of m/z 91, 210, and 119.

Discussion

For the reaction times and conditions considered in this investigation, degradation of aniline is negligible in the absence of manganese dioxide with exclusion of oxygen. This is consistent with the observations of Lyons et al. (*11*) who reported that autoxidation of aniline in the absence of light contributes little to aniline removal.

The dissolution rate of manganese dioxide by aromatic amine compounds depends on the nature of the oxidant, the reactant concentrations, and the medium composition. pH is seen to play an important role since the dissolution rate depends on the redox potential and on the extent and nature of the interaction of the aromatic solute with the oxide surface. The apparent reaction order with respect

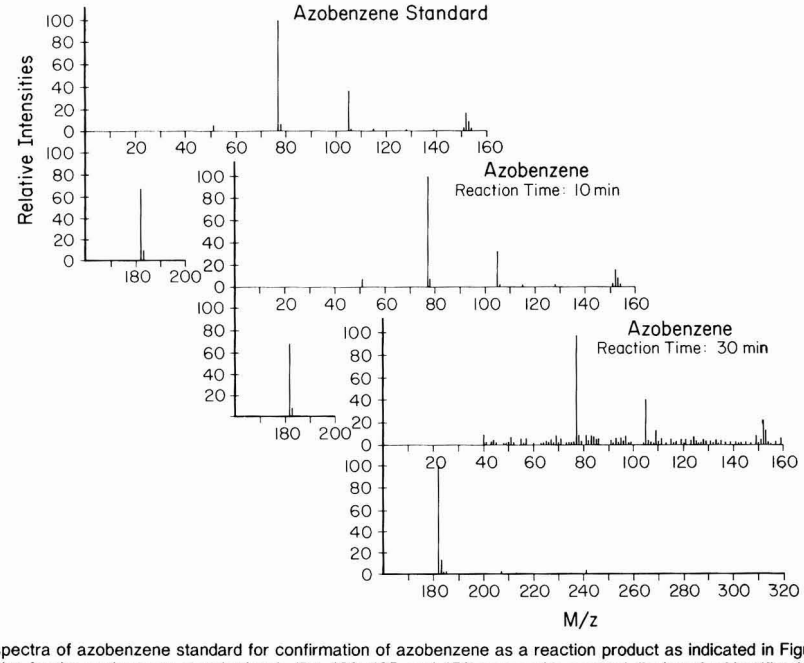

Figure 11. Mass spectra of azobenzene standard for confirmation of azobenzene as a reaction product as indicated in Figures 9 and 10. The four largest intensities for the azobenzene standard m/z (77, 182, 105, and 152) agree with spectral displays for identification of the compound as reaction product.

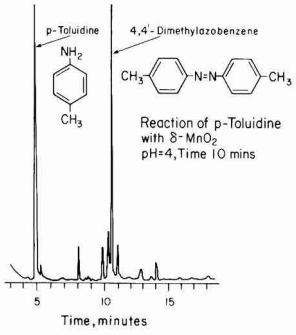

Figure 12. Chromatogram from analysis of reaction products for 10-min reaction of *p*-toluidine and manganese dioxide. 4,4′-Dimethylazobenzene is the principal reaction product.

to $[H^+]$ is derived from the slope of the logarithm of the initial reaction rates plotted as a function of pH:

$$\text{initial rate} = k[\text{organic}]^l[\text{manganese oxide}]^m[H^+]^n \quad (3)$$

or

$$\log(\text{initial rate}) = \log(k) + l \log[\text{organic}] + m \log[\text{manganese oxide}] + n \log[H^+] \quad (4)$$

The order with respect to $[H^+]$, n, need not necessarily be constant or an integer number. Figure 5 showed that reaction rate increases as the pH is decreased for the reaction of 2×10^{-3} M aniline with δ-MnO_2. The apparent order of the reaction with respect to $[H^+]$ defines a curve, rather than a straight line, varying in slope from 0.32 to 0.64. Stone (*3*) observed that the reductive dissolution of Mn(III/IV) oxide by *p*-methylphenol varied with pH, with n decreasing from about 1.2–1.3 at pH >6 to about 0.4–0.5 at pH 4. The test results with *p*-methylphenol, as with aniline, suggested that the observed pH dependence may arise from specific interactions between the reductant and the oxide surface sites, including protonation reactions that promote the formation of surface precursor complexes and/or increases in the protonation level of surface precursor complexes that increase rates of electron transfer (*3*).

The experimental results suggest an equivalent stoichiometry in the initial reaction of aniline with manganese dioxide by evidence of the principal reaction products, i.e., Mn(II) and azobenzene, and by the similarity of the rate of disappearance of the reactants. Aniline is thus a 2-equiv reductant, for which the similarity in initial reaction rate with regard to appearance of Mn(II) or depletion of aniline demonstrates that

$$d[\text{Mn(II)}]/dt = -d[\text{aniline}]/dt = \text{reaction rate} \quad (5)$$

The order of this reaction is demonstrated to be unity with respect to the concentration of both manganese dioxide and aniline, and at constant pH the rate law has the form

$$\text{reaction rate} = k_x[\text{aniline}][\text{manganese dioxide}] \quad (6)$$

Rate laws of a similar form have been proposed for reaction of aniline and substituted anilines as 2-equiv reductants in aqueous acetic acid medium for oxidation by peroxydisulfate, $S_2O_8^{2-}$ (*15*), thallium triacetate, $Tl(OAc)_3$ (*16*), and iodate, IO_3^- (*17*).

The rate constants for the oxidation of the aromatic amines may be correlated with the organic solute half-wave potential and the substituent Hammett constant. Half-wave potentials have been reported (*18*) from anodic voltammetry experiments with para- and meta-substituted

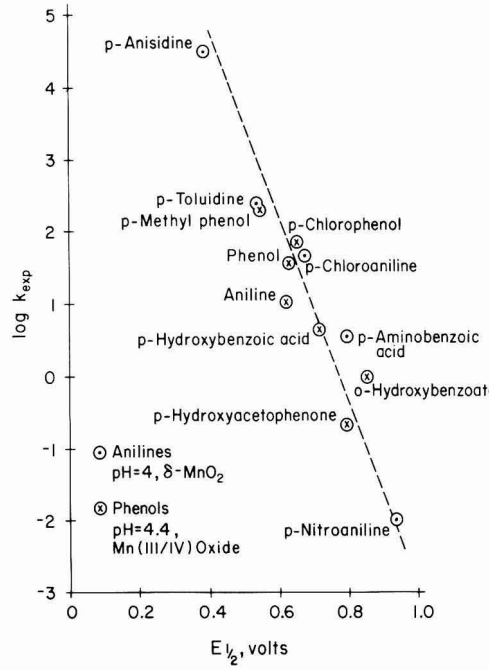

Figure 13. Correlation of half-wave potentials with experimental rate constants for redox reaction of substituted anilines with δ-MnO_2, and substituted phenols with manganese(III/IV) oxide. Rate data for the phenols are from Stone (*3*).

phenols and anilines for use in polarographic identification of oxidizable and reduced organic compounds. The half-wave reduction potentials depend upon the chemical speciation and diffusion coefficients of oxidant and reductant as well as the thermodynamic driving force for the reaction (*3*, *19*). The tendency to donate electrons increases as the solute half-wave potential decreases (*18*).

Logarithms of the experimental rate constants, k_{exp}, of substituted anilines at pH 4 are plotted against half-wave potentials, $E_{1/2}$, in Figure 13. The k_{exp} values were presented in Table III with reported values of $E_{1/2}$. The reaction rate is observed to generally decrease with increasing half-wave potential. *p*-Anisidine has the lowest half-wave potential and reacts most quickly with manganese dioxide, while *p*-nitroaniline with the highest half-wave potential is the least reactive. Data from Stone (*3*) for reaction of the substituted phenols with manganese(III/IV) oxide at pH 4.4 in acetate buffer are also presented in Figure 13, and these data agree with the trend observed for substituted anilines using $E_{1/2}$ values for the substituted phenols as reported also by Suatoni et al. (*18*). The particular manganese oxide employed by Stone (*3*), for which the rate data are compared in Figure 13, was prepared by reaction of $MnSO_4$ and $NaMnO_4$ at pH 6.6; this was similar to the manganese dioxide preparation procedure employed in this investigation except that Mn^{2+} and MnO_4^- were reacted under alkaline conditions. The chemical conditions are similar for the two sets of tests shown in Figure 13, with pH 4 used in the tests with the substituted anilines and pH 4.4 in the tests with the substituted phenols. These results suggest that the reactivities of δ-MnO_2 and manganese (III/IV) oxide in acidic environment are of the same magnitude with respect to reductive dissolution of manganese dioxide by either substituted phenols or anilines.

Hammett constants are linear free energy parameters that may be used to estimate chemical properties for or-

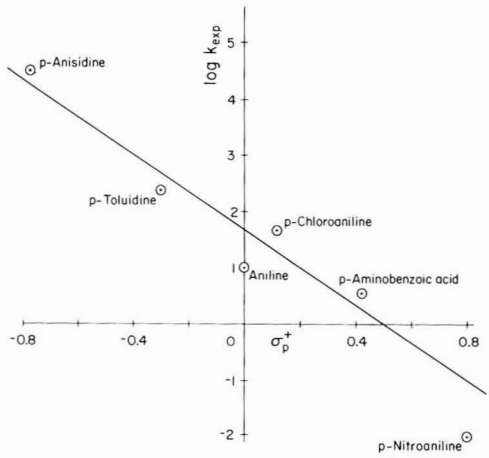

Figure 14. Correlation of Hammett σ^+ constants with experimental rate constants for redox reaction of substituted anilines with δ-MnO_2. Nitroaniline does not follow the correlation, see text for discussion on the behavior of this compound.

ganic solutes (*35*), such as acid dissociation constant or rate of hydrolysis (*20*), as well as rates for many other types of reactions of aromatic solutes (*21*). The estimation method is basically a substituent effect approach in which a correlation is established between the chemical property of the parent compound (e.g., phenol or aniline) and that of the substituted compound. It has been reported that the Hammett substituent constants, σ, are linearly proportional to the change in electron density at the aromatic ring carbon meta or para to the primary substituent group (*18*). Since the value of the half-wave potential for substituted phenols and anilines depends on the electron density at the carbon atom to which either the hydroxy or amine group is attached, the half-wave potentials of meta- and para-substituted phenols and anilines should be linearly related to Hammett's σ constants. The selection of the appropriate set of Hammett constants (σ, σ^+ or σ^-) depends on the reaction mechanism within a given series. Hammett σ^+ values are used where the substituent group can enter into direct resonance with the reaction site in the transition state for an electron-donating group (e.g., NH_2) developing a positive charge (*21*, *35*).

The rate constants for reductive dissolution of δ-MnO_2 by substituted anilines were correlated with Hammett constants σ and σ^+. A better correlation was obtained with σ^+ values, for which Figure 14 shows a general trend between the rate constant and σ^+. That the reaction series followed σ^+ better than σ suggests extensive resonance interaction in the transition state (*21*). This is consistent with the subsequent discussion, which suggests the formation of a cation-radical intermediate. Nitroaniline does not follow the sequence and may interact with δ-MnO_2 by a different mechanism, as suggested later.

Substituent effects and their correlations with physical and chemical properties provide a rational basis for estimating trends in the relative reactivity of para-substituted phenols and anilines with manganese dioxide. The order of the reactivity with substitution of the parent molecule is as follows: methoxy $\gg$ methyl > chloro > carboxy $\gg$ nitro. Those substituents that are considered classical electron-withdrawing groups make reductive dissolution of manganese dioxide by phenol or aniline more difficult by decreasing electron density, while the opposite effect on dissolution rate occurs for classical electron-donating groups. Similar orders of relative reactivity have been

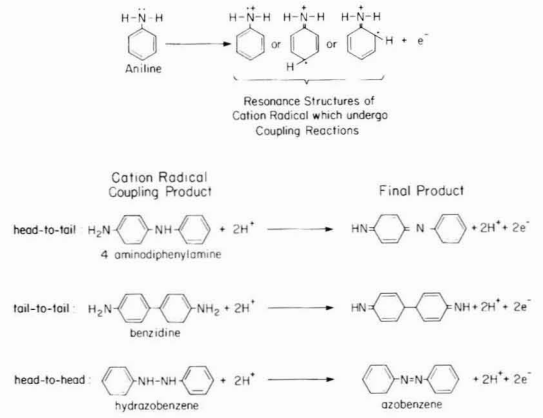

Figure 15. Postulated mechanism for oxidative coupling of aniline by reaction with manganese dioxide. The reaction proceeds from a cation radical through coupling products, which then undergo further oxidation [adapted from Sharma et al. (*31*)].

obtained for the oxidation of substituted anilines in dilute acetic acid medium by thallium triacetate and sodium iodate (*16*, *17*).

Oxidative Coupling of Anilines. The oxidation of aniline and substituted primary aromatic amines can result in the formation of a variety of products, depending on reaction conditions. The oxidation of aniline by MnO_2 in sulfuric acid gives *p*-benzoquinone (*22*), while oxidation with peroxy acids, e.g., peroxyacetic acid, or nitric acid may yield nitroso and nitro compounds (*23*, *24*). Polymeric substances result from the reaction of aniline and peroxydisulfate in acid medium (*25*). Azo compounds result from the oxidation of primary aromatic amines by lead tetraacetate in acetic acid (*26*), by phenyl iodosoacetate in acetic acid (*27*), by *N*-chlorobenzamide in methanol/hydrochloric acid medium (28), and by cuprous chloride and oxygen when pyridine is used as solvent (29). Substituted anilines can be oxidized to symmetrically substituted azobenzenes by refluxing with manganese dioxide in benzene (*30*).

The results of this work show that the principal oxidation products of aniline and *p*-toluidine by manganese dioxide in aqueous buffered solution at pH 4 were azobenzene and 4,4′-dimethylazobenzene, respectively. A postulated reaction sequence may be inferred from cyclic voltammetry studies of primary aromatic amines in acidic aqueous solution as summarized in Figure 15 from the work of Sharma et al. (*31*), who examined the anodic oxidation of aniline, 2,4- and 2,6-dimethylaniline, and toluidines. According to this oxidation mechanism, aniline loses one electron to produce a cation radical, which through resonance structures may undergo head-to-tail, tail-to-tail, or head-to-head couplings. The immediate respective products are *p*-aminodiphenylamine, benzidine, and hydrazobenzene, all of which are more readily oxidized than the parent substance and undergo further oxidation at the same potential. The overall oxidation is thus a sequential, two-electron reaction. A suggested reaction pathway for *p*-toluidine is shown in Figure 16 in which head-to-head coupling is favored because of blocking at the para position.

The results of this study confirm that the principal pathway for oxidation of aniline and *p*-toluidine by manganese dioxide in aqueous suspension at moderate acidity is a two-electron process, which results in the production of symmetrical azobenzenes. Head-to-head coupling with

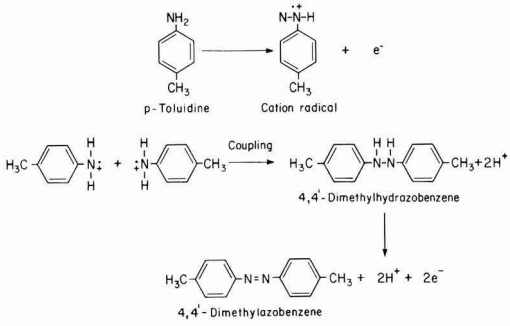

Figure 16. Postulated reaction mechanism for oxidative coupling of *p*-toluidine by reaction with manganese dioxide resulting in 4,4′-dimethylazobenzene as the principal reaction product [adapted from Sharma et al. (*31*)].

formation of azo compounds is the predominant reaction, although a variety of minor products, such as *p*-aminodiphenylamine, the aniline head-to-tail intermediate coupling product, are evident also from reaction with manganese dioxide.

These results are consistent with the work of Wheeler and Gonzalez (*30*), who demonstrated that manganese dioxide in benzene solution oxidizes substituted anilines to symmetrically substituted azobenzenes. They observed that nitroanilines and *p*-aminobenzoic acid were essentially unreactive over 24 h of refluxing in benzene with MnO_2. The lack of reactivity of nitro- and carboxy-substituted aromatic amines was attributed to the nitro or carboxyl group being preferentially adsorbed at the active oxidation centers on the manganese dioxide, thus preventing oxidation of the amino group. Although the exact nature of the mechanisms involved in the oxidation of the anilines was not explored in the investigation reported here, the general features of the reaction with regard to oxidation products and relative rates of reaction agree with the findings of Wheeler and Gonzalez (*30*) and Sharma et al. (*31*). Additional studies with multiple-substituted anilines could help elucidate the reaction mechanism with MnO_2 in aqueous medium. For example, studies with 3,5-dichloro-4-nitroaniline or 3,5-diethyl-4-nitroaniline, in which adsorption of the nitro group would be hindered by the neighboring groups, would indicate the degree to which adsorption of the nitro group impedes the reaction.

Conclusion

Transformation of Aniline and Azo Compounds. The present investigation demonstrated a redox pathway for oxidation of aniline and primary substituted anilines to symmetrical azo compounds by reaction with manganese dioxide in acidic aqueous systems. This oxidation reaction may be an important transformation process for aniline compounds in moderately acidic subsurface environments in the absence of molecular oxygen and substantial microbial activity. Analogous abiotic reductive transformations of azobenzene and selected azo derivatives have been observed by Weber and Wolfe (*32*) in sediment/water systems. The abiotic reduction of azobenzene was a four-electron, pH-dependent process for which GC–MS analyses showed production of stoichiometric amounts of aniline. The proposed scheme for the abiotic reduction of azobenzene to aniline is illustrated in Figure 17. The reaction is postulated to be a surface-mediated reaction proceeding through hydrazobenzene, which would not be stable in a highly reducing environment. The present investigation suggests that the pattern of oxidation of

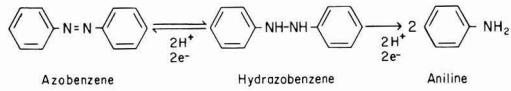

Figure 17. Proposed scheme for abiotic reduction of azobenzene to aniline in anaerobic sediment/water systems [Weber and Wolfe (*32*)].

aniline by manganese dioxide is the reverse of the reduction of azobenzene in anaerobic sediment/water systems.

The significance of the processes whereby manganese dioxide induced oxidative coupling of aniline and substituted anilines may serve as an elimination pathway for anilines depends on the accessibility and the form of manganese dioxide in natural systems, as well as the role and relative rates of competing reactions. Aniline may undergo microbial degradation through dioxygenase attack, resulting in oxidative deamination to catechol, which is further degraded by ortho cleavage and mineralized (*7*, *33*). Substituted anilines can be relatively resistant to microbial degradation, depending on the microbial community and the presence of other growth substrates (*6*, *10*, *34*).

The abiotic redox reaction of primary amines and azo compounds in mineralogical and sediment/water environments may result in various oxidative-coupling and reductive-decoupling reactions. These processes may be significant with regard to the persistence and transformation of these classes of organic contaminants in environmental systems.

Acknowledgments

S. Shanmuganantha assisted with a portion of the experimental studies. Curt M. White and Louise J. Douglas, Coal Science Division, Pittsburgh Energy Technology Center, assisted with identification of reaction products.

Registry No. δ-MnO_2, 1313-13-9; hydroquinone, 123-31-9; methyl-HQ, 95-71-6; 2,3-dimethyl-HQ, 608-43-5; *tert*-butyl-HQ, 1948-33-0; trimethyl-HQ, 700-13-0; catechol, 120-80-9; 4-methylcatechol, 452-86-8; *p*-anisidine, 104-94-9; *p*-toluidine, 106-49-0; aniline, 62-53-3; *p*-chloroaniline, 106-47-8; aminobenzoic acid, 1321-11-5; *p*-nitroaniline, 100-01-6; azobenzene, 103-33-3; 4-aminodiphenylamine, 101-54-2; 1-methyl-1-imidazole, 616-47-7; quinoline, 91-22-5; 5,5-dimethylhydantoin, 77-71-4; 4,4′-dimethylazobenzene, 501-60-0.

Literature Cited

(1) Stone, A. T.; Morgan, J. J. *Environ. Sci. Technol.* **1984**, *18*, 450.
(2) Stone, A. T.; Morgan, J. J. *Environ. Sci. Technol.* **1984**, *18*, 617.
(3) Stone, A. T. *Environ. Sci. Technol.* **1987**, *21*, 979.
(4) Murray, J. W. *J. Colloid Interface Sci.* **1974**, *46*, 357.
(5) Harrison, F. L.; Mallon, B. *Selection of Representative Organic Compounds for in-depth Studies of Mobility in Soil–Water Systems*; Lawrence Livermore National Laboratory: DE84-011 625; UCID-20031, NTIS, 1982.
(6) Lyons, C. D.; Katz, S. E.; Bartha, R. *Bull. Environ. Contam. Toxicol.* **1985**, *35*, 704.
(7) Hwang, H.; Hodson, R. E.; Lee, R. F. *Appl. Environ. Microbiol.* **1985**, *50*, 1177.
(8) Doull, J.; Klaassen, C. D.; Amdur, M. O. *Toxicology*, 2nd ed.; Macmillan Publishing Co.: New York, 1980.
(9) Sax, N. I.; Lewis, R. J. *Hazardous Chemicals Desk Reference*; Van Nostrand Reinhold: New York, 1987.
(10) Lyons, C. D.; Katz, S. E.; Bartha, R. *Bull. Environ. Contam. Toxicol.* **1985**, *35*, 697.
(11) Lyons, C. D.; Katz, S. E.; Bartha, R. *Appl. Environ. Microbiol.* **1984**, *48*, 491.
(12) Zepp, R. G.; Schlotzhauer, P. F. *Environ. Sci. Technol.* **1983**, *17*, 462.
(13) *Eight Peak Index of Mass Spectra*, 1st ed.; Mass Spectrometry Data Centre: Reading, UK, 1970.

(14) Hites, R. A. *CRC Handbook of Mass Spectra of Environmental Contaminants*; CRC Press: Boca Raton, FL, 1985.
(15) Srivastava, S. P.; Gupta, R. C.; Shukla, A. K. *Indian J. Chem.* **1977**, *15A*, 605.
(16) Radhakrishnamurti, P. S.; Pati, S. N. *Indian J. Chem.* **1980**, *19A*, 980.
(17) Rao, M. D. P.; Padmanbha, J. *Indian J. Chem.* **1980**, *19A*, 984.
(18) Suatoni, J. C.; Snyder, R. E.; Clark, R. O. *Anal. Chem.* **1961**, *33*, 1894.
(19) Bard, A. J.; Faulkner, L. R. *Electrochemical Methods*; Wiley: New York, 1980.
(20) Lyman, W. J.; Reehl, W. F.; Rosenblatt, D. H. *Handbook of Chemical Property Estimation Methods*; McGraw-Hill Book Co: New York, 1982.
(21) March, J. *Advanced Organic Chemistry*, 3rd ed.; Wiley: New York, 1985.
(22) LeNoble, W. J. *Highlights of Organic Chemistry—An Advanced Textbook*; W. B. Saunders: Philadelphia, PA, 1965.
(23) Plesnicar, B. In *Oxidation in Organic Chemistry*; Trahanovsky, W. S., Ed.; Academic Press: New York, 1973; Vol. 5-C, pp 267-270.
(24) Ogata, Y. In *Oxidation in Organic Chemistry*; Trahanovsky, W. S., Ed.; Academic Press: New York, 1973; Vol. 5-C, pp 328-330.
(25) Gupta, R. C.; Srivastava, S. P. *Indian J. Chem.* **1972**, *10*, 706.
(26) Pausacker, K. H.; Scroggie, J. G. *J. Chem. Soc.* **1954**, 4003, part II.
(27) Barlin, G. B.; Pausacker, K. H.; Riggs, N. V. *J. Chem. Soc.* **1954**, 3122, part III.
(28) Rawat, B. S.; Agrawal, M. C. *Indian J. Chem.* **1978**, *17A*, 299.
(29) Nigh, W. G. In *Oxidation in Organic Chemistry*; Trahanovsky, W. S., Ed.; Academic Press: New York, 1973; Vol. 5-B, pp 51-53.
(30) Wheeler, O. H.; Gonzalez, D. *Tetrahedron* **1964**, *20*, 189.
(31) Sharma, L. R.; Manchanda, A. K.; Singh, G.; Verma, R. S. *Electrochem. Acta* **1982**, *27*, 223.
(32) Weber, E. J.; Wolfe, N. L. *Environ. Toxicol. Chem.* **1987**, *6*, 911.
(33) Scow, K. M.; Simkins, S.; Alexander, M. *Appl. Environ. Microbiol.* **1986**, *51*, 1028.
(34) You, I. S.; Bartha, R. *J. Agric. Food Chem.* **1982**, *30*, 274.
(35) Hammett, L. P. *Physical Organic Chemistry*, 2nd ed; McGraw-Hill Book Co.: New York, 1970.
(36) Bollag, J.-M.; Minard, R. D.; Liu, S.-Y. *Environ. Sci. Technol.* **1983**, *17*, 80-83.
(37) Sillen, L. G.; Martell, A. E. *Stability Constants for Metal-Ion Complexes*; The Chemical Society: London, 1971; Supplement No. 1.
(38) Smith, R. M.; Martell, A. E. *Critical Stability Constants*; Plenum Press: New York, 1975; Vol. 2.

Received for review December 28, 1988. Revised manuscript received August 20, 1989. Accepted November 27, 1989. This work was supported by the U.S. Department of Energy, Grant DE-FG22-86PC90524; Richard P. Noceti, Technical Project Officer, provided useful comments.

Anaerobic Microbial Remobilization of Toxic Metals Coprecipitated with Iron Oxide

Arokiasamy J. Francis* and Cleveland J. Dodge

Department of Applied Science, Brookhaven National Laboratory, Upton, New York 11973

■ An anaerobic N_2-fixing *Clostridium* sp. solubilized Cd, Cr, Ni, Pb, and Zn coprecipitated with goethite (α-FeOOH) by (i) direct action due to enzymatic reduction of ferric iron and the release of metals associated with iron and (ii) indirect action due to metabolic products. The extent of dissolution depended upon the nature of the association of the metals with goethite. Substantial amounts of Cd and Zn, which were closely associated with iron, were released due to direct action. Nickel was solubilized by direct and indirect actions, while a small amount of Cr was solubilized only by direct action. The nature of association of Pb in the coprecipitate was not affected by the presence of other cations and it was solubilized by indirect action. In the presence of bacteria, the concentration of soluble Pb decreased due to biosorption. These results show that there could be significant remobilization of toxic metals coprecipitated with iron oxides in wastes, contaminated soils, and sediments due to microbial iron reduction.

Introduction

Iron oxides scavenge transition and heavy metals in soils, sediments, and energy wastes (*1-8*). These oxides are a major sink for metals in the terrestrial and aquatic environments and play an important role in regulating their availability. Sorption and coprecipitation are the predominant processes by which most of the metals are retained by iron oxide. Sorption is a process by which metals are bound to the surface of an existing solid by adsorption and surface precipitation (*9*), whereas coprecipitation is the simultaneous precipitation of a chemical element with other elements and includes mixed-solid formation, adsorption, and inclusion (*10, 11*). Although coprecipitation has not been as well studied as adsorption, it appears to remove trace metals from solution more efficiently (*12-14*). Toxic metals such as As, Cd, Co, Cr, Cu, Hg, Ni, Pb, Se, U, and Zn from fossil- and nuclear-fuel cycle waste streams, geothermal fluids, and electroplating wastes are currently removed by coprecipitation with ferric iron or are under consideration for such treatment (*3,15-17*).

The removal of toxic metals from waste streams by coprecipitation with iron seems to be a very efficient method and economically feasible, but problems remain with the disposal of the solids generated in the process and with the ultimate fate of the coprecipitated metals in the environment. Significant dissolution of metals from the coprecipitate can be brought about by chemical and microbiological action. In general, solubility of iron oxide depends upon the degree of crystallinity. Amorphous iron oxides are orders of magnitude more soluble than goethite or hematite (*1*), while amorphous synthetic goethite is 2-100 times more soluble than a well-crystallized goethite (*18*). Microorganisms play a significant role in the dissolution of amorphous and crystalline forms of iron oxides by direct action or by indirect action. Direct action involves enzymatic reductive dissolution of iron from higher oxidation state to lower oxidation state and indirect action is due to the production of metabolites (*19-23*). However, we have little information on microbially mediated disso-

0013-936X/90/0924-0373$02.50/0

lution and remobilization of metals coprecipitated with iron. In this paper, we report for the first time the anaerobic microbial remobilization of toxic metals Cd, Cr, Ni, Pb, and Zn coprecipitated with goethite.

Materials and Methods

Culture Conditions. A N_2-fixing *Clostridium* sp. (ATCC 53464) isolated from coal-cleaning residue was grown in a medium containing the following: glucose, 5.0 g; NH_4Cl, 0.5 g; glycerol phosphate, 0.3 g; $MgSO_4 \cdot 7H_2O$, 0.2 g; $FeSO_4 \cdot 7H_2O$, 2.8 mg; $CaCl_2 \cdot 2H_2O$, 0.5 g; peptone, 0.1 g; yeast extract, 0.1 g; deionized water, 1000 mL; pH, 6.8 ± 0.1. The medium was first prereduced by boiling and purging with N_2 gas for 15 min to remove the dissolved oxygen. It was then cooled under a N_2 atmosphere in an anaerobic glovebox and 40-mL quantities were dispensed in 60-mL serum bottles. The serum bottles were closed with butyl rubber stoppers, sealed with aluminum caps, and autoclaved. The medium was inoculated with 0.2 mL of an early logarithmic growth phase of the culture (optical density at 600 nm, 0.41) and incubated at 24 ± 1 °C. Growth of the bacteria was measured at 600 nm with a Bausch and Lomb Spectronic-20 spectrophotometer.

Preparation of Iron Oxide (Goethite) Metal Coprecipitate. Iron oxide coprecipitate was synthesized as described by Atkinson et al. (*24*) with some modifications. Stock solutions were prepared containing 0.25 M of each of the following metals in 100 mL of deionized water: $Cd(NO_3)_2 \cdot 4H_2O$ (Alfa Products, 95+%), $Cr(NO_3)_3 \cdot 9H_2O$ (Alfa Products, 98.5%); $Ni(NO_3)_2 \cdot 6H_2O$ (Alfa Products, 97+%); $Pb(NO_3)_2$ (Mallinckrodt, analytical reagent grade); $Zn(NO_3) \cdot xH_2O$ (Alfa Products, 95+%). Each stock solution was acidified with 0.05 mL of Ultrex nitric acid, and 5 mL of each was added to a 1.5-L Pyrex flask. $Fe(NO_3)_3 \cdot 9H_2O$, 50 g (Mallinckrodt, 98.5%) and 800 mL of deionized water were then added, and the pH was adjusted to 12 by adding 200 mL of 2.5 N KOH. A reddish brown precipitate formed immediately. The precipitate was aged for 24 h at 60 °C and then washed several times with deionized water until the nitrate levels in the supernatant were less than 5 mg/L. The washed precipitate was dried in an oven at 60 °C for 18 h, pulverized to a fine powder in an agate mortar, and stored in a desiccator. The structure of the iron oxide was confirmed by X-ray diffraction with a Phillips XRG 3100 Model analyzer.

To determine the behavior of Pb in the absence of other cations, we prepared a separate goethite coprecipitate with only Pb $(NO_3)_2$ and ferric iron, using the same procedure described.

Chemical Characterization of Metal Coprecipitates. Total Metal Content. A 50-mg aliquot of the coprecipitate was dissolved in 40 mL of 50% HCl in duplicate. The solution was filtered through a 0.22-μm Millipore filter, and the metals were analyzed by atomic absorption spectrophotometry.

Exchangeable Cations. To determine the exchangeable fraction of metals, 40 mL of a 1 M $MgCl_2$ solution was added to 50 mg of the coprecipitate in duplicate. The solution was shaken continuously for 2 h on a wrist-action shaker. The samples were then filtered through a 0.22-μm Millex filter, acidified with 0.20 mL of Ultrex HNO_3, and analyzed for each metal.

Dissolution Profile of the Metals. A 40-mL aliquot of 50% HCl was added to 50 mg of the mixed-metal–goethite coprecipitate. Six sets of duplicate samples were incubated and each sample was mixed by agitation at periodic intervals. At 0, 2, 4, 6, 8, and 10 h a set of samples was filtered through a 0.22-μm Millex filter and analyzed for each metal.

Dissolution of Metals from Goethite Coprecipitate. We determined whether the metals were released by direct action due to enzymatic reductive dissolution or by indirect action (nonenzymatic) due to production of organic acid metabolites in a series of experiments as described elsewhere (*20*) with modifications. A 50-mg sample of the mixed-metal– or lead–goethite coprecipitate was incubated in 40 mL of medium in 60-mL serum bottles fitted with butyl rubber stoppers under N_2 atmosphere for 40 h at 24 °C. All samples were incubated in triplicate.

The treatments consisted of the following:

(i) Dissolution in Sterile Medium (Control). To determine the chemical dissolution of the coprecipitate in the uninoculated bacterial growth medium (control), we added the prereduced medium to acid-washed bottles containing the coprecipitate. The samples were then sealed with butyl rubber stoppers, autoclaved, and incubated for 40 h.

(ii) Dissolution in the Presence of Bacteria. Dissolution of the coprecipitate in the presence of bacteria was determined by inoculating the autoclaved medium containing the coprecipitate with 0.2 mL of a 24-h-old culture. This treatment allowed the bacterial cells to come in direct contact with the precipitate. At the end of incubation, the total gas production and pH were determined.

(iii) Dissolution by Cell-Free Spent Medium. To determine whether metals were released from the coprecipitate by extracellular components produced by the bacterium, a cell-free spent medium was prepared. Cells were grown in culture medium in the absence of coprecipitate. After 40 h of incubation (optical density at 600 nm, 0.61), the cells were separated from the culture medium by centrifugation at 13600*g* for 30 min and filtration through a 0.22-μm Durapore filter in a 1.5-L Teflon-coated pressure filtration device (Millipore Co.) inside the anaerobic glovebox. The spent medium was divided into two equal aliquots. The first aliquot was immediately tested for its ability to solubilize metals from the coprecipitate, while the second aliquot was used to test for nonenzymatic dissolution as described below.

(iv) Nonenzymatic Dissolution of Metals. The second aliquot of filtered spent medium was transferred to serum bottles, sealed with butyl rubber stoppers, and autoclaved to inactivate the enzymes. This heat-treated spent medium was filtered again through the pressure filtration device with a 0.22-μm Durapore filter to remove any denatured cellular material. The pH of the autoclaved and filtered spent medium was measured, and the dissolution of metals from the coprecipitate was determined as described before.

The filtered spent medium and the heat-treated spent medium were checked for cells by direct microscopic examination and for viable cells by incubating an aliquot in a fresh growth medium.

(v) Dissolution of Metals by Synthetic Medium. To determine the effect of acid metabolites and pH of the medium on the dissolution of metals from the coprecipitate, a synthetic medium was prepared by adding metabolic acids to prereduced growth medium containing only inorganic salts (NH_4Cl, 0.50 g; $MgSO_4 \cdot 7H_2O$, 0.20 g; and $CaCl_2 \cdot 2H_2O$, 0.5 g/L). The metabolic acids, acetic (3.44 mM), butyric (7.90 mM), and lactic (2.62 mM), were added in the same proportions as found in an inoculated culture medium of *Clostridium* sp. (*25*). The final pH of the synthetic medium was 3.1.

At the end of incubation, the samples were filtered through a 0.22-μm Millex filter and the filtrate was acid-

Table I. Metal Content of Goethite Coprecipitate

metal	mmol added	mmol in coprecip[a]	% metal incorp
		Mixed Metals	
Fe	125	98.0 ± 0.00	78.4
Cd	1.25	0.62 ± 0.01	50.0
Cr	1.25	0.83 ± 0.00	66.6
Ni	1.25	0.62 ± 0.01	50.0
Pb	1.25	0.67 ± 0.01	53.8
Zn	1.25	0.86 ± 0.06	69.2
		Lead Only	
Fe	125	100 ± 2	80.0
Pb	1.25	0.77 ± 0.02	61.5

[a] ±1 standard error of the mean.

Table II. Exchangeable Cations in Goethite Coprecipitate

metal	mmol/g of dry wt	%
	Mixed Metals	
Fe	<0.001	<0.01
Cd	0.002	2.9
Cr	<0.002	<2.5
Ni	<0.002	<2.5
Pb	0.008	11.4
Zn	0.001	1.1
	Lead Only	
Fe	<0.001	<0.01
Pb	0.011	13.8

ified with Ultrex HNO_3 and analyzed for Fe, Cd, Cr, Ni, Pb, and Zn by atomic absorption spectrophotometry. All manipulations, except weighing the coprecipitate, were performed in the anaerobic glovebox.

Analyses of Total Gas and Organic Acids. The total volume of gas produced, and the organic acids in the culture samples, were determined as described previously (**25**).

Results

Characteristics of Goethite Coprecipitates. Analysis of the coprecipitate showed that it contained 78–80% of the added iron (Table I). There were differences in the extent of the incorporation of added toxic metals with goethite. About 69% of added Zn, 67% Cr, 54% Pb, and 50% each of Cd and Ni were found in the coprecipitate. More Pb was present in the lead–goethite coprecipitate than in the mixed-metal coprecipitate. In Table II, the exchangeable fraction of the metals in the coprecipitates is presented. Only small amounts of Cd and Zn were present in the exchangeable fraction; Fe, Cr, and Ni were not detected. A substantial amount of Pb (11%) in the mixed-metal coprecipitate and 14% in the lead–goethite coprecipitate were present in the exchangeable fraction.

Figure 1 shows the dissolution profile of the metals from the mixed-metal coprecipitate after acid (50% HCl) treatment: there was complete dissolution of all the metals after 10 h. However, the dissolution pattern of each metal was different and indicated the nature of the metal association in the coprecipitate. About 75% of Pb, 30% each of Cr and Ni, and less than 10% each of Fe, Cd, and Zn were dissolved from the coprecipitate immediately upon the addition of the acid. Pb was solubilized most readily. Ni and Cr were solubilized at similar rates. The dissolution rates of Fe, Cd, and Zn were similar but greater than Ni and Cr. In addition, the following slopes were calculated (*26*) from plots of percent toxic metal released versus iron released: Cd (1.01), Zn (1.00), Ni (0.84), Cr (0.83), and Pb (0.27). These data indicate that Cd and Zn are more closely associated with iron than Ni and Cr. Whereas, Pb is poorly associated with iron.

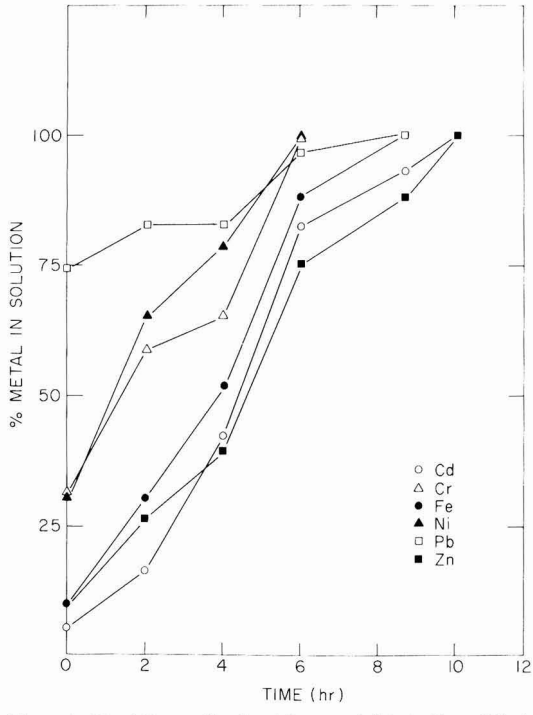

Figure 1. Dissolution profile of metals coprecipitated with goethite in 50% HCl. All points are averages of duplicate determinations and are within ±2% of the mean.

Table III. Growth of *Clostridium* sp. in the Presence and Absence of Goethite Coprecipitate

sample	goethite coprecip	final pH	total gas produced, mL	turbidity (600 nm)
		Mixed Metals		
uninoculated (control)	+	6.70	0	0
inoculated	–	3.05	24	0.62
inoculated	+	4.33	50 ± 15[a]	ND[b]
		Lead Only		
inoculated	+	4.35	52 ± 5[a]	ND[b]

[a] ±1 standard error of the mean. [b] ND, not determined because of the high background turbidity caused by the coprecipitate.

Growth Characteristics of the Bacterium. The optical density of the culture medium without the coprecipitate reached 0.62 after 40 h of incubation and the pH changed from 6.8 to 3.1. Because of the high background turbidity caused by the coprecipitate, we could not measure the optical density of the culture samples. However, the growth of the bacterium was enhanced in samples containing the coprecipitate (Table III), as evidenced by increased production of gas and changes in the pH of the culture medium during incubation from 6.7 to 4.3. The change in pH of the culture medium was due to production of acetic, butyric, and lactic acids from glucose fermentation. The higher pH of the culture medium containing the coprecipitate was probably due to the consumption of protons during the dissolution of the goethite or to the release of hydroxide from the coprecipitate. The increased growth of the bacteria accompanied by higher gas production was probably due to this higher pH of the medium. We observed a similar effect on growth of the bacterium

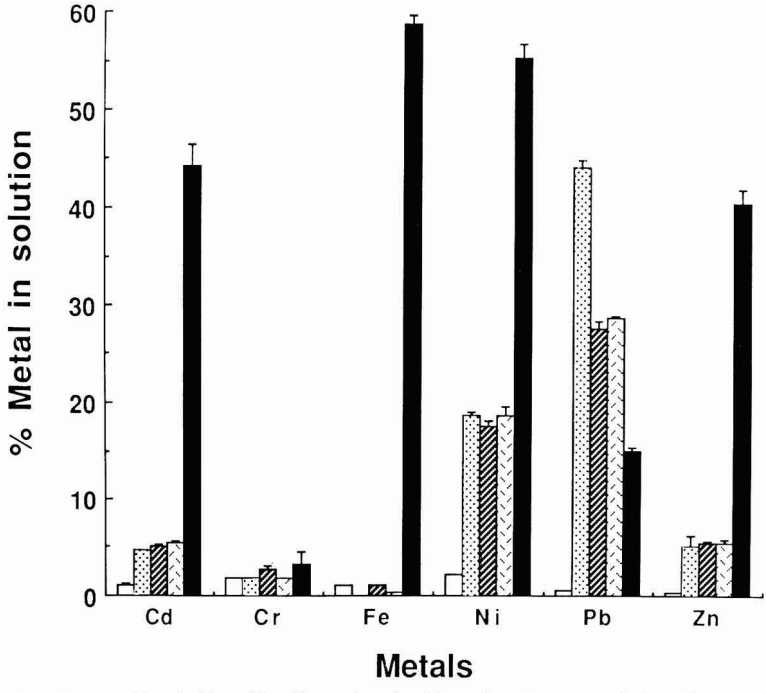

Figure 2. Dissolution of metals coprecipitated with goethite. Key: uninoculated (control) medium, □; synthetic medium, □; cell-free spent medium, ▨; autoclaved cell-free spent medium, ▨; and medium inoculated with *Clostridium* sp. ■. Error bars represent ±1 SEM.

when the culture medium was buffered with PIPES buffer or with $CaCO_3$.

Dissolution of Metals from Goethite Coprecipitate. Figure 2 shows the extent of metals solubilized from the mixed-metal coprecipitate by (i) uninoculated sterile medium (control), (ii) in the presence of bacteria (inoculated medium), (iii) cell-free spent medium, (iv) autoclaved cell-free spent medium (nonenzymatic dissolution), and (v) synthetic medium.

Dissolution of metals from the coprecipitate by uninoculated control medium (pH 6.7) was very low for Fe (1.1%), Cd (1.0%), and Zn (0.3%), while Cr, Ni, and Pb could not be detected. This finding indicates that there was little chemical dissolution effected by the culture medium.

Synthetic medium (pH 3.1) that contained the major metabolic acids (acetic, butyric, and lactic; plus mineral salts) solubilized substantial portions of Pb (44%), Ni (19%), and about 5% each of Cd and Zn. Only 0.04% of Fe was released and Cr was not detected.

Cell-free spent medium (pH 3.1) that contained the metabolites and extracellular enzymes dissolved the metals to varying degrees. More Fe was released than in the synthetic medium but the amount was similar to that in uninoculated control medium (1.1%). Similar amounts of Cd were solubilized in spent medium (5.1%) and in synthetic medium (4.8%). There were detectable amounts of soluble Cr (2.7%) in spent medium but not in uninoculated and synthetic medium, indicating that Cr dissolution was biochemically mediated. About 17.5% of Ni and 5.5% of Zn were solubilized from the coprecipitate by the cell-free spent medium, similar to their values in synthetic medium. Dissolution of Pb in the cell-free spent medium was about 15% less than that of the synthetic medium.

There was little difference in the extent of dissolution of Cd, Ni, and Zn in the spent medium, the autoclaved spent medium, and the synthetic medium, indicating that their dissolution is primarily due to the organic acid metabolites and low pH. Dissolution of Pb in the cell-free and autoclaved cell-free spent medium was similar but less than that in the synthetic medium. The soluble Fe and Cr in the autoclaved spent medium was much less than that of the spent medium. This finding indicates that heat-labile components present in the spent medium are involved in the solubilization of Fe and Cr.

A substantial increase in the concentrations of soluble Fe (59%), Cd (48%), Ni (55%), and Zn (41%) and a slight increase of Cr (3.2%) was observed in samples incubated with cells. However, soluble Pb in the inoculated culture medium was 50% less than that of spent medium and 70% less than in the synthetic medium. This difference was due to biosorption by the cellular components in the medium (25). Analysis of Fe in solution showed that it occurred as Fe^{2+}. The data clearly show that the coprecipitated metals were released into the medium when iron was solubilized only in the presence of bacteria. These results also indicate that direct contact between the coprecipitate and the bacteria was required to effect remobilization of metals associated with iron.

The extent of lead and iron dissolution from the lead–goethite coprecipitate was similar to that of the mixed-metals–goethite coprecipitate (Figure 3). Therefore, the association of Pb with coprecipitate appears to be unaffected by the presence of other cations that may compete with Pb for active sites. Dissolution of Pb from the coprecipitate was primarily due to organic acid metabolites. Soluble Pb detected in cell-free spent medium and autoclaved spent medium was much less than that of the synthetic medium. This was due to immobilization of soluble Pb by the extracellular materials present in the cell-free and autoclaved spent medium. In the presence of bacteria, however, soluble Pb detected in culture medium containing Pb–goethite coprecipitate was much less than that of culture medium containing mixed-metals–

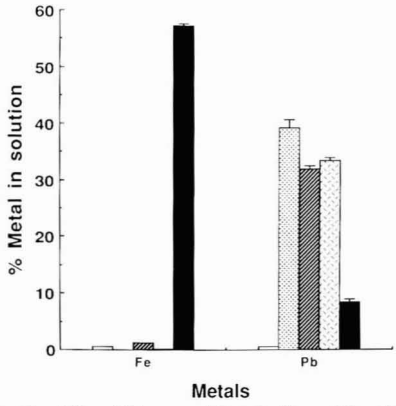

Figure 3. Dissolution of Pb coprecipitated with goethite. Key: uninoculated (control) medium, □; synthetic medium, □; cell-free spent medium, ▨; autoclaved cell-free spent medium, ▨; and medium inoculated with *Clostridium* sp. ■. Error bars represent ±1 SEM.

goethite coprecipitate. This may be due to the presence of other cations released from mixed-metals–goethite coprecipitate, which could compete for metal binding sites in the biomass.

Discussion

The dissolution profiles of the metals coprecipitated with goethite showed that the metals were incorporated into the coprecipitate to varying degrees. Although the exact chemical form and nature of the association of the metals in the coprecipitate is not known, it appears from the dissolution data that cadmium and zinc were closely associated with iron, while lead was present predominantly as a readily soluble form. Chromium and nickel were present in the acid-soluble fraction as well as in association with iron. Dissolution of metals from the coprecipitate by the bacterial action depended upon the nature of association of the metals with iron oxide. Metals that were closely associated with iron were solubilized by direct action due to enzymatic reduction of ferric iron and the others by the indirect action of the metabolites, as well as by the lowering of the pH of the growth medium. It is possible that some of the metals may exist in the oxide form in the coprecipitate. We have shown previously (*20*) that pure metal oxides such as CdO, PbO, and ZnO were solubilized by indirect action; Fe_2O_3 was solubilized by direct action. Dissolution of Cr_2O_3, NiO, and Ni_2O_3 by direct or indirect action was not observed.

In the presence of bacteria, a substantial amount of iron and metals associated with iron were solubilized from the coprecipitate. Reduction of oxyhydroxides and oxides of iron by bacteria has been reported and that direct contact of microbial cells to the oxide surface generally enhances the rate and extent of iron dissolution (*19*, *20*, *22*, *23*, *27*). The results also support the findings of the others that direct bacterial cell contact with the coprecipitate is required to effect significant dissolution of Fe and other metals. The final concentration of metals detected in solution is determined by the speciation, solubility, precipitation reactions, and biosorption by the biomass of the released metals from the coprecipitate.

Although a small amount of Cd and Zn was present as readily exchangeable forms, the concentration of these metals in solution increased by 8–9-fold when the coprecipitate was incubated in the presence of bacteria. This finding suggests that major portions of Cd and Zn are associated with iron in the coprecipitate. Chemical dissolution studies with HCl also indicate that the dissolution profiles of Cd and Zn closely parallel iron dissolution, corroborating the microbiological dissolution profile. Therefore, Cd and Zn appear to be almost stoichiometrically associated with iron and may form a complex oxide such as ferrite (*28*). These compounds may be solubilized by the bacteria at a different rate than goethite. The formation of ferrites at 65 °C has been observed when Cd, Co, Ni, and Zn were added to an aqueous suspension of lepidocrocite (γ-FeOOH) (*11*). Cadmium and zinc form tetrahedral associations in normal ferrites, while nickel and lead form octahedral coordination with Fe as inverse spinels (*29*). The tetrahedral normal ferrites are more stable than Ni and Pb ferrites (*30*). Nickel was readily solubilized by indirect action, but a 3-fold increase in the dissolution of Ni in the presence of bacteria suggests that a significant portion of the metal is associated with Fe.

Chromium dissolution from the coprecipitate was not detected in solution in any of the treatments except by cell-free spent medium and in the presence of bacteria. This result suggests that heat-labile biochemical components or enzymes are involved in the dissolution of Cr. On the other hand, lack of Cr detection in solution may partially be due to the formation of highly refractory Cr_2O_3 or chromite species. Cr^{3+} was shown to be irreversibly adsorbed to ferrihydrite and amorphous iron oxide (*12*). Dissolution of Cr_2O_3 by *Clostridium* sp. was not observed (*20*). However, dissolution of Cr from coal waste under anaerobic conditions has been reported (*31*).

Lead showed the highest solubility in synthetic medium, but the concentration of this element decreased in comparison to synthetic medium by 30% in cell-free spent medium and 65% in the presence of bacteria. This decrease in Pb was due primarily to attenuation by the bacterial biomass and by the extracellular polymeric material produced by the bacteria (*20*, *25*). The behavior of lead during the precipitation of amorphous ferric oxide in natural waters was studied by Laxen (*4*); Pb showed slow desorption kinetics in which it was transferred from the small particles to the larger particles during the aggregation of the coprecipitate. Thus, it appeared that Pb migrated outward to larger particles as they were being formed and was present predominantly in the outer surface as a readily exchangeable form. Our results with Pb as a sole metal or along with other metals in the coprecipitate confirm Laxen's conclusion (*4*). The presence of Pb in the coprecipitate as a readily exchangeable form is of concern because of the potential for its remobilization from wastes, contaminated soils, and sediments.

Although the removal of toxic metals from waste streams by iron oxide coprecipitation is an efficient process, we have shown in this study that the coprecipitates may not be stable in the waste disposal sites particularly under anaerobic conditions. Bacteria use iron as an alternate electron acceptor during the decomposition of organic compounds including organic contaminants and may indeed release the metals associated with iron. In a related study, we have shown that the dissolution of metals from coal wastes under anaerobic conditions was due to bacterial reduction of iron and manganese oxides and the release of trace metals coprecipitated with the oxides (*31*). Although, in this study, we used glucose as the carbon source, other electron donors may be used by the organism in which the iron oxide is used as the terminal electron acceptor or as sink for excess electrons generated during the decomposition process (*19*, *20*, *23*). Mobility and fate of the released metals from the coprecipitate in the natural environment is obviously regulated by the presence of

other alternate electron acceptors such as sulfate, e.g., sulfate reduction and formation of insoluble metal sulfides; attenuation by soils, subsoils, and sediments; and other geochemical interactions at the disposal site.

Conclusions

Toxic metals, which are removed from wastes and waste streams by coprecipitation with ferric iron, can be remobilized under anoxic conditions by direct or indirect microbial action. Direct action involves the enzymatic reductive dissolution of iron and the release of metals coprecipitated with iron. Dissolution of metals from the coprecipitate by indirect action is primarily due to production of metabolites and a lowering of the pH of the medium. The extent of microbial remobilization of coprecipitated metals from iron oxide depends on the nature of the association of the metals with iron. Metals that were closely associated with iron were solubilized only along with iron by direct action. Ni and Cr were solubilized by both direct and indirect action. Pb was readily solubilized by indirect action. These results indicate that toxic metals coprecipitated with iron oxides may not be very stable especially in anaerobic environments, because under appropriate conditions microorganisms can bring about dissolution of the coprecipitate.

Acknowledgments

We thank F. J. Wobber, Project Manager, for his interest and support.

Registry No. Fe, 7439-89-6; Cd, 7440-43-9; Cr, 7440-47-3; Ni, 7440-02-0; Pb, 7439-92-1; Zn, 7440-66-6; goethite, 1310-14-1.

Literature Cited

(1) Jenne, E. A. In *Molybdenum in the Environment*; Chappel, W. R., Petersen, K. K., Eds.; Marcel Dekker, Inc.: New York, 1977; Vol. 2, pp 425–553.
(2) Anderson, M. A.; Rubin, A. J. *Adsorption of Inorganics at Solid–Liquid Interfaces*; Ann Arbor Science: Ann Arbor, MI, 1981.
(3) Leckie, J. O.; Benjamin, M. M.; Hayes, K.; Kaufman, G.; Altmann, S. Adsorption/coprecipitation of trace elements from water with iron oxyhydroxide. Electric Power Research Institute Report CS-1513, Palo Alto, CA, 1980.
(4) Laxen, D. P. H. *Chem. Geol.* **1984**, *47*, 321–332.
(5) Kinniburgh, D. G.; Jackson, M. L.; Syers, J. K. *Soil Sci. Soc. Am. J.* **1976**, *40*, 796–799.
(6) Tessier, A.; Rapin, F.; Carignan, R. *Geochim. Cosmochim. Acta* **1985**, *49*, 183–194.
(7) Suarez, D. L.; Langmuir, D. *Geochim. Cosmochin. Acta* **1976**, *40*, 589–598.
(8) Stumm, W.; Morgan, J. J. *Aquatic Chemistry*, 2nd ed.; Wiley-Interscience: New York, 1981; pp 625–640.
(9) Honeyman, B. D.; Santschi, P. H. *Environ. Sci. Technol.* **1988**, *22*, 862–871.
(10) Sposito, G. In *Applied Environmental Geochemistry*; Thornton, I., Ed.; Academic Press: New York, 1983; pp 123–170.
(11) Tamaura, Y. J. *Inorg. Chem.* **1985**, *24*, 4363–4366.
(12) Schultz, M. F.; Benjamin, M. M.; Ferguson, J. F. *Environ. Sci. Technol.* **1987**, *21*, 863–869.
(13) Kurbatov, J. D.; Kulp, J. L.; Mack, E., Jr. *J. Am. Chem. Soc.* **1945**, *7*, 1923–1929.
(14) Lal, D.; Arnold, J. R.; Somayajulu, B. L. K. *Geochim. Cosmochim. Acta* **1964**, *28*, 1111–1117.
(15) Benjamin, M. M.; Hayes, K.; Leckie, J. O. *J. Water Pollut. Control Fed.* **1982**, *54*, 1472–1481.
(16) Warren, C. J.; Dudas, M. J. Mobilization and attenuation of trace elements in an artificially weathered fly ash. Electric Power Research Institute Report EA-4747, Palo Alto, CA, 1986.
(17) DeCarlo, E. H.; Thomas, D. M. *Environ. Sci. Technol.* **1985**, *19*, 538–544.
(18) Berner, R. A. *Geochim. Cosmochim. Acta* **1969**, *33*, 267–273.
(19) Ghiorse, W. C. In *Biology of Anaerobic Microorganisms*; Zehnder, A. J. B., Ed.; John Wiley & Sons: New York, 1988; pp 305–331.
(20) Francis, A. J.; Dodge, C. J. *Appl. Environ. Microbiol.* **1988**, *54*, 1009–1014.
(21) Lovley, D. R. *Geomicrobiol. J.* **1987**, *5*, 375–399.
(22) Munch, J. C.; Ottow, J. C. G. *Ecol. Bull.* **1983**, *No. 35*, 383–394.
(23) Lovley, D. R.; Phillips, E. J. P. *Appl. Environ. Microbiol.* **1988**, *54*, 1472–1480.
(24) Atkinson, R. J.; Posner, A. M.; Quirk, J. P. *J. Phys. Chem.* **1967**, *71*, 550–558.
(25) Francis, A. J.; Dodge, C. J. *Arch. Environ. Contam. Toxicol.* **1986**, *15*, 611–616.
(26) Sidhu, P. S.; Gilkes, R. J.; Posner, A. M. *Soil Sci. Soc. Am. J.* **1980**, *44*, 135–138.
(27) Jones, J. G.; Gardner, S.; Simon, B. M. *J. Gen. Microbiol.* **1984**, *130*, 45–51.
(28) Hem, J. D. In *Heavy Metals in the Aquatic Environment*; Krenkel, P. A., Ed.; Proceedings of the International Conference on Water Pollution Research, Nashville, TN, Dec 1973.
(29) Verwey, E. J. W.; Heilmann, E. L. *J. Chem. Phys.* **1947**, *15*, 174–180.
(30) Wells, A. F. *Structural Inorganic Chemistry*; Clarendon Press: Oxford, U.K., 1975; pp 489–495.
(31) Francis, A. J.; Dodge, C. J.; Rose, A. W.; Ramirez, A. J. *Environ. Sci. Technol.* **1989**, *23*, 435–441.

Received for review April 3, 1989. Revised manuscript received October 2, 1989. Accepted November 17, 1989. This research was part of the Subsurface Science Program, performed under the auspices of the United States Department of Energy, Office of Health and Environmental Research, Ecological Research Division, under Contract No. DE-AC02-76CH00016.

Environ. Sci. Technol. 1990, 24, 379–383

Degradation of the Polysaccharide Alginic Acid: A Comparison of the Effects of UV Light and Ozone

M. Shahid Akhlaq, Heinz-Peter Schuchmann, and Clemens von Sonntag*

Max-Planck-Institut für Strahlenchemie, Stiftstrasse 34–36, D-4330 Mülheim a.d. Ruhr, West Germany

■ Oxygenated aqueous solutions of alginic acid, a model compound for polyuronic acids contained in surface waters, were photolyzed in UV light (λ = 254 nm), treated with ozone, or reacted with radiolytically generated hydroxyl radicals. The average molecular weight decrease upon such treatment was measured by viscosimetry. At a fluence of 250 J m^{-2}, which is generally considered sufficient to disinfect drinking water, 0.0005 strand breaks per macromolecule are effected. Alginic acid is capable of complexing ferric ions. Their presence increases photolytic strand-break formation. At an iron concentration of 10^{-6} mol dm^{-3}, such as may prevail after flocculation with iron salts, 0.004 strand breaks per macromolecule are detected at the above fluence. Hydroxyl radicals, produced by subjecting the N_2O/O_2-saturated aqueous alginic acid solution to ionizing radiation from a ^{60}Co γ source, cause strand breakage with an efficiency of 22%, while superoxide radicals are released from the polymer peroxyl radicals with an efficiency of 71%. The efficiency of ozone in producing a strand break is 18%, relative to the total of the ozone consumed. The destruction of the alginic acid by ozone is mainly caused by the intermediate hydroxyl radicals. The polysaccharide peroxyl radicals that are formed by OH attack and subsequent addition of O_2 eliminate superoxide radicals, which in turn stimulate further hydroxyl radical production by reacting rapidly with the ozone.

Introduction

With regard to the procedures employed in the disinfection of drinking water, there is a growing reluctance to continue the use of chlorine and chlorine dioxide. Ozone is often favored as an alternative. In Europe, several large cities such as Amsterdam, Munich, and West Berlin (the latter with a water-main network of 4600 km) have stopped relying on any residual disinfectant in their distribution lines. The prerequisites for this, of course, are high-quality water and well-maintained distribution lines. As the examples show, this can be achieved, and increasingly the question is raised whether it is possible to avoid the use of chemicals altogether and instead disinfect drinking water by means of UV irradiation. This has indeed proven to be a very suitable technique. Large-scale installations were in use already at the turn of this century (cf. ref 1). At present this technique is mainly applied where the raw water carries only a small load of organic matter. It would be a breakthrough if one were to show that this method is also feasible for water from lakes and other sources that contain larger amounts of organic matter. A major component of the organic matter in lake water is the polyuronic acids, which originate from the debris of algae (*2*). These compounds appear to withstand attack by bacteria and other microorganisms reasonably well, but upon ozone treatment, their degradation products favor bacterial regrowth (*3*). This is undesirable where drinking water is concerned. Indications are that these products also impair flocculation (*4*).

In the present work, we have set out to study the degradation of the polysaccharide alginic acid as a reasonably well defined *model compound* of the more complex mixture of polyuronic acids found in lake water. Alginic acids are polymers that mainly consist of 1,4-linked β-D-mannuronic acid (A), with varying amounts of 1,4-linked α-L-guluronic acid (B) (*5*).

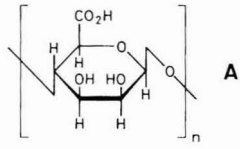

A

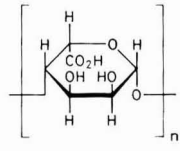

B

It is of interest to compare, with respect to strand-break formation in alginic acid, the effect of UV radiation (254 nm) with that of ozone where hydroxyl radicals are generally thought to play a major role (*6–8*). For this reason, the OH-radical-induced reduction of the molecular weight of the alginic acids was investigated separately, applying the radiation-chemical approach, which is optimally suited to this purpose.

It will be shown that UV light at a fluence of 250 J m^{-2}, which is considered to be sufficient to disinfect drinking water (cf. references given in ref (9), barely affects the alginic acids, while typical ozone treatment (a few milligrams per cubic meter) leads to their extensive degradation.

Experimental Section

Two different kinds of alginic acid were obtained from Sigma. According to our measurements (see below), the "high-viscosity" alginic acid had a molecular weight of 250 kdalton, and the "low-viscosity" one of 100 kdalton. For the most part, the experiments were carried out with the "high-viscosity" material. A typical concentration was 5 $\times$ 10^{-3} mol dm^{-3} in terms of monomer units.

The average molecular weight was determined by viscosimetry using a Ubbelohde capillary viscosimeter (Schott). The Hagenbach–Couette correction (*10*) was applied and the influence of the flow gradient was neglected. For the molecular weight determinations, after UV light, γ radiation, or ozone treatment the solutions were made 5 $\times$ 10^{-2} mol dm^{-3} in NaCl, so that the ionic strength was essentially the same in all of the samples.

For the UV photolysis, a low-pressure mercury lamp (Hanau, Sterisol NN 30/89) was used. The quartz cell, which contained the air-saturated solutions to be irradiated, was placed at a distance of 5.5 cm. The fluence rate at 254 nm was 21.7 W m^{-2} as measured by the ferrioxalate actinometer (*11*). The contribution of the longer wavelength light to the total absorbed by the actinometer was determined at some 10% of the 254-nm light, by inter-

0013-936X/90/0924-0379$02.50/0

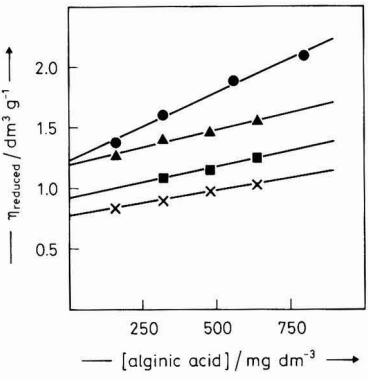

Figure 1. Reduced viscosities of UV-irradiated alginic acid (M_0 = 250 kdalton) containing 1 μmol dm^{-3} Fe(III) ions as a function of alginic acid concentration; (●) unirradiated, (▲) 6000 J m^{-2}, (■) 18 000 J m^{-2}, (×) 30 000 J m^{-2}.

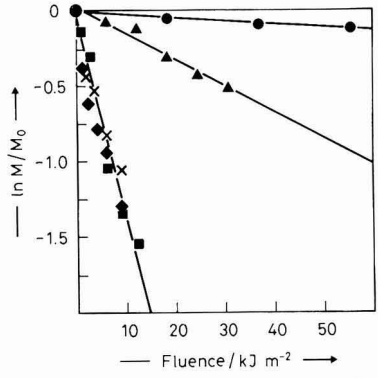

Figure 2. UV-light-induced degradation of alginic acid (1 g dm^{-3}; M_0 = 250 kdalton). The logarithm of the ratio of the average molecular weight over the original molecular weight (M/M_0) is plotted against the fluence of 254-nm quanta; (●) no additive, (▲) 1 μmol dm^{-3} Fe(III) ions, (■), 20 μmol dm^{-3} Fe(III) ions, (◆) 20 μmol dm^{-3} Fe(III) ions and 5 × 10^{-3} mol dm^{-3} tartrate, (×) 20 μmol dm^{-3} Fe(III) ions and 1 × 10^{-2} mol dm^{-3} tartrate.

position of a glass plate shutting out the 254 nm quantitatively but transparent to wavelengths of ≥300 nm.

Each time before an experiment, a stock solution of ozone was prepared by passing an ozone/oxygen mixture (Fischer Ozon-Generator Model OZI), into triply distilled water (pH 6.5) for 25 min. The ozone concentration was measured spectrophotometrically at 260 nm [molar absorption coefficient, 2900 dm^3 mol^{-1} cm^{-1} (*12*)]. Aliquots of this stock solution were added to the alginic acid solutions. Consumption of ozone was complete (10 min) before the viscosimetric experiments were started.

Hydroxyl radicals were generated by ionizing radiation using a ^{60}Co γ source at dose rates of 0.019 and 0.2 Gy s^{-1}. In these experiments, the alginic acid solutions were saturated, not with air, but with a 4:1 mixture of N_2O/O_2 prior to irradiation. Oxygen uptake was measured with an oxygen-sensitive electrode (type OXY 530, Wissenschaftlich-Technische Werkstätten, Weilheim, Germany). In some of the experiments, the formation of acidic products has been monitored by pH and titrimetric measurements.

Results and Discussion

The consequences of chemical attack on a macromolecule can be separated into two categories: (i) introduction of new functionalities without strand cleavage, (ii) modification followed by cleavage. The examination of the frequency of strand breakage is particularly relevant in the context of water treatment, since it is known (*3*) that, at equal organic content, water shows different microbiological behavior (reflected, e.g., in different rates of bacterial regrowth) depending on the relative amount of high molecular weight and low molecular weight impurities.

Determination of the Molecular Weight of the Alginic Acids. This was done by viscosimetry (*13*). The relative viscosities $\eta_{relative}$ were calculated according to eq 1, where t_{sample} and $t_{solvent}$ are the times required for the

$$\eta_{relative} = t_{sample}/t_{solvent} \quad (1)$$

alginic acid solutions and the solvent (water containing 5 × 10^{-2} mol dm^{-3} NaCl) to run through the viscosimeter. The alginic acid samples were diluted, and from the measured relative viscosities, reduced viscosities ($\eta_{reduced}$) were calculated for the various alginic acid solutions (eq 2). The reduced viscosity was plotted against the alginic

$$\eta_{reduced} = (\eta_{relative} - 1)/[\text{alginic acid}]\ (\text{g dm}^{-3}) \quad (2)$$

acid concentration and extrapolated to zero alginic acid concentration (cf. Figure 1). The extrapolated value, the intrinsic viscosity [η], is related to the average molecular weight (M) according to eq 3. The constants K = 3.17 ×

$$[\eta] = KM^{\alpha} \quad (3)$$

10^{-3} and α = 0.875 were taken from the work of Wedlock et al. (*14*). Strand break formation was calculated according to eq 4 where M_0 denotes the original molecular weight, and N is number of breaks per molecule.

$$M_0/M = 1 + N \quad (4)$$

There are good reasons (see below) to believe that the specific properties of the polyelectrolyte under study remain virtually unchanged in the course of the degradation experiments described herein. Thus, viscosimetry is a valid tool to determine the change in the molecular weight of the solute.

UV Irradiation. Pure alginic acid does not absorb significantly at 254 nm, the light emitted by low-pressure mercury lamp used in these experiments. The absorption observed at this wavelength could be partly due to hard-to-remove impurities contained in the alginic acids supplied. For this reason we will not state extinction coefficients or calculate true quantum yields but give reaction cross sections instead (*1*). The cross sections for strand breakage may then be compared with some other cross section, e.g., that of *Escherichia coli* inactivation (*1*). In Figure 2, the logarithm of the ratio of the molecular weight of UV irradiated alginic acid to that of an unirradiated sample is given as a function of dose in terms of fluence. It can be seen that there is a linear relationship. Essentially the same results are obtained with the low-viscosity alginic acid (data not shown), so that in subsequent experiments only the high-viscosity alginic acid was used. From the data shown in Figure 2 it is calculated that at a fluence of 250 J m^{-2} and in the absence of iron ions, 0.0005 strand breaks are formed on average per macromolecule. This is equivalent to a hypothetical quantum yield of ~3 × 10^{-4}, given by the ratio of the number of strand breaks and the number of 254-nm quanta absorbed, assuming that the alginic acid accounts for the entire absorptivity of the solution at this wavelength.

At this point we recall that low concentrations of transition-metal ions such as iron and manganese, in complexation with polysaccharides like the polyuronic acids,

may be present in the raw water to be disinfected. In order to investigate whether or not the presence of these ions influences photoinduced strand breakage, they were added at concentrations of 1 and 20 μmol dm^{-3}. Fe(III) is complexed by the alginic acid; at a pH near 6, where Fe(III) would normally form insoluble hydroxides, no precipitate is formed in the presence of the alginic acid. The nature of this complex is unknown. It shows a somewhat stronger absorption at 254 nm than does alginic acid itself. As can be seen from Figure 2, Fe(III) ions considerably enhance strand breakage. [1 μmol Fe(III) dm^{-3}, 0.004 strand breaks per 250 J m^{-2}; 20 μmol Fe(III) dm^{-3}, 0.04 strand breaks per 250 J m^{-2}]. In contrast to Fe(III), no effect was observed with Mn(II) (data not shown). The enhanced photosensitivity of the iron-containing alginic acids is perhaps due to a reaction akin to the well-known photodecomposition of ferrioxalate (*11*). These phenomena have not yet been investigated in detail [for a review of carbohydrate photochemistry, see ref (15); for the mechanism of the UV-radiation-induced scission of the glycosidic linkage of the related methyl(methyl D-glucopyranosid)uronate, see ref 16; for an early study on the UV-radiation-induced degradation of mucopolysaccharides, see ref 17].

Alginic acid is capable of binding Fe(III) rather tightly. This is proved by the negligible effect on the system of adding hydroxycarboxylic acids, such as tartaric acid, which are known to complex iron ions (*18*, *19*), and which therefore compete with the alginic acid for the Fe(III). However, tartrate added to the iron-containing alginic acids in concentrations equivalent to the concentration of alginic acid subunits, or even twice this value, does not protect the polymer from degradation (see Figure 2).

An additional result is worth noting: the pH does not change during irradiation (according to both pH measurement and titrimetric analysis of irradiated alginic acid solutions, total acid formation is at most 5×10^{-8} mol dm^{-3} at a fluence of 250 J m^{-2}, as indicated by an extrapolation of the data obtained at much higher fluences). This means that no significant change in the intrinsic viscosity is to be expected to account of an ionicity change; any effect would be further reduced by the relatively high ionic strength of the solutions that have been made 5×10^{-2} M in NaCl before the viscosity measurements.

Oxygen uptake measurements reveal (data not shown) that about two molecules of oxygen are consumed per strand break formed. The enhancement of photoinduced strand breakage by Fe(III) ions is also reflected in an increase in the rate of oxygen consumption. This is a strong indication that strand breakage is a major process, and any other oxidative transformation of this polymer cannot be dominant.

Hydroxyl Radicals. These were generated by subjecting N_2O/O_2- (4:1, v/v) saturated alginic acid solutions to ionizing radiation from a ^{60}Co γ source (cf. ref 20). The absorption of the ionizing radiation by the water gives rise to the formation of OH radicals, solvated electrons, and hydrogen atoms (reaction 5). The solvated electrons are converted by N_2O into further hydroxyl radicals (reaction 6). Under these conditions the yield of hydroxyl radicals is $G(^{\bullet}OH) = 0.56$ μmol J^{-1}. The rate constant for the reaction of $^{\bullet}OH$ with the alginic acids (reaction 7) is very likely close to that determined for hyaluronic acid (a carbohydrate polymer that bears some resemblance to the present substrate), for which a value of 7×10^8 dm^3 mol^{-1} s^{-1} has been determined (*21*). The H atoms [$G(H^{\bullet}) = 0.06$ μmol J^{-1}] are scavenged by oxygen, as are the carbohydrate radicals (reactions 8 and 9; $k_8 = 2 \times 10^{10}$ dm^3 mol^{-1} s^{-1} (cf. ref 22), $k_9 \approx 2 \times 10^9$ dm^3 mol^{-1} s^{-1} (cf. ref 23). The superoxide radicals do not react with the carbohydrate (cf. ref 24).

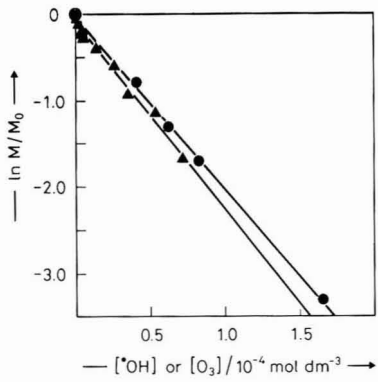

Figure 3. Hydroxyl-radical- and ozone-induced degradation of alginic acid (1 g dm^{-3}; M_0 = 250 kdalton). The logarithm of the ratio of the average molecular weight over the original molecular weight (M/M_0) is plotted against the concentration of hydroxyl radicals (▲) and ozone (●).

$$H_2O \xrightarrow[\text{radiation}]{\text{ionizing}} {}^{\bullet}OH,\ e_{aq}^-,\ H^{\bullet},\ H^+,\ H_2,\ H_2O_2 \qquad (5)$$

$$e_{aq}^- + N_2O \rightarrow {}^{\bullet}OH + OH^- + N_2 \qquad (6)$$

$$RH + {}^{\bullet}OH \rightarrow R^{\bullet} + H_2O \qquad (7)$$

$$H^{\bullet} + O_2 \rightarrow HO_2^{\bullet} \quad pK_a(HO_2^{\bullet}) = 4.8 \qquad (8)$$

$$R^{\bullet} + O_2 \rightarrow RO_2^{\bullet} \qquad (9)$$

The reduction of the molecular weight of the alginic acid is plotted in Figure 3 as a function of the amount (in terms of moles per cubic decimeter) of hydroxyl radical created by the ionizing radiation. The molecular weight as determined by viscosimetry is close to but not identical with the weight average molecular weight. In polymers with a random molecular weight distribution, the weight average molecular weight is twice the number average molecular weight (cf. ref 25). In order to calculate the efficiency of OH radicals and ozone of causing strand breakage, the number average molecular weight of the polymer must be known (see ref 25). In the present system this is not quite the case; only a small error will be introduced, however, if we assume that the average molecular weight as determined by viscosimetry is ~1.8 times the number average weight (cf. ref 26). With this assumption one calculates that hydroxyl radicals cause strand breakage with an efficiency of 22% [G(strand breakage) = 0.12 μmol J^{-1}].

Since the irradiations are carried out in the presence of oxygen, any carbon-centered radicals are rapidly transformed into their peroxyl radicals (reaction 9). In the peroxyl radical chemistry of carbohydrates, large amounts of superoxide radicals are generated in reaction 10 (for

$$HO\text{-}CH_2\text{-}O_2^{\bullet} \rightarrow >C{=}O + O_2^{\bullet -} + H^+ \qquad (10)$$

reviews see refs 20 and 27).

While $O_2^{\bullet}$ is a rather inert radical (*20*, *28*) in most respects, it does stimulate strongly the decomposition of ozone, thereby giving rise to another hydroxyl radical (see below). Thus, it is of interest to know the yield of superoxide radical formation via reaction 10. This has been achieved by reacting, in a separate radiation–chemical

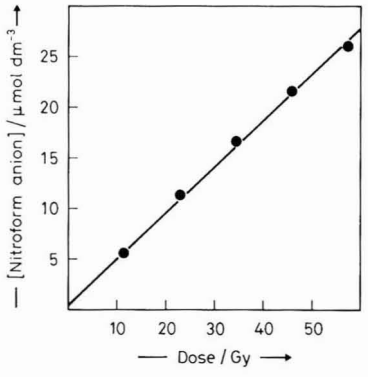

Figure 4. γ Radiolysis of N_2O/O_2-saturated aqueous solutions of alginic acid (1 g dm^{-3}) containing 3×10^{-5} mol dm^{-3} tetranitromethane. The formation of nitroform anions is plotted against the dose.

experiment, the superoxide radical with tetranitromethane (reaction 11). The product, nitroform anion, has a strong

$$O_2^{\bullet-} + C(NO_2)_4 \rightarrow O_2 + C(NO_2)_3^- + NO_2^{\bullet} \quad (11)$$

absorption at 350 nm ($\epsilon = 15000$ dm^3 mol^{-1} cm^{-1}). In the γ radiolysis of N_2O/O_2-saturated solutions of alginic acid (1 g dm^{-3}, pH 6.8) containing 3×10^{-5} mol dm^{-3} tetranitromethane, nitroform anions are produced with a G value of 0.46 μmol J^{-1} (Figure 4). After correcting for the amount of superoxide radical coming from the scavenging of radiolytically produced H atoms [$G(H^{\bullet}) = 0.06$ μmol J^{-1}; reaction 8], the yield of OH-radical-induced superoxide radicals is determined at $G(O_2^{\bullet-}) = 0.4$ μmol J^{-1}. Thus, 71% of the hydroxyl radicals that attack the alginic acid lead to the formation of $O_2^{\bullet-}$. Although the major part of this comes from reaction 10, there might be some other sources besides (cf. refs 20, 29, and 30).

In the past, the scission of the glycosidic linkage of another model compound, cellobiose, induced by hydroxyl radicals in the presence of oxygen, has been studied and many products have been determined (*31*). Analogous products should be formed in the present system where product studies have not yet been performed, but on the basis of recent pulse-radiolytic work on the hydroxyl-radical-induced strand breakage in hyaluronic acid, one expects that strand breakage is mainly caused by the bimolecular decay of those peroxyl radicals that are incapable of eliminating $O_2^{\bullet-}$ (*32*) (for some further hydroxyl-radical-induced degradation studies on this compound see refs 21, 33, and 34). That the ionicity of the polymer cannot change much upon OH-radical attack at the doses applied in these experiments is indicated by the low yield of carbon dioxide, which has been found with a yield of only 0.07 μmol J^{-1} (data not shown). This means that G(decarboxylation) ≤ 0.07 μmol J^{-1}, equivalent to the removal of at most one carboxyl group in a thousand along the polymer strand at a dose of 100 Gy (this corresonds to $\sim 0.6 \times 10^{-4}$ mol dm^{-3} hydroxyl radicals generated in the solution; cf. Figure 3). It is also in line with a very modest conductivity ($G = 0.08$ μmol J^{-1}).

Ozone. Its effect on the reduction of the molecular weight of the alginic acid is also shown in Figure 3. From these data one calculates that ozone produces strand breaks with an efficiency of 18% (with respect to total added ozone).

Ozone does not react rapidly with nonolefinic compounds such as alginic acids. For example, the rate constant for its reaction with glucose is only ~ 0.5 dm^3 mol^{-1} s^{-1} (*35*). In such cases, the hydroxyl radical pathway (cf. reactions 12–15) must predominate (*7*, *8*). For example,

$$OH^- + O_3 \rightarrow HO_2^- + O_2 \quad (12)$$

$$OH^- + O_3 \rightarrow 2O_2^{\bullet-} + H^+ \quad (13)$$

$$HO_2^- + O_3 \rightarrow O_2^{\bullet-} + {}^{\bullet}OH + O_2 \quad (14)$$

$$O_2^{\bullet-} + O_3 + H^+ \rightarrow {}^{\bullet}OH + 2O_2 \quad (15)$$

the decomposition of ozone may be stimulated by the OH^- ion present at low equilibrium concentrations (reactions 12 and/or 13; $k_{12,13} \approx 30$ dm^3 mol^{-1} s^{-1}; and the subsequent reactions 14 and 15, $k_{14} = 5.5 \times 10^6$ dm^3 mol^{-1} s^{-1}, $k_{15} = 1.5 \times 10^9$ dm^3 mol^{-1} s^{-1}) (*35*). An important step in this sequence is the rapid reaction of the superoxide radical with the ozone where an OH radical is regenerated (reaction 15). We have seen above that superoxide is formed abundantly in the hydroxyl-radical-induced peroxyl radical chemistry of alginic acid.

The efficiencies of the hydroxyl radical and of ozone in causing strand breakage in alginic acid are very similar (Figure 3). Considering the preferential formation of superoxide radical (71%; see above), it is very likely that the hydroxyl-radical-mediated pathway of ozone consumption predominates in the degradation of the polysaccharide. The alginic acid system is not accessible to a *complete* product study; this *can* be done, however, with D-glucose, where it has been shown that at pH 6.5 the same products are formed whether the compound is reacted with OH radicals in the presence of oxygen (*36*) or with ozone (*37*). It is revealing that the relative yields of the products are practically the same for these two systems. This observation supports the OH-radical pathway in the degradation of carbohydrates by aqueous ozone.

Conclusion

When one compares the effect of UV radiation with that of ozone, it is reasonable to do so on the basis of a UV fluence of 250 J m^{-2}, which suffices for water disinfection by UV radiation, and a few milligrams per cubic decimeter ozone for disinfection by ozone. We have shown that UV radiation produces hardly any strand breaks (and probably also little in the way of other byproducts), while under the conditions of ozone disinfection, the alginic acids are largely degraded. This remains true even for drinking water that has undergone Fe(III) flocculation. This treatment causes a Fe(III) concentration of ~ 1 μmol dm^{-3} to become established. We have seen above that even though this increases the frequency of polymer strand cleavage by a factor of 10, the effect is still comparatively small (0.004 strand breaks at a fluence of 250 J m^{-2}). This means that the polysaccharide component of surface waters remains essentially unaffected by UV disinfection. This is an important point, since high molecular weight material cannot be used as a nutrient by bacteria as easily as low molecular weight material (cf. ref 3). This has a bearing on the speed of bacterial regrowth. One would therefore assume that in this respect UV-disinfected water behaves superior to ozone-disinfected water.

Acknowledgments

We thank Prof. G. Fink for valuable discussions.

Registry No. $^{\bullet}OH$, 3352-57-6; Fe, 7439-89-6; alginic acid, 9005-32-7.

Literature Cited

(1) von Sonntag, C. In *Tenth Brown Boveri Symposium on Process Technologies for Water Treatment*; Stucki, S., Ed.; Plenum: New York, 1988; p 159.

(2) Hoyer, O.; Lüsse, B.; Bernhardt, H. *Z. Wasser Abwasser Forsch.* **1985**, *18*, 76.
(3) Maier, D.; Kurz, R. *Proceedings, Int. Symp. Ozon und Wasser*: Berlin, 1977; p 211.
(4) Hoyer, O.; Bernhardt, H.; Lüsse, B. *Z. Wasser Abwasser Forsch.* **1987**, *20*, 123.
(5) Clark, A. H.; Ross-Murphy, S. B. *Adv. Polym. Sci.* **1987**, *83*, 57.
(6) Hoigné, J.; Bader, H. *Water Res.* **1976**, *10*, 377.
(7) Glaze, W. H. *Environ. Sci. Technol.* **1987**, *21*, 224.
(8) Staehelin, J.; Hoigné, J. *Vom Wasser* **1983**, *61*, 337.
(9) Martiny, H.; Wlodlavezyk, K.; Harms, G.; Rüden, H. *Zentralbl. Bakteriol., Mikrobiol. Hyg.* **1988**, *B185*, 350.
(10) Elias, H.-G. *Makromoleküle, Struktur, Eigenschaften, Synthese, Stoffe*; Hüthig und Wepf: Basel, 1975; p 290.
(11) Calvert, J. G.; Pitts, J. N. *Photochemistry*; Wiley: New York, 1966; p 783.
(12) Bühler, R. E.; Staehelin, J.; Hoigné, J. *J. Phys. Chem.* **1984**, *88*, 2560.
(13) Meyerhoff, G. *Fortschr. Hochpolym.–Forsch.* **1961**, *3*, 59.
(14) Wedlock, D. J.; Fasihuddin, B. A.; Phillips, G. O. *Int. J. Biol. Macromol.* **1985**, *8*, 57.
(15) Binkley, R. W. *Adv. Carbohydr. Chem. Biochem.* **1981**, *38*, 105.
(16) Bradbury, A. G. W.; von Sonntag, C. *Carbohydr. Res.* **1978**, *60*, 183.
(17) Balazs, E. A.; Laurent, T. C.; Howe, A. F.; Varga, L. *Radiat. Res.* **1959**, *11*, 149.
(18) Ramamoorthy, S.; Manning, P. G. *J. Inorg. Nucl. Chem.* **1972**, *34*, 1977.
(19) Perrin, D. D. *IUPAC Chem. Data Ser.* **1979**, *No. 22*.
(20) von Sonntag, C. *The Chemical Basis of Radiation Biology*; Taylor and Francis: London, 1987.
(21) Myint, P.; Deeble, D. J.; Beaumont, P. C.; Blake, S. M.; Phillips, G. O. *Biochim. Biophys. Acta* **1987**, *925*, 194.
(22) Buxton, G. V.; Greenstock, C. L.; Helman, W. P.; Ross, A. B. *J. Phys. Chem. Ref. Data* **1988**, *17*, 513.
(23) Adams, G. E.; Willson, R. L. *Trans. Faraday Soc.* **1969**, *65*, 2981.
(24) Schuchmann, M. N.; von Sonntag, C. *Z. Naturforsch.* **1978**, *33B*, 329.
(25) Lemaire, D. J. E.; Bothe, E.; Schulte-Frohlinde, D. *Int. J. Radiat. Biol.* **1987**, *51*, 319.
(26) Donnan, F. G.; Rose, R. C., *Can. J. Res.* **1950**, *28B*, 105.
(27) von Sonntag, C. *Adv. Carbohydr. Chem. Biochem.* **1980**, *37*, 7.
(28) Bielski, B. H. J.; Cabelli, D. E.; Arudi, R. L.; Ross, A. B. *J. Phys. Chem. Ref. Data* **1985**, *14*, 1041.
(29) Schuchmann, M. N.; von Sonntag, C. *Z. Naturforsch.* **1987**, *42B*, 495.
(30) Das, S.; Mieden, O. J.; Pan, X.-M.; Repas, M.; Schuchmann, M. N.; Schuchmann, H.-P.; von Sonntag, C.; Zegota, H. In *Oxygen Radicals in Biology and Medicine*; Simic, M. G., Taylor, K. A., Ward, J. F., von Sonntag, C., Eds.; Plenum: New York, 1988; p 55.
(31) Schuchmann, M. N.; von Sonntag, C. *Int. J. Radiat. Biol.* **1978**, *34*, 397.
(32) Deeble, D. J.; Bothe, E.; Phillips, G. O.; Schuchmann, H.-P.; von Sonntag, C. *Radiat. Phys. Chem.*, in press.
(33) Hall, A. N.; Phillips, G.O.; Rasool, S. *Carbohydr. Res.* **1978**, *62*, 373.
(34) Lal, M. *J. Radioanal. Nucl. Chem.* **1985**, *92*, 105.
(35) Neta, P.; Huie, R. E.; Ross, A. B. *J. Phys. Chem. Ref. Data* **1988**, *17*, 1027.
(36) Schuchmann, M. N.; von Sonntag, C. *J. Chem. Soc., Perkin Trans. 2* **1977**, 1958.
(37) Schuchmann, M. N.; von Sonntag, C. *J. Water Supply Res. Technol.—Aqua* **1989**, *38*, 311.

Received for review June 16, 1989. Accepted November 15, 1989. This work has been supported by the Bundesministerium für Forschung und Technologie, Project 02-WT 8720 (Initiator, Prof. G. O. Schenck; Coordinator, Prof. H. Bernhardt).

CORRESPONDENCE

Comment on "Acidification of Adirondack Lakes"

SIR: Asbury et al. have addressed several important details necessary for a quantitative reconstruction of acidification trends in Adirondack lakes from 1929 to 1985 (*1*). We have examined additional critical assumptions that control the feasibility and reliability of such a quantitative reconstruction, using the 1929–1934 methyl orange (MO) alkalinity determinations. In this letter we summarize these results, concluding that the historic Adirondack MO alkalinity measurements have too many important, confounded errors and are too imprecise to be used in any quantitative trend analysis.

The most important source of bias accounted for by Asbury et al. is the overestimation of acid neutralizing capacity (ANC) during MO titrations (*1*), which usually continue to a fixed pH end point that is more acid than a modern Gran potentiometric determination would be for the same lake water sample. The crux of their argument is that the MO titration end point occurs at a mean pH of 4.25 (±0.10 = 2*s*, n = 60, ANC = 85 μequiv/L) (*1*) compared to an end point pH of 4.04 (±0.10, n = 24, ANC = 162 ± 1 μequiv/L) reported by Kramer and Tessier (*2*). Kramer et al. (*3*) presented both the 4.04 and a 4.19 (based on unpublished materials) pH unit end point for correcting MO alkalinity determinations in their study for the National Academy of Sciences.

Either documented approach (*1*, *2*) is affected by the accuracy and precision of the pH electrode measurement of the end point, plus the subjective choice of what is "faintest pink" (*2*) at the end point. Asbury et al. (*1*) have estimated the precision of the MO end points by a single pH measurement following 60 MO ANC titrations of one water sample by students. The ANC determined with a MO titration also depends on the accuracy of the end point pH measurement, which we estimated without pH electrodes, but was not accounted for by Asbury et al. Past quantitative investigations of pH indicator color changes have considered the sharpness of transition at the equivalence point (*5*, *6*), but only for concentrated buffer solutions.

Using a high precision spectrophotometer and the unacidified methyl orange sodium salt (*3*, *4*) (0.500 g/1000 g of solution) (*2*) at a concentration of 2 drops of MO (1 drop = 0.041 g ± 0.007 (2*s*), n = 30) per 50 mL of sample (*2*), we have measured the absorbance of dilute HCl standards, made to within ±0.003 pH unit (*7*) (except pH 5.00, within ±0.01 pH unit). With this approach we can analyze the determination of end point color on a quantitative basis. Other studies rely on pH electrode measurements, which contribute an additional imprecision of at least ±0.05 pH unit, 2*s* (*7*) and unknown bias. Table I summarizes the most important results from 25 absorbance spectra scanned from 200 to 700 nm with a Nicolet-Phillips Analytical Cambridge 8740 UV/vis scanning spectrophotometer to within ±0.001 absorbance unit within ±0.3 nm of the stated wavelength.

When the sample's pH is equal to the "apparent" dissociation constant of the indicator, the ratio [yellow form MO]/[red form MO] becomes equal to 1, and the indicator ideally will have a color due to an equal mixture of the "acid" and "alkaline" forms (*8*). In order to make such a comparison, concentration and absorbance must be linearly related at a given wavelength. We have verified that the Beer–Lambert law holds at up to 5 times the MO additions used in these experiments, as earlier workers have also observed (*9*). From Table I, the solution with a pH of 4.04 has the ratio of "yellow" to "red" absorbance equal to 1.0, but the "relative visibility factor" (relating the normal response to radiation of equal intensity) of the human eye is 0.004 at 420 nm and 0.710 at 520 nm (*10*). This means the eye is more sensitive to red than yellow solutions of equal absorbance. Thus, the pH 4.04 solution appears with a slight reddish tint, "faintest pink" (*1*), analogous to the MO titration end point. This is in agreement with the beginning of color change for similar solutions as reported by Kolthoff and Stenger (*11*). A visual comparison of the pH 4.25 and pH 4.35 solutions resulted in them being classified as the same color, a faint yellow. The pH 4.19 and pH 4.15 solutions occupy a region of transition between faint yellow and faint pink, with the actual point of demarcation being subject to individual preference, training, and confounding parameters affecting the chemistry, such as the presence of dilute amounts of organic acids. Several of these sources of variability are fixed in Asbury et al.'s estimation of the MO pH end point, which may result in statistical bias.

Table I. Absorbance Values for "Yellow", "Red", and Peak Wavelengths of Methyl Orange in Dilute HCl Standards

	absorbance		peak absorbance		
HCl std pH	"yellow" 422 nm	"red" 522 nm	λ, nm	Abs	ratio of yellow/red
2.04	0.001	0.127	508	0.135	0.008
3.02	0.006	0.063	506	0.070	0.1
4.04	0.021	0.021	480	0.042	1.0
4.15	0.029	0.024	474	0.050	1.2
4.19	0.028	0.018	474	0.051	1.6
4.25	0.025	0.016	474	0.044	1.6
4.35	0.023	0.010	471	0.041	2.3
5.00	0.035	0.015	467	0.052	2.3

The visible absorbance spectra observed in this work did not show bimodal distributions of peak absorbance corresponding to color. Instead, one absorbance peak shifted from more "yellow" wavelengths to more "red" wavelengths as the pH decreased (Table I). Obviously, we have no way of distinguishing quantitatively which subjective color end point (hence, end point pH) different analysts actually chose during the 1920–1930s. It is likely that such early work showed at least the disagreement (imprecision) seen between the modern studies (*1–3*).

A lesser concern is the average MO alkalinity correction reported by Asbury et al. (*1*) (−54.6 μequiv/L at pH 4.25) and Kramer and Tessier (*2*) (−81 μequiv/L at pH 4.04). Table II shows the results of our calculations for a MO alkalinity correction (for MO end point of pH 4.04), which varies with the dissolved inorganic carbon content (DIC) of a water sample. The calculations are based on Kramer et al.'s Appendix D, eqs 1b, 4b, 4d, and 7g (*3*).

Table II shows a representative range of corrections

 0013-936X/90/0924-0384$02.50/0

Table II. Variation of Methyl Orange Alkalinity Corrections with Dissolved Inorganic Carbon at pH 6[a]

DIC, mg/L	relation to DIC population of ELS-I region 1 lakes[b]	concn, μequiv/L		
		$[Alk_{MO}]$	[Alk]	corrctn
0.2	min. observed DIC (region 1)	96.2	4.1	−91.1
0.6	20th percentile DIC (region 1A)	106.3	14.4	−91.0
1.6	50th percentile DIC (region 1A)	131.5	40.0	−90.5
3.3	80th percentile DIC (region 1A)	174.4	83.6	−89.8
13.3	95% confid limit DIC (region 1)	426.5	339.8	−85.7
49.0	max. observed DIC (region 1)	1326.5	1254.6	−70.9

[a] At other pH values, $[Alk_{MO}]$, and [Alk] values will change, but the correction factor remains constant. [b] References 12 and 13.

calculated for DIC concentrations measured during the EPA's 1984 Eastern Lake Survey—Phase I (*12*, *13*). Region 1A contains the Adirondack lakes greater than or equal to 4 ha surface area. These are a subset of lakes sampled in region 1, also including Central and Southern New England, Maine, and the Poconos/Catskills. As a result, the MO alkalinity correction in the Adirondacks region should vary from about −91 to −86 μequiv/L, depending on a sample's inorganic carbon concentration, rather than the average correction of −54.6 μequiv/L used by Asbury et al. (*1*) (Table II). Although the individual $[Alk_{MO}]$ and [Alk] values vary as a function of pH, the MO correction does not and is dominantly controlled by the variation of [DIC].

An additional complication, which we have not noticed in the modern acidification literature, concerns the inability of MO to react with weak acids, such as organic acids (*4*, *14*). Stieglitz (*4*) hypothesized that the red form of MO reacted as a very weak base; "red" salts of weak acids were "completely hydrolyzed and incapable of existence, the liberated base reverting ... to the stable yellow isomer. That is why methyl orange is not a sensitive indicator for weak acids". This effect could prevent the detection by MO of weak acids that contribute to a solution's ANC as determined by modern potentiometric methods, resulting in underestimates of ANC. Alternatively, these reactions could also result in a higher MO pH than a potentiometric pH in the presence of organic acids, causing more titrant to be added to the fixed end point, resulting in a higher historic ANC value than would be determined potentiometrically. Additional work is necessary in order to understand the interaction of MO with organic acids during acid titrations of dilute solutions (ref 3, Appendix D). The dissolved organic carbon content (DOC) (used as a measure of organic acid content) could be approximated as we have used the modern data from the Eastern Lake Survey—Phase I. However, this would be a poor approximation to the actual lake DOC of the 1920–1930s. The qualitative correlation between high DOC content and increasing lake color is well-known, and unfortunately, one of the qualitative observations for acidification is that some lakes have turned clear since that time, which implies past lake DOC concentrations were different from today's observations.

We thank D. Heggem, U.S. E.P.A., EMSL—Las Vegas, for providing support and encouragement during the preparation of this manuscript.

Registry No. Water, 7732-18-5; methyl orange, 547-58-0.

Literature Cited

(1) Asbury, C. E.; Vertucci, F. A.; Mattson, M. D.; Likens, G. E. *Environ. Sci. Technol.* **1989**, *23*, 362–65.
(2) Kramer, J. R.; Tessier, A. *Environ. Sci. Technol.* **1982**, *16*, 606A–15A.
(3) Kramer, J. R.; Andren, A. W.; Smith, R. A.; Johnson, A. H.; Alexander, R. B.; Oehlert, G. In *Acid Deposition: Long Term Trends*; National Research Council; National Academy Press: Washington, DC, 1986; p 231.
(4) Stieglitz, J. *J. Am. Chem. Soc.* **1903**, *25*, 1112–27.
(5) Cacho, J.; Nerin, C.; Ruberte, L.; Rivas, E. *Anal. Chem.* **1982**, *54*, 1446–49.
(6) Bhuchar, V. M.; Kukreja, V. P.; Das, S. R. *Anal. Chem.* **1971**, *43*, 1847–53.
(7) Metcalf, R. C. *Analyst* **1987**, *112*, 1573–77.
(8) Bassett, J.; Denney, R. C.; Jeffery, G. H.; Mendham, J. *Vogel's Textbook of Quantitative Inorganic Analysis including Elementary Instrumental Analysis*; Longman: London, 1978.
(9) Sidgwick, N. V.; Worboys, W. J.; Woodward, L. A. *Proc. R. Soc. London* **1930**, *A129*, 537.
(10) Born, M.; Wolf, E. *Principles of Optics*, 2nd ed.; Macmillan: New York, 1964; p 185.
(11) Kolthoff, I. J.; Stenger, V. A. *Volumetric Analysis*, 2nd ed.; Wiley: New York, 1947; Vol. II, pp 57–62.
(12) Linthurst, R. A.; et al. *Characteristics of Lakes in the Eastern United States. Volume I: Population Descriptions and Physico-Chemical Relationships*; EPA600/4-86/007a; U.S. Environmental Protection Agency: Washington, DC, 1986.
(13) Overton, W. S.; et al. *Characteristics of Lakes in the Eastern United States. Volume II: Lakes Sampled and Descriptive Statistics for Physical and Chemical Variables*; EPA600/4-86/007b; U.S. Environmental Protection Agency: Washington, DC, 1986.
(14) Windholz, M., Ed. *The Merck Index*, 10th ed.; Merck & Co.: Rahway, NJ, 1983; p 874.

Richard C. Metcalf,* Robert W. Gerlach

Environmental Chemistry
Assessment and Quality Assurance Department[†]
Lockheed Engineering & Sciences Company
1050 E. Flamingo Road, Suite 209
Las Vegas, Nevada 89119

[†] Although the information in this letter has been funded in part by the United States Environmental Protection Agency under Contract 68-03-3249 to Lockheed Engineering & Sciences Co., it has not been subjected to Agency review. It therefore does not necessarily reflect the views of the Agency and no official endorsement should be inferred. The mention of trade names or commercial products does not constitute endorsement or recommendation for use. This work is a contribution to the United States Environmental Protection Agency's Aquatic Effects Research Program, which is a part of the National Acid Precipitation Assessment Program.

SIR: Asbury et al. (*1*) recently gave an assessment that suggests that there has been a median decrease in alkalinity of ~50 μequiv/L from the 1930s to the 1970–1980s for surface waters of the Adirondack region of New York. They contrast their results to those reached in a National Research Council (NRC) report (*2*), which concluded that there was a median loss of alkalinity between 0 and 44 μequiv/L. The Asbury et al. report also makes various claims to suggest that the "no change" conclusion of the NAS report is wrong. I disagree with this conclusion for the reasons stated below. I also restate important points of the NRC report that were not considered in the Asbury et al. report.

First, the problem of making a clear statement on change in alkalinity (actually acid neutralizing capacity) or change in pH for data in the 1930s is difficult because the unknowns in the colorimetric analyses are as large or larger than inferred change. The NRC report (*2*) was very clear on this point and presented a quite lengthy discussion on the nature of and magnitude of errors, which the Asbury et al. report does not consider. For example, contrary to the assertion of Asbury et al., "... in favor of direct comparison of alkalinity values which can be determined *with great precision* ..." (emphasis mine), the methyl orange

alkalinity method (MO) is not precise. Precision for the MO method in the laboratory is 20 μequiv/L (*3*) and the estimated repeatability is 53 μequiv/L (ref 2, p 273). The MO standard method used is not sensitive for analysis of these low alkalinity lakes. About 0.1 mL of titrant is equal to 20 μequiv/L. Thus, the median alkalinity change suggested by Asbury et al. of 50 μequiv/L is equal to the estimated repeatability of the method, or 0.25 mL (~5 drops) of titrant.

The lack of assessment and inability to assess other factors that would increase or decrease the estimate of loss of alkalinity is even more significant. I suggest the following biases that need to be assessed:

factor	for change in alkalinity, μequiv/L loss	gain
methyl orange end point adjusted for carbonate system		50–100
use of soft glass or porcelain titration dish in 1930s		0–100
organic acid correction for ANC	20–100	
CO_2 contamination of base (for CO_2 acidity)	0–20	

This table shows that there are probable gains or losses of alkalinity as large or larger than the loss estimated by Asbury et al.

The correction to the MO end point for low-alkalinity waters depends almost entirely upon the pH for the MO end point. For example, the median correction of Asbury et al. of 54.6 μequiv/L is within 1.6 μequiv/L of their assumed end point of 4.25; and the difference by using the MO pH end point of 4.04 can be resolved within 6 μequiv/L. The problem of accurately specifying the MO pH end point was discussed at length in the NRC report, which concluded (ref 2, pp 264–266) that a range between pH 4.0 and 4.19 was the most probable. The report made the judgment upon the following: blank and known alkalinity titrations by Kramer and Tessier (*3*) gave an average correction of 91 μequiv/L (pH 4.04); Taylor, in 1933, determined the correction for blanks was between 66 (pH 4.19) and 88 μequiv/L (pH 4.06) (he favored 66 μequiv/L); Kolthoff and Stenger (*4*) noted that the MO correction is ~100 μequiv/L, equal to a pH of "4.0"; Eilers et al. (*5*) used a regression between alkalinity and specific conductance to obtain a correction of 64 μequiv/L (pH 4.19). The pH of the MO change for dilute or blank solutions for these assessments would range between 4.0 (Stenger and Kolthoff) and 4.19 (Eilers et al.), which were the limits that the NRC report used.

It is important to note that all of the studies used in the NRC report used the actual difference between the known alkalinity of a dilute solution or blank and that obtained by the addition of titrant. On the other hand, the Asbury et al. study relied upon correctness of the pH electrode measurement (which must be concentration based and not activity based) for the MO end point. Asbury et al. contend that they are correct. I do not wish to debate which value(s) is (are) correct, but I wish to emphasize the variability in the end point for well-defined studies is nearly as large as the change inferred.

In the NRC report, we realized the difficulty in establishing a narrow limit for the MO correction. Therefore we estimated alkalinity in a second way, using total carbonate and pH. Total carbonate was estimated from the sum of the adjusted alkalinity and adjusted acidity (base titration to the phenolphthalein end point). The colorimetric pH also had to be adjusted. In order to make this second estimate of alkalinity, we had to know the colorimetric pH dye, we had to assume that carbonato species were the major protolytes, we had to assume that the base titration represented the same total carbonate as at the time of the colorimetric pH measurement, and we assumed that the CO_2 contamination of the base titrant was negligible. As Asbury et al. state, the New York study did not specify the pH colorimetric indicators. But the adjacent New Hampshire study did specify these indicators, and we assumed that New York used the same set of indicators. All of these assumptions were clearly stated in the NRC report.

The second alkalinity, calculated from the total carbonate and pH, was compared to the first alkalinity obtained by adjustment of the MO acid titration. We established a subset of data for those alkalinities agreeing within 50 μequiv/L. We also checked for any bias by comparing the subset to the entire data set (ref 2, p 280). We concluded that there was no bias.

We were also aware of major problems with the first New York DEC study as well as possible bias by addition of limed lakes, thanks to F. A. Vertucci, one of the authors of the Asbury et al. report. Therefore we compared results for the 1984 and 1980 New York DEC reports, using both the MO end points of 4.04 and 4.19 and the two data sets for 1930s data (ref 2, p 278). Asbury et al. suggest that we were not aware of problems with the recent New York DEC data, effect of limed lakes, and infer a bias due to use of a subset of alkalinity data. All of these concerns are discussed in the NRC report and are invalid comments in their paper.

Asbury et al. note that "... we find significant acidification of the lakes ($\alpha < 0.01$) even if we apply the pH 4.04 correction ...". I question this conclusion, since the major discrepancy in the two studies reduces to a difference in the MO end point, which is approximately 35 μequiv/L, resulting in ~15 μequiv/L loss for the Asbury et al. median loss.

A side issue is the concern by Asbury et al. of the incorrect formulation of the colorimetric pH dye. They cite a personal communication with J. Esposito, Hellige Co., New York, in 1985. The early studies indeed used Hellige comparators, but they were *not* the same comparators or chemicals used now. Hellige Co., New York, in the 1930s, was part of Hellige of Freiberg, Germany. We have confirmed with Hellige, Germany, that indeed they always used Merck indicator dyes. We used the 1920–1930s Merck Index recipe in our calculations, which is the same as that given in texts of the 1930s as well as Standard Methods.

The use of colorimetric pH is, however, problematical for different reasons, and I would caution against using historic colorimetric data alone for pH reconstruction. The reason for this concern is the very poor sensitivity of the bromthymol blue (BTB) dye in the pH 4–7 range. For a dilute carbonato system, one may measure a BTB colorimetric pH in the 6s, which actually spans ~2 pH units, given a colorimetric precision of ±0.2. The lack of sensitivity of colorimetric pH data can also be seen in a recent study by Blakar and Digernes (*6*).

There are other important potential biases in the comparison. The use of soft glass or porcelain crucibles in the 1930s will yield an alkalinity increase of up to 100–200 μequiv/L (*3*, *7*). If the soft glass is well aged, the effect may be small. Thus this contamination can cancel any estimation showing a loss of alkalinity over time.

On the other hand, the incorporation of organic acids will tend to lower the equivalence point pH, having the effect of a greater loss of alkalinity over time. Since Gran's

method, if carried out correctly, was used on recent samples, the acid neutralizing capacity (ANC) as referenced to the equivalence point should be used in past and present data. The equivalence point conditions would be satisfied by

$$[H]_e \sim [HCO_3^-]_e + [other^-]_e$$

where brackets refer to concentrations, the subscript, e, specifies the equivalence point and [other] are other reacting protolytes. We assume that [others] are mostly organic acids. Both the NRC study and the Asbury et al. study did not consider the influence of organics. The addition of organic acids generally would decrease the pH of the equivalence point. For example, a "back-of-the-envelope" calculation, using 40 μequiv/L organic acid (from the median dissolved organic carbon estimate for the Adirondacks and a factor of 10 μequiv/mg of C) and an average of pK of 4.2 for organic acids (*8*), gives an equivalence pH of 4.56. This adjustment for organic acids in the past data would result in a greater loss of alkalinity of ~30 μequiv/L.

An additional aspect that neither report tried to assess was the seasonal change in alkalinity and the potential bias due to mismatch of sampling periods. The recent EPA study attempted to obtain a homogeneous sample by sampling after lake overturn in the fall. Most of the 1930s studies were carried out between June and August. This factor needs to be assessed further as there are important biological and hydrological factors that affect short-term changes in lake chemistry of these small lakes.

There are some other points for discussion, perhaps of value for ongoing studies. Overall, the 1930s New York surveys are poorly documented. A footnote reference to the Standard Methods of the time was all that was made for the chemical analyses. There were no replicates, blanks, or other quality assurance procedures documented. The closest one might come to estimation of replication would be to compare results of more than one analysis for a given lake, but this comparison would require an assumption of chemical homogeneity for a water body. The parallel New Hampshire study is documented better, the specific dyes and their ranges are discussed, replicate sampling of one depth was routine, and replicate lake profiles are given. The NRC report (ref 2, pp 272–273) relied upon the New Hampshire data for quality assurance assessments and had to assume that procedures, precision replication, etc. for New York were the same as for New Hampshire studies. The Wisconsin reports, carried out at the University of Wisconsin, are by far the best documented with detailed studies on the indicator problem, blank studies, seasonal analysis, etc. The lesson is that surveys require a rigorous quality assurance protocol if they are to be useful.

In summary, given the poor precision and sensitivity of the MO alkalinity technique and given that the corrections required are in the same range as the proposed change in alkalinity, I doubt whether a definitive answer on change in ANC over time can be stated. In addition to the debate over the MO end point, both the NRC study and the Asbury et al. study did not (could not) consider a number of other important factors, as discussed above, in their calculations. An attempt to understand those specific examples that show apparent large changes (both increase and decrease) in alkalinity might be more valuable (e.g., ref 2, p 285).

Registry No. Water, 7732-18-5; methyl orange, 547-58-0.

Literature Cited

(1) Asbury, C. E.; Vertucci, F. A.; Mattson, M. D.; Likens, G. E. *Environ. Sci. Technol.* **1989**, *23*, 362.
(2) Kramer, J. R.; Andren, A. W.; Smith, R. A.; Johnson, A. H.; Alexander, R. B.; Oehlert, G. In *Acid Deposition: Long Term Trends*; National Research Council; National Academy Press: Washington, DC, 1986; p 231 ff.
(3) Kramer, J. R.; Tessier, A. *Environ. Sci. Technol.* **1982**, *16*, 606A.
(4) Kolthoff, I. M.; Stenger, V. A. *Volumetric Analysis. Titration Methods*; John Wiley and Sons: New York, 1947; Vol. II, pp 61–62.
(5) Eilers, J. M.; Glass, G. E.; Pollack, A. K. Water quality changes in northern Wisconsin lakes, 1930–1980. RL-D Draft 539; U.S. Environmental Protection Agency.
(6) Blakar, I. A.; Digernes, I. *Verh. Int. Ver. Limnol.* **1984**, *22*, 679.
(7) Bacon, F. R.; Burch, D. G. *J. Am. Ceram. Soc.* **1941**, *24*, 29.
(8) Perdue, E. M. In *Humic Substances in Soils, Sediment and Water*; Wiley-Interscience: New York, 1985; pp 504.

James. R. Kramer

Department of Geology
McMaster University
1280 Main Street West
Hamilton, Ontario, Canada L8S 4M1

SIR: The historic chemical data available for lakes in the Adirondack Mountain region of New York provide a rare opportunity to measure directly the magnitude of lake acidification. Our conclusions about lake acidification (*1*) have been questioned by Kramer (*2*) and Metcalf and Gerlach (*3*). Kramer (*2*) suggests that we did not consider important points related to the validity of the methods employed by Kramer et al. (*4*) in the study of lake acidification. Although it is fair to evaluate our work on the basis of our published results, our original version submitted to ES&T considered many additional points, but was reduced by editorial constraints.

We considered two types of errors in our paper: precision and bias. As we stated, bias is the important consideration because the low precision was overcome by the large number of lakes used in the analysis; any bias present in the data, however, indeed could have contributed to erroneous conclusions about acidification in these lakes. Both Kramer et al. (*4*) and our study examined possible sources of bias in detail. The differences in the results of our studies appear to be largely the result of differing methods used to correct for or eliminate such bias in these data.

As Kramer pointed out in ref 2, an important difference in the correction for bias was the treatment of the methyl orange (MO) titration end point. For their estimate of acidification in Adirondack lakes, Kramer et al. (*4*) used two pH values of the MO end point, 4.04 and 4.19, concluding that the occurrence of acidification of these lakes was sensitive to the choice between these end points. In our view they also implied that it was equally likely that either of these end points was used by the historic survey, and thus that a conclusion regarding acidification would be ambiguous. Our experimental results quantifying the MO end point, and other information gathered from the literature, led us to conclude that it is not equally likely that these two end points were used. Instead, we found that the most likely MO end point was pH ~4.2–4.3.

In Table I we summarize information on the MO end point pH, much of it also discussed by Kramer et al. in ref 4. We concluded that different color end points have been used with this indicator; we believe that these end points have been the cause of much of the controversy over the historic use of this indicator. We found substantial agreement that a color transition in MO from yellow to

0013-936X/90/0924-0387$02.50/0

Table I. Methyl Orange End Points for Alkalinity Titrations As Determined from Different Sources

color	end point pH	alk corrctn[a]	method[b]	ref
"orange"	4.6	21	a	5
"orange"	4.6	21	b	6
"faint orange"	4.6	21	a	7
"deeper orange"	4.4–4.5	37–29	a	7
"definite orange"[c]	4.0–4.27	99–52	c	8
"faintest pink"	4.04	90	d	9
"faintest pink"	4.3–4.5	48–29	c	8
"faintest pink"	4.25	55	e	1
"very faint pink"	4.3	48	b	6
"fainter end point"	4.18	65	f	10
"pink"	4.0	99	b	6
"pink"	4.0	99	a	5

[a] For comparison; theoretical value calculated for a pure solution with CT = 225 μM (equivalence point pH 5.0). [b] Methods: (a) not given; (b) titration of standard $CaCO_3$ solution by two analysts; (c) titration of waters of various alkalinities by several analysts; (d) titration of diluted Lake Ontario water by three analysts; (e) titration of Mirror Lake, NH, water by 20 analysts; (f) titration of boiled distilled water by one analyst; value shown is given as "safest blank to use". [c] The pH range given for this color appears to be inconsistent with the range for "faintest pink" cited in the same study (*8*), but Haines explained that two independent groups of analysts were working from different sets of instructions defining the end point color. The group titrating to the "faintest pink" end point was following the methods used in the New York survey.

yellow-orange and orange occurs at pH ~4.6 and that the color changes further to faint pink at pH ~4.2–4.3 and to pink at pH ~4.0. Kramer and Tessier (*9*) found a lower mean "faintest pink" end point (pH 4.04), based on work of three analysts; however, this mean value (precision of 0.1 with 2 degrees of freedom based on three analysts) may not be statistically different from other reported values as large as pH 4.2–4.3. We were uncomfortable about inclusion in Table I of Kolthoff and Stenger (*11*), (cited as supporting evidence by refs 2 and 4), because all other works in the table discuss alkalinity titrations specifically, while ref 11 is a general work, and because we found contradictory information regarding the pH range of MO at several points in the book.

We are aware that the contradictory discussions of this subject in refs 1, 2, and 4, as well as here, may be taken by some as evidence enough that the correct historic MO end point cannot be determined unambiguously. We suggest that the interested reader may wish to obtain direct evidence on this matter by preparing a series of water samples containing MO indicator (concentrations given in ref 12), within the range of pH 3.5–6, and examining the series for the pH at which the color first begins to change, i.e., "the faintest pink coloration appears: that is, until the color of the solution is no longer pure yellow" (*12*). According to the documentation of the historic New York survey, this pH should be an estimate of the pH used for alkalinity titrations in that survey. We have found 13 general works on chemistry in addition to the information in Table I, which refer to the beginning of the MO color transition as occurring at pH 4.4 or above.

We are puzzled by Metcalf and Gerlach's (*3*) use of spectrophotometry data to attempt to show the end point of field alkalinity titrations. The problem is to determine the pH to which human technicians, employing MO indicator but unaided by spectrophotometers, titrated lake samples to "faintest pink" color. Clearly the choice of the absorbance ratio of 520 nm (yellow) to 420 nm (red) of unity is extremely arbitrary, and no evidence is given by the authors that such a ratio corresponds to the color

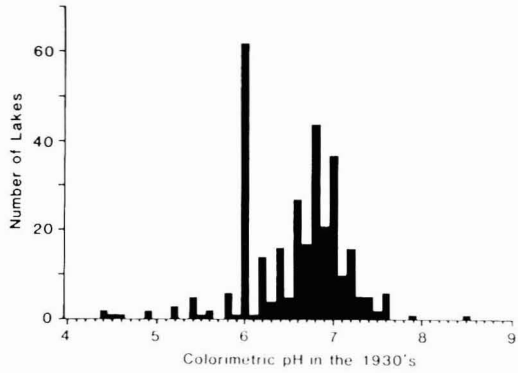

Figure 1. Histogram of historic colorimetric data from 274 Adirondack lakes. Sources of data as in ref 1.

"faintest pink". The crucial connection to human color perception and verbal translation of the perceived colors is missing, thus the data are of limited relevance to the problem.

Apparently Metcalf and Gerlach (*3*) have misunderstood the method that we used to correct MO alkalinity values; we did not use a constant correction factor for all lakes. We stated (*1*) that we used the procedure outlined in ref 4 to correct the MO alkalinity data for each lake. This procedure involved dissolved inorganic carbon (DIC) estimates based on alkalinity and CO_2 acidity data from each lake in the original reports.

We do not understand the final question addressed by Metcalf and Gerlach (*3*). Weak acids do not react with MO when they do not lower the pH enough to include the MO color transition interval (e.g., less than pH ~4.6). We are not aware of any literature documenting a direct effect between anions of weak acids and MO.

Kramer (*2*) is probably correct about the compositions of historic colorimetric indicators, although it appears that no definite information regarding these compositions can be obtained. However, evidence of the incorrect *use* of color indicators is available. The unusually large frequency of pH class 6.0 (Figure 1) in the historic data suggests that the indicator used for many of those measurements was at the extreme of its range, and that the alternate type of indicator with an appropriate pH range should have been used. Either of these types of errors could have resulted in bias in the data set of Kramer et al. (*4*), since alkalinity values calculated from colorimetric pH were averaged with the measured alkalinities.

We did not use the "consistency test" procedure of Kramer et al. (*4*) because we tested it and found it to be seriously flawed. The discussion of this issue was deleted from our paper for editorial reasons. Briefly, the procedure of Kramer et al. (*4*) was as follows: (1) for each lake, MO alkalinity and phenolphthalein (P) acidity were used together to estimate DIC; (2) MO alkalinity and P acidity were adjusted for the measurement error resulting from the difference between the pH of their respective end points and the resulting equivalent points; (3) colorimetric pH was adjusted for error caused by indicator buffering, the adjusted pH and P acidity were used to estimate alkalinity, the result was compared with the estimate of adjusted MO alkalinity, and all samples for which the two alkalinity values differed by more than 50 μequiv/L were eliminated from the data set as erroneous; (4) for each remaining lake, the change in alkalinity was calculated as the difference between modern Gran alkalinity and the mean of the two estimated historic alkalinity values.

Table II. Measured and Calculated Alkalinity (μequiv/L) for 51 Adirondack Lakes

source	measd Gran alk	MO[b] alk[a]	DIC and pH[a]	P[b] acidity and pH[a]
mean (SE)	78.2 (13.5)	75.3 (10.5)	66.7 (12.6)	53.7 (70.7)
median	36.7	29.4	24.4	22.6

[a] Calculated by procedure of ref 4. [b] MO, methyl orange; P, phenolphthalein.

We tested the accuracy of the above procedure empirically with quality-controlled data from the EPA Eastern Lakes survey for 1984 (*13*). We used detailed data on acid and base titrations supplied by EPA for 51 Adirondack lakes to estimate MO alkalinity and P acidity (using end points of pH 4.25 and 8.25, respectively) and obtained data on Gran alkalinity, sample pH, and DIC. For each lake we used the procedures of ref 4 with the above data to adjust MO alkalinity and P acidity to the appropriate equivalence points as in steps 1 and 2 above, derive another estimate of alkalinity from pH and adjusted P acidity (P acyalkalinity), and obtain a third estimate of alkalinity from pH and DIC (DIC alkalinity). We used equilibrium constants that were somewhat different from those employed by ref 4 because the EPA titrations were conducted in constant ionic strength medium; of the several pH values measured by EPA, we used the most appropriate value for each estimate.

Our results are summarized in Table II. For both means and medians of values for these 51 lakes, corrected MO alkalinity, P acyalkalinity, and DIC alkalinity all underestimated Gran alkalinity. The greatest underestimates were found for P acyalkalinity, while MO alkalinity provided the best approximation to Gran alkalinity. The difference between Gran alkalinity and DIC alkalinity was highly correlated with DOC ($r = 0.49$) but not with extractable aluminum ($r = 0.04$), indicating that organic bases may be a significant source of non-carbonate alkalinity in these waters. We concluded that estimates of alkalinity derived from pH and P acidity were biased, probably because non-carbonate protolytes caused violation of the assumptions of the model on which the calculation was based. The small difference (mean 2.9 μequiv/L; maximum 9 μequiv/L) between mean Gran and MO alkalinities was evidence that organic anions present were titrated above the MO end point and that no significant bias exists between corrected MO alkalinity and Gran alkalinity.

The apparent bias in P acyalkalinity may have affected conclusions in Kramer et al. (*4*) about acidification in Adirondack lakes. When we compared corrected MO alkalinity and P acyalkalinity, as done in ref 4 to test for consistent data, 8 of the 51 lakes had differences between these values greater than 50 μequiv/L and thus would have been rejected as inconsistent despite the fact that they were all quality-controlled data that should pass an unbiased test. The mean Gran alkalinity of the rejected lakes was 214 μequiv/L; the mean Gran alkalinity of the remaining lakes was 54 μequiv/L. In our complete data set, the difference between historic and modern alkalinity was weakly correlated with the historic alkalinity ($r = 0.12$; $a = 0.04$); thus, elimination of lakes with high historic alkalinity values as "inconsistent" would have resulted in a decrease in estimated acidification. Bias in the remaining data would also have resulted from the practice employed in Kramer et al. (*4*) of averaging P acyalkalinity, which apparently is biased low, with the adjusted MO alkalinity. Because steps 1 and 2 above apparently were valid in our test sample but steps 3 and 4 were not, we adopted the former procedure but not the latter in our analysis (*1*).

Table III. Effect of Storage of Water in Soft Glass on Alkalinity[a]

lake	storage treatment	mean alk, μequiv/L	SE
Minnewaska	plastic	−10.1	1.2
Minnewaska	soft glass	−5.9	1.3
Stissing	plastic	1946.8	2.2
Stissing	soft glass	1956.6	1.8
Stissing	plastic, porcelain[b]	1948.6	0.9

[a] Samples were stored for 50 h after collection. Means and standard errors are shown for triplicate titrations. [b] Titrated in porcelain crucible.

We did not claim that the data of Kramer et al. (*4*) were biased due to limed lakes; we stated that bias in their data could occur due to the inclusion of lakes sampled in 1979 when a faulty pH meter was used and the Gran plots were nonlinear. Much of the faulty 1979 data present in the 1980 New York State report (*14*) were not eliminated from the 1984 report (*15*). Anyone using data from *either* report should eliminate data collected in 1979, which Kramer et al. (*4*) did not do.

To examine our data statistically, we used a conservative Wilcoxon signed rank test for paired samples. As we stated, we found significant ($a < 0.01$) lake acidification even when we applied the correction for the lower pH 4.04 titration end point suggested by Kramer et al. (*4*). Kramer (*2*) has called into question the validity of our calculations. We have rechecked the statistics and found no mistakes. We would be happy to make our data set available to Kramer if he wishes to conduct additional statistical analysis.

Kramer (*2*) indicates that the use of soft glass bottles and porcelain crucibles contributed up to 100–200 μequiv/L alkalinity to the historic lake samples, and that this effect invalidates the significant lake acidification reported by us (*1*). We were genuinely surprised at the magnitude of the effect suggested by Kramer (*2*), reversing his previously stated position on this subject: "... glass contamination would not be a factor in some analyses done in the field immediately after sample collection ..." (*9*). We decided to investigate this issue further with a simple test. We collected water from two New York lakes, Stissing Lake (pH 8.2) and Lake Minnewaska (pH 4.9), and stored the samples for 50 h in new, soft glass (Qoropak) bottles as well as in plastic carboys. Samples were titrated in plastic beakers and analyzed by the Gran procedure (*16*). Additional samples from Stissing Lake stored in plastic were titrated in porcelain crucibles. The results (see Table III) showed a small alkalinity increase of 9.8 μequiv/L ($a < 0.05$) in 50 h of storage for Stissing Lake and a nonsignificant increase for Lake Minnewaska samples. These rates of increase are roughly similar to those found by Kramer and Tessier (*9*). We found no significant effect of the porcelain titration vessel. Since the historic samples were titrated in the field without delay (and the analysts presumably reused aged glass bottles, which would release less alkalinity), the effect of storage was probably less than 0.5 μequiv/L; this contrasts markedly with the estimate of 100–200 μequiv/L given by Kramer (*2*). On further investigation we were surprised to discover that a reference cited by Kramer (*2*) to support this estimate was a study reporting the effect of storage of sulfuric acid solutions (N/1000) on new glass bottles held at room temperature for time periods of 6 months to 1 year (*17*). These conditions hardly seem comparable with storage of water samples for a few hours. The second reference (*9*) showed

results similar to ours, with small, nearly linear increases in alkalinity during several days of storage. Kramer's application of the results of the long-term storage in new glass from these references to the few hours of storage employed by the historic lake surveys is unreasonable.

We are concerned about seasonal variations in surface water alkalinities as suggested by Kramer (2). However, much of the modern data is based on the New York D.E.C. data set (*18*), which was collected during the summer months (as was the historic survey). The modern EPA surveys collected samples in the fall, but alkalinities in Adirondack lakes tend to be highest during this time (*19*). Thus the actual acidification is probably somewhat greater than we have estimated it to be. As stated in our original paper, whenever possible we chose the more conservative interpretation.

In summary, we believe we have conducted a careful and thorough examination of both the historic as well as the modern chemistry data. A thorough review of these analyses supports our previous conclusion that significant acidification of Adirondack Mountain lakes has occurred during the past 50 years and also is in agreement with the results of earlier chemical and biological studies of lake acidification in this region.

Registry No. Water, 7732-18-5; methyl orange, 547-58-0.

Literature Cited

(1) Asbury, C. E.; Vertucci, F. A.; Mattson, M. D.; Likens, G. E. *Environ. Sci. Technol.* **1989**, *23*, 362.
(2) Kramer, J. R. *Environ. Sci. Technol.*, preceding correspondence in this issue.
(3) Metcalf, R. C.; Gerlach, R. W. *Environ. Sci. Technol.*, preceding correspondence in this issue.
(4) Kramer, J. R.; Andren, A. W.; Smith, R. A.; Johnson, A. H.; Alexander, R. B.; Oehlert, G. In *Acid Deposition: Long Term Trends*; National Research Council; National Academy Press: Washington, DC, 1986; p 231.
(5) American Public Health Association *Standard Methods for the Examination of Water and Waste Water*, 13th ed.; A.P.H.A.: New York, 1971.
(6) Eilers, J. M.; Glass, G. E.; Pollack, A. K. RL-D Draft 539; U.S. EPA, 1985.
(7) Wetzel, R. G.; Likens, G. E. *Limnological Analyses*; Saunders: Philadelphia, PA, 1979; p 116.
(8) Haines, T. A. Unpublished data and personal communication; U.S. Fish and Wildlife Service, Orono, ME.
(9) Kramer, J. R.; Tessier, A. *Environ. Sci. Technol.* **1982**, *16*, 606A.
(10) Taylor, F. L. Letter of February 23, 1933, to C. Juday. Archives University of Wisconsin, Madison, WI, 1933.
(11) Kolthoff, I. M.; Stenger, V. A. *Volumetric Analysis*; Wiley: New York, 1947; Vol. II.
(12) American Public Health Association *Standard Methods for the Examination of Water and Sewage, 4th ed.*; A. P.H.A.: New York, 1926. *Standard Methods for the Examination of Water and Sewage, 6th ed.*; A.P.H.A.: New York, 1930.
(13) *Characteristics of Lakes in the Eastern United States*; EPA/600/4-86/007; U.S. Environmental Protection Agency. U.S. Government Printing Office: Washington, DC, 1986; Vols. 1–3.
(14) Pfeiffer, M. H.; Festa, P. J. *Acidity Status of Lakes in the Adirondack Region of New York in Relationship to Fish Resources*; New York State Department of Environment Conservation: Albany, NY, 1980.
(15) Colquhoun, J. R.; Kretser, W. A.; Pfeiffer, M. H. *Acidity Status of Lakes and Streams in New York State*; New York State Department of Environmental Conservation: Albany, NY, 1984.
(16) Gran, G. *Analyst* **1952**, *77*, 661.
(17) Bacon, F. R.; Burch, O. G. *J. Am. Chem. Soc.* **1941**, *24*, 29.
(18) Adirondack Lake Survey Corp. *Lake Survey*; NY Dept. of Environmental Conservation: Albany, NY, 1984–85; Vols. 1–10.
(19) Driscoll, C. T.; Yatsko, C. P.; Unangst, F. J. *Biogeochemistry* **1987**, *3*, 37.

C. E. Asbury*
Center for Energy and Environment Research
G.P.O. Box 3682
San Juan, Puerto Rico 00936

M. D. Mattson
Institute of Ecosystem Studies
The New York Botanical Garden
Box AB Millbrook
New York 12545

F. A. Vertucci
Rocky Mountain Forest and Range Experiment Station
Department of Biology
Colorado State University
Ft. Collins, Colorado 80526

G. E. Likens
Institute of Ecosystem Studies
The New York Botanical Garden
Box AB
Millbrook, New York 12545

By the time you get regulatory information, is it too late?

Let Regulated Chemicals Listing (CHEMLIST) help.

There's a lot of regulations to know about these days—

PMN, CHIP, PAIR, CAIR, SNUR, FYI, Section 12B to mention a few. One way for your staff to find the information they need concerning regulations on commercial chemicals is to review every issue of key sources such as the EPA TSCA Inventory, the Federal Register, Chemical Regulation Reporter, TSCA Chemicals-in-Progress Bulletin, TSCATS (TSCA Unpublished Test Submissions), and Pesticide & Toxic Chemical News.

A better solution is to search online

A faster, easier solution is to have your staff access Regulated Chemicals Listing (CHEMLIST) online. We've already reviewed the important sources and input the data to our database. And your staff will get current information—in general—not more than two weeks old.

To get additional details about how searching Regulated Chemicals Listing (CHEMLIST) online can help your staff comply with government regulations, write to

Chemical Abstracts Service, Dept. 31790, P.O. Box 3012, Columbus, OH 43210.

Regulated Chemicals Listing is produced by the American Petroleum Institute; is marketed by Chemical Abstracts Service; and is available online only through STN International.

STN®
INTERNATIONAL
The Scientific & Technical Information Network

How gun cotton and a twist of the wrist made the world a safer place.

In 1855, a German scientist named Fick created quite a stir in the scientific community.

He took a glass rod, dipped it in some gun cotton (nitrocellulose), and literally started "stirring," or rolling the rod. Much to his delight, a thin "sac" formed on the surface of the rod. And the first membrane filter was created.

Fick was excited. Unfortunately, his colleagues weren't. Which explains why it took almost a century for his discovery to make an impact.

Today, refined offsprings of Fick's crude filter monitor workplace and environmental air quality, detect and treat diseases, uncover impurities in foods and drugs, and ensure water supplies are safe to drink.

Millipore membranes have led to more rapid, accurate monitoring of coliform densities in water supplies.

Surprisingly, these and hundreds of other uses were advanced or developed by one company. Millipore.

But then, maybe it's not a surprise. Anyone who's worked in a lab has probably used a Millipore filter. In fact, over 100 million will be used this year.

For good reason, too. Over 120 contaminants are regulated by the EPA, NIOSH and OSHA. Millipore has membranes to sample them all.

Millipore test kits can detect fine sand and metal particles to ensure airplane fuel reliability.

Their filters undergo as many as 25 individual tests.* (More than most people get during a routine physical.)

All this has helped Millipore learn a lot about membranes.

Consistent pore sizes allow Millipore filters to better detect and analyze gas line impurities.

* Depends upon application

But it's also given people the idea they're the only manufacturer of membranes. "So," they conclude, *"it doesn't matter what brand I buy. It's all Millipore."*

Millipore originated many of the procedures which use membranes for pollution monitoring.

Not so. To ensure you get accurate results—time after time—you've got to ask for Millipore by name.

Try it right now. Call 800-225-1380, or the nearest Millipore office, and ask for a free sample pack, featuring the new Isopore™ track-etched membrane

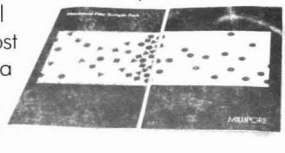

After all, it's a lot easier than making your own.

MILLIPORE

CIRCLE 1 ON READER SERVICE CARD